Self-Optimisation of Automated Continuous Reactors

Nicholas Holmes

Submitted in accordance with the requirements for the degree of Doctor of Philosophy

School of Chemistry

&

School of Chemical and Process Engineering

May 2017

The candidate confirms that the work submitted is his/her own, except where work which has formed part of jointly-authored publications has been included. The contribution of the candidate and the other authors to this work has been explicitly indicated below. The candidate confirms that appropriate credit has been given within the thesis where reference has been made to the work of others.

The work in Chapter 3 has appeared in: **N. Holmes**, G. R. Akien, A. J. Blacker, R. L. Woodward, R. E. Meadows and R. A. Bourne, *React. Chem. Eng.*, 2016, **1**, 366-371. NH was responsible for carrying out all experimentation and helping improve the optimising program. The contribution from other authors was writing the initial optimising and control programs (GRA. RAB), donating equipment, analytical methods and compounds (RLW, REM) and project supervision (RLW, REM, AJB, RAB).

The work in Chapter 5 has appeared in: **N. Holmes**, G. R. Akien, R. J. D. Savage, C. Stanetty, I. R. Baxendale, A. J. Blacker, B. A. Taylor, R. L. Woodward, R. E. Meadows and R. A. Bourne, *React. Chem. Eng.*, 2016, **1**, 96-100. NH was responsible for carrying out all practical experimentation, initial MS method development experiments, making significant changes to the optimising program to include MS, calibration of the MS to HPLC and DoE model regression and analysis. The contribution from the other authors was, writing the initial optimising and control programs (GRA. RAB), fitting and analysis the DoE models (RJDS, BAT, RAB), carrying out initial MS method development experiments (CS) and project supervision and support (IRB, AJB, RLW, REM, RAB).

To Tom Poyser,

Ken Tate

and Eric Holmes

Acknowledgements

Firstly I would like to thank my supervisor Richard Bourne for his tireless help and support over the years and for providing me with an interesting project with such exciting opportunities. I don't think I'll ever forget the early days of my project, us both sitting and staring at HPLC chromatograms until late into the evening with me desperately trying to learn MatLab code and wondering what the hell I'd got myself in for. Also for allowing me to prioritise my MSc work over lab work during my first year. My thanks go to my co-supervisor John Blacker for his help and guidance and unparalleled industrial knowledge that was available whenever I needed it. Also to Bao Nguyen and Frans Muller for project contributions.

I would like to thank all members of the iPRD, past and present and give special praise to two members in particular. Geoff Akien, who set up the basic automated reactor and whom I learned I was more and more in debt to the more I learned about coding; and Katie Jolley who would *always* give up her time to go above and beyond to help, I rarely needed to ask. The other postdocs during my time at Leeds who would give their advice, support and constant bullying that I was only a lazy computer scientist: John Cooksey, Jess Breen, Will Reynolds and Alastair Baker. All other members of the group and department over the years who made it should a crazy but fun place to work: Lisa, Phil, Mike, Andy, Yuhan, Jake, Mo, Paul, Seb, Tarn, Chris, Grant, Rachel, James, Ilias, Maria, Adam, Pete, Jing, Mary, Ahmed and Prof. Kocienski. I'd also like to thank the Masters students I mentored for, above all, teaching me patience: Mo, Alex, Rob and Jamie.

This project wouldn't be anything without the help and contribution of equipment and resources from AstraZeneca. My thanks to Rebecca Meadows for her supervision over the years as well as reading early drafts of thesis chapters, papers and departmental reports and getting me on my feet during my placement at Macclesfield. Rob Woodward for project help and with Martin Jones for championing the project internally at AZ. Brian Taylor for his DoE help both in person and at the end of an e-mail. Anne O'Kearney-McMullan, Ali Boyd, Mubina Mohammed and the rest of the flow team for their help as well as Tony Bristow for MS help and discussions. Rich Hart and Joel Le Bars for help during my placement and also the AZD9291 team for letting us use such a valuable compound on such an unknown technology.

I have benefitted from many collaborations over the years so I would like to thank Andy Baker, Clive Aldcroft and Mark Allen from Advion and Jeremy Reddish and Alessio Zammataro from Microsaic. Christian Stanetty and Ian Baxendale from Durham University for our combined work on the Advion spectrometer as well as allowing me to present at a Baxendale group meeting. Artur Schweidtmann and Alexei Lapkin for working together with such an exciting algorithm. Simon Doherty and Julian Knight for optimisation studies with heterogeneous catalysts.

I'd like to thank all departmental support staff: Matthew Broadbent for mechanical workshop support, Martin Huscroft LC/MS, Simon Barrett NMR and Tarsem Hunjan for electronic workshop support, all chemical stores staff and all departmental administration staff. Thank you to the University of Leeds, EPSRC and AstraZeneca for funding my studentship.

Thank you to my family, Mum, Dad and Kate for their constant support over the years and always providing well-earned escapes from Leeds on weekends where I didn't need to worry about coding errors, clogged up reactors or broken pumps.

My last and most heartfelt thank you goes to Lisa. I can't begin to put into words my gratitude for all you have done. You know how important you are.

Abstract

The optimisation of problematic reaction steps in the synthesis of a drug compound is crucial for pharmaceutical process development. In recent traditions, this has carried out using design of experiments (DoE), which shows the key reaction variables and provides optimum reaction conditions. The process can require a lot of experiments and be time and resource consuming. The speed of optimisation experiments can be increased by using automated platforms complete with online analysis, which carry out reactions and acquire analytical samples without any human intervention. If these experiments can be carried out in continuous reactors then they will benefit from faster kinetics, enhanced heat and mass transfer, improved safety and higher productivity over their batch counterparts.

An automated self-optimising flow reactor combines a continuous reactor with online analysis and feedback loop. The feedback loop contains full computerised control and monitoring of all equipment as well as a minimising algorithm, which will use the results from the online analysis to predict new optimum conditions. The technique has been shown to optimise the synthesis of small organic compounds but has, so far, yet to be widely used in pharmaceutical process development.

This thesis has improved self-optimising technologies in order to make it a useful technique in pharmaceutical process development. First, the final bond forming step in the synthesis of an active pharmaceutical ingredient was optimised for yield. Studies were primarily carried out on a model compound in order to establish the correct reactor setup before transferring to the active compound, which found an optimum yield of 89%. The work also provided mechanistic evidence for generation of impurities.

Next, response surface models were successfully fitted to the data obtained from a branch and fit algorithm optimisation of a Claisen-Schmidt condensation. In depth statistical calculations show how DoE models can be generated from self-optimisation data with good fit and predictability ($R^2 > 0.95$, $Q^2 > 0.90$), and with the aid of commercial DoE software.

Further work developed the use of direct mass spectrometry (MS) as the online analytical method. The short method times and real-time analysis of MS allowed a steady state detection function to be built, followed by a linear calibration model of all the species in the amidation of a

methyl ester. The reaction was optimised for yield using branch and fit algorithm, and DoE, with excellent agreement between the two techniques in both optimum conditions and responses.

Finally, changes were made to the optimisation program to reduce the amount of material required for automated optimisations. Reaction pulses of sub-reactor volumes were pumped through the reactor, dispersed in a continuous phase of miscible solvent. Residence time distribution experiments were carried out to characterise the dispersion of the reactor and calculate the minimum reactor pulse volume. Optimisations were primarily carried out using pattern search algorithm and a multi-objective evolutionary algorithm, the latter of which generated a three target function optimum, reducing the amount of waste by 81%.

Overall this work has shown how self-optimisation can be a valuable tool for pharmaceutical process development. The existing technique has been improved by demonstrating its use in the synthesis of pharmaceutical compounds, combining it with existing DoE techniques, adding new forms of online analysis, and reducing the amount of material required to deliver a multi-target optimum.

Table of Contents

List of Figures

List of Schemes

List of Tables

List of Abbreviations

ANOVA	Analysis of variance
APCI	Atmospheric pressure chemical ionisation
API	Active pharmaceutical ingredient
aq	Aqueous solution
Ar	Aromatic
ATR	Attenuated total reflectance
ATR-kinase	Ataxia telangiectasia and Rad3-related protein kinase
AZ	AstraZeneca
BPR	Back pressure regulator
Boc	tert-Butyloxycarbonyl
Bu	Butyl
cat.	Catalyst/Catalytic amount of
CCF	Central composite face centred
CMS	Compact mass spectrometer
COSY	homonuclear correlated spectroscopy
DBA	Dibenzylidene acetone
DBU	1,8-Diazabicyclo[5.4.0]undec-7-ene
DCE	1,2-Dichloroethane
DF	Degrees of freedom
DIB	(diacetoxyiodo)benzene
DMC	Dimethyl carbonate
DME	Dimethoxy ethane
DMF	*N*,*N*-dimethyl formamide
DMPU	1,3-Dimethyl-3,4,5,6-tetrahydro-2(1*H*)-pyrimidinone
DMSO	Dimethyl sulfoxide
DoE	Design of experiments
DSR	Deleted studentised residual
EGFR	Epidermal growth factor receptor
eq	molar equivalents
ESI	Electrospray ionisation
Et	Ethyl
FDA	Food and Drug Administration (US government)
FED	Fractional factorial design
FFD	Full factorial design

FT-IR	Fourier transform infrared (spectroscopy)
GC	Gas chromatography
GSK	GlaxoSmithKline
GUI	Graphical user interface
HPLC	High performance liquid chromatography
HSQC	heteronuclear single quantum correlated spectroscopy
ID	Internal diameter
IntPo	Interior point (algorithm)
IPA	Isopropyl alcohol
IR	Infrared (spectroscopy)
IUPAC	International Union of Pure and Applied Chemistry
Me	Methyl
MLE	Maximum likelihood estimation
MLR	Multiple linear regression
MOAL	Multi-objective active learner (algorithm)
mol	moles
mp	Melting point
MS	Mass spectrometry
Ms	Methanesulfonate
NIRS	Near infrared spectroscopy
NMP	*N*-methyl pyrrolidinone
NMR	Nuclear magnetic resonance (spectroscopy)
NMSim	Nelder-Mead simplex (algorithm)
OD	Outer diameter
OVAT	One variable at a time
PC	Personal computer
PEEK	Polyether ether ketone
PFC	Perfluorinated compound
PFR	Plug flow reactor
Ph	Phenyl
PMI	Process mass intensity
ppm	parts per million
PRESS	Prediction error sum of squares
PS	Pattern search (algorithm)
psi	Pounds per square inch

PTFE	Polytetrafluoroethylene
RS	Raman spectroscopy
RSM	Response surface methodology
RT	Room temperature
RTD	Residence time distribution
RV	Reactor volume
sat.	Saturated
sc	Supercritical
SD	Standard deviation
SL	Sample loop
SMSim	Super modified simplex (algorithm)
S_NAr	Nucleophilic aromatic substitution
SNOBFIT	Stable noise optimisation by branch and fit
SSE	Residual sum of squares
SST	Total sum of squares
STY	Space time yield
^{t}Bu	*tert*-butyl
TEAC	Triethylammonium chloride
Tf	Trifluoromethanesulfonyl
TFA	Trifluoroacetic acid
TFAA	Trifluoroacetic anhydride
THF	Tetrahydrofuran
TIC	Total ion chromatogram
TLC	Thin layer chromatography
TMOF	Trimethyl orthoformate
TREAT-HF	Triethylamine trihydrofluoride
TS-EMO	Thompson sampling-evolutionary global optimisation (algorithm)
UHPLC	Ultra high performance liquid chromatography
USB	Universal serial bus
UV	Ultraviolet
UV-Vis	Ultraviolet-Visible light (spectroscopy)
wrt	with respect to
XIC	Extracted ion chromatogram

1. Introduction

The pharmaceutical industry relies on innovative and novel technological advances in the chemical sciences to drive forward drug discovery and development. Medicinal chemists discover chemical compounds for new medicines and their structure scrutinised until the active pharmaceutical ingredient (API) is decided. Next, the company is heavily reliant on the research of process development scientists to redesign and improve the synthetic route in order to create a robust and efficient manufacturing process.[1] One aspect of process development is the optimisation of problematic reaction steps, which is typically carried out using design of experiments (DoE).[2, 3] Whilst this approach is highly effective at improving chemical understanding and finding optimal conditions, there is always scope to find better techniques.

In order to facilitate safe and efficient manufacture, continuous flow processing has been seen as an attractive technology for API manufacture.[4-7] Flow reactors have several unique characteristics that allow for more efficient syntheses over batch counterparts. One particular aspect is the ease of integration of online analytics and equipment automation. The combination of this automated technology with a feedback loop containing an optimising algorithm creates a "self-optimising" reactor, which can carry out multiple experiments and optimise a reaction without any user intervention (Figure 1.1).[8-10] The concept was first introduced by Krishdnadasan *et al.* for the highly selective synthesis of CdSe nanoparticles,[11] and has since been developed by the groups of Jensen[12-14] and Poliakoff[15-18] for the synthesis of simple organic molecules. In parallel to the work in this thesis, the field of self-optimisation has benefitted from further development from Jensen[19-21] and Poliakoff[22, 23] with additional contributions from other groups.[24-28]

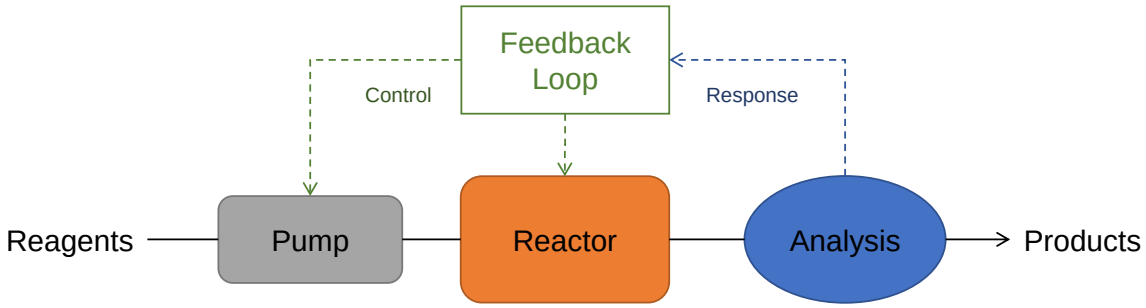

Figure 1.1 Schematic of a self-optimising flow reactor

This thesis will explore the use of self-optimisation as a technique for improving and optimising troublesome steps in pharmaceutical process development. This chapter will introduce this subject with a literature review that explores the recent advances in flow chemistry, online analysis and automated optimisations.

1.1 Flow Chemistry

In batch reactors, reagents are added either instantaneously or with slow controlled addition in order to control exotherms. If the reaction needs to be heated, the temperature will change over a period of time and it can take minutes to hours to achieve the desired temperature depending on the reaction scale and temperature. The maximum temperature that the reaction can be heated to is also limited to the boiling point of the solvent. Similarly, cooling a reaction back to room temperature occurs over a period of time and sometimes this is required before a reaction can be quenched. Very fast exothermic reactions need to be cooled, sometimes to cryogenic temperatures in order to slow down the reaction to controllable rates and prevent runaway reactions. Overall batch reactions suffer from a lack of control and non-uniform reaction conditions as well as slow reaction kinetics.

Flow reactors have smaller dimensions and volumes, resulting in a higher surface area to volume ratio, which results in more efficient energy transfer. The smaller volumes also allow for the safe operation of elevated pressures whereby it is possible to heat a reaction above the boiling point of the solvent and even pump molten reaction mixtures.[29-31] Efficient heat transfer enables typically cryogenic transformations to be carried out at warmer, and more efficient, temperatures;[32-34] including "flash chemistry" with sub-second reaction times.[35, 36] Highly efficient energy transfer has also been applied to increased performance with non-thermal energy sources.[37] The safety of reactions is also increased due to the decrease in exothermic hotspots,[38] and lower chemical inventory allowing for a lower exposure of highly hazardous reagents.[39-44] The surge of academic and industrial research into continuous flow chemistry over the past few decades has contributed to the advancement of a variety of techniques and technologies that have improved the field immensely.[45-55] The following sections provide selected examples of these advances.

1.1.1 High Energy Transfer

Chemical reactions in flow can be carried out at more forcing conditions than in batch, resulting in improved performance, be that yield, selectivity, rate or productivity. The term was derived as "novel process windows" by Hessel *et al*. in 2009 and has since been used for a variety of applications,[29-31] most often enhancing performance by carrying out reactions at higher temperatures and pressures.[50] Elevated pressures are easily achieved by simply forcing the flow through an extremely narrow channel in a back pressure regulator. It should be noted that for liquid phase reactions, increasing the pressure is unlikely to significantly increase the reaction kinetics but simply allows for higher operating temperatures before the reaction boils (Boyle's Law).

Borhukova *et al.* benefitted from novel process windows in the synthesis of rufinamide (Scheme 1.1),[56] an anticonvulsant used to treat epilepsy in children. The first step used hydrogen chloride gas and neat benzyl alcohol **1** to facilitate the efficient synthesis of a benzyl chloride **2** with water as the only by-product.[57] The second step proceeded *via* a simple substitution between the benzyl chloride **1.2** and sodium azide to yield the benzyl azide **1.3**. Sodium hydroxide was added to prevent formation of the highly toxic and explosive hydrogen azide gas. The last step, a Huisgen cycloaddition, typically requires a copper catalyst to control regiochemistry, however with process intensification the reaction was carried out catalyst free with excellent yield and selectivity.[58] A stream of methanol was added to the reaction outlet in order to aid crystallisation, which occurred upon standing in the product collection pot.

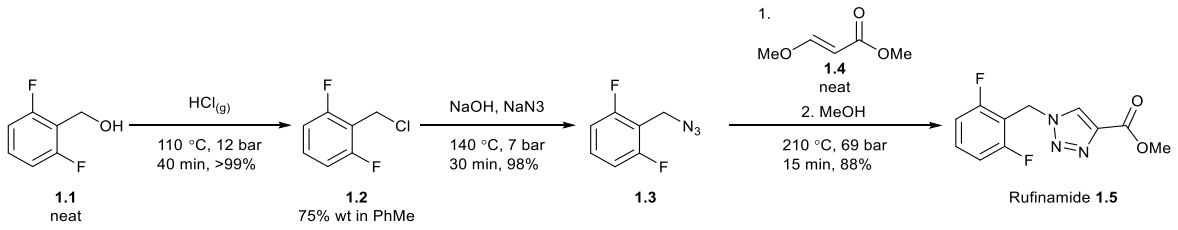

Scheme 1.1 Synthesis of rufinamide **1.5** under continuous flow conditions, by Borhukova *et al.* The conditions for each step are shown underneath each reaction arrow. Yields were improved by using novel process windows.[56]

In a similar approach, Snead and Jamison reported the highly atom economic synthesis of diphenhydramine hydrochloride **1.8** (Scheme 1.2).[59] By introducing the chlorodiphenyl methane **1.6** and *N*,*N*-dimethylethanolamine **1.7** as neat reagents and using high temperatures and pressures,

the product **1.8** could be pumped out of the reactor as a molten salt after first reacting with the HCl by product *in situ*.

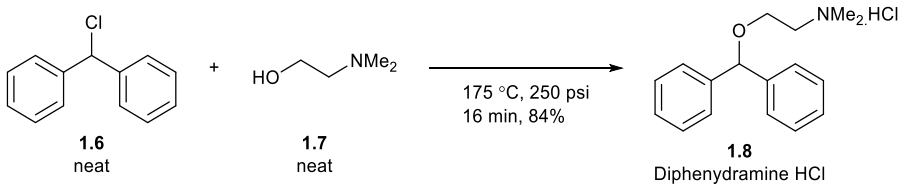

Scheme 1.2 Continuous flow synthesis of diphenhydramine hydrochloride **1.8**. High temperatures and pressures enabled the product to be pumped as a molten salt.

Improving synthetic methods is not the only benefit of novel process windows; Hone *et al.* showed that through process intensification, multistep kinetic models can be generated by using higher forcing conditions rather than longer reaction times. The approach accelerated kinetic model development and as such 72 reactions were carried out in 3 hours of total experiment time, which were used to fit 8 kinetic parameters.[60]

High energy transfer can be used not only for safe operation at high temperatures and pressures but also for sudden changes in reactor temperatures, which would not be possible in batch due to the lengthy temperature gradients. Gutman *et al.* carried out the synthesis of sulfoximide **1.10**, an intermediate towards the synthesis of an ATR-kinase inhibitor.[61] The combination of azide salt and fuming sulfuric acid generated hydrogen azide *in situ*, which could perform the desired functional group transformation with high atom economy.

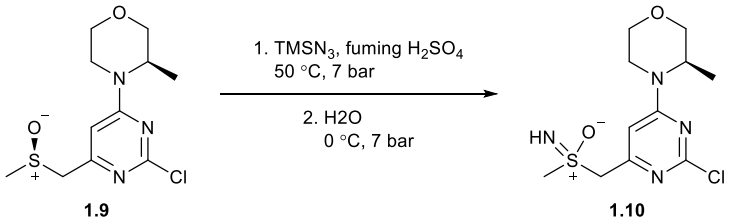

Scheme 1.3 Formation of sulfoximide **10** under continuous flow conditions. The reaction step was carried out at 50 °C followed by an aqueous quench, which needed to be cooled rapidly to 0 °C.

The sulfoximidation reaction was carried out at 50 °C and followed by a quench with ice cold water. This required a rapid temperature change to 0 °C, which was easily facilitated using two separate continuous reactors and resulted in minimal by product formation.

Rapid heat removal has been exploited by the Yoshida group for "flash chemistry" reactions, which can be carried out in micro to millisecond time scales.[35, 36] For example, with rapid mixing and heat removal, it was possible to carry out a desired chemoselective *ortho*-functionalisation of iodophenyl carbamate **1.11** without suffering from a Fries rearrangement (Scheme 1.4).[62] In other work, it was possible to carry out a Swern oxidation at room temperature with high yields and selectivities (Scheme 1.5), a reaction that would ordinarily be performed at -78 °C to control the highly exothermic reaction between dimethyl sulfoxide (DMSO) and trifluoroacetic anhydride (TFAA).[63] These reaction conditions are only possible with the strict control of residence time and efficient removal of heat achieved with flow reactors.

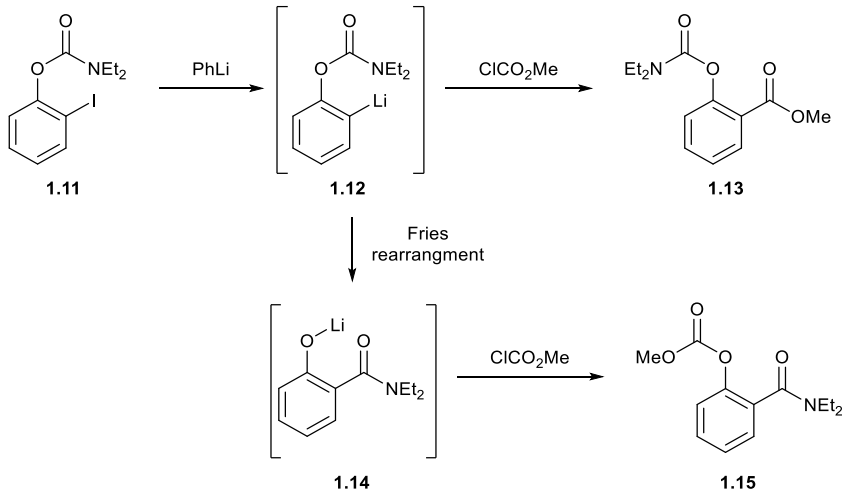

Scheme 1.4 Schematic outlining the desired transformation of *ortho* iodophenyl carbamate **1.11** with phenyl lithium, then methyl chloroformate to form 1-carbamate-2-ester product **1.13**. In poor mixing reactors, the intermediate **1.12** undergoes Fries' rearrangement to form **1.14** and the undesired 1-carbonate-2-amide product **1.15**. The best selectivities were achieved at residence times of 330 μs for the first step.

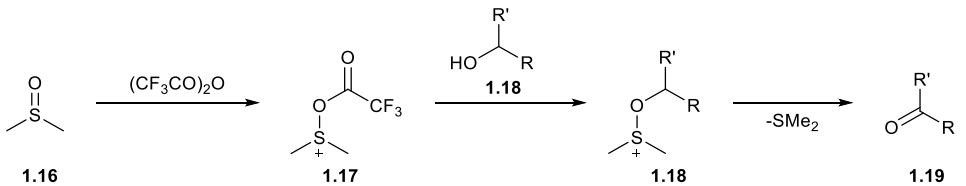

Scheme 1.5 Swern oxidation reaction Scheme . The reaction requires temperatures of -78 °C under batch conditions to prevent formation of impurities but was carried out at room temperature in flow.

Energy transfer does not just apply to heat. Photochemical reactions in continuous flow have been highly successful because of the short distances photons have to travel to react with the reaction media. Arguably the most successful application of continuous photochemistry is

converting oxygen to its singlet and triplet states to perform key oxidation steps in the synthesis of artemisinin, an effective antimalarial drug.[64-67]

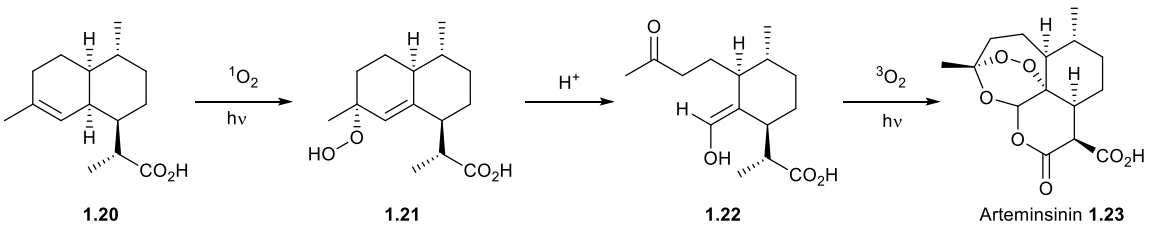

Scheme 1.6 Reaction Scheme to artemisinin **1.23** from dihydroartemisinic acid **1.20** using a combination of oxidation steps using singlet (**1.20** to **1.21**) and triplet oxygen (**1.22** to **1.23**).

Electrochemical reactions also see an improvement in continuous flow because of the high interfacial area between the electrodes and reaction mixture, short distances between electrodes allowing for enhanced mass transfer as well as the ability to operate the reactions without electrolytes.[68, 69] Energy can also be successfully applied to continuous reactors using microwave irradiation,[70, 71] inductive heating from magnetic fields to heat magnetic particles,[72, 73] or sound waves to either breakup solid by-products[74, 75] or supply energy.[76]

1.1.2 Hazardous Chemistries

The low chemical inventory in continuous flow reactors means that highly hazardous and reactive reagents can be safely used at all scales. This is most evident in the use of gases. Increased interfacial areas between liquid and gas streams by means of segmented or annular flows means that reactions with gases in flow are incredibly efficient with high atom economy and minimal by-products.[41] The disadvantages with gaseous reagents is that its physical state means that it is highly reactive and they can be dangerous to use due to specific safety hazards, such as being toxic (F_2, CO, O_3), highly flammable/explosive (O_2, H_2, C_xH_y) or simple asphyxiants (N_2, CO_2).

Fluorine is a highly reactive element yet is also very important in the synthesis of pharmaceuticals and it appears in many APIs or intermediates towards them. Chambers *et al.* developed a stainless steel/nickel falling film reactor for the fluorination of 1,3-dicarbonyl substrates and their scale-up.[77, 78] A solution of 10% F_2 in N_2 (v/v) was used because pure F_2 gas would have uncontrollable reactivity. This type of reactor could then be coupled to an additional stream of hydrazine to yield 1,2-pyrazoles.[79]

The synthesis of heterocycles is a potentially dangerous process if the necessary hazards have not been addressed. Nitrogen containing heterocycles are popular for commercial explosives because they form and then release benign N_2 gas upon detonation. Therefore the synthesis of nitrogen containing heterocycles is not without its dangers. In the previous section, examples showed inorganic azides (M-N_3, highly toxic) forming triazole rings by reacting with a terminal alkyne.[56-58] Disregarding their toxicity, all azides can from the explosive gas hydrogen azide and some are explosive in their natural state, either with ignition from sparks or shocks. Deadman *et al.* avoided preparing a stock of tosyl azide **1.25** (explosive, highly toxic) by reacting tosyl chloride **1.24** with the less hazardous sodium azide, *in situ* then carrying on to react with a ketone **1.26** to form an aza-*α*-carbonyl compound **1.27**. Any unreacted tosyl azide **1.25** could be quenched by a mixture of sodium hydroxide with acetylacetone.

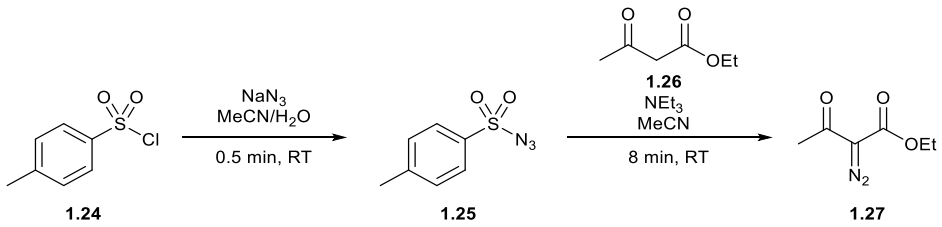

Scheme 1.7 Synthesis of aza-*α*-carbonyl compounds *via* the *in situ* formation of tosyl azide **1.25**, preventing the use of preparing hazardous stock solutions.[40]

Formation of hazardous reagents *in situ* is a commonplace practice for flow chemistry because of the ease in which reagent streams and reactor coils can be combined to existing setups. For example there have been multiple uses of generating gases *in situ* for laboratory scale applications, avoiding the more intensive task of installing a gas cylinder and the expense of a mass flow controller.[80]

1.1.3 Multistep Synthesis of Pharmaceuticals Using Automated Flow Reactors

The modular nature and small footprint of continuous reactors means that it is simple to integrate multiple equipment types into one reactor setup. Examples have been shown in the previous sections where multiple reaction steps have been integrated for synthesis of hazardous reagents[40, 80] or desired organic compounds,[56-58] however flow technology has advanced to allow sophisticated syntheses of organic compounds, all in a single continuous process. This not only includes coupling continuous reaction modules but also liquid/liquid separators,[81-83] solvent

extractors,[84-86] by-product scavengers,[87] back pressure regulators,[88] crystallisers[89, 90] and filtration devices.[91]

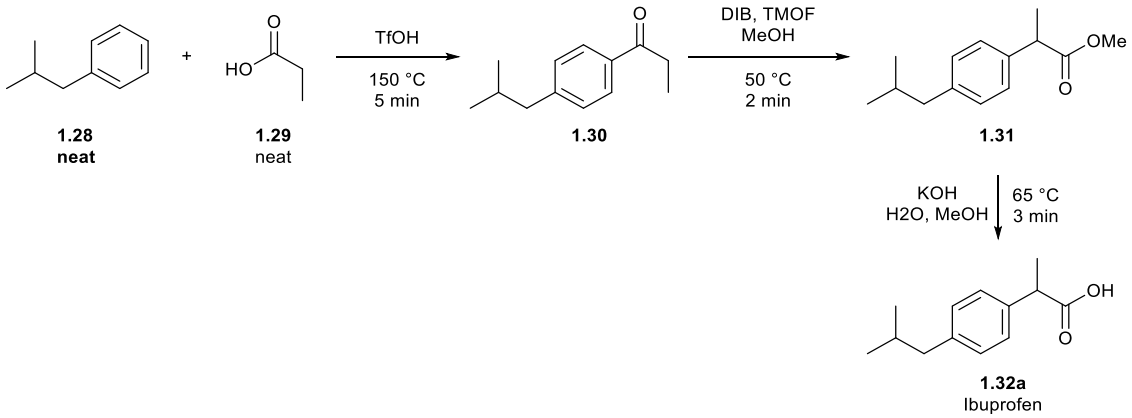

Scheme 1.8 Continuous flow synthesis of ibuprofen **1.32** by Bogdan *et al*.[93] All steps were incorporated into a single process to produce crude **1.32a**, which was recrystallised in batch. DIB = (diacetoxyiodo)benzene, TMOF = trimethyl orthoformate

Ley and Baxendale used solid supported reagents and scavenging columns in the multistep continuous synthesis of compounds including complex alkaloids.[92] This method required no isolation or purification steps, however the columns are too expensive to use in any realistic scale up and manufacturing process. A more attractive procedure is to optimise each single step to minimise excess waste or ensure that it will not interfere in any downstream reactions or processes. Bogdan *et al*. provided one of the first examples of this in their continuous synthesis of ibuprofen **1.32**.[93] An excess of TfOH was used for the Friedel-Crafts acylation in the first step, and the DIB mediated 1,2-aryl migration in the second to yield the target compound in a 51% yield in 7 min (after batch recrystallisation, Scheme 1.8). Snead and Jamison pushed this synthesis further using neat reagents wherever possible, inline liquid-liquid separation, continuous crystallisation and novel process windows to produce pure **1.32** in an 83% yield in 3 min (Scheme 1.9).[94]

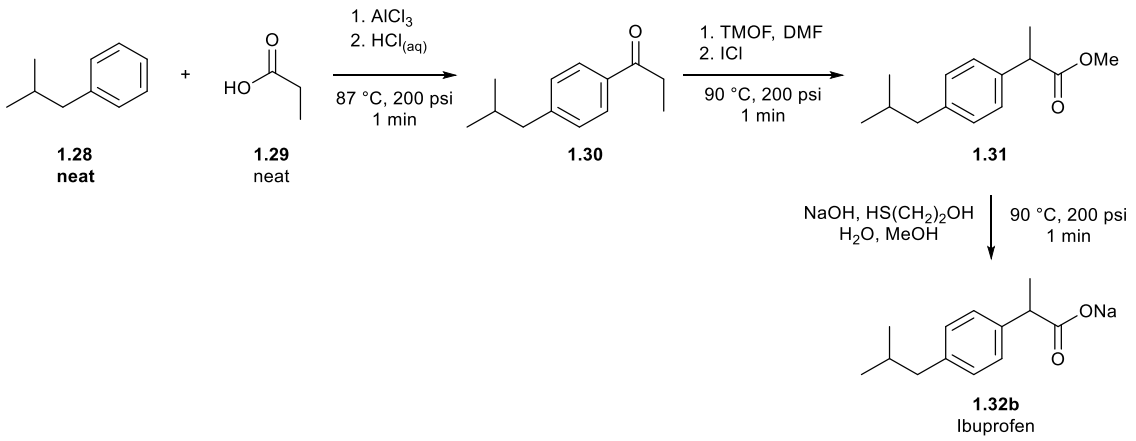

Scheme 1.9 Continuous flow synthesis of ibuprofen **1.32** by Snead and Jamison.[94] The first step was quenched using aqueous HCl solution then product **1.30** extracted using continuous inline separation. The final step featured a combined ester hydrolysis and continuous crystallisation to produce pure **1.32b**. TMOF = trimethyl orthoformate.

The danger with multistep continuous flow synthesis is that it relies on the process running perfectly. In reality continuous flow can be fraught with potential pitfalls caused by variable reagent quality, equipment malfunction or material blockage.[95] The best way to prevent this is to use intelligent control platforms to monitor equipment and have emergency shutdown procedures in case of malfunctions. Ingham *et al.* used this approach for the continuous synthesis of adamantine amino acid **1.38** (Scheme 1.10).

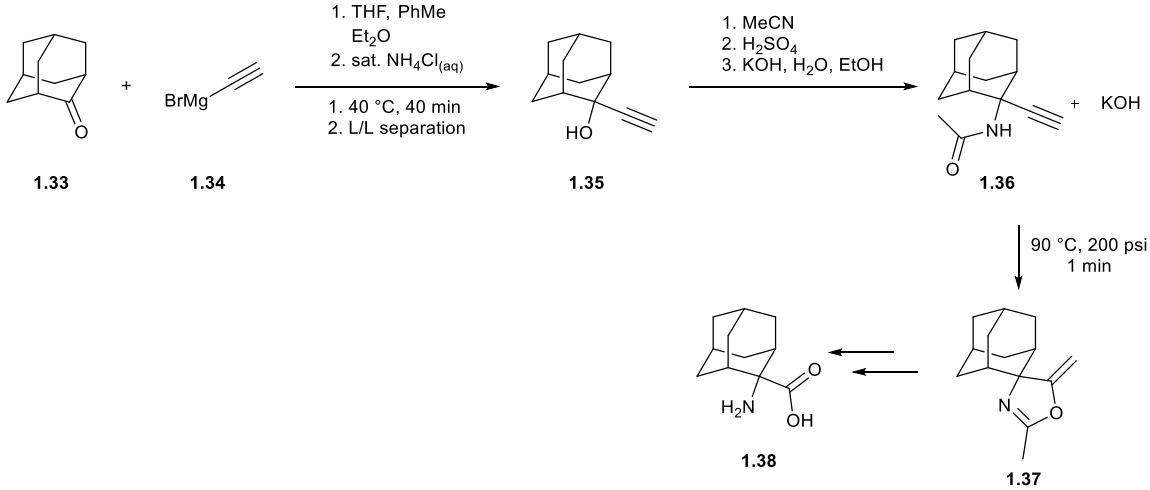

Scheme 1.10 Continuous flow synthesis of oxazole intermediate **1.37**. All steps were controlled by a computer platform which used online IR and webcam liquid level monitoring to stop and start each step. Amide **1.36** was collected as a filtrate in a solution with KOH, which was directly pumped into the next reactor to facilitate cyclisation to **1.37**. Adamantane amino acid **1.38** was synthesised in separate steps.

The formation of the propargyl alcohol **1.35** from the solutions of adamantone **1.33** (in toluene and diethyl ether) and ethynyl magenesium bromide **1.34** (in THF), was monitored by

online infrared spectroscopy (IR) to control the quench stream of saturated ammonium chloride. Computer controlled liquid/liquid separation resulted in a solution of **1.35** in a mixture of organic solvents, which were evaporated and then acetonitrile was introduced to produce a solution of **1.35** for which the level was controlled by webcam monitoring. This acetonitrile solution was reacted with sulfuric acid to produce amide **1.36,** then quenched with potassium hydroxide. The by-product salt was filtered and the filtrate (containing KOH) was collected into a webcam monitored reservoir and then pumped through a reactor to induce the cyclisation to oxazole **1.37**. Through the use of online IR analysis and monitoring of liquid levels using webcams, the synthesis of **1.37** was enabled in a fully automated continuous process with 10 separate unit operations.

Whilst the combination of these technologies is impressive, there is a development and integration timescale to connect all the equipment together both physically and with computer communications. This configuration of equipment is specific to this process and requires setup and disassemble time. Adamo *et al.* developed a single reconfigurable automated reactor platform that was capable of synthesising 4 different formulated drug products: diphenhydramine hydrochloride, lidocaine hydrochloride, diazepam and fluoxetine hydrochloride (Figure 1.2).[96] The platform was the size of a household refrigerator and contained computer controlled modules with online IR to monitor product formation and ultrasonic probes to quantify the concentration of solution phase parenteral and dermal doses (Figure 1.3). The time to reconfigure the system to synthesise different drugs varied from 15 min to 2 h and could produce up to 4500 doses over a 24 h period.

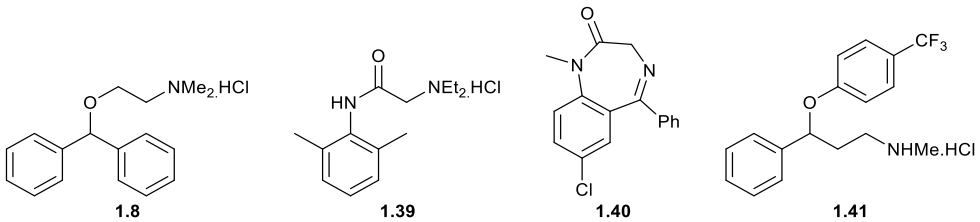

Figure 1.2 Structures of pharmaceuticals manufactured by Adamo *et al*.[96] Diphenyhydramine hydrochloride **1.8**, lidocaine hydrochloride **1.39**, diazepam **1.40** and fluoxetine hydrochloride **1.41**.

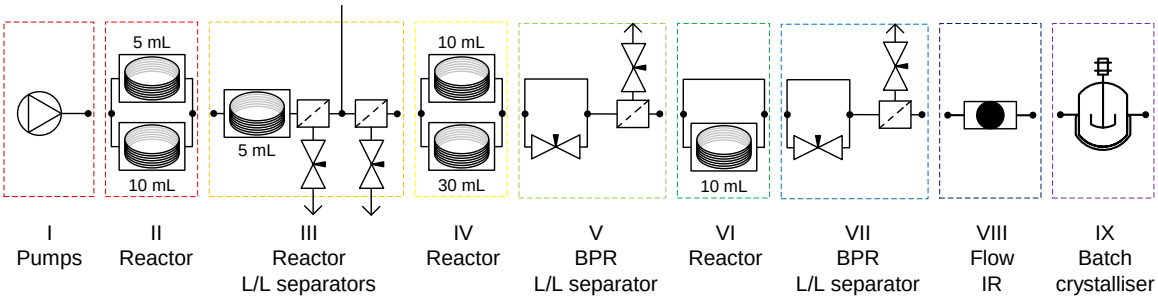

Figure 1.3 Schematic of the reconfigurable automated reactor designed by Adamo *et al.*, used for the synthesis of pharmaceuticals in Figure 1.3 Each unit could be interchanged/bypassed depending on the target product.[96]

1.2 Online Analysis

Analysis of reaction progress is not a new concept in chemical synthesis. For example, it is commonplace for standard batch laboratory reactions to be monitored offline by thin layer chromatography (TLC), gas chromatography (GC) or high performance liquid chromatography (HPLC). Typically, offline analysis requires neutralisation and possibly workup for the sample to be suitable for analysis. During these steps, reaction intermediates and crucial information about the reaction could be lost.

Online analysis, describes the *in situ* analysis of a reaction, and can be used for a variety of applications, including reaction intermediate screening and gathering kinetic data. Techniques such as IR,[97-104] Raman spectroscopy[98, 99, 105] ultraviolet-visible light spectroscopy (UV-Vis)[98, 100, 106] and nuclear magnetic resonance spectroscopy (NMR);[107-110] HPLC[111-113] and GC;[114-116] as well as mass spectrometry[117-119] have been used extensively to monitor reactions in flow reactors.

1.2.1 Infrared Spectroscopy

IR offers a convenient and non-destructive method for inline monitoring. The majority of applications of modern IR instruments for continuous monitoring utilise flow-through cells with attenuated total reflectance (ATR) technology and are capable of fast acquisition for near real-time monitoring.

Fourier transform IR (FT-IR) monitoring of functional groups was used by Qian *et al.* in the telescoped flow synthesis of a δ-opioid receptor antagonist **1.45** (Scheme 1.11).[104] Each step of the synthesis was carried out and optimised in individual reactor coils followed by polymeric scavenging columns to generate pure product without the need for work-up or purification.[87] The

optimisation studies consisted of injecting sample loops containing the substrates and reagents, an online FT-IR was used to measure the presence of the intermediate, *via* the characteristic stretching frequency of the amide **1.44**, so that the addition of the Burgess reagent stream could be synchronised. It was also possible to calculate the concentration and volume of reagent required using the IR spectra.

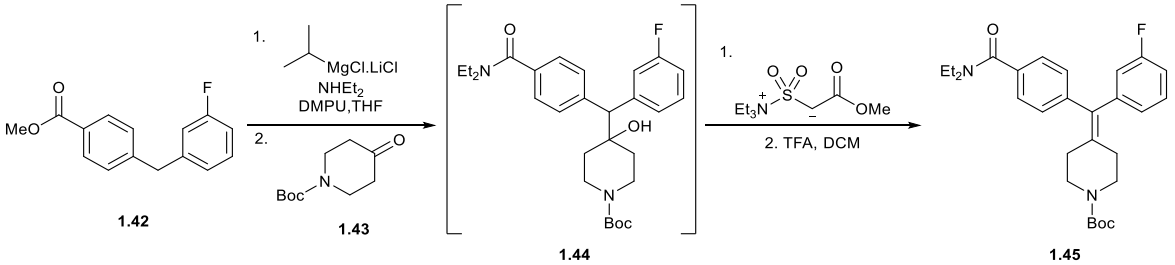

Scheme 1.11 Telescoped synthesis of *δ*-opioid receptor antagonist **1.45**. Online IR was used to observe the amide formation **1.44** and notify when to introduce the Burgess reagent for the dehydration.[104]

Skilton *et al.* used the fingerprint region for online analysis of the *O*-methylation of *n*-pentanol using dimethyl carbonate and a fixed catalyst bed containing *γ*-alumina.[18] Calibration of the IR data was performed by correlation of non-convoluted peaks with calibrated GC data. The use of FT-IR significantly enhanced throughput compared to the GC experimentation. The average experiment time of 32 min when using GC was reduced to 3.5 min with FT-IR as the near real-time analysis could both detect steady state performance and much more rapidly quantify the outlet concentration of the desired product, enabling detailed scans of the parameter space.

1.2.2 Nuclear Magnetic Resonance Spectroscopy

NMR spectroscopy could be described as the go-to method for compound identification by synthetic organic chemists, but its inherent insensitivity generates spectra with low signal to noise ratios, especially with samples sizes of microlitres and smaller. Recent developments have been made into using microcoils and flow capillaries to reduce the signal to noise ratio.[107, 108] Olson *et al.* demonstrated that microcoils and capillaries could be used to provide high resolution NMR spectroscopy for small quantities of material.[107] Recently, miniaturised low-field NMR systems with permanent magnets have been developed for online analysis in the laboratory and production environments. These devices typically operate at field strengths of 2 tesla and up to 85 MHz ^{1}H-

frequency.[120] This low field strength normally produces complex spectra and the magnetisation of the sample is influenced by the flow velocity and further complicated by the absence of deuterated solvents in process monitoring applications. Therefore, they are not ideally suited to detailed assignment of spectral features but can be readily used for near real-time analysis of reaction mixtures. However it may be impractical to accurately quantify low concentrations or systems containing a large number of compounds.

Wensink *et al*. used a microcoil NMR at 60 MHz for generating a kinetic profile of an imine formation (Scheme 1.12) in continuous flow.[108] Syringe pumps with the benzaldehyde and aniline in separate solutions of nitromethane-*d*3 were fed into the reactor. Clearly separated singlet signals of the aldehyde proton (C*H*O, δ 9.9 ppm) and the imine proton (Ar-C*H*N-Ar, δ 8.4 ppm) were chosen to monitor reaction conversion. Rate constants were collected and results shown to be comparable to offline measurements. Improvements were proposed, by adding multiple microcoils along a flow reactor; an approach later used by Ciobanu *et al*.[110]

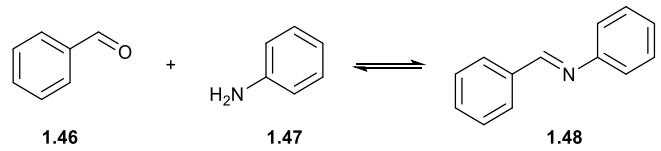

1.46 1.47 1.48

Scheme 1.12 A kinetic profile of the reversible imine formation was measured with NMR spectroscopy. Product formation and substrate degradation was easily monitored in crude spectra due to the distinctive changes in proton environments.[108]

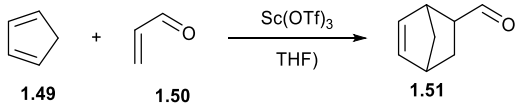

1.49 1.50 1.51

Scheme 1.13 Diels-Alder reaction between cyclopentadiene **1.49** and acrylaldehyde **1.50**, catalysed by scandium triflate. The stereochemical ratio of the product was determined by deconvoluting ^{1}H NMR spectroscopy.[25]

The advancement of commercial low-field NMR spectrometers[121, 122] has allowed researchers to monitor more challenging reactions by NMR. Sans *et al.* used online NMR to distinguish between two stereoisomer products of a Diels-Alder reaction between cyclopentadiene **1.49** and acrylaldehyde **1.50**, catalysed by scandium triflate (Scheme 1.13).[25] Deconvolution of the low resolution spectra was achieved by fitting Gaussian trends to the chemical shift peaks in the aldehyde region (δ 9.0 to 9.6 ppm). It was also possible to carry out structural characterisation of

the product of a fluorination reaction (Scheme 1.14) using ^{1}H homonuclear correlated spectroscopy (COSY) and $^{1}H^{13}C$ heteronuclear single quantum correlated spectroscopy (HSQC) and ^{19}F NMR. However, the machine used had a scan time of 10 s, which resulted in total acquisition times of 9 min (COSY) and 38 min (HSQC) for the two techniques.

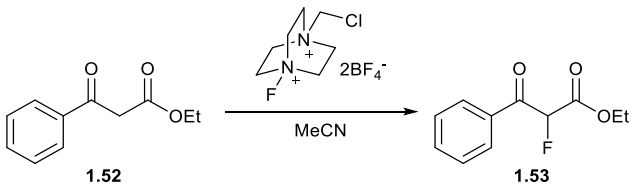

1.52 1.53

Scheme 1.14 Fluorination of keto-ester **1.53** using Selectfluor. The product was identified using homo- and heteronuclear correlated spectroscopy.[25]

Online NMR has also been used for monitoring the DIB mediated cyclopropanation of styrenes in flow, using a variety of different substrates. Geminal and vicinal correlations within the cyclopropane ring could be determined by using COSY with acquisition times of 10 min.[123]

1.2.3 Ultraviolet-Visible Spectroscopy

UV-Vis spectroscopy is conducted in the 200-800 nm wavelength range. It is especially applicable to compounds with high conjugation and active chromophores. Unlike NMR, IR and Raman Spectroscopy, UV/vis spectra consist of relatively broad absorption peaks due a multitude of electronic and vibrational levels, this makes quantification difficult in the majority of cases. Smith *et al.* showed the applicability of UV-Vis for measuring dispersion for product collection in a react and release system for the synthesis of triazoles.[124]

1.2.4 Raman Spectroscopy

Raman spectroscopy (RS) is another form of vibrational spectroscopy, which measures the inelastic scattering of light emission. RS, like ATR FT-IR spectroscopy, offers a convenient and non-destructive analytical technique for analysis of flow reactors. In particular, RS is particularly suited to systems containing water. A recent example by Chaplain *et al.* discussed the development of a Raman Flow Cell for the continuous Suzuki reaction shown in Scheme 1.15.[125]

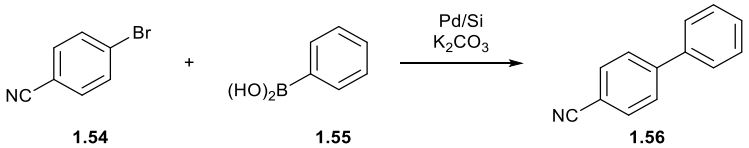

1.54 1.55 1.56

Scheme 1.15 Suzuki reaction used to develop inline Raman spectroscopy using potassium carbonate base and a palladium on silica monolith catalyst.

Quantitative analysis was achieved by partial least squares regression to obtain a calibration model which was validated using offline GC-MS analysis. Furthermore, kinetic profiles of the reaction could be compiled to give rate constants for reaction optimisation. This achieved 61% yield of the product.

1.2.5 Near Infrared Spectroscopy

Near Infrared Spectroscopy (NIRS) covers a spectral range between visible and mid-IR wavelengths (800-2500nm). NIRS measures the absorption bands resulting from overtones or combinations of the fundamental mid-IR bands, mainly of –CH, -OH, -SH and –NH bonds.[126] NIR spectra consist of many overlapped spectral features which necessitate the use of chemometrics to gain quantitative data regarding the composition of samples.[127, 128]

Cervera-Padrell *et al.* used NIRS for the online monitoring of a Grignard reaction (Scheme 1.16) in a tubular reactor.[127] The Grignard reaction is a useful technique in organic synthesis for forming carbon-carbon bonds in functionalised compounds. It can be however problematic in scale up as it is incredibly fast, highly exothermic and therefore difficult to control. The increased heat transfer found in flow reactors has resulted in many Grignard transformations being scaled up in continuous reactors but heat spots are still observed at mixing sections,[127] where it is assumed the reaction occurs.[129] To counter these potential problems, the Grignard was introduced into the reactor through multiple entries. The reaction was sensitive to changes in the relative stoichiometry of the Grignard reagent and ketone, with increases in the former creating impurities, and the latter reducing the yield. NIRS was used to monitor the concentration of the substrates in the system, with a feedback loop controlling the pump ratios.

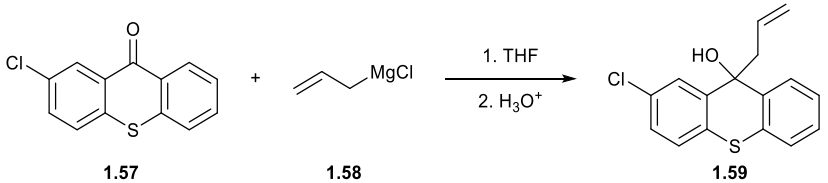

1.57 **1.58** **1.59**

Scheme 1.16 Formation of tertiary alcohol **1.59** by Grignard reaction with ketone **1.57**. The reaction was sensitive to reactant stoichiometry and excesses of ketone and Grignard were monitored using online NIRS.

1.2.6 Gas Chromatography

Chromatography separates compounds based on their differential affinity for mobile and stationary phases. It is commonly used as an accurate measure of purity as well as product identification, if compared with known standards, or combined with other analytical techniques (such as mass spectrometry). Chromatography is typically regarded as an at-line technique as sampling must be performed discretely with analysis results typically requiring 2-30 min, compared to the continuous real-time nature of most spectroscopy techniques.

GC uses a gaseous mobile phase and has been successfully used in the online monitoring of reactions that produce extremely volatile products or by-products that are normally lost during work-up or extraction procedures. Online GC is typically conducted using a sample loop, a switching valve between two separate flow streams, which can introduce a small volume of the sampled stream into the carrier flow of the GC. Walsh *et al.* used online GC analysis to create an automated continuous system to analyse the formation of highly volatile short chain ether species in the solid acid catalysed etherification of short chain alcohols (Scheme 1.17) in supercritical carbon dioxide ($scCO_2$) which could not easily be contained for offline analysis.[114] *O*-Alkylations using short chain alcohols can be a greener alternative to their alkyl halide counterparts due to their non-toxicity.

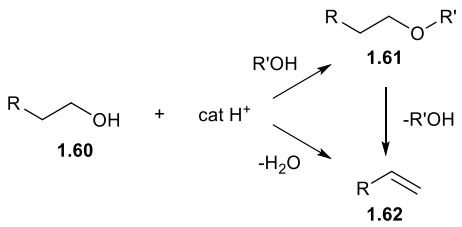

Scheme 1.17 Various reactions in the *O*-alkylation of alcohols using short chain alcohols (note, the etherification can be symmetrical or asymmetrical)[114]

The symmetrical etherification of alcohols with methyl to *n*-pentyl chains was investigated and the results showed that the highest yield was achieved with *n*-propanol. It was proposed that the longer carbon chain increased the nucleophilicity of the alcohol, but for the longer butyl and pentyl chains, the elimination reaction was preferred.

The implementation of online GC with an automated reactor resulted in a queue of experiments that could be run without any user intervention. GC was appropriate for analysing the

highly volatile short chain ether and alkene products. However GC is restricted to compounds that have significant volatility and has been estimated to be useful for only 20% of known organic compounds.[130]

1.2.7 High Performance Liquid Chromatography

HPLC separates materials based on their differing affinity to a pressurised liquid carrier and a column filled with a solid sorbent material (typically 2-50 micrometers particle size). Several different detectors can be fitted including UV/Vis, photodiode array or MS. HPLC has several advantages over GC, including:

- A greater library of compounds that can be analysed.
- A smaller diffusion coefficient, increasing the speed of analysis.
- Higher viscosities of the mobile phase, reducing the diffusion coefficient.
- Greater flexibility in changing the stationary and mobile phases.

HPLC technologies have developed over the past few decades to improve the speed and efficiency of column separation. The newer technologies have been denoted as ultra-high performance liquid chromatography (UHPLC) or simply ultra-performance liquid chromatography (UPLC).[131] Part of the advancement has been to decrease the theoretical plate height in a column, which is a measure of the resolution. The plates in a column are thought of as theoretical discrete steps that the compounds have to "climb" and the smaller the steps, the higher the number of these steps in a column and the better the separation. There are two particular methods that have been used to decrease the plate height: reduce the particle size to < 2 µm and change the particle composition to have partial porosity. The relationship between theoretical plate height, particle size and optimum flow velocity is calculated by the Van Deemter plot and shows that the optimum flow velocity is greater for smaller particle sizes (Figure 1.4).[132, 133] The invention of core shell particles, with partial porosity reduce the longitudinal diffusion and therefore peak broadening.[133, 134]

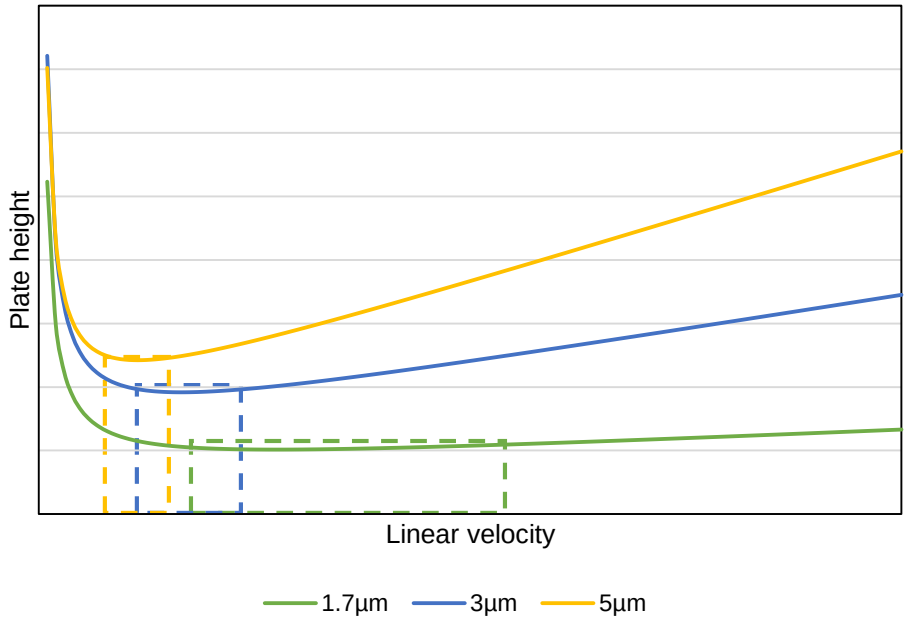

Figure 1.4 Van Deemter plots showing the optimal linear velocities for HPLC columns with different particle sizes. Optimal linear velocity zones are highlighted by the dashed boxes. Smaller particle sizes result in higher linear velocities.[132, 133]

At-line HPLC was used by Antes *et al*. to monitor the nitration of toluene in microreactors to assess the performance of a silicon microreactor.[113] Silicon has high heat transfer properties and high resistance to acid corrosion. At-line HPLC was chosen for the speed and reliability of analytical feedback; plus the UV detector on the machine was suitable for the aromatic substrates and products. In this research they replaced the typical mixture of aqueous sulfuric and nitric acid with fuming nitric acid, removing the need to regenerate and purify the resulting nitrating acid mixture. The effective mixing and high heat transfer that is achieved in microreactors enabled rapid reaction with effective control of the reaction exotherms. The reactor was set up with three separate syringe pumps for toluene, fuming nitric acid and an ice water quench; with at-line HPLC sampling through a sample-loop.

The nitration of toluene can generate a high number of different isomers (Scheme 1.18) but only mono-substituted products were targeted. During initial screening tests, the highest yields (89 to 92%) of nitrotoluene were observed at residence times of 3 s, with isomer ratios of 53% *ortho*, 3.5% *meta* and 44% *para*. Because the reaction time was so short, a quench stream was introduced before sampling, so that strict control over the reaction could be achieved. When the flow rate of

the quench stream was reduced the observed yield, by at-line HPLC, decreased by almost half, due to the reaction progressing to di-substituted products.

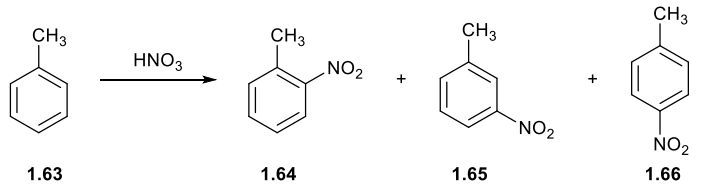

1.63 1.64 1.65 1.66

Scheme 1.18 Different mono-isomers formed in the nitration of toluene.[113]

1.2.8 Mass Spectrometry

Online MS is a stand-alone technique that measures the molecular mass of compounds and their constituent fragments. MS is commonly coupled to chromatographic techniques (GC-MS, LC-MS) but has been used solely for online analysis in reaction monitoring and has several advantages over other techniques. It can directly detect metal species; and particular elements, such as chlorine and bromine can be identified by their isotope patterns. However it does come with some disadvantages. If structural isomers do not form different fragments, then they can only be identified with ion mobility,[135] which is not readily available on most spectrometers. Different ionisation techniques are required for different compounds, so a compromise may have to be reached in the spectra obtained in terms of how many components can be characterised.

Browne *et al*. capitalised on the speed of analysis and identification opportunities to monitor short lived and unstable intermediates formed in a tandem benzyne and Diels-Alder reaction (Scheme 1.19) using electrospray ionisation (ESI) MS.[118] The reaction uses a nitride to convert the anthranilic acid **1.72** to a diazonium salt **1.73**, which undergoes rapid loss of CO_2 and N_2 to yield the benzyne **1.74**. Introduction of furan initiates a Diels-Alder reaction to form the epoxy naphthalene **1.76**.

This follows the traditional route to benzynes, which is no longer popular in batch processes because the diazonium intermediate is explosive if produced in large quantities or isolated to its pure crystalline form. The substrates have now been replaced with starting materials that introduce triflates and trimethylsilanes as leaving groups but these are expensive reagents that require multistep processes, generating more waste. The use of continuous processing offers a direct route because the low inventory of the hazardous intermediate can be handled safely.

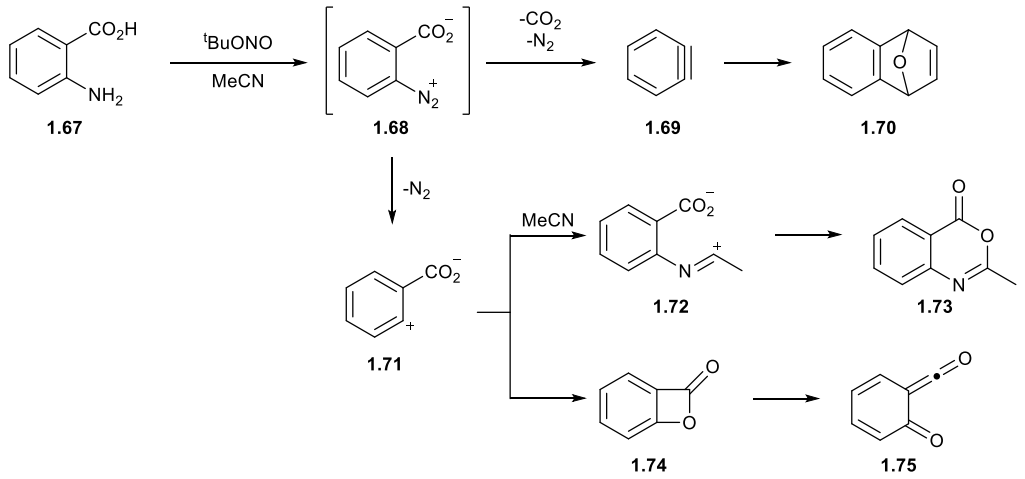

Scheme 1.19 Single step benzyne generation and Diels-Alder reaction. Online MS was used to monitor intermediates and show evidence of competing reaction pathways.[118]

Preliminary studies with the mass spectrometer showed that the explosive diazonium intermediate was still present in the out stream mass spectrum when the reactor was at room temperature, so sodium thiosulphate was added to the collection vessel to reduce the intermediate and thus minimise the risk of explosions. Further optimisation of the operating conditions using the mass spectrometer data enabled complete consumption of the explosive intermediate and prevented formation of undesired side products.

1.3 Automated Optimisations using Flow Reactors

1.3.1 Self-Optimisation

Self-optimisation describes the use of automated reactors combined with online analysis and adaptive feedback algorithms to generate optimal conditions without the need for human intervention. The procedure depends on the algorithm used but will likely start with a set of conditions either user defined or calculated from the algorithm, which are carried out with the reactor, then the optimising target calculated from the online analytical data. Next, the algorithm will use the results of the experiments to predict new experimental conditions and this will continue in a cycle until the user stops the process or a tolerance limit is reached.

Flow systems are ideally suited for such experimentation, as integration of analytical equipment is facile and rapid measurement and adjustment of operating parameters such as flow rate, temperature and pressure can be accomplished quickly within a single reactor system. The concept was first used by Krishnadasan *et al.*[11] for the synthesis of CdSe quantum dot nanoparticles

using a microreactor, online UV and SNOBFIT algorithm.[136] The reaction was optimised for a wavelength function that was termed the 'dissatisfaction coefficient', which assigned an error from the current to desired wavelength, which the SNOBFIT algorithm could minimise. This allowed the synthesis of highly tuned target-optimised CdSe quantum dot nanoparticles.

SNOBFIT (Stable Noise Optimisation by Branch and Fit) is a branch and fit algorithm used in linear programming.[136] It is so called because it will plot global (or exploratory) experimental points and then calculate polynomials based on the responses to find optimal (or local) points; essentially branching out and then finding a fit. The algorithm will continue to plot both exploratory and local points, as it continues to seek optima.

McMullen *et al.* used the Nelder-Mead simplex (NMSim), steepest descent DoE and SNOBFIT algorithms for the optimisation of a Knoevenagel condensation in a microreactor equipped with at-line HPLC (Scheme 1.20).[12] A 2-dimensional experimental space was selected using residence time and temperature as the variables; and optimised for a combined function of yield and production rate (also called Space Time Yield, STY).

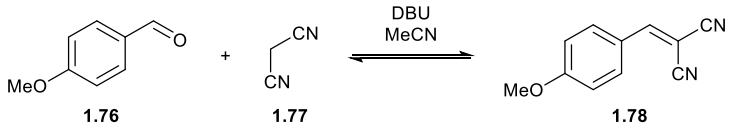

1.76 **1.77** **1.78**

Scheme 1.20 Knoevenagel condensation used by McMullen for self-optimisation studies.[12]

Simplex is an algorithm that will start by plotting $n + 1$ experimental points, where n is the number of variables, then ranking the results of the experiments from best to worst. A new point is created by reflecting the simplex shape from the worst point through the mid-point between the resultant points.[137] There are various modifications to the simplex algorithm, including Nelder-Mead, which can expand or shrink the simplex depending on the ranking of points.[138, 139]

The boundary constraints for temperature and residence time were between 40 and 100 ºC, and 30 and 300 s respectively. Each algorithm found the same optimum conditions of 30 s and 100 °C. The simplex algorithm quickly started merging towards short residence times and high temperatures; it reached the border range at 30 s and after trying to plot an experiment outside the defined constraints, started contracting as it moved towards 100 °C. The algorithm finished after 30 experiments. The SNOBFIT algorithm required the highest number of experiments with 36,

however it created the highest amount of scatter across the experimental space and thus provided more confidence in the optimum conditions. The steepest descent algorithm started by plotting a 2-level factorial design,[a] with 3 mid-point repeats. Analysis of the design by the algorithm showed that there was no quadratic curvature, then the algorithm calculated the gradient and progressed towards higher temperatures and lower residence times. When trying to plot an experiment outside of the design space, the algorithm changed the experiment to the constraint boundary and then terminated, after 13 experiments. Although the algorithm required the fewest number of experiments of the 3 tested, it relied on calculating the correct gradient after the first design, whereas the SNOBFIT algorithm will explore new space then re-evaluate the current model fit.

Bourne *et al*. compared the approaches of standard and super modified simplex (SMSim) algorithms for the acid catalysed methylation of *n*-pentanol in supercritical CO_2 (Scheme 1.21) using dimethyl carbonate (DMC).[16] The reaction was optimised for yield using the parameters of temperature, pressure, CO_2 flow rate; and equivalence of DMC.

In the comparison between standard simplex and SMSim algorithms, it was shown that an optimum can be reached with the SMSim in fewer simplexes due to its ability to expand and contract as it moves towards the optimum. The self-optimisation technique was well suited to reactions in supercritical fluids because the solvent can be highly tuned by only slight changes in the temperature and pressure.[140] This high level of precision would be difficult to achieve over a large experimental area, using other techniques.

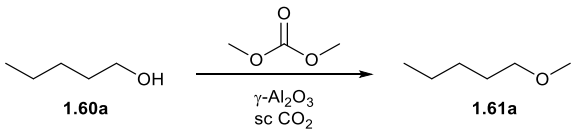

Scheme 1.21 Methylation of *n*-pentanol **1.60a** in supercritical CO_2 using dimethylcarbonate as a methylating agent and catalysed by γ-Alumina.[15, 16]

In work that was either parallel or published subsequently to the start of experimental work in this thesis, the concept of "cloud chemistry" was introduced to the field of self-optimisation.[22] This used the concept of cloud networking, where any piece of equipment that is connected to a network can be remotely accessed from another location. Therefore, because almost all of the

[a] DoE factorial designs will be discussed in detail in Chapter 3

experiments are carried out by computerised control, the operating user does not actually need to be present at the equipment. Instead, the chemicals and equipment are prepared by a local technician and then the user remotely connects to the laboratory computer and controls all aspects of the automated optimisation until completion of the experiments, where the local technician then cleans and shuts down the reactor. The Poliakoff group at the University of Nottingham, UK managed to connect to remote operators at international campuses in Ningbo, China and Kuala Lumpur, Malaysia; as well as other institutions in Ethiopia (Addis Ababa University), Brazil (Universidade Federal do Rio Grande do Sul) and Turkey (Petkim Petrochemical Holding). Successful optimisations included the etherification of propanol and the γ-Al_2O_3, Nb_2O_5 and $NbOPO_4$ catalysed DMC methylation of butanol.

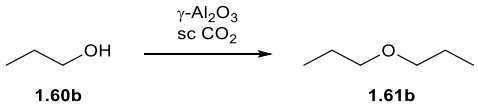

Scheme 1.22 Symmetrical etherification of *n*-propanol **1.60b** used for cloud controlled self-optimisation.[22]

The main advantage with cloud chemistry is that it makes available equipment that would be too expensive for some institutions, especially those in the developing world. The only challenges experienced with this technique were general local technological techniques, such as low bandwidth or poor weather limiting connection speeds.

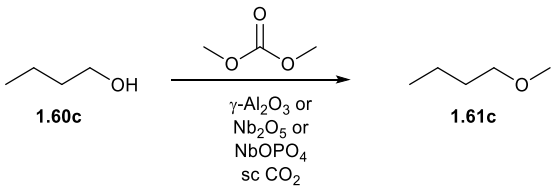

Scheme 1.23 Inorganic heterogeneous catalysed methylation of *n*-butanol **1.60c** using dimethylcarbonate as a methylating agent. These reactions were optimised using cloud control self-optimisation.[22]

There has also been considerable work towards integrating new forms of online analysis for self-optimisation. Previous techniques involving FT-IR require some form of chemometrics to deconvolute the output[126] and some chromatographic methods can be up to an hour in length. As discussed above, NMR spectroscopy is a very good for product identification and requires very little effort in calibration due to the identical relative responses of products to an internal standard.

The ability to reduce the spectral complexity by only monitoring specific nuceli (e.g. ^{19}F) reduces the time spent developing methods. Sans *et al*. used a commercial NMR spectrophotometer for the self-optimisation of an imine condensation (Scheme 1.24), using a NMSim algorithm to maximise the STY.[25]

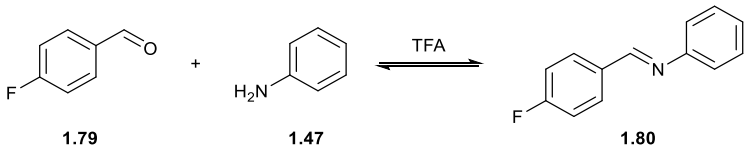

1.79 **1.47** **1.80**

Scheme 1.24 Imine condensation used for the maximisation of imine STY using online NMR and Nelder-Mead simplex algorithm (NMSim).

1.3.2 Feedback Controlled Statistical and Kinetic Models

Self-optimisation systems have typically used minimising algorithms in their feedback loops, however work by the Jensen group has replaced these algorithms with statistical and kinetic models. McMullen and Jensen aimed to optimise and scale up the Diels-Alder reaction between isoprene and maleic anhydride by using automated feedback controlled kinetic model determination and at-line HPLC (Scheme 1.25).[13]

1.81 **1.82** **1.83**

Scheme 1.25 Diels-Alder reaction between isoprene **1.81** and maleic anhydride **1.82** used by McMullen and Jensen for the automated feedback controlled kinetic model determination.[13]

Four separate kinetic models (1.1 to (1.4) were proposed with varying orders with respect to the concentrations of the starting materials and reversible/irreversible reactions, where C_A is the concentration of **1.81**, C_B is the concentration of **1.82**, C_C is the concentration of **1.83**, r_i and k_i are the rates and rate constants of equation (1.i), respectively. A Bayesian statistics approach was then used to discriminate between the different models and calculate a probability that each model describes the true reaction kinetics. Five separate experiments were carried out to determine which model was the most accurate and a sixth experiment confirmed that the best model was (1.1). Next a D-optimal DoE was carried out to find the kinetic parameters for model (1.1) (Arrhenius pre-exponential constant A and activation energy E_A) then these were used to predict the reaction

performance upon scale up from custom etched plate microreactor 120 µL to 60 mL Corning Advanced-Flow reactor (500 fold).

$$r_1 = -k_1 C_A C_B \tag{1.1}$$

$$r_2 = -k_2 C_A^2 C_B \tag{1.2}$$

$$r_3 = -k_3 C_A C_B^2 \tag{1.3}$$

$$r_4 = -k_{4,f} C_A C_B + k_{4,r} C_C \tag{1.4}$$

The advantage with using kinetics to optimise a reaction is that an empirical kinetic model that accurately interpolates and extrapolates is obtained, which can thus be used to optimise any reaction metric. In this example the reaction is simple and the kinetic model only needs to incorporate 3 different species. If the example was a reaction that required multiple chemical species (e.g. metal catalysed cross coupling) then there could be potentially hundreds of kinetic models to distinguish between and the reaction could proceed down unpredicted impurity pathways. Black-box optimisation methods, such as minimising algorithms, only need to measure the target response and therefore can easily incorporate unpredictable reaction pathways.

Further work by the Jensen group has used empirical statistical designs for automated reaction optimisation. Reizman studied the mono-alkylation of diamine **(±)1.84** to optimise for solvent selection and continuous reaction conditions using online LC-MS and a feedback controlled DoE algorithm (Scheme 1.26).[20] The feedback algorithm proceeded through the following steps:

1. Initial fractional factorial design (FED) for each solvent. Fit models for each solvent.
2. FED in smaller experimental area where the initial set of models predicted an optimum.
3. Feedback G-optimal DoE search to minimise the uncertainty in the best performing solvent designs.
4. Steepest descent gradient search optimising only continuous variables with the best solvent.

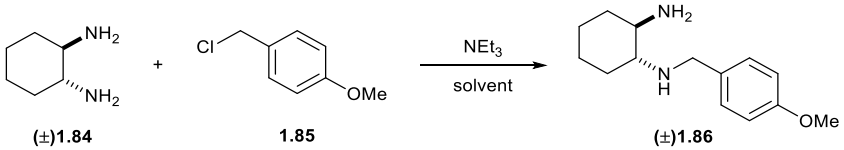

(±)**1.84** **1.85** (±)**1.86**

Scheme 1.26 Amine mono-alkylation reaction used by Reizman and Jensen to carry out discrete and continuous feedback DoE optimisations.[20]

The solvents screened were: DMC, DCE, IPA, MeCN, THF, DME, pyridine, DMSO, toluene and DMF; and the continuous variables were: residence time, temperature and amine concentration. In the first step, 20 experiments were carried out at the least and most forcing conditions of the continuous variables for each of the 10 solvents screened (a 2^{3-2} FED design). A response surface was fitted to each solvent design and was used to decrease the design space towards the predicted optimum conditions. Therefore the new least forcing conditions were the old centre-point and the new centre-point was scaled accordingly. A new set of 20 experiments (10 FEDs) were carried out and the worst performing solvents were eliminated: MeCN, DME and DMC.

Next the algorithm used response surface refinement to search through the continuous conditions using the resultant solvents. A G-Optimal design was used, which aims to minimise the maximum variance in the predicted models, i.e. carrying out experiments with solvents that have the highest error with the predicted optima. This search required a further 27 experiments before deciding that DMSO was the best performing solvent. The last step was a steepest descent gradient search optimising for only the continuous variables using DMSO as the reaction solvent.

In total the optimisation required 97 experiments but there was no note of the overall optimisation time. The feedback DoE algorithm managed to optimise 10 discrete and 3 continuous variables to find the optimum conditions. The disadvantage with the approach is that the initial set of FED designs had a very low resolution and predicted optimum yields of 191 ± 121% and therefore possibly missed higher performing solvents that did not obtain a good initial model fit. Plus, the algorithm was custom written and required extensive statistical knowledge to implement, an expertise that is not commonplace amongst process chemists or engineers. However the only way to screen the same number of discrete variables using existing self-optimisation techniques would be to carry out separate optimisations for each solvent, which would likely require much more than 97 experiments.[b]

[b] Further advantages and disadvantages with optimisation using DoE will be discussed in Chapter 4

1.4 Project Motivations and Thesis Outline

A large part of pharmaceutical process development is the optimisation of each reaction step in order to maximise product yield and purity and minimise waste. This is often not a trivial problem and as such techniques including DoE and kinetic modelling are required to provide quantitative descriptions and optimum conditions. With the increasing development of continuous manufacturing steps in the pharmaceutical industry, it is perhaps a surprise that the ever-growing field of self-optimising flow reactors has not yet been applied to pharmaceutical process development. However self-optimisation is not without its problems. Some of the challenges are:

- Chemical suitability – Self-optimisation has only currently been applied to model reactions and it is difficult to know if it would lend itself to much more complex substrates such as pharmaceuticals.
- Conflicting with existing techniques – DoE is used extensively in process development and it could be hard to convince people to use new technologies that they are unfamiliar with. Even feedback DoE algorithms (as used by Jensen) are new and more work is required to combine the two techniques.
- Analytical techniques – The existing analytical techniques for self-optimisation are primarily IR or chromatography and do not match the number of online analytical techniques available to process development scientists.[141]
- Algorithm and target function – The algorithm and target function is incredibly important because different choices can deliver different results, not only for the target optimum but also about the chemical design space as a whole.
- Material waste – A minimal amount of material is required for chemical analysis, however large quantities of material and pumped and simply discarded. Material is often a limited and precious resource in process development.

The work in this thesis aims to address all of these points. This first chapter has reviewed the existing literature in the field of flow chemistry, online analysis of flow reactors and self-optimisation techniques. Chapter 2 introduces the automated flow reactor and other automated techniques used in this thesis. Chapter 3 provides the first known example of using self-optimisation to optimise the final bond-forming step in the synthesis of an API. It also shows how feedback controlled minimising algorithms can provide more information about a chemical system than just the optimum conditions. Chapter 4 discusses the possibility of obtaining empirical

response surface models, the same as obtained using DoE, from minimising algorithm data; therefore finding a way that existing optimisation techniques can be complimented by self-optimisation. A new form of online quantitative analysis in self-optimising reactors is introduced in Chapter 5 – mass spectrometry. The chapter explores methods to quantify and calibrate the response with minimal manipulation or chemometric analysis of the raw data. Chapter 6 introduces practices to reduce the amount of material used during optimisations. This is covered by a two pronged approach of introducing sub-reactor volume reaction pulses and intelligent algorithms that can optimise for more than one target function at once. The final conclusions chapter summarises the significant contributions that have been made in this thesis and provides new directions for the future of automated self-optimising flow reactors.

The ultimate desire for any pharmaceutical process development research is to obtain the maximum amount of data from the minimal amount of material in the minimal amount of time. It is believed that the work in this thesis can deliver towards this target by presenting novel research ideas combined with practical and interesting applications.

2. Description of Automated Reactor and Processes

2.1 Reactor Description

All automated flow experiments were carried out using a modular reactor containing commercially available equipment, which was monitored and controlled through a custom written program with graphical user interface (GUI). A generic diagram is shown in Figure 2.1; a detailed description of all components is in the following sections. Please note that these are general descriptions of how the equipment was set up and may vary in different chapters.

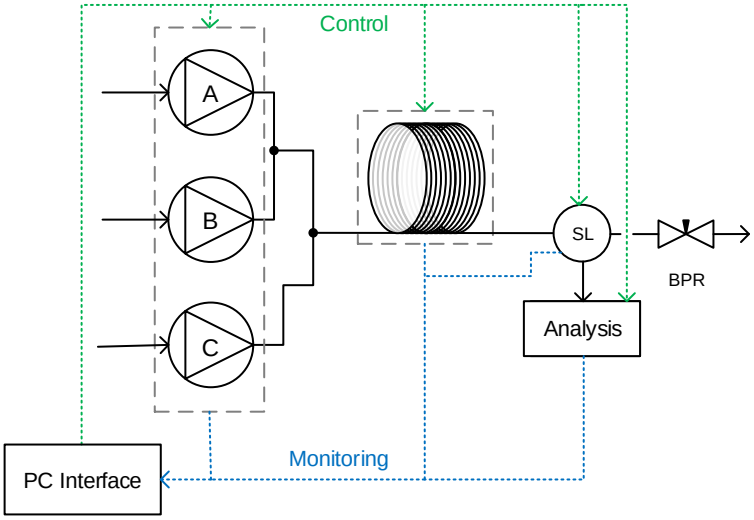

Figure 2.1 Generic schematic of the automated reactor. SL – sample loop, BPR – back pressure regulator.

Pumps

All reagents were pumped using Jasco dual piston HPLC pumps (PU-980). The minimum flow rate for each pump was 0.02 mL/min, as this was measured as the lowest reliable flow rate against a total flow of 1 mL/min from the other pump(s). The pump heads were primed with isopropanol when left idle.

Reactor

Reactions were carried out using a Polar Bear Plus Flow Synthesizer (Cambridge Reactor Design) which has active heating and cooling. The specified temperature ranges from -50 to 150 °C; however temperature testing showed that the reactor would not reach temperatures less than -40 °C. Tubular reactors of various volumes were constructed by wrapping tubing around the

heating mantle. A Syrris 250 µL chip was used as a micro-reactor/mixer, with a pressure rating of 30 bar but no temperature control module.

Sample Injectors

At-line HPLC and MS samples were acquired using a VICI Valco 4-port internal sample injector (Figure 2.2). Samples were delivered to the analytical mobile phase without prior quench or dilution. HPLC: CI4W.06 manual valve with a DCI4W.06 rotor, volume of 0.06 µL, and medium torque EUDA actuator. MS: CI4WE.06 manual valve with DCI4W.06 rotor, volume of 0.06 µL, and high torque EUHA actuator.

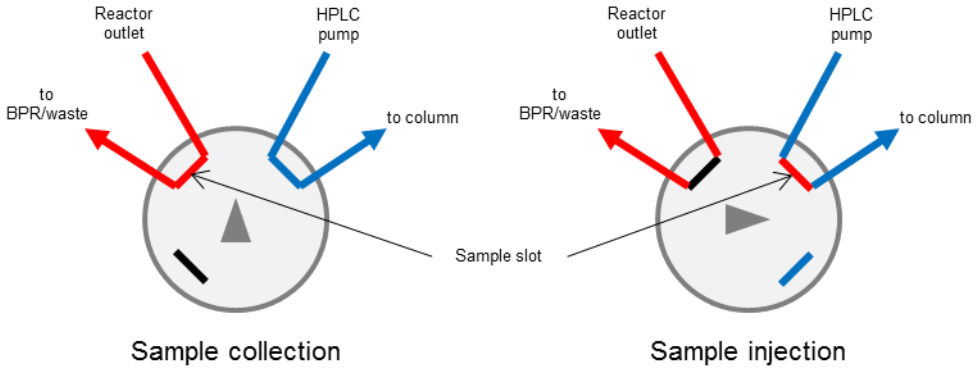

Figure 2.2 Schematic of a 4-port internal sample injector. Left – reaction mixture is pumped from the reactor, through the sample slot and then to waste (red). Right – the injector is rotated 90 °C and delivers the sample slot to the HPLC mobile phase (blue).

Back Pressure Regulators

Upchurch Scientific back pressure regulators (BPRs) were used and the pressure altered using replaceable cartridges (75, 100 and 250 psi). The pressure was kept constant through reactions at a value that would prevent boiling of the solvent. Pressure was kept constant throughout all experiments and therefore was not used as a variable.

Tubing and Fittings

Polyflon PTFE tubing (1/16" OD, 1/32" ID) was primarily used through the reactor. All connections and fittings to equipment were the individual brand (Jasco, VICI, Agilent etc.), all other tubing connections were Swagelok 316 stainless steel. Reagent feeds were mixed in mixing tees (Swagelok) unless otherwise stated. A Swagelok SS-2F-2 inline filter was fitted during some reactions to prevent particulates clogging the sample injector or BPR.

At-line HPLC

At-line HPLC analysis was carried out using an Agilent 1100 system. All tubing between the pump head and UV detector outlet was green Agilent capillary tubing (ID 0.17 mm). Descriptions of the HPLC methods are in the experimental chapter.

Online MS

Online MS was carried out using an Advion Expression CMS operating in APCI mode. This was fitted with an APCI ionisation probe and corona discharge needle. The sample injector and ionisation probe was connected using red PEEK tubing (1/16" OD, 0.005" ID) with Rheodyne RheFlex fittings. Nitrogen was used for all gas feeds at a total flow rate of 4 L/min. The mobile phase was supplied using an Agilent G113A HPLC pump and made up of 50% H_2O and 50% MeCN (0.1% formic acid). MeCN was purchased from commercial vendors at HPLC grade and H_2O collected from departmental water purification module generating H_2O at a resistivity of 18.2 MΩ cm.

Software and Communication

Automated reactions were monitored and controlled using an in-house program written in MatLab, which ran on a conventional desktop PC (IBM running Windows 7). Control and monitoring of the HPLC was achieved using Agilent ChemStation (revision B.04.05-SP1) and the MS by Advion Mass Express (version 3.1.21.1). These software generated reports in .xls (ChemStation) and .cdf (Mass Express) file formats, and then scripts were written to transcribe the data from the reports into MatLab. All equipment command and monitoring signals were communicated through RS-232 (Jasco pumps and sample injectors), ethernet (Polar Bear reactor and HPLC) or USB (MS). Commands received from RS-232 controlled equipment were processed by Realterm.exe open source freeware.

2.2 Automated Optimisation Process

Automated optimisations typically proceeded according to the following set-up. All equipment was arranged to the desired configuration and connected with necessary tubing. HPLC software was launched and modules were turned on and allowed to equilibrate and the reactor was set to its minimum temperature whilst pump reservoir solutions were prepared. The pump heads

were primed through the priming valve and then allowed to pump at 1 mL/min until it was deemed the outlet tubing was primed to its next connection, typically 10 min. The operating program was launched (in MatLab) and all available communication lines to the equipment were connected. The optimisation control program was launched and all the necessary user inputs were entered. The optimisation was started. During this time, the only user actions required were replenishing the mobile phase and reagent reservoirs and emptying the HPLC and reactor outlet waste.

2.2.1 Optimisation Control Program

For each experiment, the optimisation control program would run according to the description in Figure 2.3.

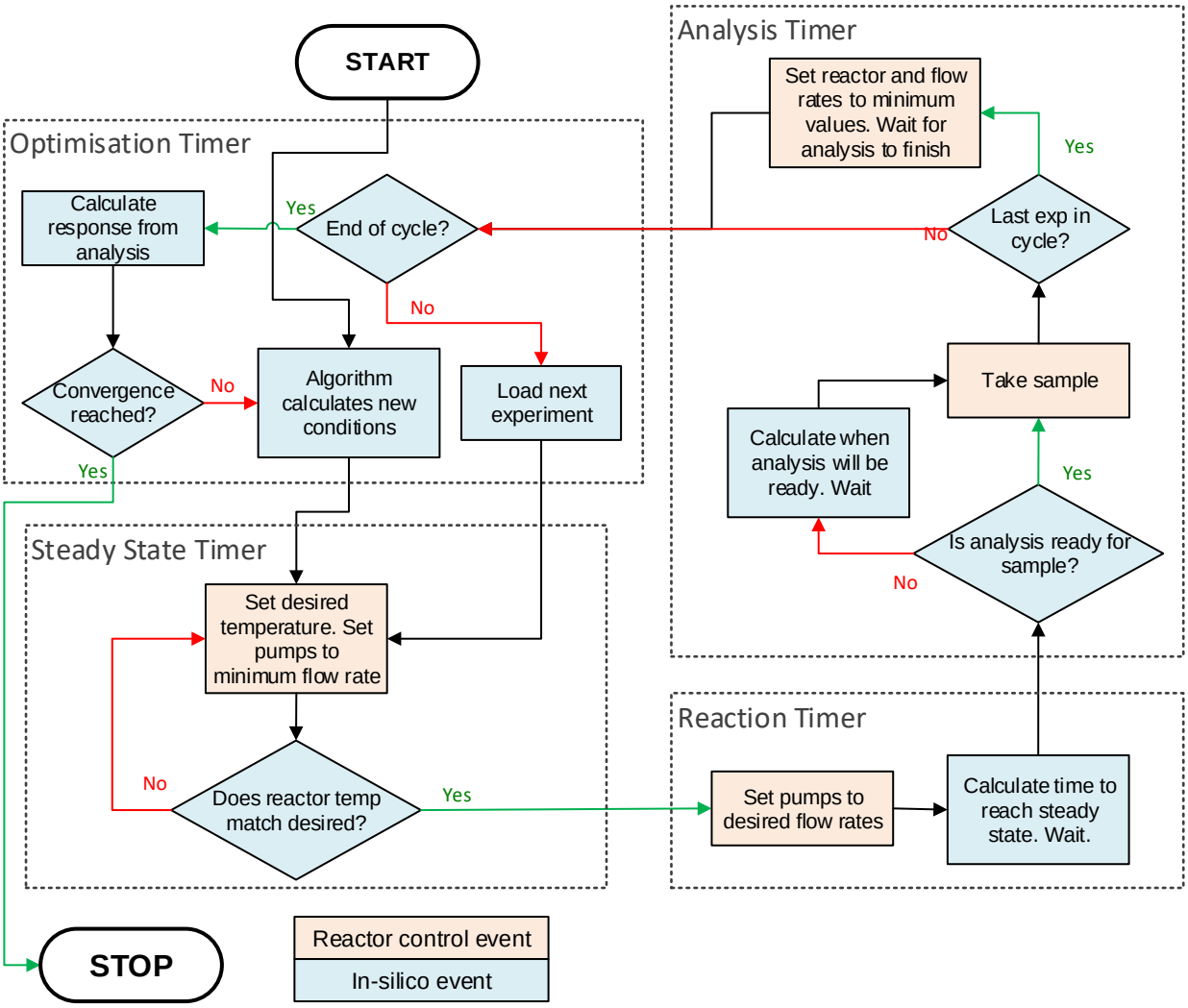

Figure 2.3 Flow diagram depicting the actions carried out by the optimisation control program.

The program is split into 4 separate timers – optimisation, steady state, reaction and analysis. Timers are individual functions that can start and stop depending on various commands. In the

optimisation program, a new timer will not start until the existing one has finished. Firstly, the algorithm parameters are loaded from the user inputs entered into the program's GUI (not shown on Figure 2.3). Next, the algorithm timer starts and calls the algorithm to calculate new conditions. The algorithm timer then stops and the program moves onto the steady state timer, which sets the reactor to its desired temperature and the pumps to their lowest values. Waiting for the reactor to cool is the greatest contributor to the overall optimisation time and with this approach the reactor only needs to cool once per cycle. Setting the pumps to its lowest values prevents unnecessary waste of material.

Once the reactor has reached temperature, the reaction timer starts and the pumps are set to their desired flow rates. The time to reach steady state is calculated and the program continually monitors the equipment for clogging or malfunctions whilst it waits for analysis. When steady state is reached, the analysis timer checks that the analytical equipment is ready for a new sample, if not, it calculates when it will be ready and waits until a sample can be acquired. When a sample is acquired, the timer checks if it is the last experiment in the cycle. If this is the case, it waits for the analysis to finish and sets all the equipment to its minimum values. This prevents material waste and cools the reactor for the start of the next cycle.

When the optimisation timer starts, it checks if there are any more experiments in the current cycle left to run. If there are more experiments, the new conditions are loaded and the steady state timer starts. If not, the timer calculates the responses to the existing experiments, checks to see if convergence has been reached then calls the algorithm to calculate new conditions. Once convergence is reached, the program stops.

2.2.2 HPLC Automated Calibrations

HPLC calibration curves were obtained with high precision and low error using an automated procedure. Two separate reservoir solutions were prepared, the first with the analyte and internal standard at known concentrations, the second with internal standard at the same concentration as the first. The solutions were fed into two separate pumps, mixed in a micro-mixer before entering the sample loop. The flow rates were adjusted to change the analyte concentration whilst maintaining constant internal standard concentration. The example in Figure 2.4 shows a solution of analyte (1.0 mol L^{-1}) and internal standard (IS, 0.2 mol L^{-1}) feeding pump A and a

solution of internal standard (0.2 mol L^{-1}) feeding pump B. The total flow rate through the micro-mixer always equals 1 but the flow ratio, and therefore concentration of analyte, varies. The concentration of internal standard remains constant throughout. The example assumes a 10 min HPLC cycle and turns off the pumps during analysis to prevent unnecessary material usage. HPLC samples are acquired at the end of each pump pulse.

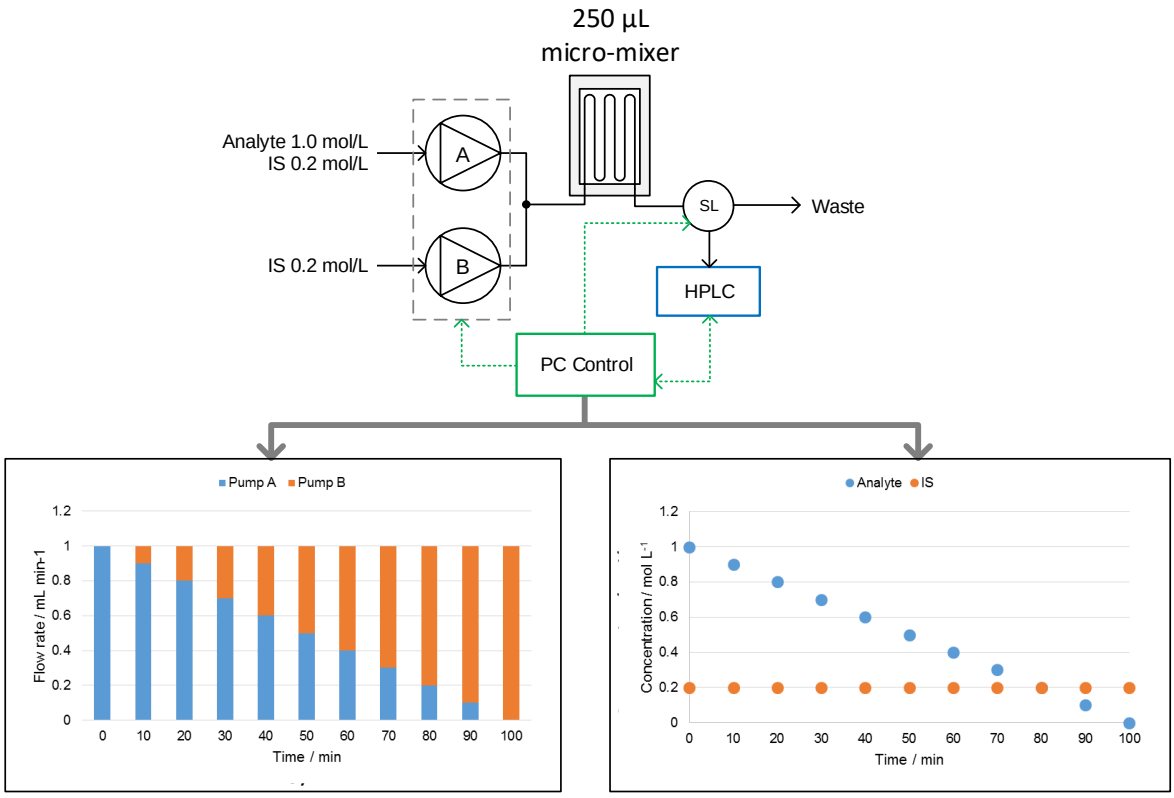

Figure 2.4 Schematic of the automated calibration procedure. Top shows the equipment setup, left shows flow rate vs time, right shows analyte and IS concentration vs time.

The relative response factors (f_{RR}) were calculated

$$\frac{A_x}{A_{IS}} = f_{RR}\left(\frac{C_x}{C_{IS}}\right) \tag{2.1}$$

where A_i is the HPLC area of species i at a given wavelength, C_i is the known concentration of species i, x is the analyte and IS is the internal standard. For a linear response, a plot of A_x/A_{IS} vs C_x/C_{IS} gives a straight line of best fit with gradient f_{RR}. If this plot showed a non-linear trend then the calibration was repeated at a wavelength that provided a linear trend. An alternative would be to use a more dilute solution. However, during reactions, this approach would require an extra dilution/quench stream after the reactor – increasing the engineering complexity – or running the reaction at lower concentrations – compromising on the kinetics.

2.3 Description of Optimising Algorithms

2.3.1 Genetic Algorithm

The genetic algorithm optimises a process using the same rules of natural selection in evolution.[142, 143] Algorithm cycles are described as generations, containing populations instead of conditions. The initial population can either be assigned by the user or chosen by the algorithm at random. Populations are ranked by their response and the best individuals are chosen as parents to create children for the next generation, falling into three types: elite, crossover and mutated. Elite children are carried through without any modification. Crossover children are generated from two parents by sharing their vectors, much like how genetic information is shared between parents during reproduction. A parent can be selected to create more than one child with the same or different parent. Mutated children are created by a random mutation of a vector from the parent (*Figure 2.5*).[144]

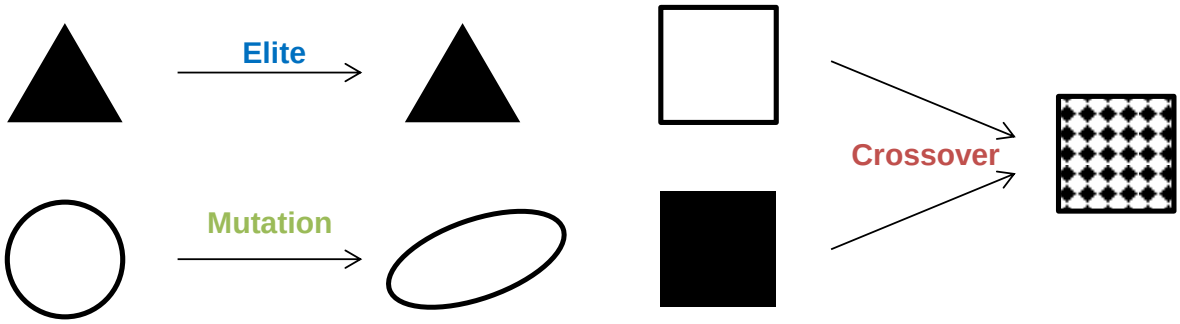

Figure 2.5 The creation of elite, mutated and crossover children in the genetic algorithm.

2.3.2 Pattern Search

Pattern Search (PS) is a derivate-free algorithm based on the OVAT approach to optimisation. New points are generated by only changing one variable at a time and the size of the distance between the points changes throughout.[145, 146] A base point (or initial point) is generated by the user and the procedure of going from the base point to the next point is called a move. If the response at the new point is better, then the move is considered a success. If no improvement is made then the move is a failure.

The MatLab process for PS optimisation[147] (*Figure 2.6*) plots a user defined initial point (or base point), followed by points that are a single step size away only varying one condition at a time. If a successful move occurs, the step size (or mesh) is doubled and the successful point

becomes the new base point. If a successful move is no longer possible, the mesh is halved. The mesh can expand and contract until it is too small to initiate any significant change in the response, in which case the optimisation is terminated.

The initial mesh size is calculated based on the upper and lower bounds of the algorithm:

$$mesh = 2^{\frac{log_2|Bo_l|+log_2|Bo_u|}{2}} \tag{2.2}$$

where Bo_l and Bo_u are the lower and upper bounds, respectively.

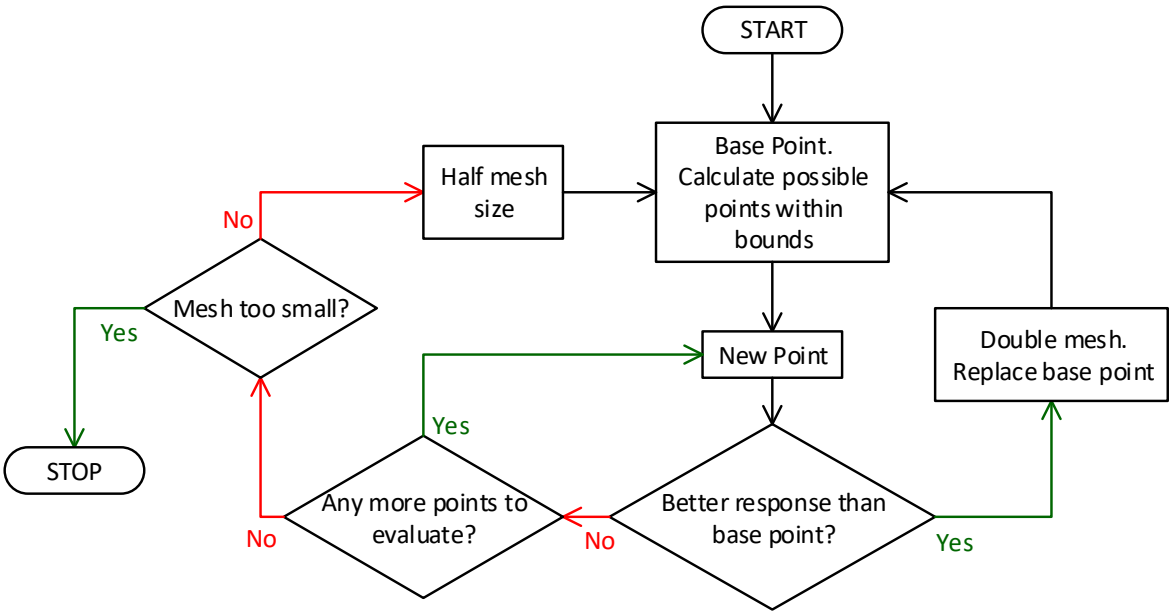

Figure 2.6 Flow chart following the key decisions made during the MatLab version of the pattern search algorithm.[147]

2.3.3 Super-Modified Simplex

The super-modified simplex (SMSim) is an algorithm adapted from the simplex algorithm.[137] In a classic simplex algorithm, a simplex is created with the number of vertices, $n + 1$ where n is the number of variables. Each vertex (or point) is ranked based on its response, and a new vertex is created by reflecting from the worst vertex through the midpoint of the resulting vertices, thus creating a new simplex. The new point, and the resultant points make up a new simplex and then the points are reranked to form a new vertex and subsequent simplex The process continues until the optimum is surrounded by simplicies (Figure 2.7).[137]

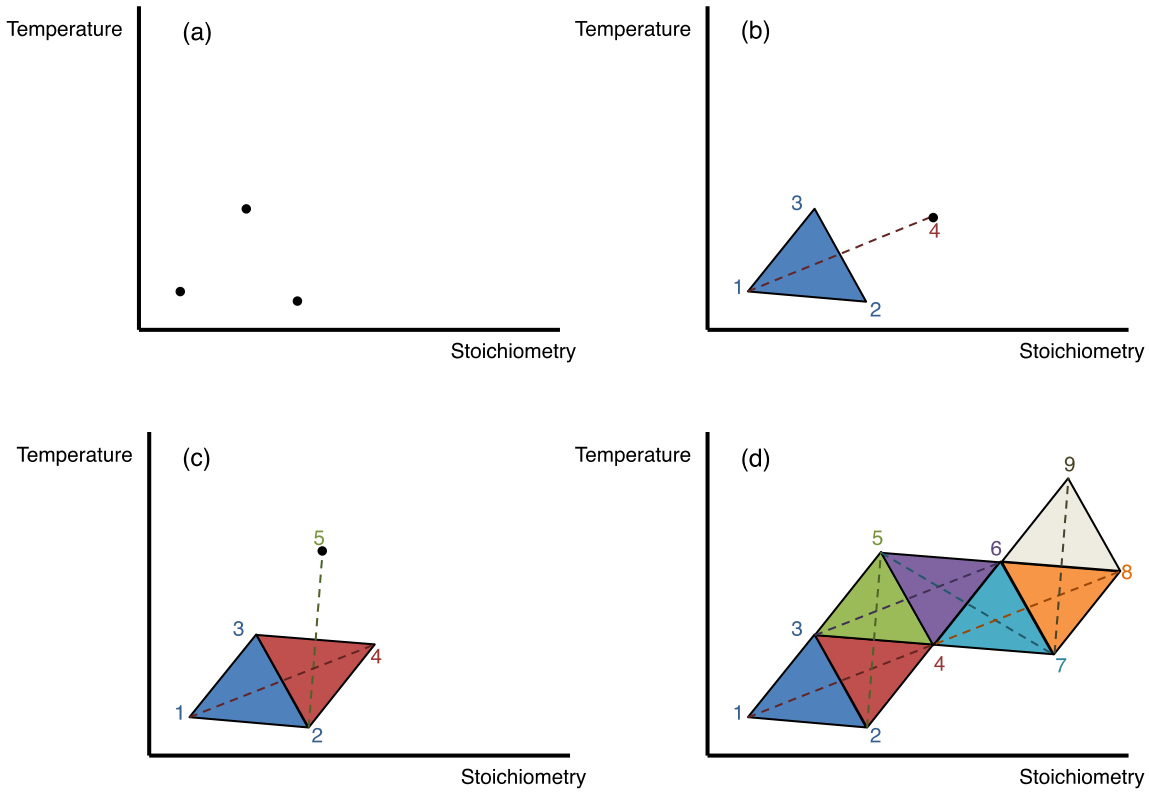

Figure 2.7 (a) The variables of temperature and stoichiometry are selected and three initial data points are plotted with three different conditions (N=2, N+1=3). (b) The three data points are ranked (1=worst, 2=middle, 3=best) for how close they reach to the optimum and a vertex is plotted from the lowest ranked point, through the midpoint between the top two ranked points and finishes at a new point generated by the algorithm. (c) A new simplex is formed between points 2, 3 and 4 and then these points are re-ranked. A new vertex is generated from the lowest ranked point to the newest point, 5; points 3, 4 and 5 form the new vertex. (d) The process is continued forming new simplexes until the optimum point is reached.[137, 148]

The SMSim algorithm[139] (Figure 2.8) follows the same rules to calculate the reflected vertex as the simplex algorithm. However the response of the mid-point (vertex $\bar{P}$, response $\bar{p}$)[c] is also calculated and a curve is fitted between the worst (W), reflected (R) and midpoint vertices to calculate an expansion coefficient (Y_{opt}) subject to either a polynomial fit

$$Y_{opt} = \frac{w - \bar{p}}{w - 2\bar{p} + r} + 0.5 \tag{2.3}$$

or Gaussian fit:

$$Y_{opt} = \frac{ln\, w - ln\, \bar{p}}{ln\, w - 2\, ln\, \bar{p} + ln\, r} + 0.5 \tag{2.4}$$

where w and r are the responses for vertices W and R respectively. The expansion coefficient is used to calculate an improved reflected vertex (O)[149]

[c] For all formulae during the simplex sections, i is the response of vertex I

$$O = Y_{opt}\bar{P} + (1 - Y_{opt}) \times W \tag{2.5}$$

The value of Y_{opt} is bound by constraints and must be between the values of -1 and 3 so that the simplex doesn't grow more than twice the size of the original.[150] The initial value of Y_{opt} is normalised so that the distance between W and $\bar{P}$ is 1.

If a boundary is reached, a boundary coefficient (Y_a) is introduced

$$Y_a = \frac{Bo_j - \bar{P}_j}{\bar{P}_j - W_j} + 1 \tag{2.6}$$

where Bo_j is the boundary value for variable j. The value of Y_a is set to 0.5 if $Y_a < 1.5$ to ensure reasonable spacing between R, $\bar{P}$ and W and that the simplex doesn't shrink more than half the size of the original.[150] Once a boundary is reached a new value for Y_{opt} is calculated, which for a polynomial fit takes the form

$$Y_{opt} = \frac{(Y_a^2 - Y_a)}{2} \frac{w - \bar{p}}{w(Y_a - 1) - Y_a\bar{p} + r} + 0.5 \tag{2.7}$$

and for a Gaussian fit:

$$Y_{opt} = \frac{(Y_a^2 - Y_a)}{2} \frac{ln\, w - ln\, \bar{p}}{ln\, w\,(Y_a - 1) - Y_a\, ln\, \bar{p} + ln\, r} + 0.5 \tag{2.8}$$

which is subject to additional conditions. When Y_a > 1, $\bar{p}$ must be greater than $\frac{r+w(Y_a-1)}{Y_a}$ (for polynomial fit) or $r^{1/Y_a}w^{(1-1/Y_a)}$ (for Gaussian fit), otherwise Y_a is set to -1. When $Y_a \leq 1$, $\bar{p}$ must be less than $\frac{r+w(Y_a-1)}{Y_a}$ (polynomial) or $r^{1/Y_a}w^{(1-1/Y_a)}$ (Gaussian), otherwise Y_a is set to 3.[149]

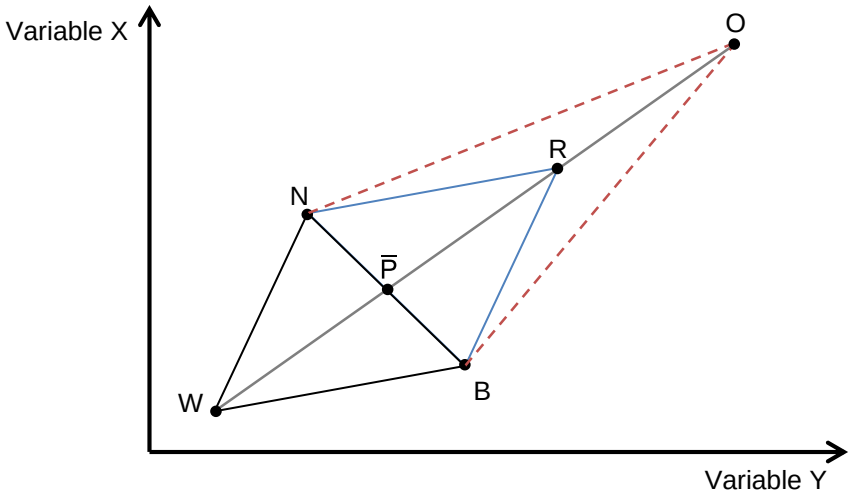

Figure 2.8 Transformations during the SMSim. Points W, N and B make up the original simplex and are ranked best (B), worst (W) and other (N). Point R is created by reflecting through the mid-point $\bar{P}$ from W. The W$\bar{P}$ distance is equal to $\bar{P}$R distance; WO distance (Y_{opt}) and position of O is calculated by fitting a polynomial or Gaussian curve between W, $\bar{P}$ and R.

2.3.4 Nelder-Mead Simplex

The Nelder-Mead Simplex[138] (NMSim) algorithm follows the same initial rules as the classical simplex algorithm where a reflected vertex R is created. If r is better than b, an expanded vertex (E), which is reflected twice as far as R, is calculated:[151]

$$E = 2R - \bar{P} \tag{2.9}$$

If e (response of E) is better than r then vertex E is retained. If r is not an improvement on the optimum then a new R is calculated, reflecting from the next worse vertex, and this process continues until r is an improvement on the optimum. If r never improves then the current simplex must surround the true optimum and will start to contract. The first contraction vertex (C_1) occurs from W:

$$C_1 = \frac{W + \bar{P}}{2} \tag{2.10}$$

If c_1 is better than w then C_1 replaces W in the new simplex, otherwise a second contraction vertex (C_2) is calculated, which contracts from R.

$$C_2 = \frac{R + \bar{P}}{2} \tag{2.11}$$

If c_2 isn't better than w then the simplex must shrink towards B, and a new vertex S is calculated:

$$S = \frac{\sum_i N_i}{i} \tag{2.12}$$

where N is any vertex that isn't B, W, R, E or C and i is the number of those vertices. It should be noted that the cycle is refreshed upon iteration and the simplex can still reflect and expand after a contraction or shrink. Figure 2.9 shows geometric representations of the transformations.

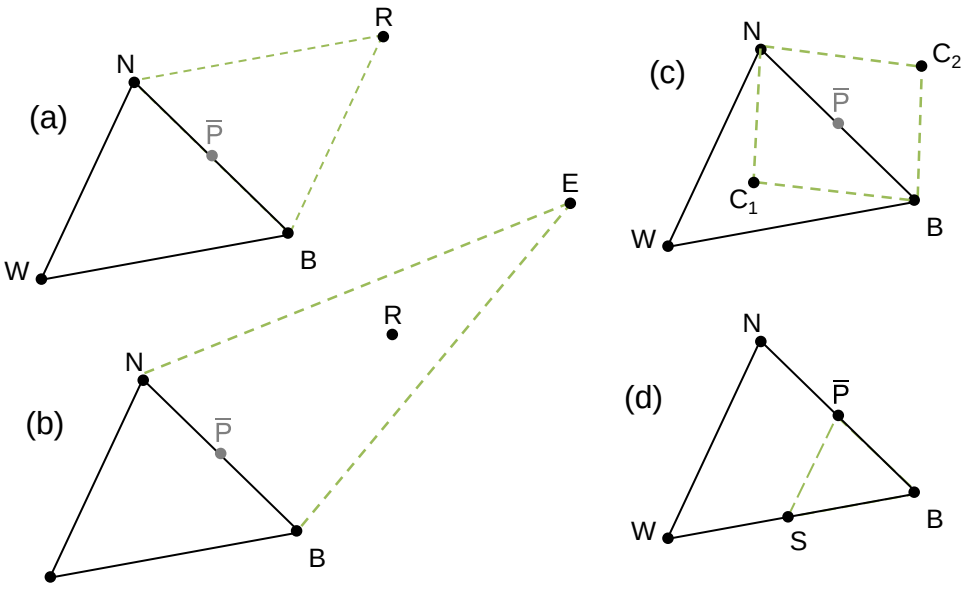

Figure 2.9 Transformations that occur during NMSim algorithm: (a) reflection through midpoint $\bar{P}$ to new point R; (b) expansion of R to new point E; (c) contraction from W to new point C_1 or from R to new point C_2; (d) shrinking towards point B to make new point S. During a reflection, expansion or contraction the conditions of midpoint $\bar{P}$ are calculated but not its response. During a shrink, both the conditions and response of $\bar{P}$ are calculated.

2.3.5 SNOBFIT

SNOBFIT (Stable Noisy Optimisation by Branch and Fit) is a branch and fit algorithm used in linear programming for a computationally expensive function.[136] The algorithm starts by plotting random points until it has enough to fit a polynomial surface. It will then plot exploratory and local points to improve the surface fit and find optimal points. The algorithm will continue to plot both exploratory and local points as it continues to seek optima.

Each algorithm cycle contains a property called n_{req}, which is the number of requested points and is a user input at the beginning of the optimisation. Other user inputs include *call*, the number of total n_{req}, *dx*, the precision of each variable, the upper and lower boundaries, and *prob*, the probability of exploring empty space. Each experimental data point is assigned one of 5 types:

1. Global minimum
2. Secondary minima
3. Local point to improve the polynomial fit
4. Random exploratory point
5. Initial scatter if there is insufficient data to fit a polynomial

Typically, the first 2-3 n_{req} only contain type 5 points in order to gain more information about the system. Afterwards, per cycle, the algorithm will plot a single type 1 point and, if

applicable, a single type 2 point. The number of type 4 points is determined by the value of $prob$ and any resultant points in the cycle are filled with type 3 points. Sometimes the algorithm will increase the value of n_{req} to increase the number of type 3 points and improve the polynomial fit.

3. Optimising the Continuous Synthesis of a Pharmaceutical Intermediate using a Self-Optimising Flow Reactor

3.1 Introduction

To achieve effective optimisation of a reaction process, careful consideration is needed of the various synergistic interactions that occur between reaction variables such as temperature, reaction time and reagent concentrations. It is important to ensure that suitable parameter-defining experiments have been carried out during the course of process development to deliver a robust process that can be easily transferred to a manufacturing facility. Design of experiments (DoE) is a commonly used approach which implements statistical methods to screen and optimise a reaction, particularly for problematic steps and has been used in the synthesis of many pharmaceutical products.[2]

A DoE is traditionally constructed using a full factorial design (FFD), which requires experiments at the minimum and maximum of each variable split across each level in all possible combinations, plus centre-points.[152] Centre-points are used to show curvature in the response between the variable extremes and are repeated to show how reproducible the model results are. The number of experiments for a full factorial is calculated by:

$$n^k + m \tag{3.1}$$

where n is the number of levels, k is the number or variables and m is the number of centre-points.[153] This number increases exponentially with increasing variables and can be too large to carry out efficiently for a high number of variables. Table 3.1 shows the number of experiments per number of variables for 2- and 3-level full factorial designs.

A 2-level full factorial will show which of the variables (or main effects) contribute most to the response, as well as interactions between variables. For example, temperature and time could be an interaction as reactions are faster at higher temperature and *vice versa*. Interactions can occur between 2-, 3- and up to k-variables.

Table 3.1 **The number of experiments in full factorial experiments.**

No. of variables	No. of experiments	
	2-level	3-level
2	$2^2 = 4$	$3^2 = 9$
3	$2^3 = 8$	$3^3 = 27$
4	$2^4 = 16$	$3^4 = 81$
5	$2^5 = 32$	$3^5 = 243$
6	$2^6 = 64$	$3^6 = 729$
7	$2^7 = 128$	$3^7 = 2187$
8	$2^8 = 256$	$3^8 = 6561$

A fractional factorial (FED) reduces the number of experiments required by at least half.[154] The number of experiments in an FED is calculated by:

$$n^{k-f} + m \tag{3.2}$$

where f is the factor that the design is reduced (i.e. half=1, quarter=2, either=3 etc.).

A

2-level 3-variable
full factorial
$n = 2^3 + 2 = 10$

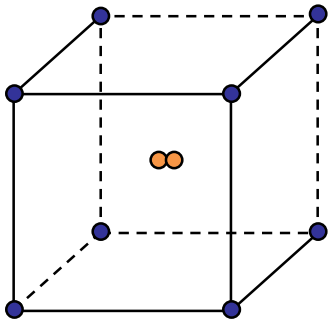

Exp	a	b	c
1	+	+	+
2	-	+	+
3	+	-	+
4	-	-	+
5	+	+	-
6	-	+	-
7	+	-	-
8	-	-	-
9	0	0	0
10	0	0	0

B

2-level 3-variable
½ fractional factorial
$n = 2^{3-1} + 2 = 6$

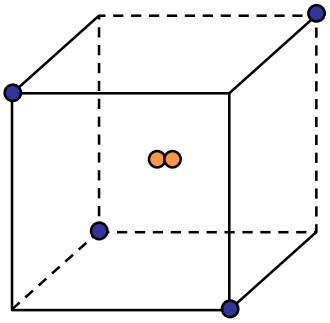

Exp	a	b	c=ab
1	+	+	+
2	-	+	-
3	+	-	-
4	-	-	+
5	0	0	0
6	0	0	0

Figure 3.1 Example of a 2-level 3-variable FFD (A) and 1/2 FED (B). The tables show how the design is constructed. The vector of c is calculated from the product of ab (e.g. exp 1, 1×1=1; exp 2, -1×1=-1 etc.)

The reduction in experiments is achieved by replacing (or confounding) a main effect with an interaction (Figure 3.1B). This means that it is impossible to distinguish between a main effect and its confounded interaction. As the number of variables in an interaction increases the coefficient of that interaction (i.e. how much it contributes to the model) decreases. Therefore a main effect will be confounded with the highest available interaction. If a design has a lot of variables then the reduction in experiments is justified as it would be uncommon for an interaction of greater than 3 variables to contribute anything towards the fit of the model. However as the variables increase, or the degree of the FED decreases, the chance of a main effect confounding with an interaction with a large coefficient is high. In Figure 3.1B, the highest available interaction is a 2-variable interaction, which results in c being confounded with ac. It may not be clear if a high coefficient for c is a result of the ac interaction.

The resolution of an FED describes the amount and extent of confounding in the model:

- Resolution III: main effects are confounded with 2-variable interactions
- Resolution IV: main effects are not confounded with 2-variable interactions; 2-variable interactions are confounded with other 2-varibale interactions.
- Resolution V: main effects are not confounded with 2-variable interactions; 2-variable interactions are confounded with 3-variable interactions etc.

The FED shown in Figure 3.1 was constructed by setting

$$c = ab \tag{3.3}$$

If both sides are multiplied by c:

$$c^2 = abc \tag{3.4}$$

or

$$I = abc \tag{3.5}$$

where I is the generator. The resolution of a design is determined by the shortest possible generator. For this example the FED is a resolution III half factorial, otherwise notated as 2_{III}^{3-1}. Table 3.2 shows how the confounding changes for models of different resolution for designs with 3 to 6 variables.

Table 3.2 Construction of 2-level fractional factorial designs for 3 to 6 variables of differing resolution[154, 155]

Variables	2_{III}^{3-1}	2_{IV}^{4-1}	2_{V}^{5-1}	2_{III}^{5-2}	2_{IV}^{6-2}	2_{III}^{6-3}
a	a	a	a	a	a	a
b	b	b	b	b	b	b
c	ab	c	c	c	c	c
d	-	abc	d	ab	d	ab
e	-	-	abcd	ac	abc	bc
f	-	-	-	-	bce	ac
No. exps	4	8	16	8	16	8

The final step of the synthesis of the Src kinase inhibitor saracatinib (**3.3** AZ), a nucleophilic aromatic substitution between a fluoroanilidine and an alcohol (Scheme 3.1),[156] was optimised using a fractional factorial DoE[154, 155] due to a poor isolated yield. The key issues upon scale up were: increased impurity formation at temperatures higher than 90 °C, a high charge of alcohol was required for acceptable reaction times and the unknown role of water in the reaction that appeared to increase the reaction rate and improve selectivity. The design carried out was a two level resolution IV design of four reaction variables (stoichiometry of base, water and alcohol **3.2**; and temperature) totalling 10 experiments (2 centre-points).

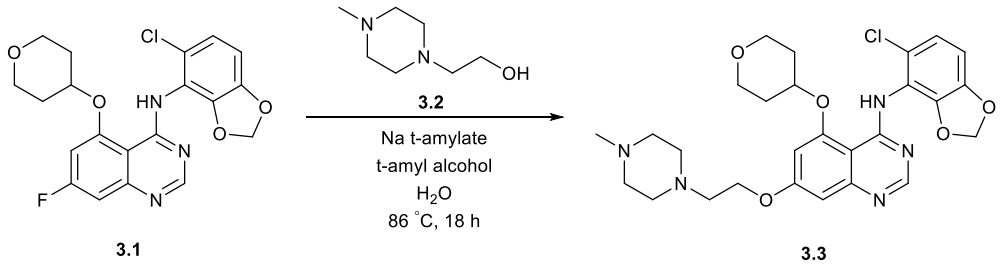

Scheme 3.1 Final step S_NAr reaction in the synthesis of saracatinib **3.3**.[156]

The results of the design revealed four key findings: an excess of base above 2.2 eq did not affect the reaction; water stoichiometry higher than the equivalents of base greatly reduced the reaction rate; higher temperatures improved the rate but increased impurity formation and increasing the equivalents of alcohol **3.2** improved the rate although this would be undesirable due to the cost implications.

The disadvantage with FEDs is that extra experimentation might be required to distinguish between a main effect and interaction, and no 2-level factorial designs (FFD and FED) can be used

for accurate prediction because only linear coefficients are included. A different design is required to predict and define process parameters, called a response surface method (RSM, Figure 3.2).[153, 157, 158]

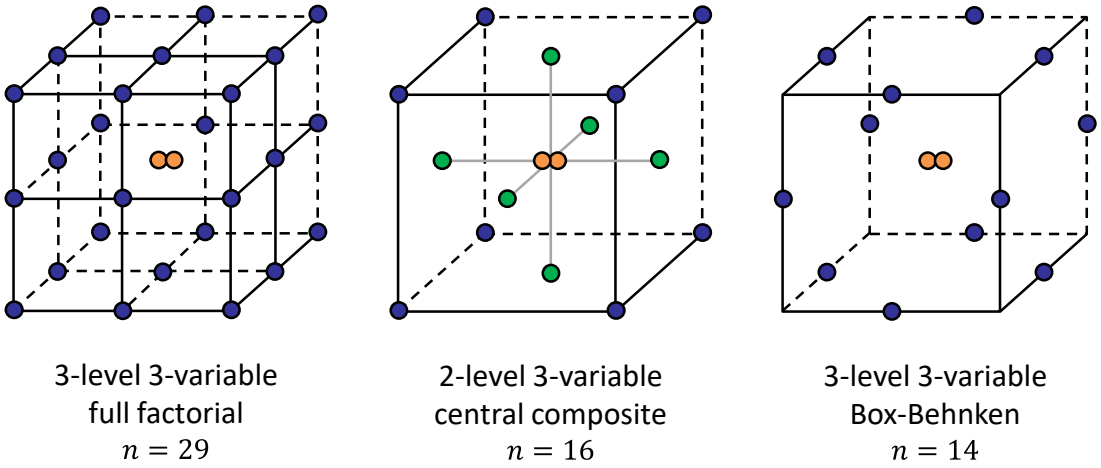

Figure 3.2 Experimental plots of 3-variable RSM designs. The blue points are experimental data points, axial "star" points (central composite) are highlighted in green, centre-points are highlighted in orange.

A troublesome step in the synthesis of an antibiotic (GSK) was the deprotection of silyl ether **3.4** to alcohol **3.5**.[3] Lactone **3.6** is formed from the product **3.5** and the compounds were found to co-crystallise upon isolation. The reaction was optimised using RSM with the aim to improve the yield of **3.5** (>75% by HPLC area), reduce the presence of **6** in the crude product (<2% by HPLC area, which would translate to <0.5% isolated product) and minimise the amount of TREAT-HF for cost purposes.

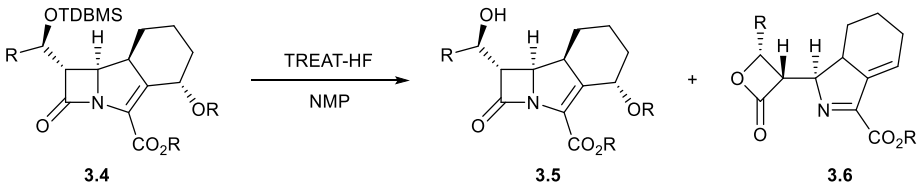

Scheme 3.2 Deprotection of silyl ether 4 in the synthesis of **3.5** towards an antibiotic. Lactone **3.6** is an undesired impurity (TREAT-HF = $Et_3N{\bullet}3HF$, NMP = N-methyl pyrolidine).

A four variable central composite circumscribed design[157, 158] was carried out using temperature, time, volumes of NMP and molar equivalents of TREAT-HF as variables with a total of 30 experiments. The model predicted different regions where the alcohol yield was maximised and the lactone yield was minimised. However, superimposing these conditions generated an operating region that fulfilled the criteria of alcohol yield >93% and lactone yield <2%. These

conditions increased the alcohol yield during manufacture from 68% to 94% whilst still maintaining low levels of impurities in the final product.

However, further experiments were required to verify the model and ensure sufficient robustness of manufacture. An additional 6 experiments were carried out to confirm the conditions predicted from the model. Whilst this number is not excessive it adds to the overall experiment number and therefore increases the time and resources required.

The study suggests a route for choosing an experimental design for progression from uncertain process conditions to robust manufacture (Figure 3.3). Initial scoping experiments provide boundary limits for each variable. The screen shows key main effects and interactions and can be used to eliminate variables from the design for the next optimisation step. This step adds curvature to the model allowing a response surface to be fitted which can be used to predict responses. The final robustness step shows how far away from the optimum the response will be and is the basis of operating limits for manufacture.

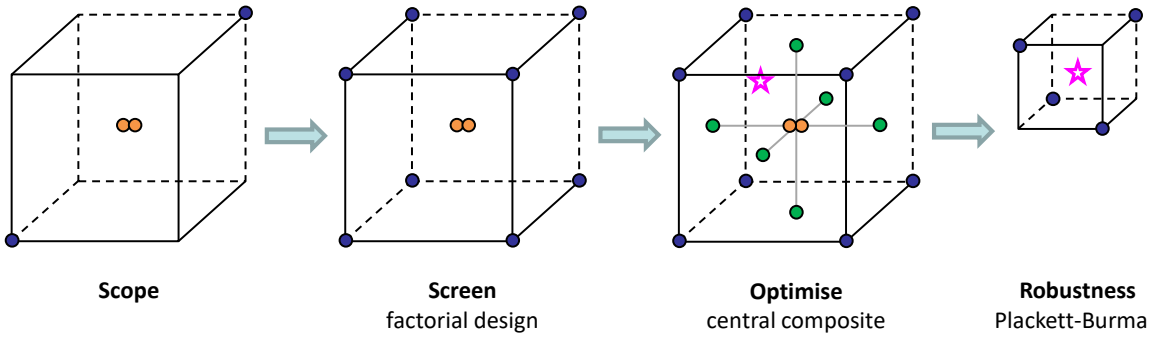

Figure 3.3 Recommended steps for selecting experimental designs to choose conditions for manufacture. Blue points are experimental data points, axial "star" points (central composite) are highlighted in green, centre-points are highlighted in orange, the optimum point is highlighted by the star.[3]

The scope might seem a trivial step and could be eliminated in order to progress to the screen where more information is obtained. However, the variable limits are decided in this step and are incredibly important to obtain a good overall fit. Models are generated by fitting a polynomial to the responses of the experimental data points. Polynomial curves are very poor at fitting sharp changes in response, especially over a broad range. Instead it is sensible to choose limits where the maximum change in response is happening over the minimum change in a variable. Figure 3.4 shows how a polynomial fit can be improved by reducing the variable limits.

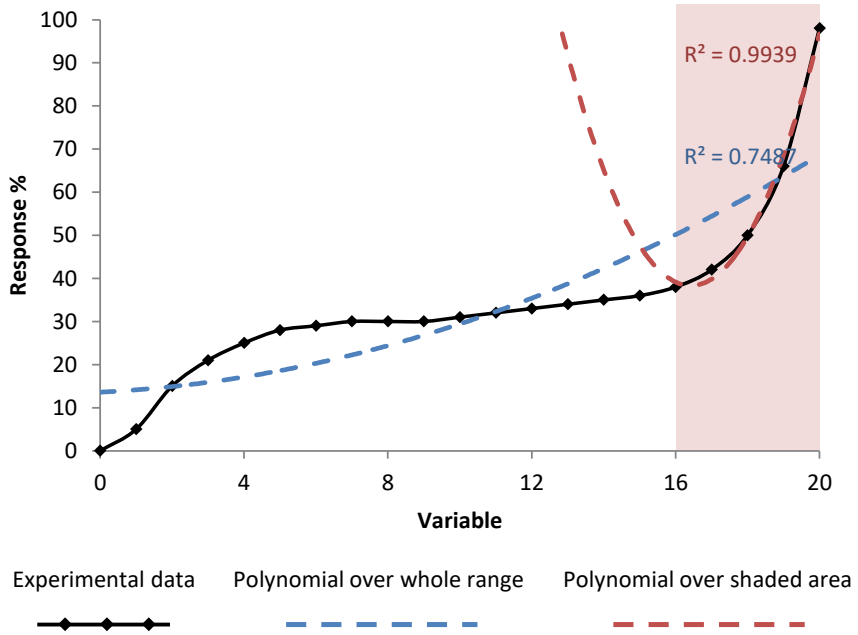

Figure 3.4 Examples of how the fit of a polynomial can improve between different limits. The blue line shows a polynomial fit over the whole data range, the red line shows a polynomial fit in the shaded section only. The red polynomial shows a better fit over the shaded area; the polynomial is extended to outside this space to show how poorly it will extrapolate.

The disadvantages of reducing the variable limits range might not seem apparent as the model will optimise and deliver manufacturing conditions within this limit. However, developing a process for the manufacture of an active pharmaceutical ingredient (API) requires focus on more than just yield as control of impurities is crucial. This can involve synthesising sufficient quantities of an impurity to characterise and asses any toxicological hazards. Therefore the ability to screen and optimise in a larger experimental space than that available in DoE is highly advantageous.

A self-optimising reactor with adaptive feedback algorithm can explore a larger experimental space than DoE. The rejection of points that contribute to a lower response means that only the important main effects and interactions are explored thus providing the same information as a full factorial in fewer experiments. The algorithms also generate a more concentrated scatter of points around the optimum illustrating the robustness of the reaction. Therefore a single self-optimisation can provide all the information that required 4 separate steps by using a DoE.

However, the choice of algorithm is very important. Some algorithms will directly move towards the optimum region but not provide additional information about experimental space that

does not lie between the starting point and optimum. If an exploratory algorithm, such as SNOBFIT (stable noisy optimisation by branch and fit), is used then the data will be spread across all of the experimental space and can still provide a replica of a response surface.

The SNOBFIT algorithm is a branch and fit algorithm that will generate random scatter across the experimental space until it has enough data points to fit a polynomial. It will then plot points that simultaneously target improving the optimum, the polynomial fit and exploring empty space. It does not suffer from the poor polynomial fit demonstrated in DoE as the concentration of points around the optimum will naturally improve the fit, and therefore predicted response, in that area. The exploration of empty space means that the scatter can show how the response changes in areas of poorer response and can also find and distinguish between local and global optima.

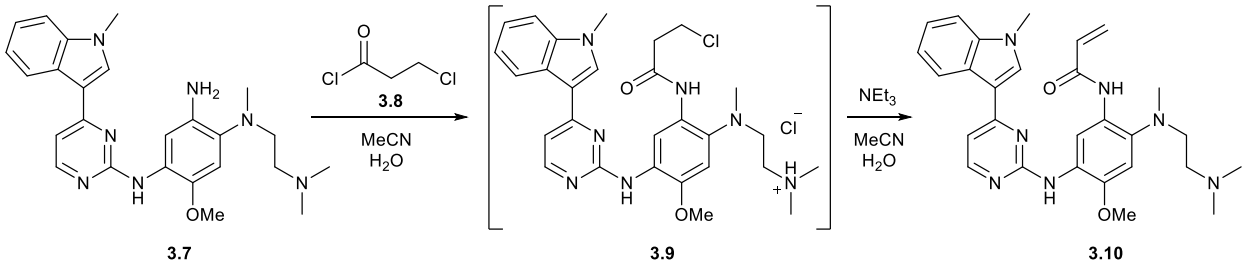

Scheme 3.3 Synthesis of acrylamide **3.10**, the freebase of the AZD9291 API. Aniline **3.7** is treated with acid chloride **3.8** to give unisolated intermediate **3.9**, which undergoes base mediated elimination to generate **3.10**.

There is motivation to develop adaptive feedback control technologies to explore a greater area of experimental space than DoE, providing optimum response and robustness. An automated flow reactor is ideally suited for such an initiative as monitoring and control of reaction variables, such as flow rate, temperature and pressure can be achieved rapidly within a single system.[8, 9, 53, 54, 159] This chapter explores the applicability of using this technology in process development by optimising a model reaction then transferring the knowledge gained towards the final bond forming step in the synthesis of AZD9291 (osimertinib, **3.10**), an irreversible epidermal growth factor receptor (EGFR) tyrosine kinase inhibitor with T790M mutation, developed for treating non-small cell lung cancer (Scheme 3.3).[160-162]

3.2 Model Optimisation Study

A model reaction study was carried out, using the same chemical transformation as in the AZD9291 synthesis but with a commercially available substrate. With this approach, an experimental set-up could be developed without wasting high value material. The reaction carried out was the telescoped synthesis of acrylamide **3.13**, which proceeded *via* an amidation between aniline **3.11** and acid chloride **3.8,** to form the unisolated *β*-chloroamide **3.12**, followed by base mediated elimination (Scheme 3.4).

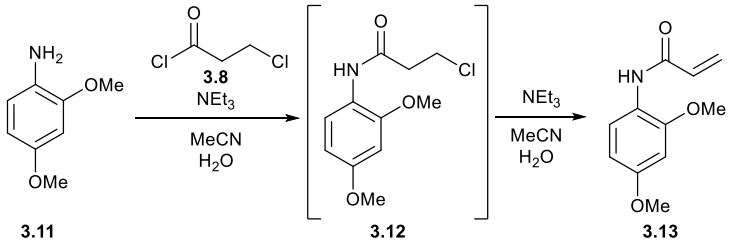

Scheme 3.4 Telescoped synthesis to acrylamide **3.13** via the unisolated intermediate *β*-chloroamide **3.12**

3.2.1 Initial Reaction Screening

The aim of the initial reactions was to minimise the amount of solvent by pumping neat triethylamine and acid chloride with the aniline dissolved in acetonitrile, but the high concentrations resulted in clogging in the tee-piece from the resultant triethylammonium chloride (TEAC). The acid chloride was diluted with anhydrous acetonitrile but it was only possible to pump without clogging when water was added to the aniline reservoir.

A temperature profile was carried out using an acetonitrile:water mixture (7:2, v:v) for the aniline solution (0.25 mol L^{-1}, 4.4 mmol L^{-1} biphenyl IS), anhydrous acetonitrile for the acid chloride solution (2.2 mol L^{-1}) and neat triethylamine. The flow rates were adjusted to correspond to 1.05 eq acid chloride and 10 eq triethylamine, with a 2.5 min residence time. The high excess of base was to ensure the HCl byproduct was quenched and prevent corrosion of the stainless steel reactor parts; and to encourage high yields of acrylamide **3.13**.

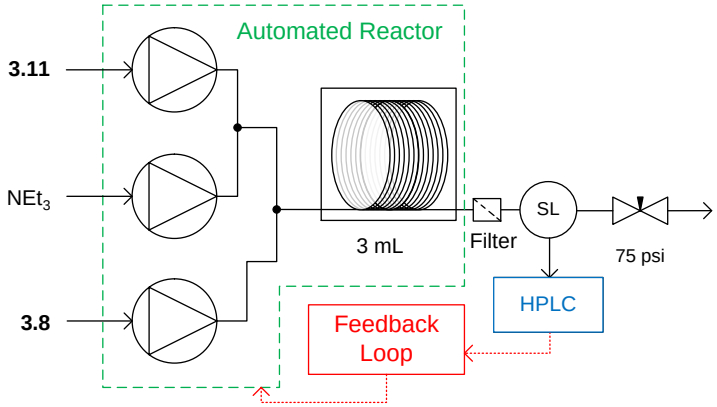

Figure 3.5 Reactor setup for the model compound study. SL – sample loop

The results of the temperature profile (Figure 3.6) show that the first step in the reaction is very fast, as full conversion of **3.11** to **3.12** is achieved after 2.5 mins at all temperatures. The second elimination step is slower and requires higher temperatures to maximise the yield of **3.13** under the conditions for the temperature ramp. An unknown impurity (imp1) was formed that had a higher yield at lower temperatures and decreased with increasing temperature. This could be rationalised by three explanations: imp1 is formed from the chloroamide, which is at higher concentrations at lower temperatures; the desired reaction route is faster at higher temperatures; or imp1 is formed in an equilibrium which favours the reactants at higher temperatures. No other major impurities were identified at this stage, but the conversion of **3.12** was incomplete so more impurities could form at longer residence times.

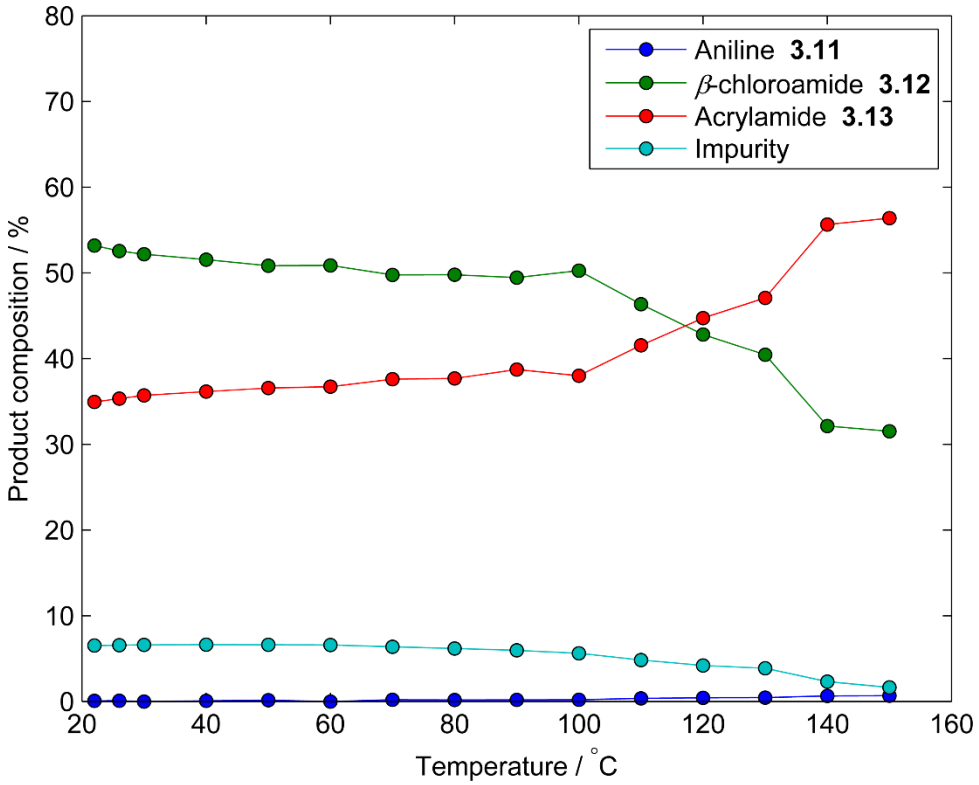

Figure 3.6 Temperature profile of the continuous reaction shown in Scheme 3.4. Reaction conditions were 1.05 eq **3.8**, 10 eq NEt_3 and 2.5 min. The product composition is measured by HPLC area % after removing the internal standard peak.

3.2.2 Reaction Optimisation

The reaction yield, measured using at-line HPLC, was optimised using the SNOBFIT algorithm, with the flow rate of the aniline **3.11** (pump A), molar equivalents of acid chloride **3.8** (pump C - wrt aniline), triethylamine (pump B – eq, wrt acid chloride) and the reactor temperature as variables. The pump reservoir solutions were diluted from those used in the temperature profile so that the volumetric flow rates were similar and all the TEAC would be in solution. The real-time yield was calculated from the ratio of the HPLC peaks of **3.13** and biphenyl internal standard; the algorithm was set to find conditions to maximise this value. The boundary condition limits and reservoir concentrations are displayed in Table 3.3. The temperature range was decreased from the temperature profile as the increased dilution resulted in the reaction boiling and it was decided that a lower maximum temperature was preferable to increasing the pressure of the BPR.

Table 3.3 Optimisation boundary limits for the conditions of the model aniline reaction

Limit	Pump A / mL min^{-1}	Pump B / mol eq	Pump C / mol eq	Temperature / °C
Minimum	0.100	4.5	0.9	0
Maximum	0.500	20	2.1	130

Pump A reservoir 0.241 mol L^{-1} aniline **3.11**, 0.0156 mol L^{-1} biphenyl, pump B reservoir 3.73 mol L^{-1} triethylamine, pump C reservoir 1.00 mol L^{-1} acid chloride **3.8**.

The results of the optimisation are displayed in Figure 3.7. The optimum conditions are 0.1 mL min^{-1} **3.11**, 117.8 °C, 1.7 equivalents of **3.8**, 16 equivalents of triethylamine and a residence time of 12.2 min, generating **3.13** in a 92% yield. A low aniline flow rate correlates to an increase in the residence time and higher yields are achieved at higher temperatures. The excess of **3.8** is likely to compensate for the competing hydrolysis reaction and high equivalents of triethylamine are possibly required to accelerate the slower elimination step. Further scrutiny of the HPLC chromatograms show >99% conversion of **3.11** in all experiments with the other main component being the intermediate **3.12**, highlighting that the elimination step is probably rate limiting. In the optimum chromatogram, complete conversion of **3.11** is achieved with the resulting impurities totalling 8% (2.7% **3.12**).

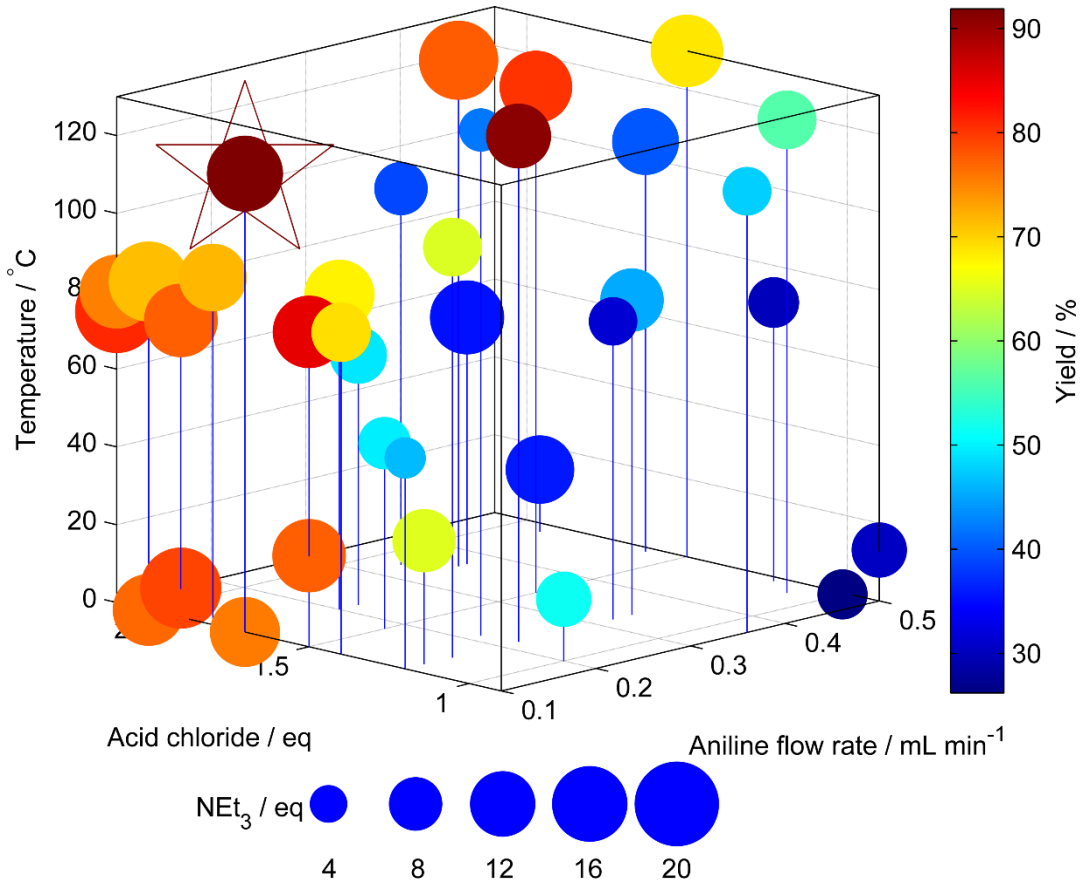

Figure 3.7 Multi-dimensional plot of the optimisation of acrylamide **3.13**. The 3-axis plot show the aniline **3.11** flow rate (x-axis), acid chloride **3.8** eq (y-axis) and temperature (z-axis). The size of the point represents the eq of NEt_3, and the colour represents the product yield. The optimum conditions: 12.2 min, 118 °C, 16 eq NEt_3, 1.7 eq **3.8** are highlighted by the star.

3.2.3 Impurity Identification and Optimisation

Using the optimisation data, it was possible to create multi-dimensional plots for all the significant impurities observed by HPLC, and find the experimental space where impurity yield is high (Figure 3.8). This is important, not only to find operating conditions where impurities are minimal for manufacture but to find where impurity formation is high in order to synthesise it for characterisation. The US Food and Drug Administration (FDA) guidelines dictate that any non API compounds present in the drug substance above 0.05%[d] must be identified.[163] The ability to use automated equipment that can track substance composition in experimental space is a great asset for impurity identification

Impurities in the optimisation were identified using offline LC-MS and by comparing the relative retention times with known impurity standards in the API HPLC method. An impurity

[d] Impurity threshold of 0.05% for drug products with a daily dose of >1 g; 0.1% for drug products with a daily dose of ≤1 g. For more information see reference 18.

(imp1) had already been observed during the temperature profile but did not match anything in the API HPLC method. An impurity of particular concern in the current API synthesis was known to be a dimer. In this model system, a dimeric impurity with a molecular weight equivalent to two monomers of **3.13** was also detected. Two potential mechanisms were proposed that could lead to dimeric species: nucleophilic substitution between **3.11** and **3.12** followed by amidation with **3.8** and subsequent elimination to give **3.15a**; or a Rahut-Currier mechanism[164] (a variation on the Baylis-Hillman reaction)[165-167] *via* the enolate **3.14** to give dimer **3.15b** (Scheme 3.5). In the LC-MS analysis, imp1 had a mass of m/z 309 and further LC-MS-MS analysis showed a fragment of m/z 208 in the second MS spectrum. These data suggest that imp1 is the enolate **3.14** and from the potential mechanistic motifs proposed in sub-chapter 3.2.1, it is proposed that formation of the enolate **3.14** is reversible.

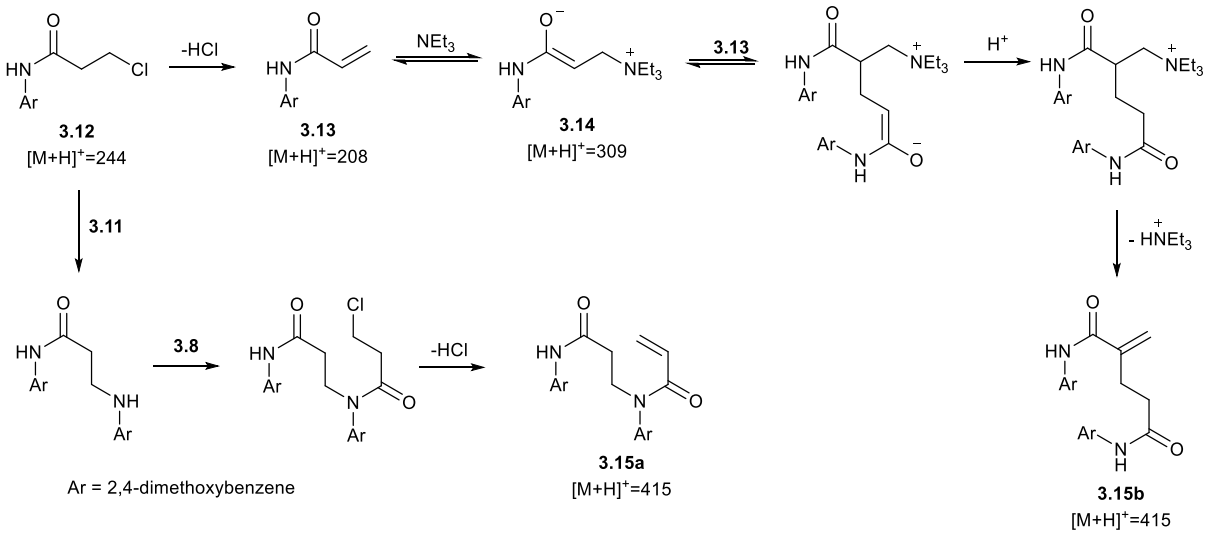

Scheme 3.5 Proposed mechanisms to dimers **3.15a** and **3.15b**. The observation of a peak corresponding to **3.14** favours the Rahut-Currier mechanism to **3.15b**. All observed peaks from offline LC-MS are displayed.

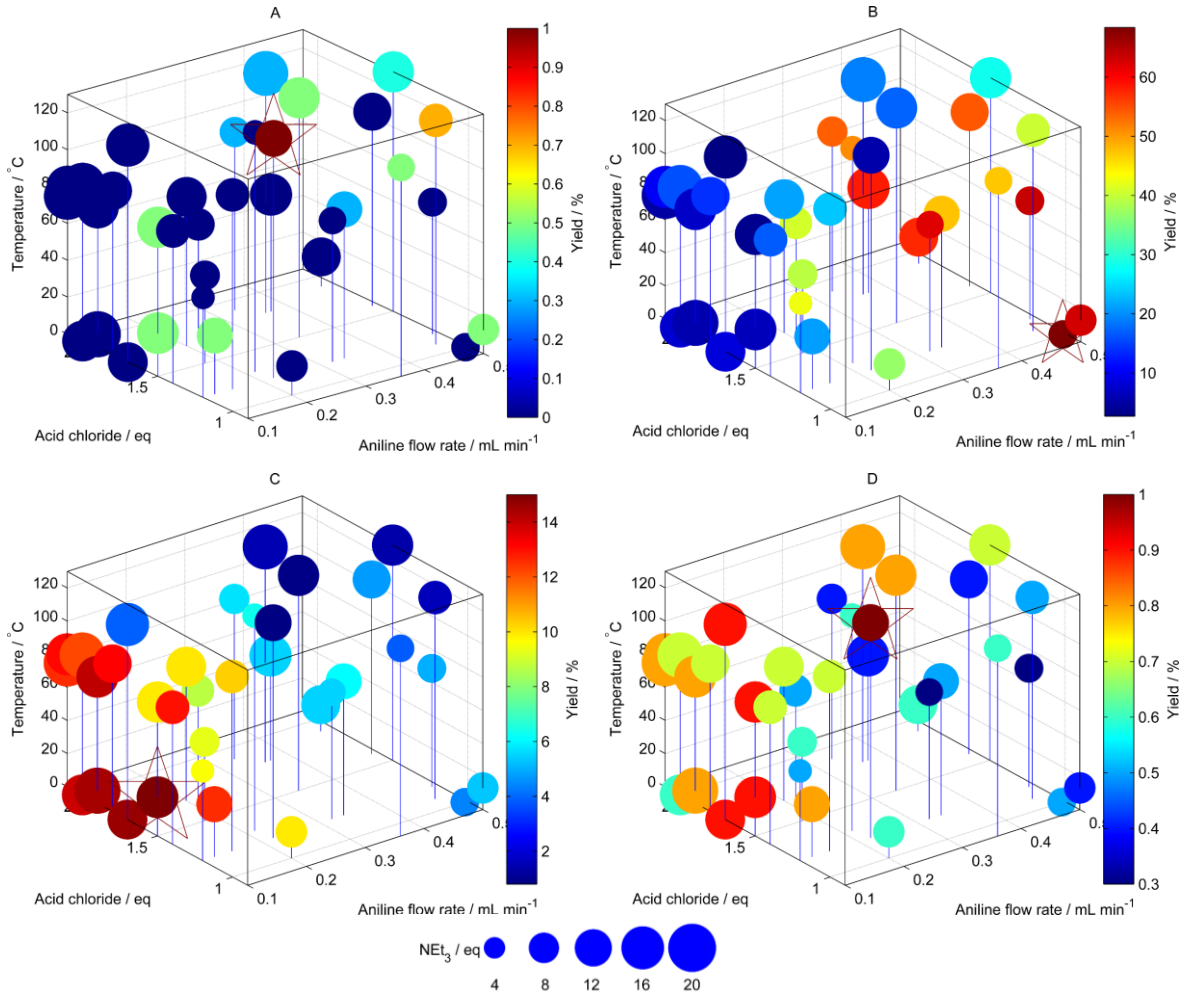

Figure 3.8 Multi-dimensional plots showing the compositions of the major impurities: aniline **3.11** (a), *β*-chloroamide **3.12** (b), enolate **3.14** (c) and dimer **3.15** (d). The maximum composition for each compound is highlighted by the star.

A further optimisation was then run in order to maximise the amount of **3.14**, and find experimental regions where the impurity formation is high. The yields of by-product **3.14** from the original optimisation (Figure 3.7) were inputted to SNOBFIT as preliminary data and the algorithm continued from the last data set using the same boundary limits (Table 3.3).

It should be expected that the optimum region for the formation of **3.14** (Figure 3.9) is similar to that of the acrylamide **3.13**, as the acrylamide is a precursor for the formation of the enolate. However, **3.14** is formed in higher yields at much lower temperatures, suggesting two possibilities for its formation. Firstly, it could be that increased temperatures favour the onward reaction of **3.14** with another molecule of **3.13**, resulting in the formation of the dimer **3.15b**. Secondly, as the reaction from **3.13** to **3.14** (Scheme 3.5) is likely to be reversible, it is possible that increased temperatures favour the acrylamide **13** in the equilibrium. However, any mechanistic

assumptions would need to be confirmed with further kinetic experimentation. It was hoped that these optimal conditions for **3.14** could be used for its full characterisation but attempts to isolate the compound were unsuccessful.

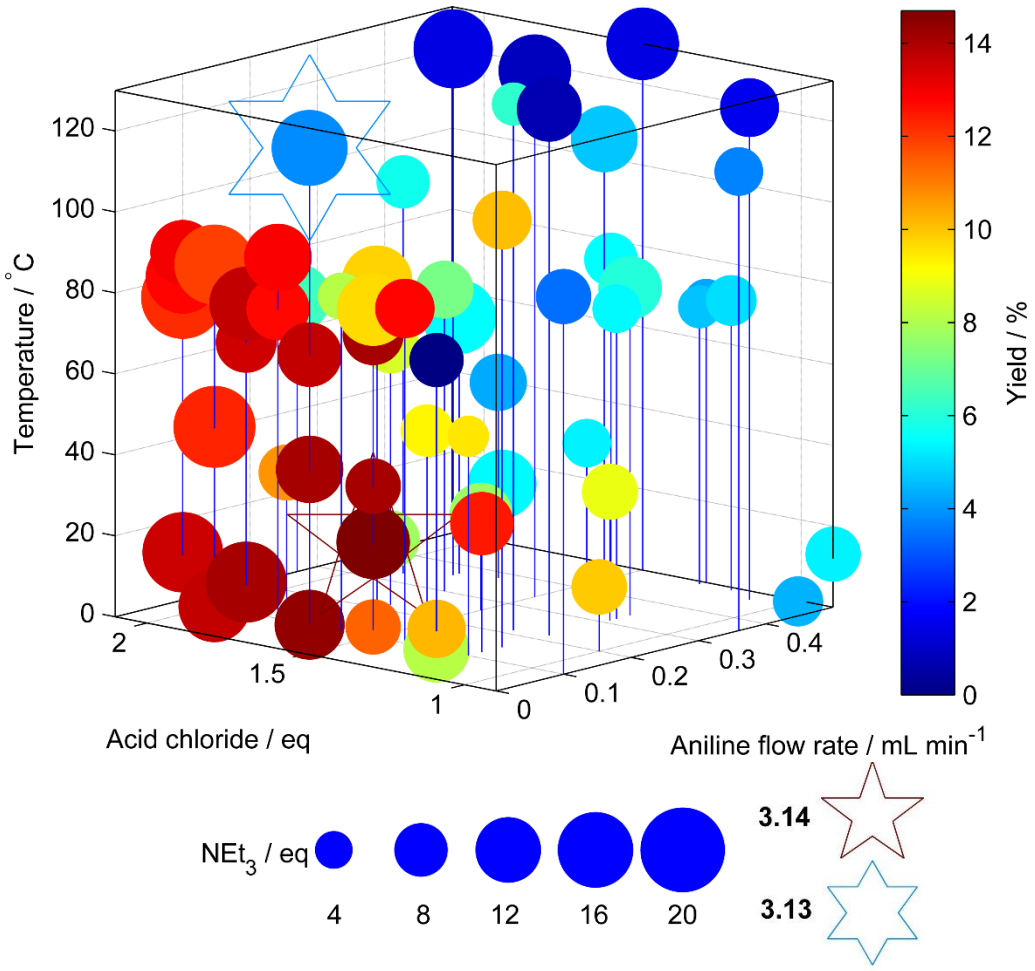

Figure 3.9 Multi-dimensional plot, showing the results of the optimisation of enolate **3.14**. The 3-axis plot show the aniline **3.11** flow rate (x-axis), acid chloride **3.8** eq (y-axis) and temperature (z-axis). The size of the point represents NEt_3 eq, and the colour represents the product yield. The optimum conditions: 0.1 mL min^{-1} **3.11**, 117.8 °C, 1.5 eq **3.8**, 15.2 eq NEt_3 and 12.7 min are highlighted by the 5-pointed star. The optimum conditions of **3.13** are highlighted by the 6-pointed star.

Further LC-MS-MS analysis was carried out using samples acquired from the optimisation to find a reasonable explanation of the dimer structure. The presence of enolate **3.14** favours the Rahut-Currier route to **3.15b**. LC-MS-MS of the dimer peak (m/z 437, $[M+Na]^+$) showed a fragment of m/z 230, which is assumed to be a sodium adduct. Each dimer can produce that fragment, but the C-N disconnection of dimer **3.15a** looks more probable than the C-C of **3.15b**.

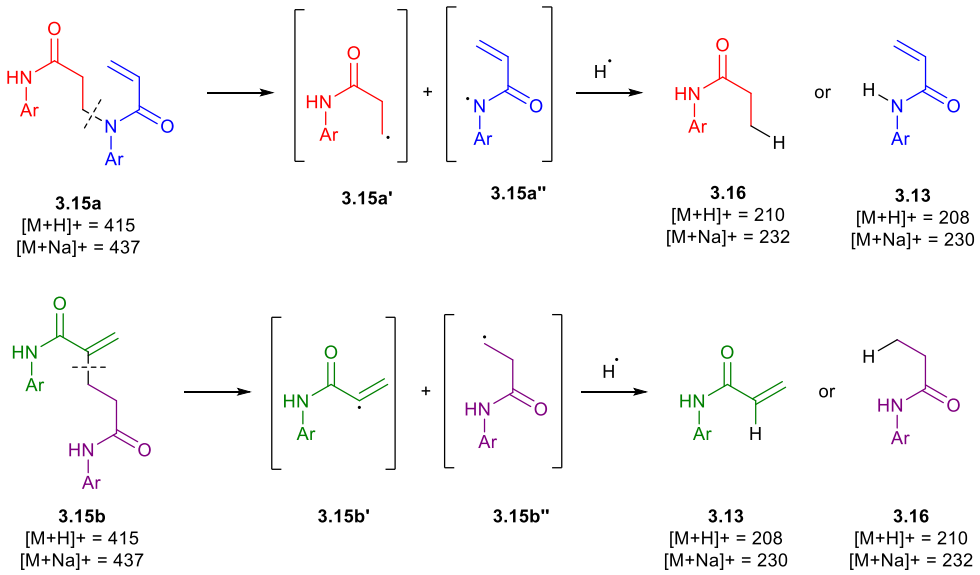

Scheme 3.6 Proposed adduct fragments of dimers **3.15a** and **3.15b**. The final adducts assume that the respective radical is quenched by a hydrogen radical and undergoes no further isomerisation or elimination. It should be noted that only one of the radical intermediates will be quenched to form an adduct after a single fragmentation.

3.3 Optimisation of AZD9291 Freebase

The data obtained from the model compound was used for optimising the final bond forming step of AZD9291.[160-162] Phase I clinical trials showed an encouraging response to the drug, which prompted the FDA to award it breakthrough status for fast track through Phases II and III.[168] Therefore rapid development and optimisation was required to meet the demands put in place by the regulatory bodies, something that a self-optimising reactor would be highly suitable for.

3.3.1 Optimisations Using AZD9291 Free Aniline

Under the batch conditions developed at AZ, a slurry of aniline **3.7** is cooled to 0 °C before addition of acid chloride **3.8**. The presence of a tertiary alkyl amine on the starting material facilitates the first amidation step without requiring base. Next, triethylamine is added and the reaction is heated at reflux to undergo elimination to acrylamide **3.10** (AZD9291 freebase, Scheme 3.7). It had been observed at AZ that the impurities were forming during the heating gradient to reflux and the model optimisations showed that selectivity and yield of the eliminated product was greater at elevated temperatures. Therefore, it was proposed that the reaction would benefit from the safer operation of elevated temperatures and excellent heat transfer in flow reactors to increase the selectivity of the reaction and minimise impurity formation.

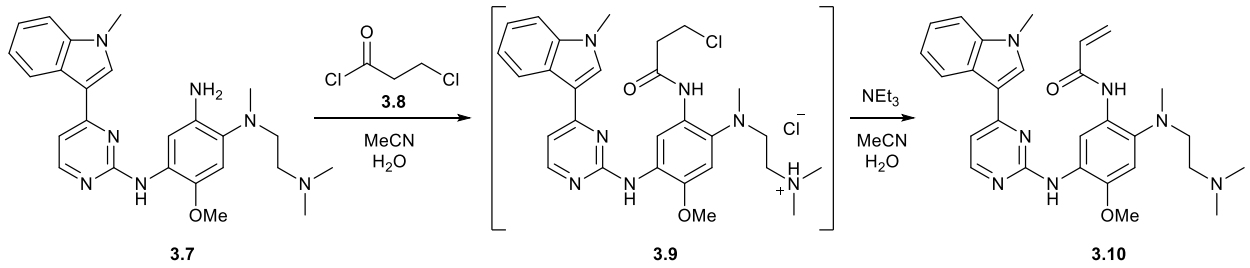

Scheme 3.7 Synthesis of acrylamide **3.9**, the freebase of the AZD9291 API. Aniline **3.7** is treated with acid chloride **3.8** and triethylamine to yield unisolated intermediate **3.9**, which undergoes base mediated elimination to generate **3.10**.

3.3.2 Development of Process Conditions for the Continuous Synthesis of AZD9291 Acrylamide

One of the challenges of transferring the process from batch to continuous was the low solubility of **3.7** in the solvent mixture. The reactor pumps require homogeneous solutions, and dissolution of **3.7** was only achieved with 60 relative volumes (RV) of solvent. This would not be suitable for a manufacturing process due to the excess of solvent. Therefore a brief solvent screen compared the solubility of **3.7** in methanol, acetone, ethyl acetate, anisole, diethyl carbonate, dioxane and tetrahydrofuran. Saturated solutions of **3.7** in each solvent were filtered and then the absorbance of the filtrate was measured using HPLC-UV/Vis; a solubility model was built using DynoChem software.[169] This was coupled with separate thermodynamic solubility calculations[e] and both studies showed that anisole was an attractive replacement to aqueous acetonitrile.

In anisole, aniline **3.7** dissolved in 25 RV, which is higher than ideal for manufacture but is a lot lower than the existing solvent mixture. Anisole also scores more favourably than acetonitrile in solvent comparison studies based on safety, environmental and occupational health factors.[170] However, the reaction was much slower and multiple experiments over a period of time resulted in accumulation of solids and clogging. Anisole was replaced with acetonitrile in the triethylamine reservoir to improve the reaction kinetics but the reaction was still slow and it required addition of water to prevent clogging. The water content was only 10% (v:v) in the triethylamine reservoir but this coalesced to a biphasic mixture upon leaving the reactor, which could incur problems for HPLC sampling if aqueous material was sampled rather than organic.

[e] Thermodynamic solubility calculations were carried out using COSMOTherm software by S. Tomasi, AstraZeneca

Instead, a solution of the hydrochloride salt of **3.7** (0.8 eq HCl) was prepared, which would dissolve in 15 RV of the aqueous acetonitrile mixture. Sub-stoichiometric equivalents of acid were used to maintain a non-acidic pH thus preventing corrosion of stainless steel within the reactor. The boundary limits were adjusted from the initial AZD9291 optimisation to explore a larger chemical space. In particular, the temperature range was increased from the model reaction as poor conversion of **3.7** was achieved during initial experiments at lower temperatures. The optimisation limits are displayed in Table 3.4, the flow rates of which correspond to a calculated residence time between 4 and 22 minutes. The optimisation results are shown in Figure 3.10.

Table 3.4 Optimisation boundary limits for the AZD9291 aniline reaction

Limit	Pump A / mL min^{-1}	Pump B / mol eq	Pump C / mol eq	Temperature / °C
Minimum	0.080	2.2	0.75	80
Maximum	0.150	15	3.0	150

Pump A reservoir 0.136 mol L^{-1} aniline **3.7**, 0.0255 mol L^{-1} biphenyl, pump B reservoir 1.20 mol L^{-1} triethylamine, pump C reservoir 0.500 mol L^{-1} acid chloride **3.8**.

The optimum conditions (0.11 mL min^{-1} **7**, 2.65 eq **3.8**, 10.5 eq NEt_3, 123.9 °C, 9.36 min in 89%) are slightly different to that of the model compound, with higher equivalents of triethylamine and **3.8**, resulting in a shorter residence time than the free aniline, but this could be a consequence of the higher concentration resulting in a higher reaction rate.

The flow rate of **3.7** is not at the minimum boundary and it exhibits a clear interaction with temperature. As the flow rate of **3.7** is increased there is a concurrent increase in temperature required to achieve high yields as the residence time decreases. The decrease in residence time could also be a result of improved mixing. Whilst this was proposed in the initial optimisation, this system involves an extra pre-equilibrium step to deprotonate the HCl salt of **3.7**, which could be mixing sensitive. Further analysis of the HPLC chromatographs for each experiment show that the relative composition of **3.7** is typically higher than **3.9** indicating that the elimination is faster and the pre-equilibrium is most likely the rate limiting step. Unfortunately there is no way to identify the degree of protonation of **3.7** by HPLC and further kinetic experimentation would be required to support this hypothesis.

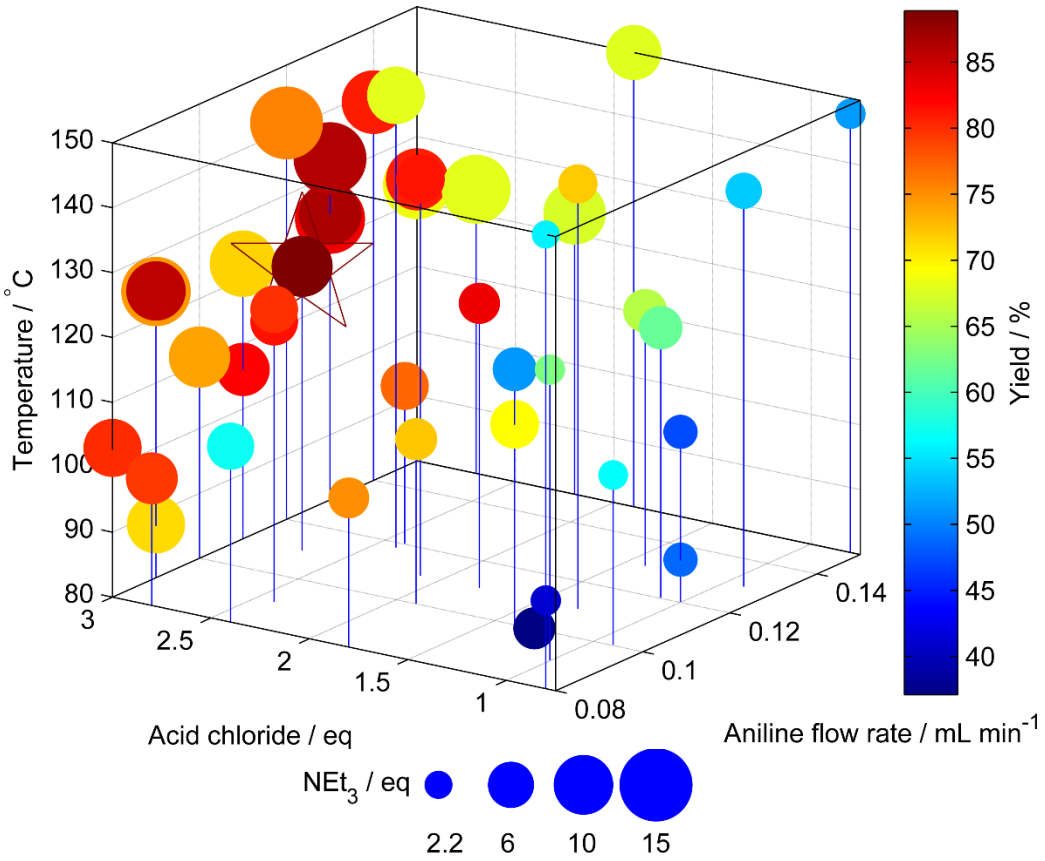

Figure 3.10 Multidimensional plot of the optimisation of acrylamide **3.10**. The 3 axis flow rate shows the aniline **3.7** flow rate (x-axis), acid chloride **3.8** eq (y-axis) and temperature (z-axis). The size of the point corresponds to the triethylamine eq, the colour is the yield. Optimum conditions: 9.36 min, 123.9 °C, 10.5 eq NEt_3, 2.7 eq **3.8** are highlighted by the star.

The equivalents of triethylamine across the two optimum conditions vary significantly from 10.57 to 16. It could be that each reaction requires different concentrations of base but there could be an alternate explanation. The flow rate of each pump controls the respective concentrations of the reaction components but also the overall residence time. The residence time wasn't a main variable but was confounded from the flow rate of aniline and the equivalents of triethylamine and **3.8**. Therefore it could be proposed that the concentrations of aniline and **3.8** and the residence time were the most important factors, ignoring temperature, and the effect of the changes in equivalents, and subsequently flow rate, of triethylamine has more impact as an adjustment of residence time and concentration of **3.7** than as a concentration of triethylamine.

3.4 Conclusions

Presented is the novel application of implementing a self-optimising flow reactor for the continuous optimisation of the final bond forming step in the synthesis of an active pharmaceutical

ingredient. The concept was first tested on a model reaction to develop the experimental set up and data analysis for the ultimate optimisation of the API. The model optimisation was the telescoped synthesis of acrylamide **3.13** from aniline **3.11**. Initial reaction conditions were developed by carrying out a temperature profile, where impurity formation was first observed. With the reaction set up in hand, the yield of acrylamide **3.13** was optimised using the SNOBFIT algorithm, providing conditions for its formation in 92% yield. The model optimisation also provided enough information to predict a mechanistic route to and possible structures for the impurities enolate **3.14** and dimer **3.15**.

The final optimisation of **3.10** required 42 separate experiments, which used 10 g of material and lasted 37 hours (average of ~240 mg per experiment) providing the desired product in 89% yield. The overall time would have been less but clogging resulted in some periods of down time before the reactor could be restarted. One of these events occurred at 1 am and therefore was not noticed until the following morning. Fortunately, an automatic trip written into the optimisation program prevented wasteful continuous pumping of material by stopping all the pumps. Had the reactor pumped continuously without clogging through its whole operation, the optimisation would have finished in 26 hours. The impracticalities of performing the reaction in flow influenced the decision to carry out the reaction in batch for the manufacturing route. Ultimately, neither the work in this chapter, nor the complementary work by the AZ flow chemistry team could develop a reliable set-up where the reaction could be pumped continuously without problems.

Nevertheless, the use of self-optimising systems allowed swift exploration and process optimisation even of multistage reaction systems without human intervention. The data obtained not only provided optimum regions of high product yield but aided the identification and mechanistic route to impurities. Crucially, this technology enables a shift in focus towards the scientifically challenging aspects whilst the automated system performed the routine experimentation.

4. Empirical response surface models generated using self-optimising algorithms[f]

4.1 Introduction

Multivariate optimisation describes the changing of more than one variable at a time to track the change in response and ultimately find optimum conditions. This method has multiple advantages over only changing one variable at a time (OVAT) because the systematic approach to carrying out experiments does not lead to an increase in the number of total experiments and does not omit inter-variable interactions.

Design of experiments (DoE) is the common approach, where statistical analysis is carried out on a predetermined grid of experiments (design). The result is an empirical model, which can predict the behaviour of the process within the limits for the variables studies. This differs from a conclusive model, which can predict all outcomes across all condition ranges. The information acquired from the model depends on the type of design: a linear design (screen) can show the important main effect variables and interactions; a quadratic design can show curvature in the model and can be used to interpolate, predict responses and optimise.

Quadratic designs are typically labelled response surface methodology (RSM) because the curvature of the model allows a surface to be plotted using the terms generated from the model.[157, 158] Common designs for RSM include 3-level full factorial, central composite and Box-Behnken. Each of these designs feature 3 levels which allow the quadratic fit. The number of experiments per design depends on the number of factors, but it follows the order: Box-Behnken ≤ central composite << full factorial.

All three of these designs have at least three levels and require experiments at the minimum and maximum extremes of each variable, either in the corners, edges or faces of the experimental cube. However, there are a few examples of using RSM with data that does not follow a conventional factorial design. The data generated from exploratory algorithms, such as SNOBFIT, provides a scatter across the experimental space but is used solely for optimising purposes rather than for acquiring information about a chemical system.[136] There are examples of optimisation by

[f] The work in this chapter was carried out in collaboration with MChem student M. Jeraal. The Author and MJ carried out the experimental optimisations and all model and data analysis was carried out by the Author.

algorithm with multiple target functions,[26, 171] but it is typical for an optimisation to be run for a single function and repeated for a new target or metric.[17, 64, 172] Some algorithms will only generate new experiments with the aim of improving the existing optimum. Therefore only providing information about the reaction system in experimental space that lies between the initial and optimum points. It is hypothesised that RSM models can be fitted to data obtained from exploratory algorithms in order to provide more information about the chemical process and find optimum conditions for new single or compound target functions. This will be carried out by fitting quadratic models using commercially available DoE software and then applying statistical treatments and analysis that result in accurate models with good fit.

4.2 Response surface model generation

4.2.1 Example: Claisen-Schmidt condensation

The reaction studied was a Claisen-Schmidt condensation between benzaldehyde **4.1** and acetone **4.2** to yield benzylideneketone **4.3** (Scheme 4.1). The reaction proceeds with NaOH base catalysis and will readily form the bis adduct, dibenzylideneacetone (DBA, **4.4**), under mild conditions.[173] A SNOBFIT optimisation was carried out to optimise the yield of the kinetic product, ketone **4.3**, by varying the flow rate of benzaldehyde, molar equivalents of acetone, flow rate of base catalyst and reactor temperature. The flow reactor setup (Figure 4.1) consisted of three pumps, 6 mL tubular reactor, inline filter and 6 bar back pressure regulator. The pump reservoirs contained benzaldehyde (1.95 mol L^{-1}) and biphenyl internal standard (0.032 mol L^{-1}) in ethanol, sodium hydroxide (0.2 mol L^{-1}) in ethanol, and neat acetone. Online analysis was carried out using HPLC and the algorithm limits are displayed in Table 4.1.

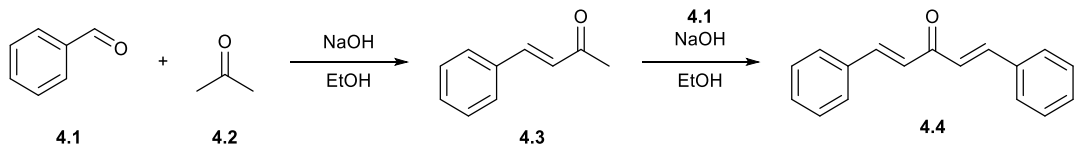

Scheme 4.1 Base catalysed Claisen-Schmidt condensation between benzaldehyde and acetone.

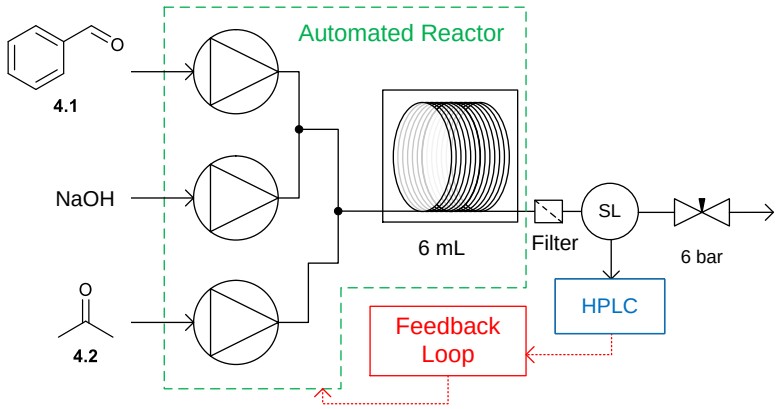

Figure 4.1 Reactor setup for the Claisen-Schmidt condensation. SL – sample loop

Table 4.1 Boundary limits for the Claisen-Schmidt condensation optimisation

Limits	**4.1** flow rate / mmol min^{-1}	NaOH flow rate / mmol min^{-1}	**4.2** / mol eq	Temperature / °C
Minimum	0.4	0.008	1	10
Maximum	2.0	0.100	7	80

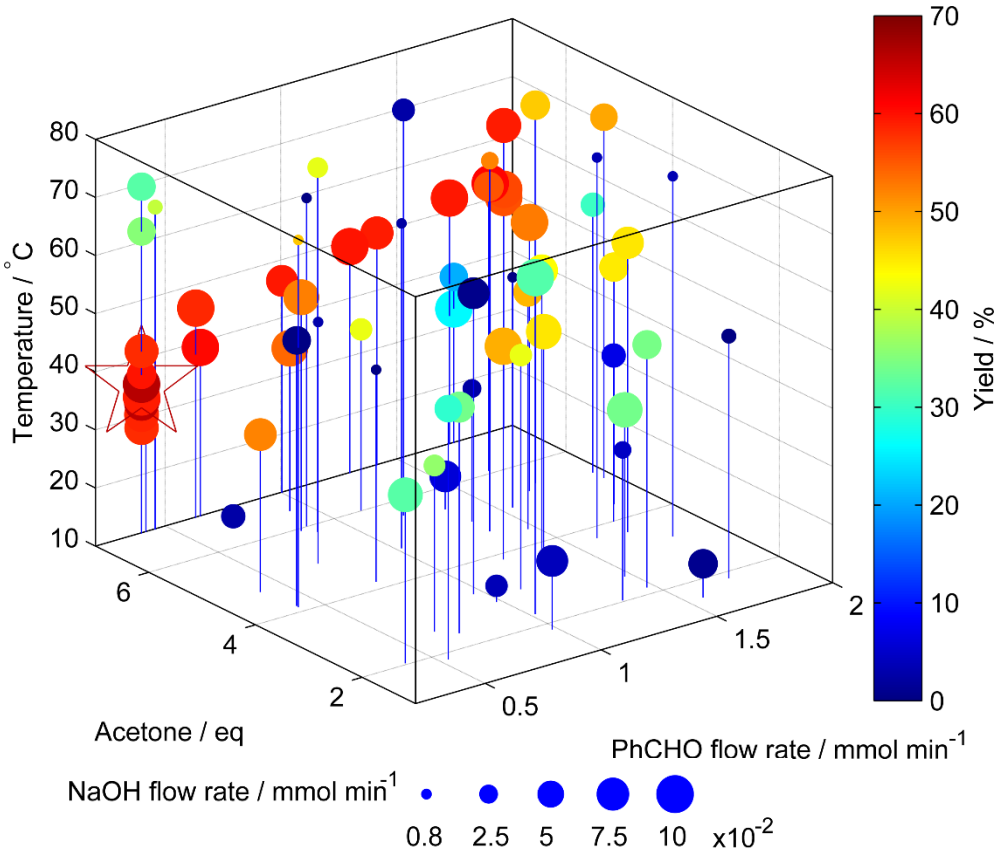

Figure 4.2 Optimisation plot for the SNOBFIT optimisation of ketone **4.3**. x-axis = **4.1** flow rate; y-axis = acetone eq; z-axis = temperature; size of the point denotes NaOH flow rate; colour of the point denotes yield . The optimum point is denoted by the star: 0.4 mmol min^{-1} 1, 7.0 eq acetone, 0.25 mmol min^{-1} and 35.8 °C.

The algorithm generated optimum conditions of 0.4 mmoL min^{-1} **4.1**, 7.0 eq acetone, 0.25 mmol min^{-1} and 35.8 °C (Figure 4.2). The spread of data is scattered across the experimental space but generally concentrated towards low benzaldehyde flow rates and high acetone equivalents.

4.2.2 Basic model generation

The percentage yield of compounds **4.1**, **4.3** and **4.4** were used as the responses for three separate quadratic models. Saturated models were generated by including all square and interaction terms and fitted using multiple linear regression (MLR). The model can be written as

$$\hat{y} = \beta_0 + \beta_1 x_1 + \beta_2 x_2 + \beta_3 x_3 + \beta_4 x_4 + \beta_{11} x_1^2 + \beta_{22} x_2^2 + \beta_{33} x_3^2 + \beta_{44} x_4^2 + \beta_{12} x_1 x_2 + \beta_{13} x_1 x_3 + \beta_{14} x_1 x_4 + \beta_{23} x_2 x_3 + \beta_{24} x_2 x_4 + \beta_{34} x_3 x_4 \quad (4.1)$$

where $\hat{y}$ is the model response, β_i is the coefficient of each term, x_i. The terms are displayed in Table 4.2.

Table 4.2 Description of terms from equation (4.1)

Term	Variable	Abbreviation
x_1	Flow rate of **1**	P1
x_2	Acetone eq	Ace
x_3	Flow rate of NaOH	NaOH
x_4	Temperature	Temp

Following construction of the model, the success of the fit can be quantified according to two terms R^2 and Q^2. R^2 measures how well the model fits the existing data, and is calculated by

$$R^2 = 1 - \frac{SS_E}{SS_T} \quad (4.2)$$

where SS_E is residual sum of squares and SS_T is the total sum of squares

$$SS_E = \sum_{i=1}^{n} (y_i - \hat{y}_i)^2 \quad (4.3)$$

$$SS_T = \sum_{i=1}^{n} (y_i - \bar{y})^2 \quad (4.4)$$

where $\hat{y}_i$ is the modelled (or predicted) response, y_i is the experimental (or observed) response and $\bar{y}$ is the mean experimental response. Q^2 measures how well the model will predict the response of new data, and is calculated by

$$Q^2 = 1 - \frac{PRESS}{SS_T} \tag{4.5}$$

where $PRESS$ stands for the prediction error sum of squares, and is calculated by refitting the model with a point i removed, then calculating SS_E when predicting the response of the i^{th} point, $\hat{y}_{(i)}$

$$PRESS = \sum_{i=1}^{n} \left(y_i - \hat{y}_{(i)}\right)^2 \tag{4.6}$$

4.2.3 Methods to improve the fit

A model will have the maximum R^2 value when all possible interaction and square terms are included because the degrees of freedom (DF) of the model (the number of terms subtracted from the total number of points) is low. The R^2 fit can also be increased by removing data points that have a large deleted studentized residual when plotted as a normal distribution, which also decreases DF. The deleted studentized residual (DSR) measures the ratio of a residual ($e_i = y_i - \hat{y}_i$) by the estimation of its standard deviation (SD). In conventional DoE it is typical to repeat an anomalous experiment rather than remove it but in this case the spread of data and number of data points (high initial DF) allows deletion. However, reducing the DF too much can result in a poor model.

The total DF is a measure of how much the data can vary without changing the model and is calculated by $n - 1$, where n is the number of experiments. For example, a survey of the details of a group of people is carried out and a model generated, which shows the average height of a male adult is 180 cm. The heights of four adult males are measured and they are 170, 180 and 190 cm. For the model to be correct, the height of the fourth man must be 180 cm. Therefore the model has 3 DF; the heights of the first three men can be anything but the height of the final must be a value that supports the hypothesis. In this case, an average height of 180 cm. The complexity can be increased by adding an additional term so that the average height and weight of an adult male is 180 cm and 85 kg, respectively. The model now has 2 DF; the height of the fourth man and weight of the third must be values that support the hypothesis. If it is discovered that the first man is not a fully grown adult, they must be removed from the model. Now the model only has 1 DF, meaning

only one data point can have any variation. Therefore it is important to increase the DF to generate a more robust model.

The model is improved by removing terms where the potential to contribute to the model is calculated to be zero. This generally does not greatly decrease the R^2 value but will increase the DF and Q^2 value because the model is better at predicting with fewer terms and higher DF.

The saturated model (4.1) for ketone **4.3** is shown in Figure 4.3 with all coefficients, normal probability *vs* deleted studentized residuals plot and R^2 and Q^2 values. The model had an average fit ($R^2 = 0.753$) but poor predictability ($Q^2 = 0.495$). However, as described above, there were steps to be taken to improve the fit.

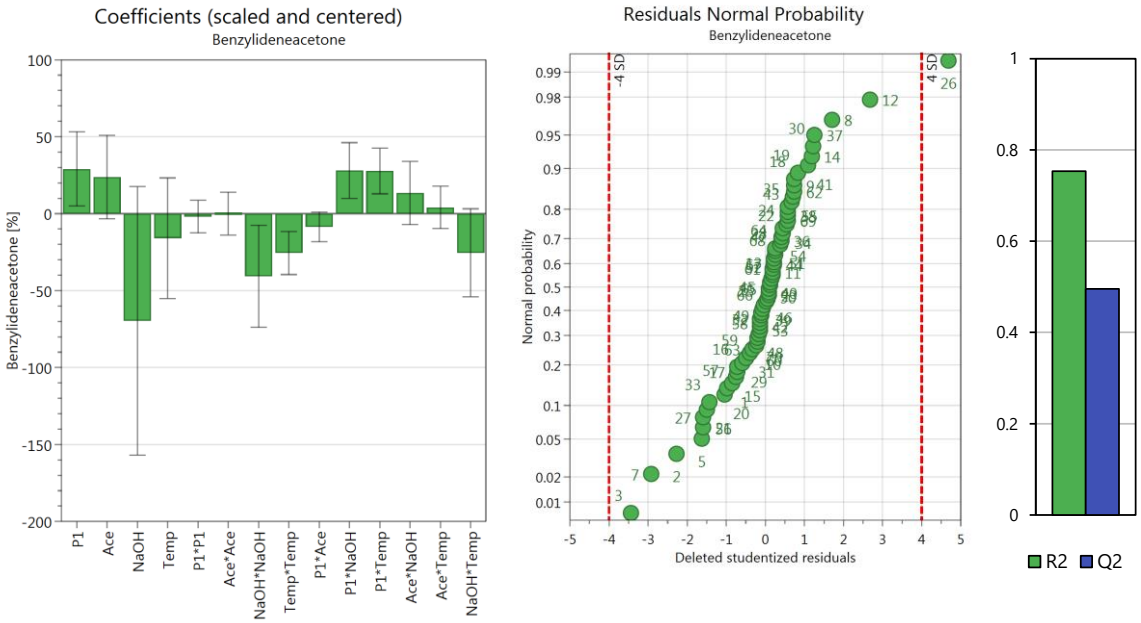

Figure 4.3 Model coefficients (left) and normal probability distribution (centre) and $\boldsymbol{R^2}$ and $\boldsymbol{Q^2}$ (right) for the saturated model of ketone **3**.

The normal probability plot showed an S-shape fit, which demonstrated that the data was not normally distributed and also showed that experiment 26 had high residual error. Removing this experiment, along with a further 7, improved the R^2 and Q^2 values to 0.961 and 0.907, respectively. It is standard procedure to repeat anomalous results in a DoE, however the high number of experiments obtained during the SNOBFIT optimisation justified their removal. The anomalous experiments could be caused by faulty pumps or integration error with HPLC analysis.

The statistical significance of a coefficient is measured by its p-value, which is a measure of whether the null hypothesis of the model should be rejected.[174] A p-value of $>\alpha$ (for 95%

confidence interval, $\alpha = 0.05$) shows significance towards the null hypothesis and can therefore be rejected from the model. Coefficients with p-values of $>\alpha$ had error bars that overlapped the x-axis (Figure 4.3), stating that their contribution to the model was potentially zero, and were removed from the model. After a coefficient was removed, the model was re-fitted and the p-value could change. Therefore it was important to only remove a single coefficient at a time and reassess the p-values of each coefficient. Figure 4.4 shows the model coefficients and summary of fit for the improved model. Removing insignificant coefficients and anomalous experiments improved the overall fit and predictability as well as the normal distribution of the data.

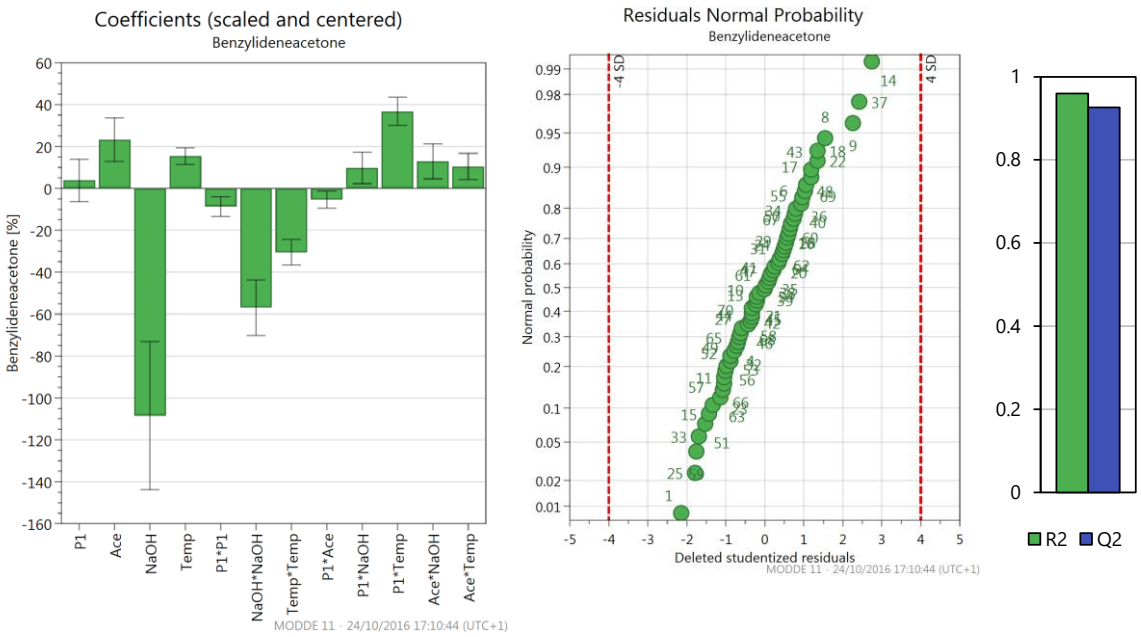

Figure 4.4 Model coefficients (left) and normal probability distribution (centre) and $\boldsymbol{R^2}$ and $\boldsymbol{Q^2}$ (right) of the model for ketone **4.3** after removing anomalous experiments and non-significant coefficients.

4.2.4 Transformations

The model for ketone **3** had the advantage of good initial R^2 and Q^2 values, requiring only slight modification of the model to improve both fits. However the model for benzaldehyde **4.1** needed much more treatment. The R^2 value for the initial saturated model (4.1) was only 0.55 and the Q^2 was 0.06 (Figure 4.5).

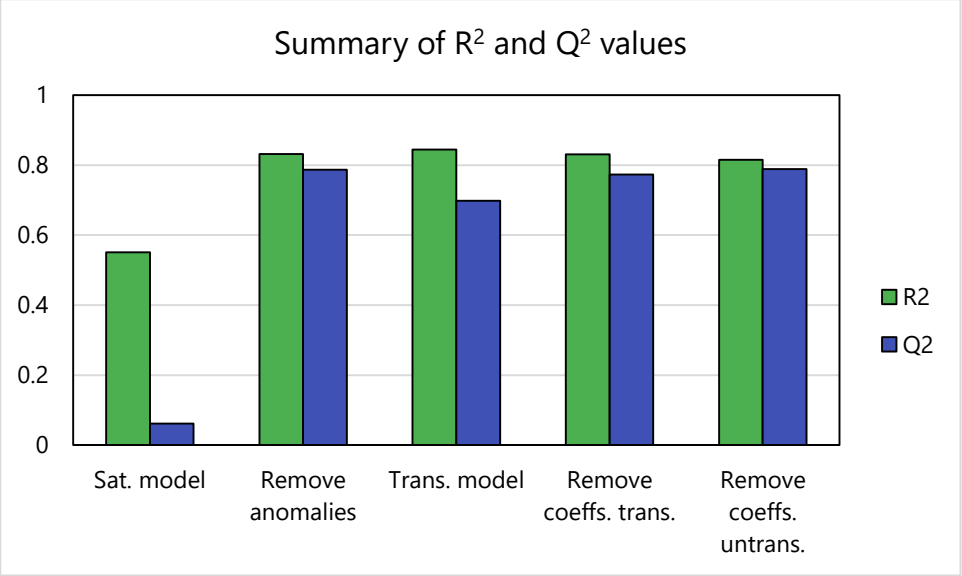

Figure 4.5 Monitoring how the $\boldsymbol{R^2}$and $\boldsymbol{Q^2}$ values change with treatments to improve the fit of model for aldehyde **4.1**. Sat. = saturated; trans. = transformed; untrans. = untransformed; coeffs. = coefficients.

All of the experiments were within ±4 SD on the normal probability plot; however five points were deleted, which resulted in a spread of data where all points were within ±3 SD. As shown in Figure 4.5 (remove anomalies), this greatly improved the fit but no further improvements were witnessed after removal of coefficients.

Next, the model was investigated to see if it could be a good candidate for a transformation, where the response is treated with a mathematical transformation such as a logarithm or indices.[175, 176] Transformations are calculated according to

$$y(\lambda) = \begin{cases} y^{\lambda} & if\ \lambda \neq 0 \\ log(y) & if\ \lambda = 0 \end{cases} \tag{4.7}$$

for $y > 0$ where where λ is a parameter that defines the transformation and $y(\lambda)$ is the transformed response. λ is determined using the maximum likelihood estimation (MLE, $L_{max}(\lambda)$), of the regression of transformed responses

$$L_{max}(\lambda) = -\frac{1}{2} n\, ln\left(\frac{SS_{R,\lambda}}{n}\right) + (\lambda - 1)\sum_{i=1}^{n} ln(y_i) \tag{4.8}$$

Where n is the number of experiments and $SS_{R,\lambda}$ is calculated by

$$SS_{R,\lambda} = \sum_{i=1}^{n} (y(\lambda)_i - \bar{y})^2 \tag{4.9}$$

A plot of $L_{max}(\lambda)$ *vs* different values of λ (Box-Cox plot)[175] will show the best recommended transformation, which can be approximated within a $(1-\alpha)$ confidence region using

$$L_{max}(\lambda^*) - L_{max}(\lambda) < \frac{1}{2}\chi^2_{DF_\lambda}(\alpha) \tag{4.10}$$

where λ^* is the value that supports the best transformation, $\chi^2_{DF_\lambda}$ is the chi-squared distribution for the degrees of freedom of λ and α is the confidence interval (for 95%, $\alpha = 0.05$). Transformations are typically calculated for $-2 \leq \lambda \leq 2$, a summary of which are displayed in Table 4.3.

Table 4.3 – Summary of common transformations based on the MLE λ value

MLE λ value	Transformation
-2	$y(\lambda) = \frac{1}{y^2}$
-1	$y(\lambda) = \frac{1}{y}$
0	$y(\lambda) = \ln(y)$
0.5	$y(\lambda) = \sqrt{y}$
1	$y(\lambda) = y$ No transformation
2	$y(\lambda) = y^2$

The Box-Cox plot for the aldehyde **1** model supports a logarithm transformation because the λ value is closest to zero (Figure 4.6). The Q^2 value decreased after the transformation, however when the non-significant terms were removed a greater R^2 was achieved with transformation than without (Figure 4.5) (after trans.). The transformation also supported an improvement in the in normal distribution of the data (Figure 4.7).

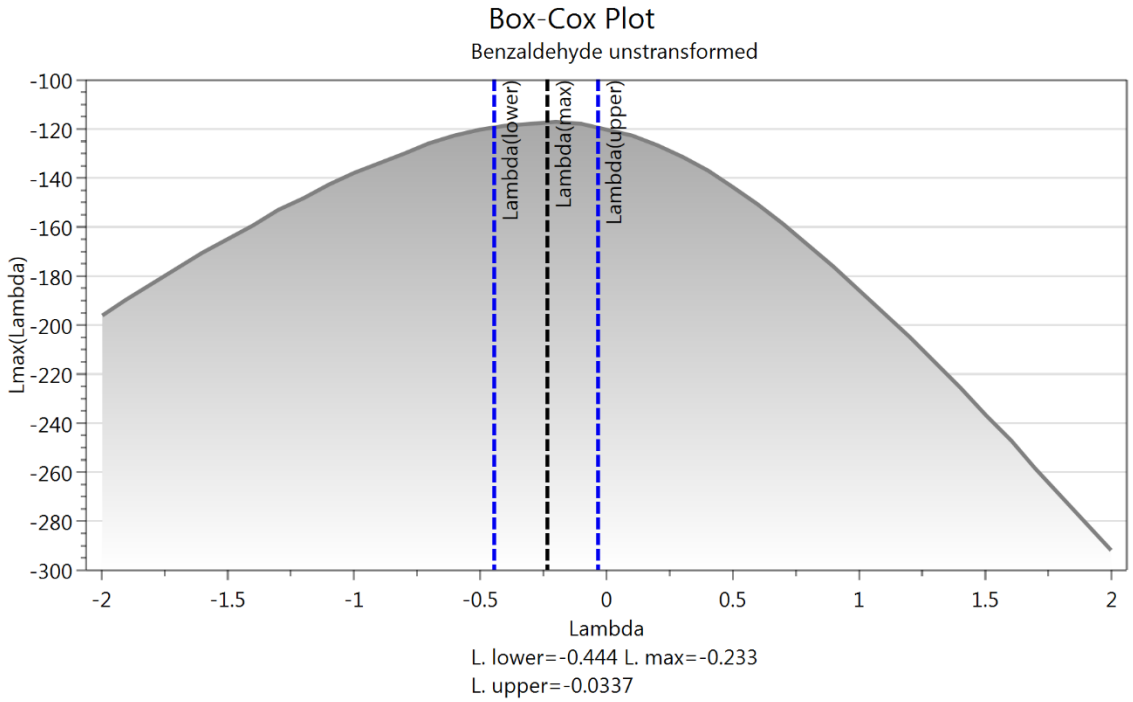

Figure 4.6 Box-Cox plot for benzaldehyde **1** model. The $\boldsymbol{L_{max}(\lambda^*)}$ value is approximated to 95% confidence interval.

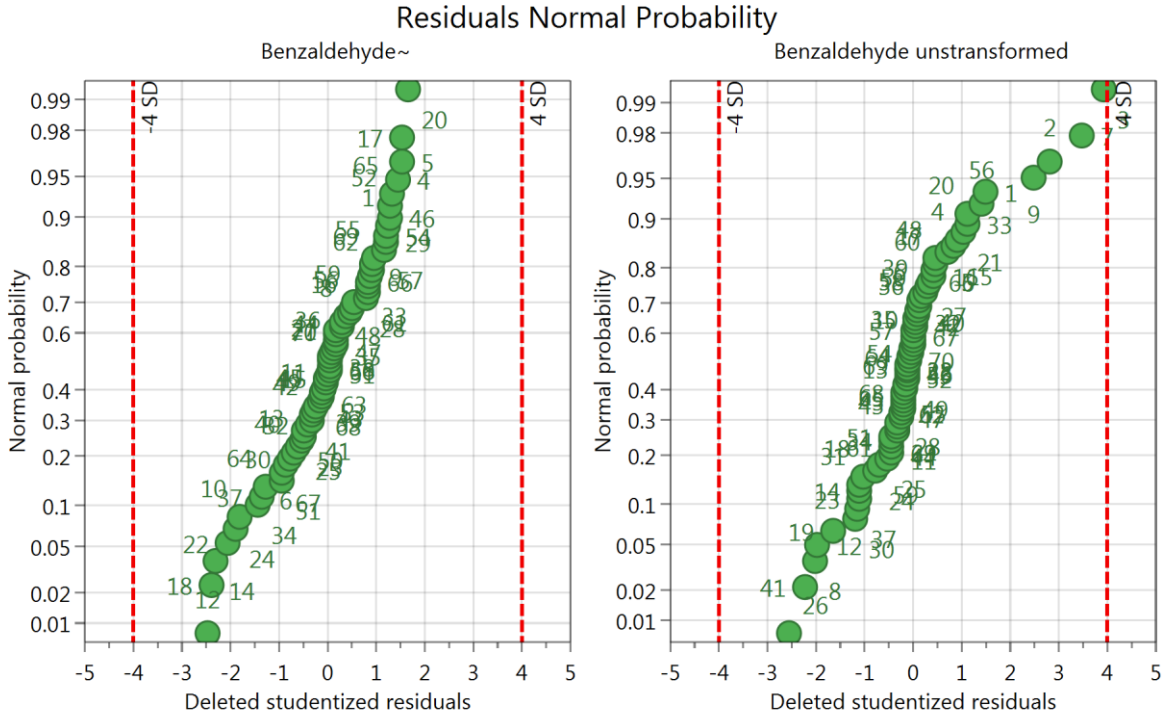

Figure 4.7 Comparison of the normal probability distribution for the transformed (left) and untransformed (right) benzaldehyde **1** models. The transformed data fits a straight line and shows an improved normal distribution.

A design feature of some response surface methods is that they are rotatable, which means that the variance in each experimental point is constant for points that have the same distance from

the centre-point, regardless of their location.[177] Constant variance is simple to determine for conventional RSM models, such as central composite or Box-Behnken, as it is easy to calculate experiments with the same distance. It is simple to see visually that these models have rotational symmetry. The data generated from SNOBFIT is much more random and if there is more than two data points with the same distance from the centre-point, they would be difficult to spot visually. However, constant variance can be qualitatively confirmed by looking at the spread of DSR against each variable. A random spread of data shows constant variance, whereas a trend that follows a shape such as cone or curve can be the result of a missing model term or non-constant variance. The initial untransformed model showed a cone shape for the benzaldehyde flow rate variable vs DSR, indicating non-constant variance. As shown in Figure 4.8, the randomness of the variable vs DSR increases after transformation.

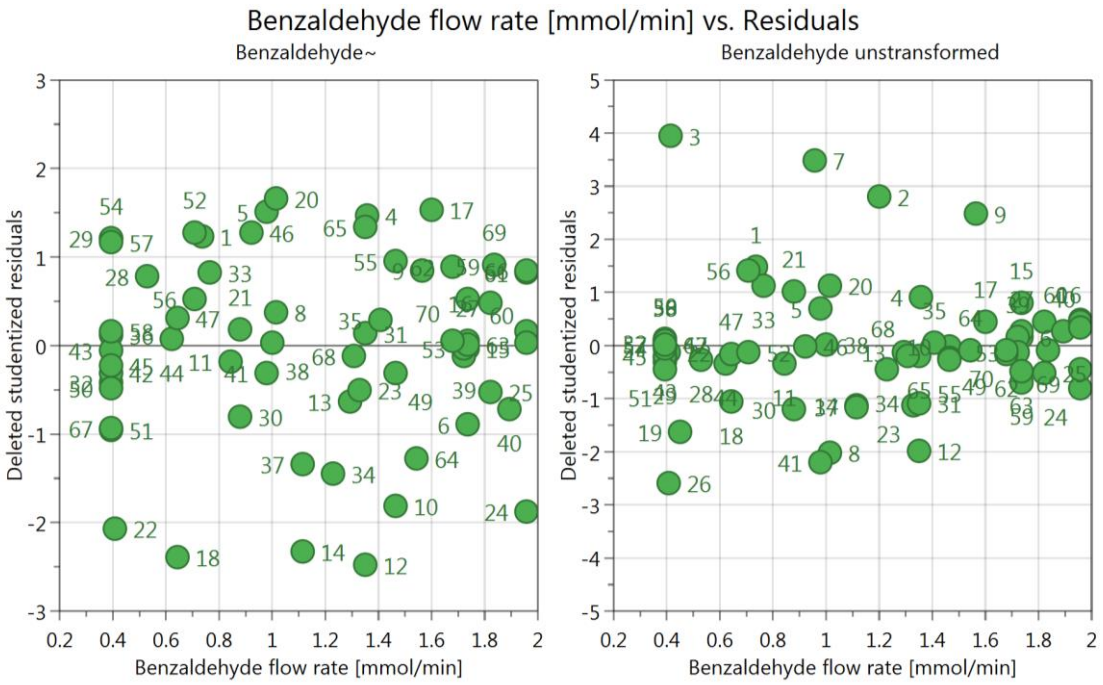

Figure 4.8 Comparison of deleted studentized residuals vs flow rate of **4.1** for the transformed (left) and untransformed (right) models of benzaldehyde **4.1**.

4.2.5 Analysis of variance and lack of fit

The quality of fit has been described above as having high values for R^2 and Q^2, however these quantities do not completely explain all aspects of the model. A method of quantifying the model in terms of testing the null hypothesis is by using analysis of variance (ANOVA). This

separates the total sum of squares (SS_T) associated with the model into regression error (SS_R), due to the model fit and residual error (SS_E), due to the noise

$$SS_T = SS_R + SS_E \tag{4.11}$$

where

$$SS_R = \sum_{i=1}^{n} (\hat{y}_i - \bar{y})^2 \tag{4.12}$$

The total degrees of freedom (DF_T) can also be separated into regression and residual so that

$$\begin{aligned} DF_T &= DF_R + DF_E \\ &= (k) + (n - k - 1) \\ &= n - 1 \end{aligned} \tag{4.13}$$

where k is the number of coefficients in the model. The model null hypothesis is tested by calculating the F_0 value

$$F_0 = \frac{SS_R/DF_R}{SS_E/DF_E} = \frac{MS_R}{MS_E} \tag{4.14}$$

which looks at the ratio between the regression and residual errors, where MS is the mean square. As the F_0 value greatly increases above 1, the regression error is much larger than the residual error and a poorly fitting model will be due to problems with the model itself rather than random noise. The null hypothesis can be accepted or rejected by calculating the p-value of the F-distribution having degrees of freedom DF_R and DF_E. This p-value calculates the probability of a F_0 value that is greater than the observed value and the null hypothesis is rejected if the p-value is less than the significance level for the confidence interval (α).

Further scrutiny of the data looks at how well the model fits the trend of the data, which is tested using lack of fit. Lack of fit measures the error variance σ^2 in the replicate experiments, which could be caused by instrument, analytical and human random error. It is measured by first partitioning the residual sum of squares into two components

$$SS_E = SS_{PE} + SS_{LOF} \tag{4.15}$$

where SS_{PE} is sum of squares due to pure error and SS_{LOF} is sum of squares due to the lack of fit. This is measured based on the replicate experiments in the model, the experiments with the same conditions where the responses are measured separately of each other (i.e. not one experiment

measured multiple times). For every replicate level $i = 1,2 \dots m$ there will be $j = 1,2 \dots n_i$ replicate responses, such that the $(i,j)^{\text{th}}$ residual is

$$y_{ij} - \hat{y}_i = \left(y_{ij} - \bar{y}_i\right) + (\bar{y}_i - \hat{y}_i) \tag{4.16}$$

Squaring and summing for all values of i and j converts (4.16) to

$$\sum_{i=1}^{m}\sum_{j=1}^{n_i}\left(y_{ij} - \hat{y}_i\right)^2 = \sum_{i=1}^{m}\sum_{j=1}^{n_i}\left(y_{ij} - \bar{y}_i\right)^2 + \sum_{i=1}^{m} n_i(\bar{y}_i - \hat{y}_i)^2 \tag{4.17}$$

where the left hand side of equation (4.17) is SS_E, the first summation term on the right hand side is SS_{PE} and the second summation term is SS_{LOF}. If the error due to lack of fit is higher than the pure error then there is a significant lack of fit in the model, possibly caused by a missing term or lack of transformation. The F_0 test for lack of fit is

$$F_0 = \frac{SS_{LOF}/DF_{LOF}}{SS_{PE}/DF_{PE}} = \frac{MS_{LOF}}{MS_{PE}} \tag{4.18}$$

Models with a high reproducibility can sometimes result in a lack of fit because the pure error is so low. The reproducibility is calculated as such

$$Reproducibility = 1 - \frac{MS_{PE}}{MS_T} \tag{4.19}$$

Therefore the SS_{LOF} may not be of a magnitude that would lead to a lack of fit, but the SS_{PE} is so low that the model appears to have a high lack of fit. This can sometimes be highlighted in the model validity, which gives a measure of lack of fit. The validity is calculated such that a model with a p-value for lack of fit (p_{LOF}) that is less than the confidence interval (α = 0.05) will total < 0.25. Any model that has a high validity will have no lack of fit.

$$Validity = 1 + 0.57647 \times log(p_{LOF}) \tag{4.20}$$

The summary of fit for models **4.1**, **4.3** and **4.4** shows how the high reproducibility can result in a poor model validity (Figure 4.9). The model for ketone **4.4** was fitted and treated according to the techniques described in sections 4.2.2 and 4.2.3 and did not require a transformation.

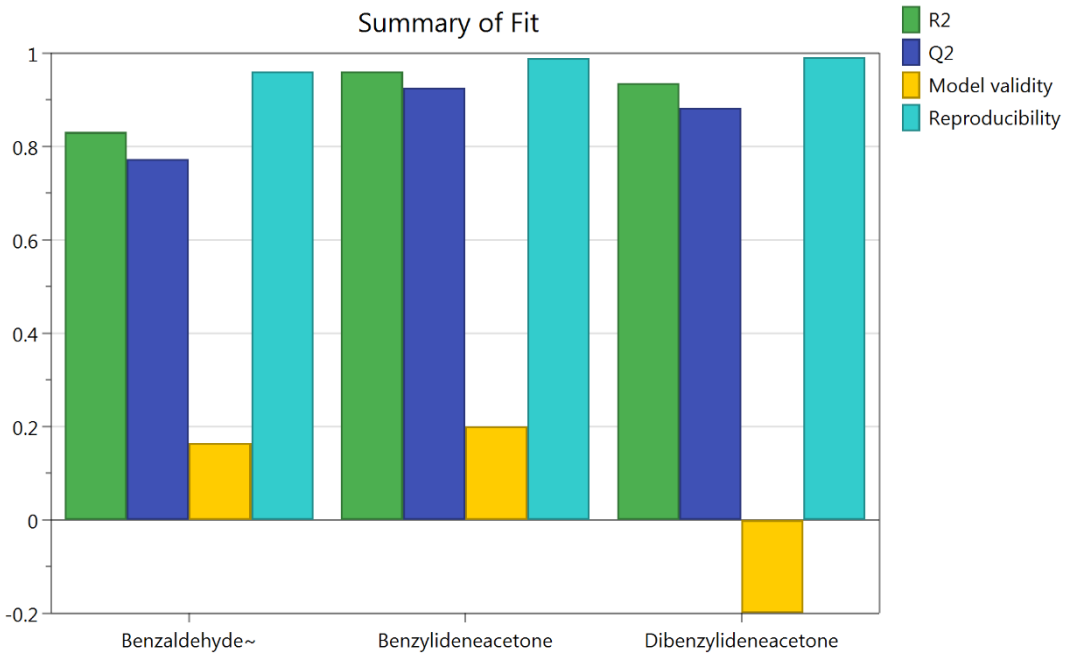

Figure 4.9 Summary of fit for the benzaldehyde **4.1**, benzylideneketone **4.3** and dibenzylideneacetone **4.4**.Green - $\boldsymbol{R^2}$, blue - $\boldsymbol{Q^2}$, yellow – model validity and turquoise = reproducibility.

4.2.6 Optimisations and predictions

The addition of square terms is a feature of RSM that gives the model curvature and means that interpolation and optimisation can be carried out. Optimisations are carried out by minimising or maximising a response within a user defined value using the Nelder-Mead simplex algorithm.[138] This is achieved by calculating a desirability function (d_k) for all of the included models, which normalises the response y to the range

$$0 \leq d_k \leq 1$$

and searches for the variables that predict responses that are closest to the desired targets. If there are multiple model responses then the desirability function will compromise between each target equally.[178] In such a case the compromise is expressed as an overall desirability function

$$ds = \left(\prod_{k=1}^{m} d_k\right)^{\frac{1}{m}} \tag{4.21}$$

where ds is the overall desirability function, m is the number of responses, d_k is the desirability function for each model $k = 1, \ldots, m$. Optimum conditions are achieved by minimising the value of ds. The desirability function has different notation depending on the optimisation requirements.[179, 180] If the response y is to be maximised

$$d = \begin{cases} 0 & y < L \\ \left(\frac{y - L}{T - L}\right)^r & L \leq y \leq T \\ 1 & y > T \end{cases} \quad (4.22)$$

where r is the user defined weight of the desirability function ($0 < r < 1$). If $r = 1$ then the function is linear, if $r > 1$ then the function concentrates on being closer to the target value, choosing a value of $r < 1$ places less emphasis on this response. If the response y is to be minimised

$$d = \begin{cases} 0 & y < T \\ \left(\frac{U - y}{U - T}\right)^r & T \leq y \leq U \\ 1 & y > U \end{cases} \quad (4.23)$$

If the target value (T) is between the lower (L) and upper (U) tolerances, the desirability function is defined as

$$d = \begin{cases} 0 & y < T \\ \left(\frac{y - L}{T - L}\right)^r & L \leq y \leq T \\ \left(\frac{U - y}{U - T}\right)^r & T \leq y \leq U \\ 1 & y > U \end{cases} \quad (4.24)$$

The models were used to predict an optimum yield of ketone **3** by maximising the response of **3** (lower tolerance 65%) and minimising **4.1** and **4.4** (upper tolerance 5%). Optimum conditions were calculated that satisfied the tolerances for responses **4.1** and **4.4**: 1.56 mmol min^{-1} **4.1**, 7.0 eq acetone, 0.11 mmol min^{-1} NaOH and 80.0 °C, generating **4.3** in a 64% yield. These conditions did not match the yield optimum observed by the SNOBFIT algorithm of 0.4 mmol min^{-1} **4.1**, 7.0 eq acetone, 0.099 mmol min^{-1} and 35.8 °C, generating **4.3** in a 66% yield. When the model for ketone **4.3** was used to predict the response from the SNOBFIT optimum conditions, it predicted a yield of 61%.

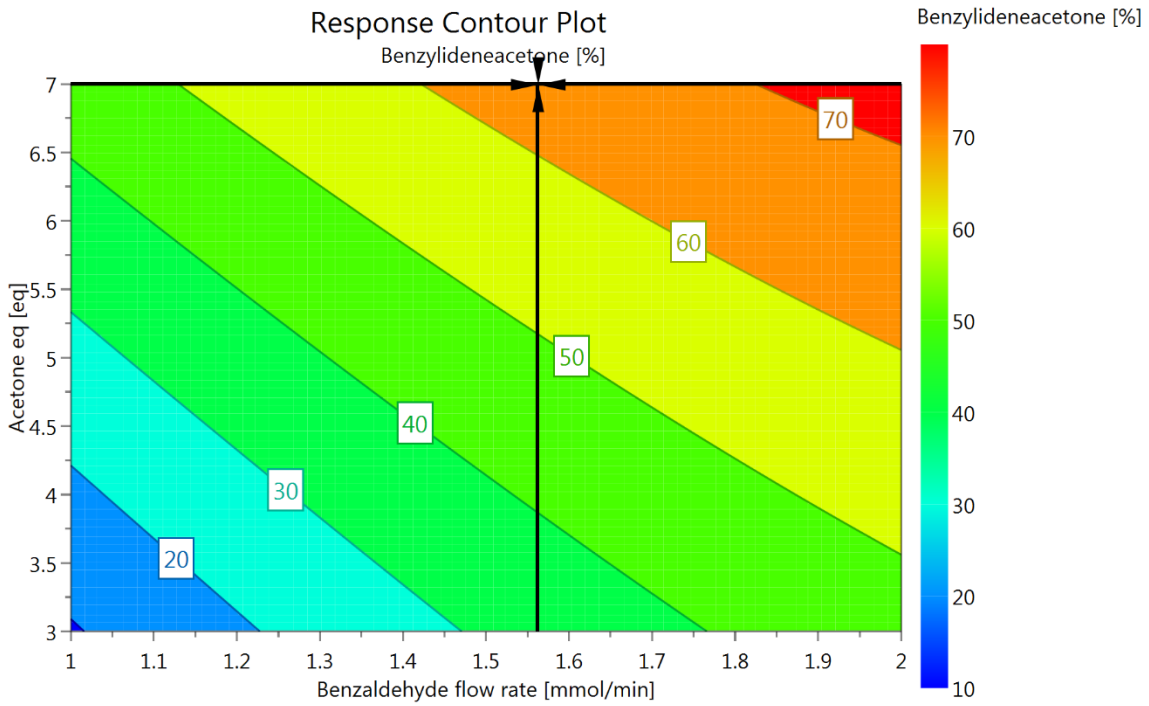

Figure 4.10 Response contour plot for the model of ketone **4.3** where NaOH flow rate (0.11 mmol min^{-1}) and temperature (80.0 °C) are fixed. The black cross-hair shows the predicted optimum conditions to maximise **4.3** and minimise **4.1** and 4.**4**.

A contour plot of fixed temperature and NaOH flow rate shows a strong interaction between benzaldehyde flow rate and equivalents of acetone. The model shows that for a constant response, a reduction in benzaldehyde flow rate leads to a corresponding increase in equivalents of acetone required, which was not initially observed from the SNOBFIT results. In addition the maximum yield the model predicts is at high flow rate and eq, whereas the algorithm optimisation found the highest yields at low flow rate and high acetone eq.

Further scrutiny of the SNOBFIT optimum data point showed that there is a significant rise in yield compared to points in close vicinity. For maximum values of acetone eq and NaOH flow rate, there are a lot of points that are ~59 ±2% creating a plateau that the polynomial of the RSM possibly has difficulty fitting. This, coupled with the disagreement in optima between the two techniques prompted some further experimentation to study the reproducibility of the algorithm optimum. Three further experiments were carried out at the optimum conditions, which generated **4.3** in a mean yield of 64.4% ± 0.3% (arithmetic mean ± 1 SD). This shows that the previous optimum value was possibly caused by an integration error from HPLC analysis. It was decided to carry out a second self-optimisation, expanding on the existing experimental space.

4.3 Improved experimental space

The SNOBFIT algorithm was restarted using the existing data points within the new boundary limits (Table 4.4). The new optimisation required 36 further experiments with an optimum point of 0.76 mmol min^{-1} **4.1**, 14 eq acetone, 0.15 mmol min^{-1} and 43 °C, generating **4.3** in a 67% yield (Figure 4.11). The new optimum is close to the centre of benzaldehyde **1** flow rate and temperature limits, indicating that the new experimental space is an improvement over the original.

Table 4.4 New boundary limits for the second Claisen-Schmidt condensation optimisation

Limits	**4.1** flow rate / mmol min^{-1}	NaOH flow rate / mmol min^{-1}	**4.2** / mol eq	Temperature / °C
Minimum	0.4	0.01	5	10
Maximum	1.0	0.15	14	60

The data collected over the two optimisations were collated into a new data set that included experiments within the ranges shown in Table 4.5. This was an attempt to include as many experiments as possible in an experimental space that would deliver good fitting and accurate models.

Table 4.5 Boundary limits for the second generation RSM models

Limits	**4.1** flow rate / mmol min^{-1}	NaOH flow rate / mmol min^{-1}	**4.2** / mol eq	Temperature / °C
Minimum	0.4	0.008	1	10
Maximum	1.0	0.15	14	60

New MLR models were fitted according to the techniques discussed in Section 4.2. No transformations were required and each model either had values for all summary of fit terms that were either an improvement over the first models, or within the same magnitude. The exception is for the model validity, which saw a large improvement for all three models, with models **4.1** and **4.3** no longer showing evidence for lack of fit (Figure 4.12).

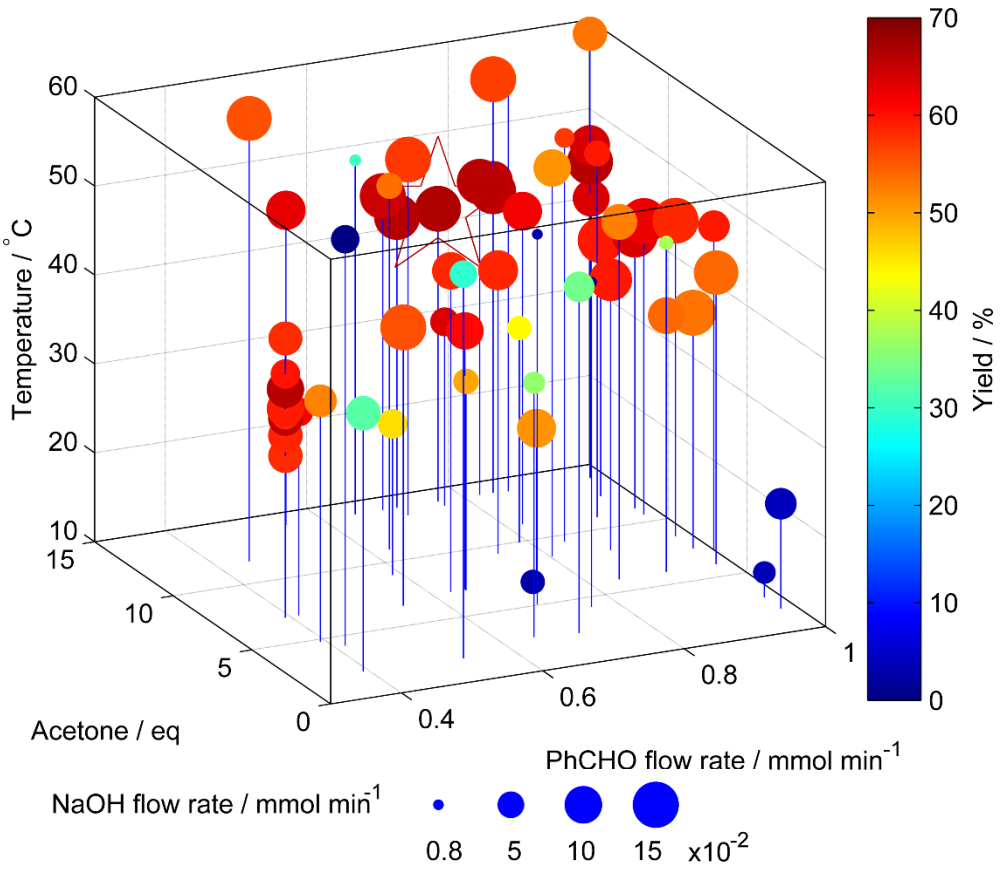

Figure 4.11 Plot for the SNOBFIT optimisation of ketone **4.3** using an improved experimental space. x-axis = **4.1** flow rate; y-axis = acetone eq; z-axis = temperature; size of the point denotes NaOH flow rate; colour of the point denotes yield. The optimum point is denoted by the star: 0.76 mmol min^{-1} **1**, 13.9 eq acetone, 0.15 mmol min^{-1} and 43.0 °C generating **3** in a 67% yield.

The new models were used to predict an optimum yield by maximising **4.3** and minimising **4.1** and **4.4** with the conditions 0.57 mmol min^{-1} **4.1**, 12.3 acetone eq, 0.09 mmol min^{-1} NaOH and 50 °C, generating ketone **4.3** in a 63% yield. These optimum conditions were in greater agreement with the SNOBFIT optimum when compared to the original experimental space. This re-enforced that the new boundary limits had improved the experimental space explored.

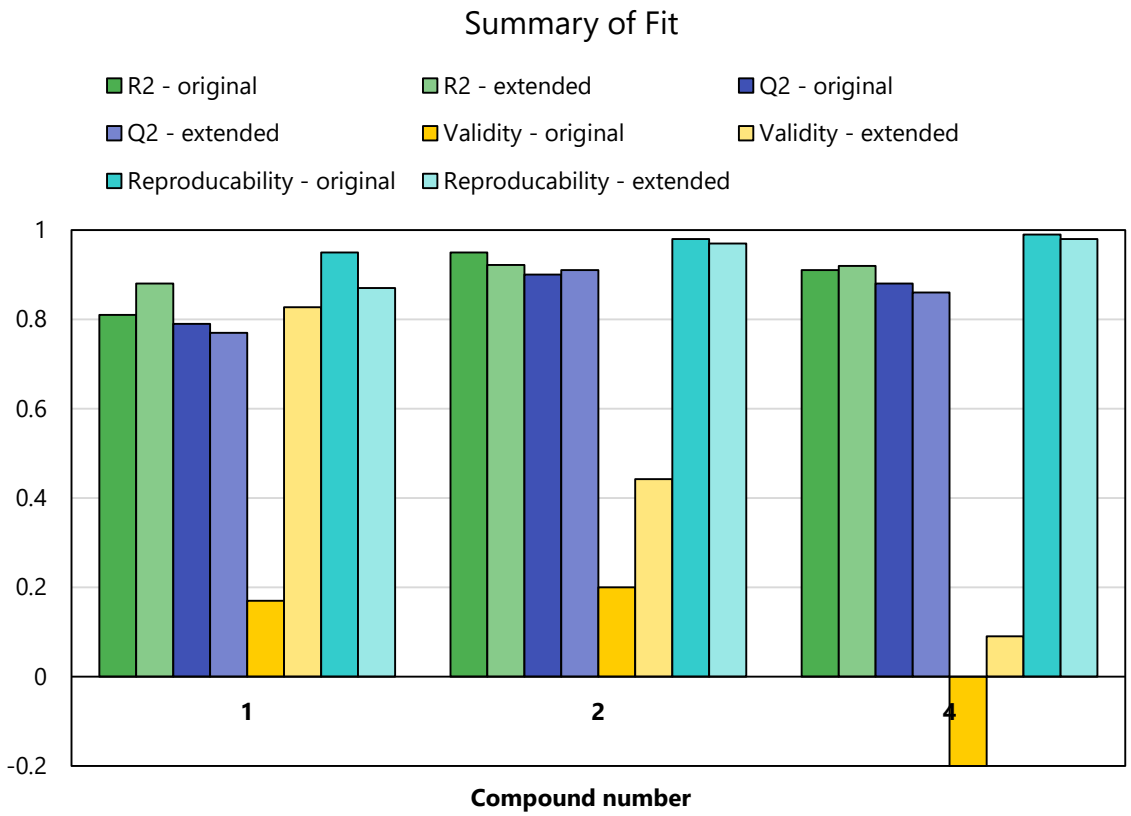

Figure 4.12 Comparisons of summary of fit terms for the original (solid colour) and extended (faded colour) experiment spaces. Green - $\boldsymbol{R^2}$, blue - $\boldsymbol{Q^2}$, yellow – validity, turquoise – reproducibility.

4.3.1 Reaction metrics

It is possible to try and increase the yield of ketone **4.3** by increasing the limits for acetone eq and NaOH flow rate, however it is worth considering if the increase in reagent eq would be worth the financial and material cost, especially for reaction scale up. Especially as doubling the eq of **4.2** only resulted in an increase of 1% yield. Although yield was the target function for the optimisations so far, previous research has shown how yield is not the best target and other metrics such as E-factor, process mass intensity (PMI), material cost and reaction productivity can be a better target for an efficient manufacturing process.[12, 17, 18, 27, 181] The advantage of a statistical model means that additional responses can be calculated and new models fitted without carrying out further experiments, whereas algorithm optimisations need new experiments to find new optima.

Therefore, metric analyses were carried out by calculating the values for different metrics from the experiments used to fit the existing models. The new metrics were PMI, a measure of the total chemical resource per mass unit

$$PMI = \frac{\sum_{i=1}^{n} Q_m(i)}{Q_n(\mathbf{4.1})\, Y\, MW(\mathbf{4.3})} \tag{4.25}$$

where Q_m is mass flow rate, Q_n is molar flow rate, Y is yield and MW is molecular weight;[182] Space time yield (STY), the mass of product per unit volume per unit time

$$STY = \frac{Q_n(\mathbf{1})MW(\mathbf{3})}{V} \tag{4.26}$$

where V is reactor volume; and material cost per mass unit of ketone **4.3** produced

$$Cost = \frac{\sum_{i=1}^{n} Q_v(i)\, £(i) C_0(i)}{Q_n(\mathbf{4.1})\, Y\, MW(\mathbf{4.3})} \tag{4.27}$$

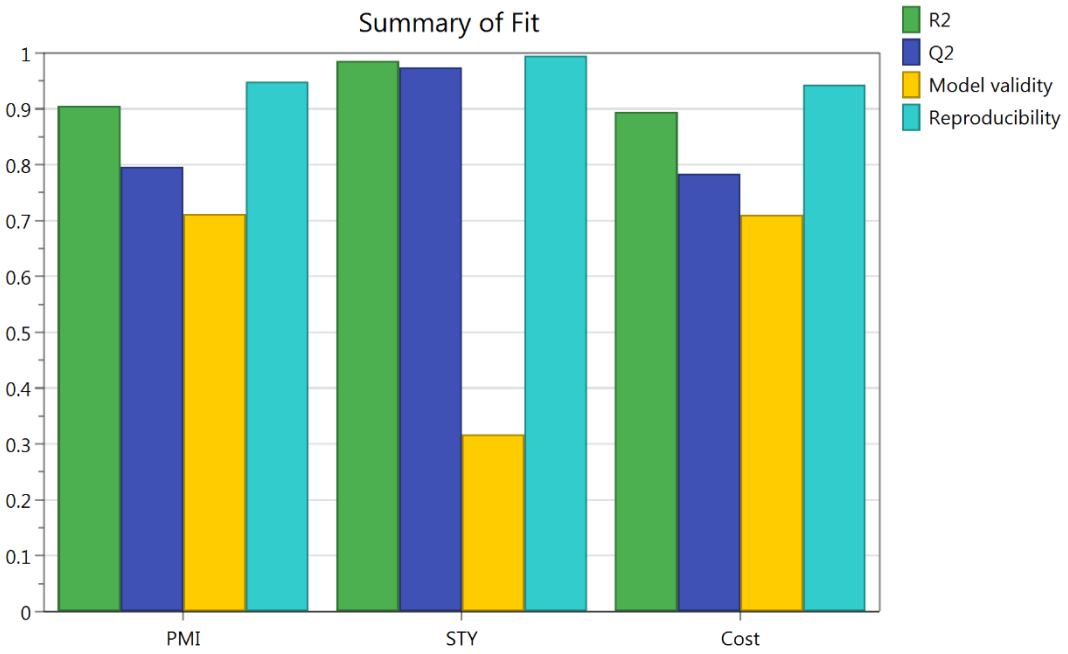

Figure 4.13 Summary of fit for the new metrics. Green - $\boldsymbol{R^2}$, blue - $\boldsymbol{Q^2}$, yellow – validity, turquoise – reproducibility.

New models for these metrics were fitted using MLR with R^2 values of 0.93 (PMI), 0.92 (STY) and 0.90 (cost); and Q^2 values of 0.86 (PMI), 0.86 (STY) and 0.83 (cost). Each model also had high reproducibility (> 0.9) and no evidence of lack of fit (Figure 4.13).

Table 4.6 Effect of different metrics on the product composition of compounds **1**, **3** and **4**

Metric target	**4.1** / %	**4.3** / %	**4.4** / %	PMI / kg kg^{-1}	STY / g L^{-1} h^{-1}	Cost / £ kg^{-1}
Yield	*3.22*	**65.62**	*3.01*	18.48	633.20	33.45
PMI	4.54	47.90	6.02	*13.81*	614.36	27.92
STY	3.06	62.15	4.45	19.11	**872.69**	34.50
Cost	4.15	58.81	4.13	14.30	798.39	*26.72*
Yield PMI[a]	*4.28*	**55.32**	*4.70*	*13.99*	729.52	26.91
PMI Cost[b]	2.96	64.81	3.66	*16.35*	769.93	*29.57*

The first column shows the metric target, responses are shown in the rows. Maximized values are highlighted in bold, minimized values and highlighted in italics. Unformatted values display the models' predicted values. [a]maximize the yield of 3, minimize the PMI; [b]minimize both PMI and cost.

Table 4.6 shows how the model responses change with optimum conditions for different metric targets. The maximum yield has poor responses for PMI, STY and cost, showing that high yielding reactions are wasteful and unproductive. The optimum response for PMI is the least productive and predicts the lowest yield of ketone **4.3**. There is good correlation between the responses of PMI and cost for all the metric targets. This should be expected as they are calculated by the ratio of product to substrates and reagents. The raw material cost calculation aims to put bias on reducing the excess of expensive material, although this reaction example is perhaps not the best to show this as all substrates are relatively inexpensive. It should be noted, however, that lower cost promotes a higher yield rather than lower PMI, indicating that raw material cost could be the most important metric, assuming that a cheaper reagent does not increase the complexity, and therefore cost, of work-up and purification.

The conditions for the optimal responses are shown in Table 4.7. The flow rate of **4.2** is towards its upper limits for every target which reduces the residence time, therefore increasing the reaction productivity (STY). The acetone equivalents are generally lower than the self-optimisation thus limiting the reagent waste (PMI and cost). Strict temperature control is required to both maintain the high yields of **4.3** and minimise polymer formation.

Table 4.7 Predicted conditions for the optimum responses to different metric targets

Metric target	**4.1** flow rate / mmol min^{-1}	NaOH flow rate / mmol min^{-1}	**4.2** / mol eq	Temperature / °C
Yield	0.741	0.112	12.4	47.2
PMI	0.846	0.044	6.0	44.1
STY	1.000	0.150	13.9	42.2
Cost	0.986	0.067	9.2	47.1
Yield PMI[a]	0.915	0.055	7.5	45.5
PMI Cost[b]	0.998	0.096	10.5	46.8

[a]maximize the yield of 3, minimize the PMI; [b]minimize both PMI and cost.

4.4 Conclusions

The yield of ketone **4.3** in a Claisen-Schmidt condensation was self-optimised using an automated flow reactor equipped with an at-line HPLC system and feedback loop with SNOBFIT algorithm. With the data obtained from the self-optimisation, response surface models were fitted to the main compounds of interest in the reaction (**4.1**, **4.3** and **4.4**). After analysis of the models and self-optimisation data, it was decided to carry out further optimisations in a larger chemical space. The second experimental optimisation improved upon the yield of **4.3** and the increased correlation between the new optimum and surrounding experimental points, provided a greater range of conditions at which optimal yields could be obtained. The subsequent statistical models of the extended optimisation predicted similar optimal conditions and exhibited an overall improved model fit.

It should be noted that the choice of algorithm in the initial self-optimisation step is critical to achieving a good fit to the RSM. The simplex algorithm and modifications thereof,[137-139, 183] is a popular choice in self-optimising systems.[12, 14-17, 23, 25, 27] However, during its operation it will only execute experiments with an improved predicted response therefore not providing any information about experimental space that does not lie between the initial and optimum points. The execution of random conditions and exploration of free space offered by SNOBFIT provides a scatter of data, without which the additional response surface fitting would not be possible. In this study, the increased robustness resulting from the additional experimental points around the optimum would also have been forfeited with a simplex approach.

Because the experimental optimum was identified at the edge of the initial optimisation space, prediction of the optimum *via* the statistical model was compromised due to its inability to fit a polynomial to changes induced by the cliff edge. The experimental self-optimisation, however, freely explored the edge of the optimisation space to identify the point of maximum yield. For these reasons, it can be concluded that self-optimisation is the superior technique for chemical process optimisation. However, when used in tandem the subsequent response fitting of self-optimisation data can predict the responses of different species and even alternate metrics without additional experimentation. It therefore follows that self-optimisation and DoE can be interdependent, rather than conflicting techniques, which can combine to provide a wealth of information in the scale-up and process optimisation of chemical systems.

5. Adaptive feedback controlled optimisations using at-line quantitative mass spectrometry[7]

5.1 Introduction

Online analysis describes the *in-situ* monitoring of a chemical reaction by any analytical technique without any manual intervention from the user. This can be separated into two distinct categories: at-line analysis, which describes the automated extraction of a reaction aliquot for analysis; and inline analysis, which describes the direct analysis of the whole reaction by the analytical equipment.

Quantitative online analysis is a requirement for the optimisation of reactions using an adaptive feedback loop. Self-optimisation has been carried out using UV-Vis,[11] IR[18, 27, 97, 184] and NMR spectroscopy;[25] and gas[15-18, 23] and liquid chromatography.[12, 14, 21, 172, 185] Depending on the self-optimising setup, the analysis time can have the highest contribution to the overall optimisation time, especially if using an algorithm where the results of the previous experiment are required before calculating a new one.[18] The criteria for the ideal analytical techniques are:

- Quantitative – must be able to accurately calculate the response
- Short method lengths – minimising the amount of time that the reactor is left idle
- Simple data analysis – allows fast acquisition of experimental response from the analytical data file
- Minimal method development – reduces the time it takes to develop the analytical method, enabling an easier process for the user
- Easy (or no) calibration of response – reduces the equipment setup time prior to starting the optimisation
- Minimal data analysis by chemometrics required – analytical data provides the discrete composition of all species, without requiring complex deconvolution
- Can monitor unknown species – provides information about the composition of by-products and/or impurities

[7] Themes from this chapter appear in: N. Holmes, G. R. Akien, R. J. D. Savage, C. Stanetty, I. R. Baxendale, A. J. Blacker, B. A. Taylor, R. L. Woodward, R. E. Meadows and R. A. Bourne, *React. Chem. Eng.*, 2016, **1**, 96-100.

- Can identify unknown species – provides information about the structure of by-products and/or impurities

In a laboratory environment, online analytical equipment is typically denoted as "benchtop" and is designed to have a smaller footprint, thus making it easier to fit into a fumehood and integrate with existing equipment. Benchtop machines typically generate data at a lower resolution to their offline counterparts but are easier to use for a non-specialist. As is shown in Table 5.1, there is not an existing analytical technique that satisfies all the criteria, however mass spectrometry (MS) satisfies most. Despite this, it is surprising that online MS is sparingly used to monitor reactions. Existing examples in flow reactors are only qualitative[27, 118, 186-188] and quantitative monitoring has required the use of specialist spectrometers.[189-191]

Table 5.1 Properties of online analytical techniques

	UV	IR	NMR	GC	HPLC	MS
Quantitative	●	●	●	●	●	●
Short method length	●	●	●			●
Simple data analysis			●	●	●	●
Minimal method development	●	●	●			●
Easy calibration			●	●	●	
No requirement for chemometrics				●	●	●
Monitor unknown species				●	●	●
Identify unknown species		●	●			●

UV – ultraviolet/visible spectroscopy, IR – infrared spectroscopy, NMR – nuclear magnetic resonance spectroscopy, GC – gas chromatography, HPLC – liquid chromatography, MS – mass spectrometry. N.B. all criteria are applied to general benchtop specification and might change depending on the reaction case study.

MS is an analytical technique that measures the mass of a charged compound and can separate multiple species according to their mass to charge ratio (*m/z*). A compound is charged by ionisation, which is achieved using a variety of techniques. Electrospray ionisation (ESI) is the most common technique for measuring the mass of organic compounds and therefore is the most available for benchtop spectrometers. ESI generates ions by injecting the liquid sample through a nebulising needle into an electrically charged chamber, creating a mist of positively charged droplets. The chamber is exposed to hot dry gas, which evaporates solvent from the droplets. As the amount of solvent evaporates, the repulsive electrostatic forces exceed the surface tension of the droplet and it desorbs into the gas phase, where it is attracted to pass through a negatively

charged capillary and into the mass analyser (Figure 5.1). ESI can sometimes create multiply charged species and is best used for large polar molecules.

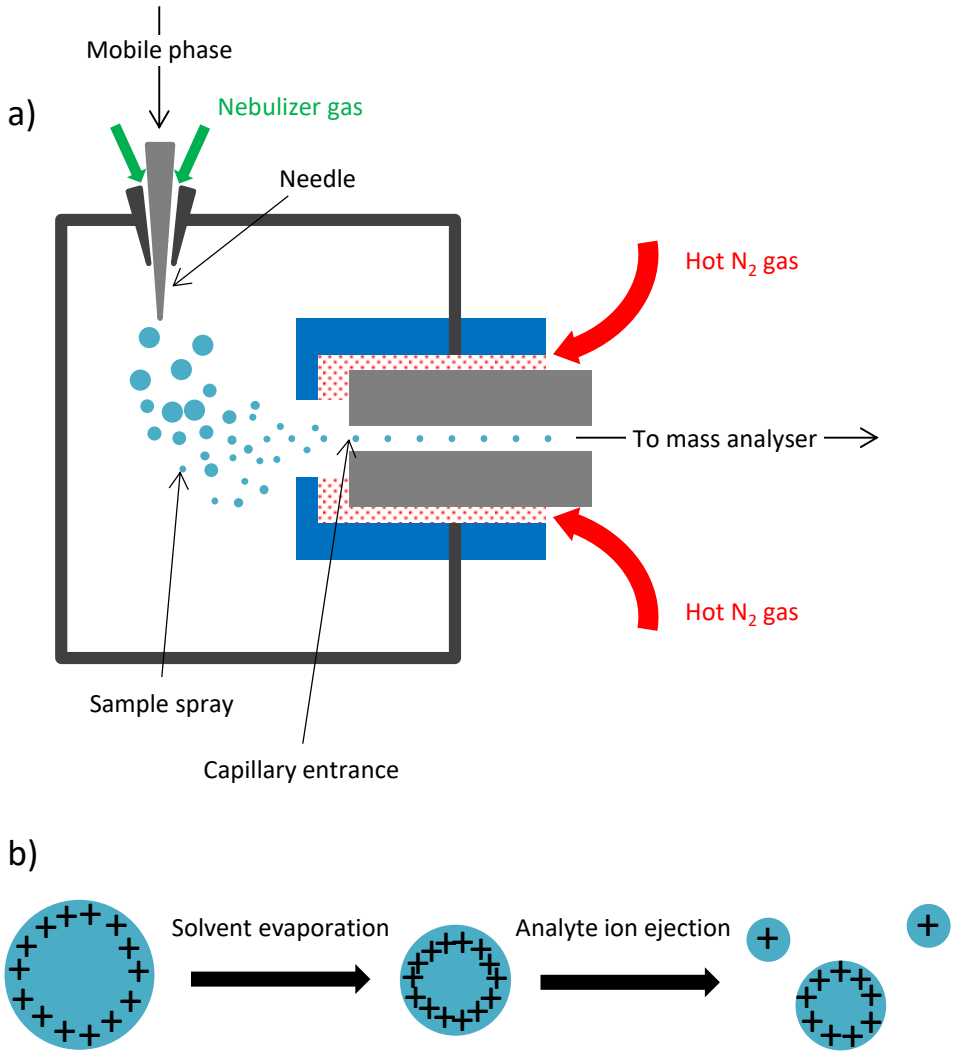

Figure 5.1 a) Diagram of ESI ion source. Liquid sample is injected through needle and nebulised to produce a spray. Hot N_2 gas aids desorption of the spray to create a positively charged mist that is attracted to the capillary tube and fed to the mass analyser. b) Desorption of sample to produce a positively charged analyte mist. Figures adapted from ref [192].

Atmospheric pressure chemical ionisation (APCI) is a similar ionisation technique to ESI. The liquid sample is heated to very high temperatures using a hot nebulising gas stream, which transfers the sample into the gas phase. The gas particles are then charged by being exposed to electrons that are generated from a corona discharge needle. Like ESI, these charged gas particles are then attracted through a capillary into the mass analyser. APCI generally does not create multiply charged species and it best used for smaller polar and non-polar compounds that will not undergo thermal degradation.

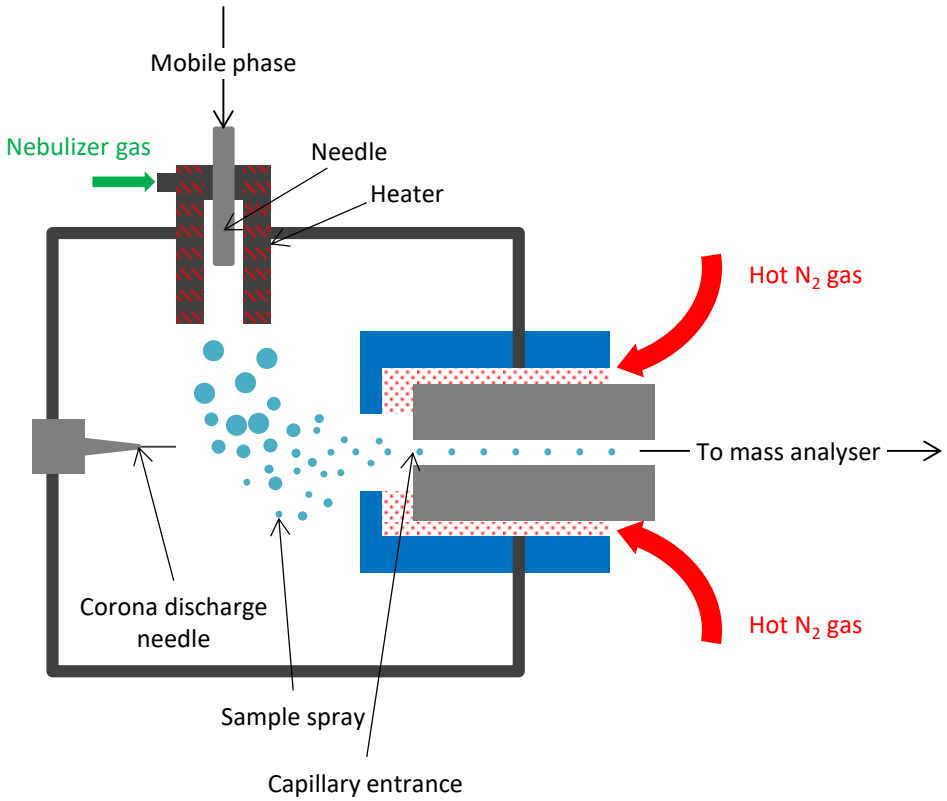

Figure 5.2 Diagram of APCI ion source. Liquid sample is nebulised using a hot gas stream and the gaseous particles are then charged with electrons from a corona discharge needle. Adapted from ref [192].

Both APCI and ESI are classified as soft ionisation sources because they generate a large quantity of molecular ions with minimal fragmentation ions. ESI is typically used for molecules with a high polarity and large molecular weight because of its ability to generate multiple positively charged species. APCI is suited to compounds with a lower polarity and molecular weight.[192-195] The molecular weight range is much lower for APCI because the high temperatures during its ionisation procedure can make it unsuitable for thermally labile compounds (such as enzymes and proteins). As a result ESI generally performs better at ionising cationic or anionic compounds whereas APCI is better at neutral or basic compounds.[195]

The main reason for the lack of examples using online quantitative MS is due to the difficulty in calibrating a signal that has a variable sample matrix. Existing analytical techniques use a calibration curve where a number of samples are prepared at different concentrations then a plot of response vs concentration will have a straight line fit. However this is not representative of the signal when using MS due to a phenomenon called “matrix effects”.[196] The sample matrix describes everything else in the sample that is not the desired analyte (e.g. reaction solvent, mobile

phase solvents and modifiers, reagents, substrates, by-products, impurities etc.) and these can supress the response of the analyte resulting in an unpredictable response that changes with reaction conditions[197-199] and MS method.[186]

There are several examples of inline MS analysis of flow reactions, where the reactor outlet is fitted to capillary tubing directly into the spectrometer, resulting in full destruction of the sample;[200-208] and using multiple ionisation techniques that are unfortunately unavailable with commercial benchtop spectrometers.[117] This technique also means that reactions have to be performed at very low concentrations and therefore are not representative of kinetics at manufacturing scales.

One of the first examples of monitoring a reaction at process relevant concentrations using atmospheric pressure ionisation (AtmPI) MS was reported by Dell'Orco *et al.* for the Knoevenagel condensation to produce an intermediate **5.3** towards eprosartan, an angiotensin II receptor antagonist, using a batch reactor (Scheme 5.1).[209] The MS setup featured a series of HPLC pumps to sample the reaction then quench and dilute by 3000 fold before ESI-MS analysis. The work was used to identify reaction intermediates and propose a mechanism, which aided separate kinetic investigations. The MS data was not used to determine the kinetic parameters due to the difficulties in calibrating all species, some of which were only stable in solution.

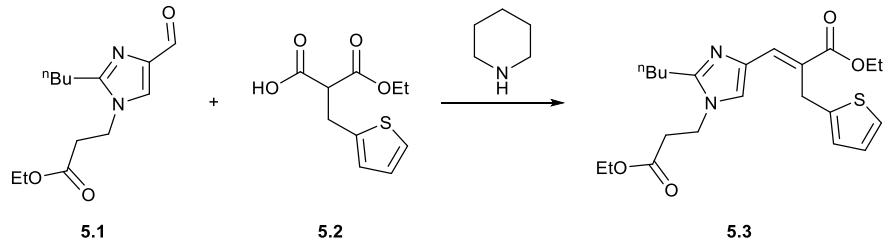

5.1 **5.2** **5.3**

Scheme 5.1 Knoevenagel condensation reaction to intermediate **5.3** towards eprosartan

Quantitative MS analysis was achieved by Owen *et al*. for the base catalysed esterification of butyl acetate **5.7** from acetic anhydride **5.4** (Scheme 5.2).[191] The reaction was carried out at two different scales using batch reactors and was monitored online by ATR-IR and ESI-MS and offline by GC. Calibration of the MS signal was carried out by applying a least squares linear regression fit to the reaction data from the response of the pure components of acetic anhydride, acetic acid, butyl acetate, butanol, pyridine, ethanol and ethyl acetate.

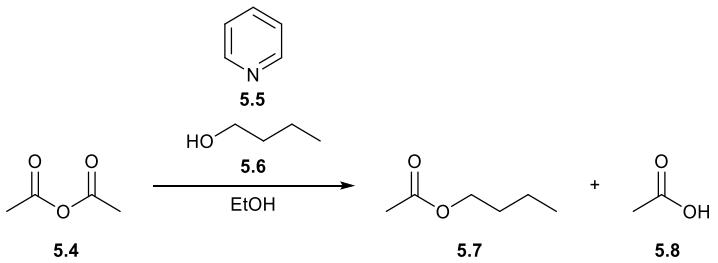

Scheme 5.2 Base catalysed hydrolysis and esterification of butyl acetate.

Zhu *et al*. monitored a Michael addition between 2-phenylethylamine **5.9** and acrylonitrile **5.10** to form 3-phenethylamino-propionitrile **5.11** using APCI-MS (Scheme 5.3).[190] The reactants were placed in a syringe then infused (using a syringe pump) through a 4-port microvolume internal sample injector, replicating a batch reaction that continually refreshes the sample delivered to the MS. Quantification of the MS signal was achieved by preparing stock solutions and binary mixtures of the starting amine and product at concentrations ranging from 0.165 to 1.65 mol L^{-1}. These calibration curves showed a linear response across the experimental range covered and could be used to show the change in concentration of the two species over the course of the reaction.

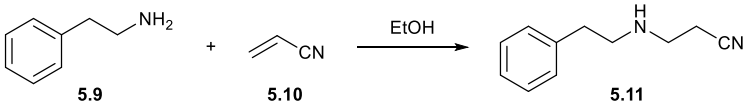

Scheme 5.3 Michael addition between 2-phenylethylamine **5.9** and acrylonitrile **5.10** to form 3-phenethylamino-propionitrile **5.11**.

The above quantitative techniques are possible due to the availability of pure compounds, the linearity of the response and, most importantly, the predictable composition of species in the reaction. Other calibration techniques require the first two points but not the final. For example, when monitoring a reaction by chromatography, where the compounds of interest have been calibrated by calculating relative response factors, the response from the machine does not change with the amount of reagent or catalyst added to the reaction; and therefore the calibration does not need to be recalculated for changing reaction conditions. However, in the Michael addition by Zhu, the amount of acrylonitrile is kept constant throughout the reactions. Whilst the compound is not detected by the MS, it is likely that it is still ionised and therefore its concentration in the reaction will change the potential for the other compounds to be ionised thus changing their response.

Moreover, both quantified techniques have been carried out using modified analytical equipment, which would be daunting for a non-specialist to use.

5.1.1 Aims and objectives

It is the aim of the work in this chapter to use a benchtop MS for quantitative analysis of the automated optimisation of the amidation of methyl nicotinate **5.12** with methylamine to form *N*'-methyl nicotinamide **5.13** (Scheme 5.4). The cheapest commercial source of methylamine is available in an aqueous solution, which promotes the hydrolysed nicotinic acid **5.14** as an impurity in the reaction. The presence of the pyridine group should provide a good site for ionisation and high loadings of methylamine may cause suppression of the MS response.

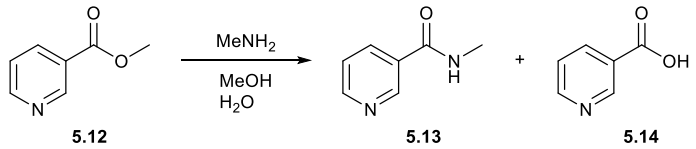

Scheme 5.4 Amidation of methyl nicotinate **5.12** with methylamine in methanol and water to form the desired N'-methyl nicotinamide **5.13** or the hydrolysed nicotinic acid **5.14**.

The objectives for this work were:

- Develop a method to use fast sample acquisition (<1 min) to identify steady state within the reactor.
- Calibrate the MS response and calculate response factors for the three compounds of interest (**5.12**-**5.14**).
- Optimise the reaction using adaptive feedback controlled minimising algorithm.

5.2 Mass spectrometry and reactor setup

5.2.1 Equipment

The reactor was configured as shown in Figure 5.3; three pumps were used to deliver the ester **5.12**, methylamine and methanol. Pump reservoir solutions were prepared to concentrations of 1.45 mol L^{-1} ester **5.12** in methanol and 5.77 mol L^{-1} of methylamine in water (unless otherwise stated). A length of tubing equalling 3 mL was fitted to the reactor. A detailed description of the equipment used is available in the equipment chapter; preparation of pump reservoir solutions is available in the experimental chapter.

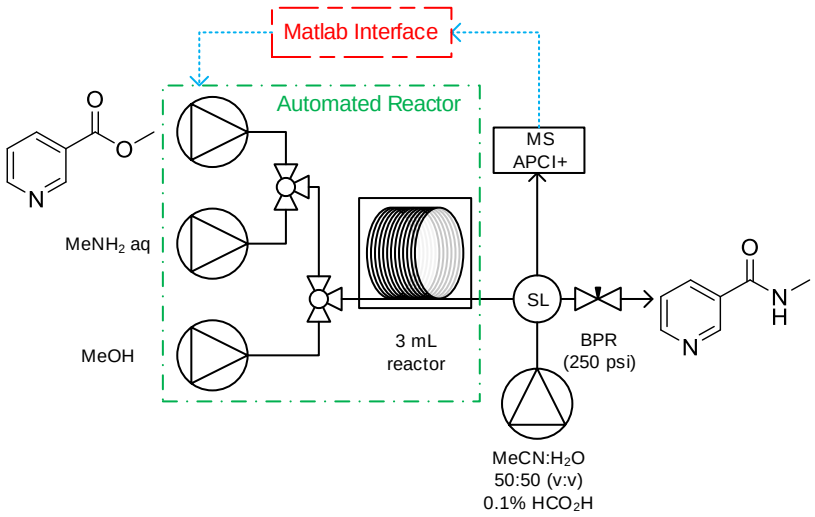

Figure 5.3 Reactor set-up for the optimisation of *N'*-methyl nicotinamide **13**.

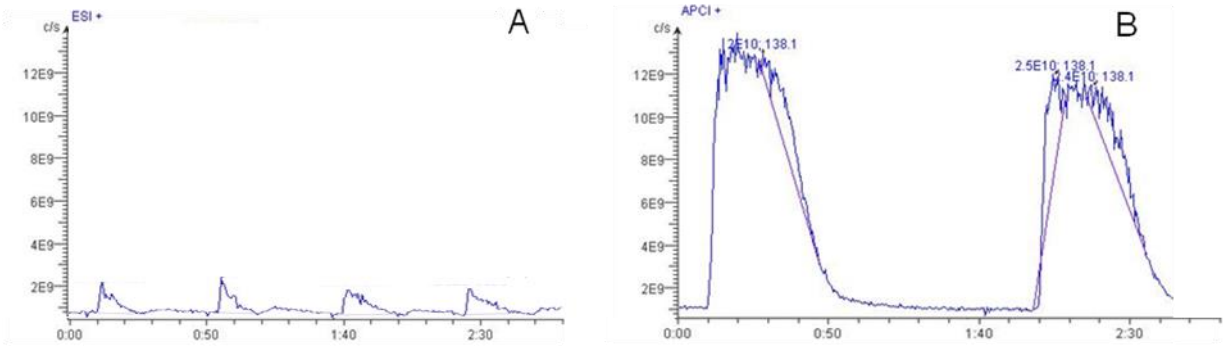

Figure 5.4 Comparison of sampling frequency for ESI+ (A) and APCI+ (B) over a 3 minute period.

The spectrometer used for all online analysis was an Advion expression CMS[210] operating using APCI+ ion source. The machine is capable of operating with either ESI± or APCI+, and whilst a higher frequency of sampling was possible with ESI, APCI was chosen for its reduction in baseline noise (Figure 5.4), higher mobile phase flow rate tolerance, increased signal strength and reduced likelihood of ion suppression.[199] Reaction aliquots were introduced to the mobile phase using a 4-port VICI micro-volume sampling valve. It is possible to sample MS quasi-continuously using a mass rate attenuator,[211, 212] which delivers aliquots of volume 20 to 300 nL at a frequency of up to 2 Hz at a constant sample concentration. The advantage with this approach is that real-time monitoring is achieved with the continuous sampling; however it is difficult to detect accumulation of analyte within the spectrometer.

A mobile phase of 1:1 (v:v) MeCN:H_2O with 0.1 % formic acid modifier was pumped using an agilent G1311A quaternary pump module. Agilent stainless steel capillary tubing (green, 0.17

mm ID) delivered the mobile phase to the sample loop and PEEK tubing (red, 0.005" ID) from the sample loop to the spectrometer. All other equipment is described in the equipment chapter.

A 2:5 flow splitter was created by connecting 6.5 and 16.5 cm PEEK tubing (red) to a PEEK microvolume tee-piece (rheodyne), where the input was sample in mobile phase. The shorter tubing was directed to waste and the longer tubing to the APCI input. The change in pressure drop between the different tubes was used to control the flow ratios. The mobile phase flow rate to the MS was calculated to be 0.057 mL min^{-1}, based on a flow rate of 0.200 mL min^{-1} from the pump (0.200 mL $min^{-1} \times \frac{2}{7} = 0.057$ mL min^{-1}).

Assuming that the sample injection into the mobile phase is the same as two fluid streams meeting in a tee-piece with a total flow rate of the mobile phase flow rate, the maximum concentration of **5.12**-**5.14** can be calculated

$$C_X = \frac{C_A q_X}{Q} \tag{5.1}$$

where C_X is the concentration of analyte (mol L^{-1}), C_A is the concentration of nicotinic species in the reactor (mol L^{-1}), q_X is the theoretical flow rate from the sample loop injection (L min^{-1}) and Q is the total flow rate of mobile phase. Assuming that the reservoir of **5.12** is pumped without any other pump streams, the analyte concentration is calculated

$$C_X = \frac{1.45 \text{ mol L}^{-1} \times 0.06 \times 10^{-3} mL\ min^{-1}}{0.200\ mL\ min^{-1}} = 4.35 \times 10^{-4} mol\ L^{-1}$$

and when accounting for the split ratio

$$C_X = \frac{2}{7} \times 4.35 \times 10^{-4} mol\ L^{-1} = 1.24 \times 10^{-4}\ mol\ L^{-1}$$

The concentration of the analyte within all reactions will depend on the ratio of methylamine flow rate to ester **5.12** flow rate. For example, if the ester and methylamine pumps are set to the same flow rate, the total of all nicotinic species in the reactor (C_A) will be 0.725 mol L^{-1} and the analyte concentration will thus be 6.21×10^{-5} mol L^{-1}.

Product composition from MS is determined from two separate chromatograms: total ion chromatogram (TIC), which calculates the total number of ions detected over a time period; and extracted ion chromatogram (XIC), which calculates the number of ions for a specific mass over

the same time period. The composition of a product is calculated from the ratio between the XIC and TIC. Advion Mass Express software was used to record all chromatograms and the program would bin mass peaks to the nearest 0.5 mass unit (Dalton, Da) and then create a data report in a .cdf format. Data could be extracted from the .cdf file using MatLab commands and a script was written to calculate the XIC for a particular mass over all of the sample range. A percentage yield was calculated from the ratio between the desired XIC and the XIC for all known compounds.

5.2.2 Steady state determination

In a batch reactor the relative concentrations of species in the reactor change with respect to time. In a plug flow reactor, the relative concentrations change with respect to the length of the reactor tubing or channel.[213-215] Therefore, a sample acquired at a fixed point in a continuous reactor will have constant composition, assuming the conditions remain constant throughout the reactor's residence time. This concept is known as steady state and is fundamental for the performance of a reaction in flow. The time to reach steady state depends on the physical dimensions of the reactor, which firstly affects the dispersion, where the frictional forces from the walls of the reactors result in a non-uniform flow velocity across the tube; and secondly the residence time distribution, which describes the average amount of time the fluid spends in the reactor.[213]

It is typical for the material from the first two reactor volumes to be disposed of before analysis of the reaction is carried out, which obviously creates a large amount of waste. Online IR has been used to detect the steady state of a reactor due to its fast acquisition time. It is hypothesised that the same approach can be achieved with MS.

To test this, the reactor was set up according to the configuration shown in Figure 5.3, with methanol replaced with isopropyl alcohol. Ester **5.12** was prepared to 0.787 mol L^{-1} in methanol, and methylamine was used as a 40 % (w/v) aqueous solution without any modification. The reactor was set to 30 °C then **5.12** pumped at 0.200 mL min^{-1} and methylamine pumped at 0.023 mL min^{-1} (2 mol eq) for 30 min; MS acquisition was set to a period of 1 min. Solvent was then pumped for 10 min at 0.500 mL min^{-1} to clean the reactor, prevent accumulation in the MS and check that the MS response returns to zero. This cycle was then repeated using 3 and 4 mol eq of methylamine

(full conditions shown in Table 5.2). The mobile phase was as stated above but without the splitter, resulting in a total flow rate of 0.200 mL min^{-1}.

Table 5.2 – Conditions screened to test steady state

12 flow / mL min-1	MeNH2 flow / mL min-1	IPA flow / mL min-1	Duration / min	Time from start / min
0.200	0.023	0	30	30
0	0	0.500	10	40
0.200	0.034	0	30	70
0	0	0.500	10	80
0.200	0.046	0	30	110
0	0	0.500	10	120

The results from the steady state test (Figure 5.5) showed that linearity of the MS signal was reached when the standard deviation in the internally normalised data (0-100) was less than 1.5 %, corresponding to an analytical error of ± 0.75%.

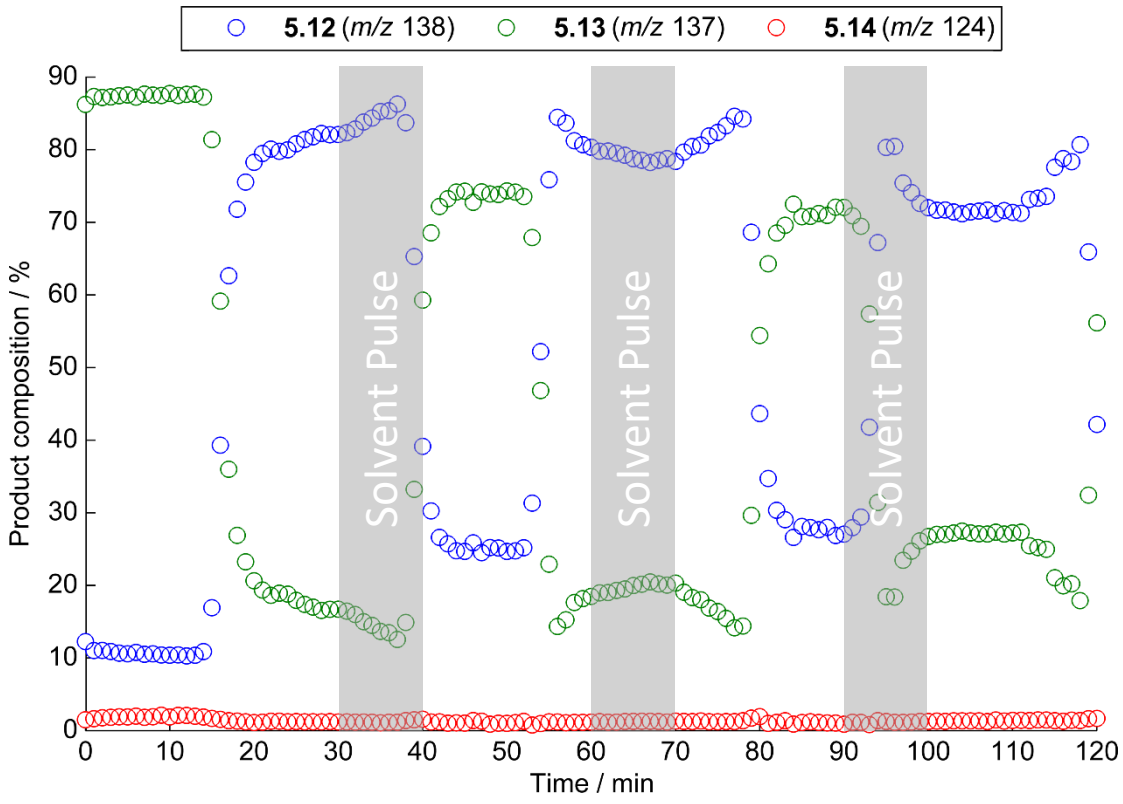

Figure 5.5 Test for steady state monitoring by MS. The graph shows change in MS ion count for compounds **5.12-5.14** over total time. The reactor was initially filled with solvent, and then pumped with the desired reagents. The signal of all three compounds changes as the reactor reaches the outlet (~20 min). Linearity is reached, indicating steady state, then the signal for all three compounds drops when the reactor is flushed with solvent (30-40 min). This cycle is repeated a further two times.

If steady state was calculated based on 2 reactor then this would be 27 min (1st experiment), 26 min (2nd) and 24 min (3rd). However Figure 5.5 shows that linearity in the signal, and therefore the true reactor steady state, is reached before these calculated values; indicating that time can be saved by detecting when the reactor reached steady state rather than calculating it. Using this data it was possible to construct a steady state function to run during the automated optimisations (Figure 5.6). Development of optimum split ratio and mobile phase flow rate resulted in an MS method of 25 s allowing a sampling period of 40 s during optimisations.

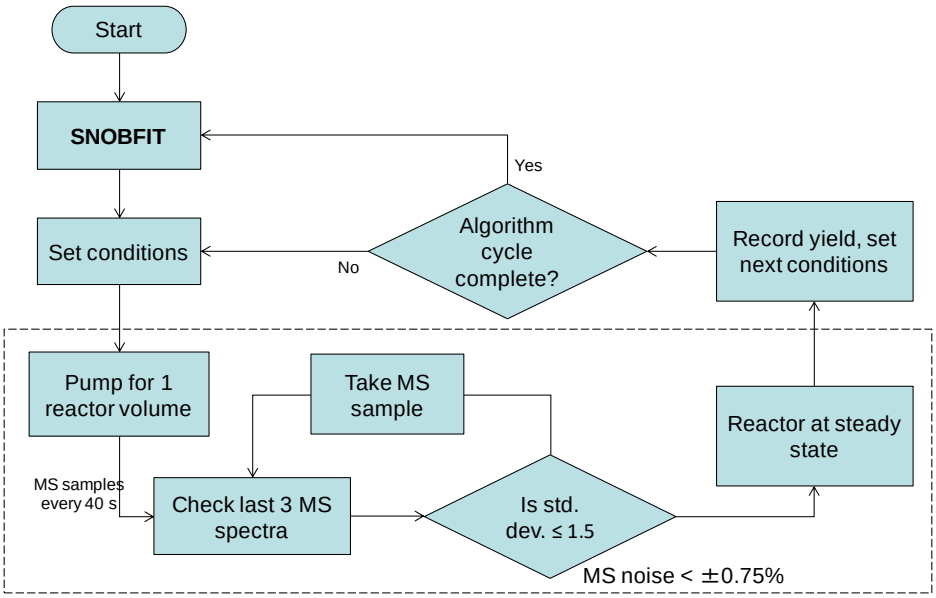

Figure 5.6 Flow chart showing the optimisation process with steady state function (dashed lines)

5.3 Calibration

Quantitative MS response was achieved by calibrating against HPLC. The MS spectra of each compound showed peaks corresponding to both $[M+H]^+$ and $[M+MeCN+H]^+$ adducts, but the response was only calibrated to the $[M+H]^+$ peaks as the $[M+MeCN+H]^+$ adduct for the acid **14** had a *m/z* peak of 149, which can be a plasticiser contaminant.[216] It was assumed that the degree of acetonitrile adduct formation would be constant throughout all reaction conditions because its source is the mobile phase.

5.3.1 Isotope deconvolution

The molecular weight of the ester **5.12** and amide **5.13** is only separated by one mass unit (Dalton, Da) and it is therefore possible that full conversion of **5.12** is achieved but cannot be

detected due to the presence of a ^{13}C $[M+H]^+$ peak of **5.13**. Therefore the isotopic abundance of carbon in each compound was calculated so it could be accounted for in the calibration.

MS spectra will normalise the highest peak to 100%, so the peak corresponding to the highest isotope abundance must also be normalised to the same value.

$$I_{En} = \frac{x_{En}}{x_{E0}} \tag{5.2}$$

where I_{En} is the isotope composition of element E isotope n, x_{En} is the molar ratio of element E isotope n, and x_{En} is the molar ratio of the most abundant isotope of element E. For example, the molar ratio of ^{12}C:^{13}C in carbon is 0.9893:0.0107, which means the percentage isotope composition of ^{13}C is:

$$I_{C13} = \frac{0.0107}{0.9893} = 1.1\%$$

according to the IUPAC defined molar ratios.[217] Therefore, for every atom of carbon in a molecule, the $[M+1+H]^+$ isotope peak will increase by 1.08%. The ester **5.12** has a molecular formula of $C_7H_7NO_2$, therefore the size of the +1 isotope peak, P_{I+1} can be calculated by the abundance of ^{13}C in the compound:

$$P_{I+1} = 7I_{C13} = 7.7\%$$

because all other elements in the compound have negligible abundance in their +1 isotopes. The acid **5.14** has a formula of $C_6H_5NO_2$ and therefore a calculated isotope peak of 6.6%. Using these values, the response of each compound was calculated using the following equations:

$$Ester(\mathbf{5.12}) = (P_{137} - (P_{138} \times 0.077)) \times 1.077 \tag{5.3}$$

$$Amide(\mathbf{5.13}) = P_{138} \times 1.077 \tag{5.4}$$

$$Acid(\mathbf{5.14}) = P_{124} \times 1.066 \tag{5.5}$$

5.3.2 Calibration of relative response factors

Firstly calibration solutions were prepared to 1.4 mol L^{-1} in methanol for compounds **5.12** and **13** and to 0.49 mol L^{-1} dimethylsulfoxide for compound **5.14**. The acid **5.14** was sparingly soluble in most solvents and so the lower concentration calibration solution was justified as its formation in high quantities would clog the reactor. Calibrations were carried out by preparing

samples at concentrations of 0.14 to 1.4 mol L^{-1}, in 0.14 mol L^{-1} increments, and analysis by HPLC analysis at 254 nm. A plot of HPLC peak area vs concentration showed a linear response.

Next a single stock solution containing all three compounds was prepared to a concentration of 0.332 mol L^{-1} and HPLC samples were prepared at dilutions of 1/2, 1/4, 1/8 and 1/16, corresponding to concentrations of 0.332, 0.166, 0.083 and 0.042 mol L^{-1}. Response factors for the compounds were calculated from the gradient of regression analysis of a plot of HPLC peak area vs concentration.

Table 5.3 Boundary limits for the optimisations by algorithm and design of experiments

Limits	**5.12** flow / mL min^{-1}	$MeNH_2$ eq	Temperature / °C
Upper	0.100	1	0
Lower	0.400	10	130

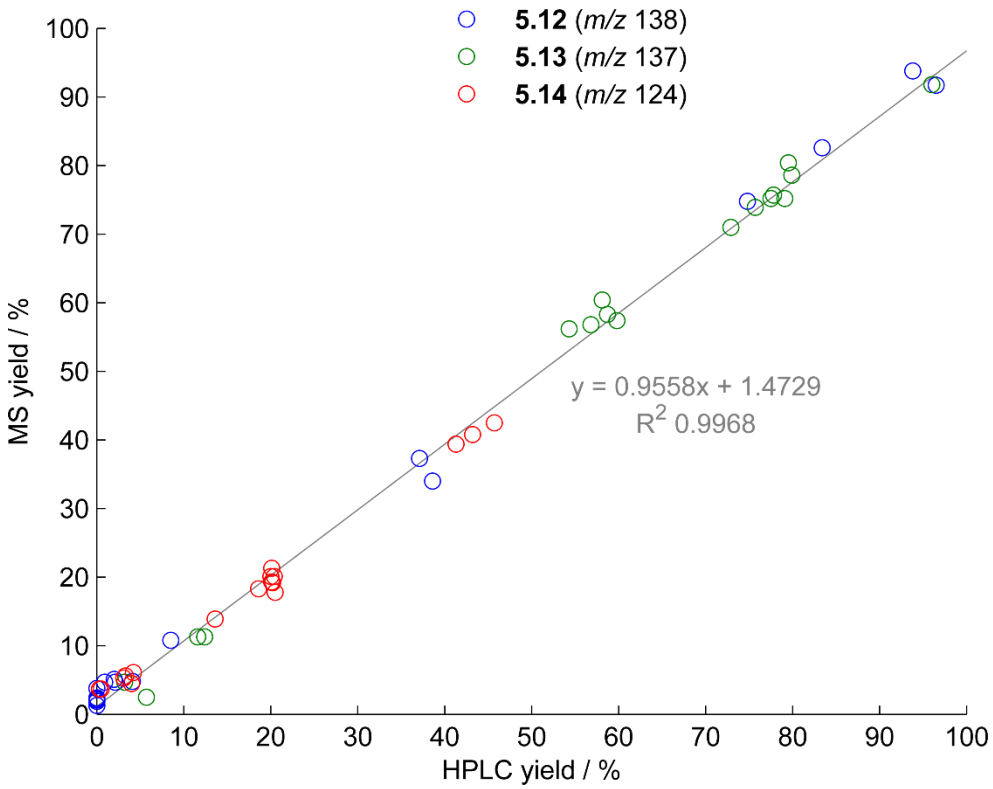

Figure 5.7 Comparison between HPLC and MS responses. Individual points are shown for the ester **12** (blue), amide **13** (green) and acid **14** (red). Linear regression analysis is shown for all three compounds combined (grey).

MS calibration was carried out by running experiments at the upper and lower extremes for each variable. A central composite faced (CCF) design of experiments (DoE) was carried out, analysing by both HPLC and MS, according to the limits shown in Table 5.3.

The HPLC was analysed by internal normalisation of the peaks of compounds **5.12-5.14** after correcting the areas from the response factors. MS was analysed by internal normalisation of the intensity of the $[M+H]^+$ peaks for compounds **5.12-5.14**, corrected for isotope deconvolution. A new MS response was calculated by multiplying the existing response by a response factor, initially set to 1, and internally normalising the results. The difference between the two techniques was calculated using a sum of squares approach

$$Error = \sum_{i=12}^{3} \left(R_{i,HPLC} - R_{i,MS}\right)^2 \tag{5.6}$$

where R_i is the response of compound $\boldsymbol{i}$ after treatment with necessary response factors and deconvolution calculations. This error was then minimised by changing the MS response factors using a generalised reduced gradient non-linear algorithm from the solver function in Microsoft excel. Comparison between the HPLC and MS responses are shown in Figure 5.7.

5.4 Automated optimisations

Automated optimisations were carried out using the SNOBFIT algorithm[136] and response surface methodology (RSM) of a CCF DoE[157] using the boundary limits shown in Table 5.3. The optimum function was to maximise the yield of amide **5.13**, the actual experimental limits for the equipment are shown in Table 5.4. For each experiment, the reactor was set to the desired temperature and methanol pumped at 0.5 mL min^{-1} and the other pumps at 0.02 mL min^{-1} to minimise reagent usage, clean the reactor and prevent accumulation in the MS during temperature changes. During experiments the methanol pump was set to 0.001 mL min^{-1} because a value of zero would trigger the safety trips included within the program code. It was not anticipated that these low values would affect the results of the experiments.

Table 5.4 – Conversion of limits shown in Table 5.3 into experimental limits

Limits	Pump 1 flow / mL min^{-1}	Pump 2 / mol eq[a]	Pump 3 flow / mL min^{-1} [b]	Temperature / °C
Upper	0.100	1	0.001	0
Lower	0.400	10	0.002	130

Pump 1 – ester **5.12**, pump 2 – $MeNH_2$, pump 3 – MeOH. a) Flow rate for pump 2 was calculated as a ratio of the flow rate for pump 1. b) The MeOH pump was used to clean the reactor between algorithm cycles and prevent accumulation in the MS

When the reactor reached the set temperature the reagent pumps were set to their desired flow rates and allowed to pump for 1.1 residence times. Next the steady state function (Figure 5.6) monitored the last three samples and when variation of the % yield of the amide **5.13** was less than a deviation of ± 0.75% the system is deemed to be at steady state. The composition of the fluid was then recorded and the next experiment conditions are set and the process above repeated.

5.4.1 SNOBFIT optimisation

Optimum conditions were reached in 21 experiments, which corresponded to less than 12 hours of overall experiment time. The optimum conditions generated **5.13** in 93% yield (Ester **5.12** flow rate 0.1 mL min^{-1}, $MeNH_2$ 10 eq, 10.6 °C).

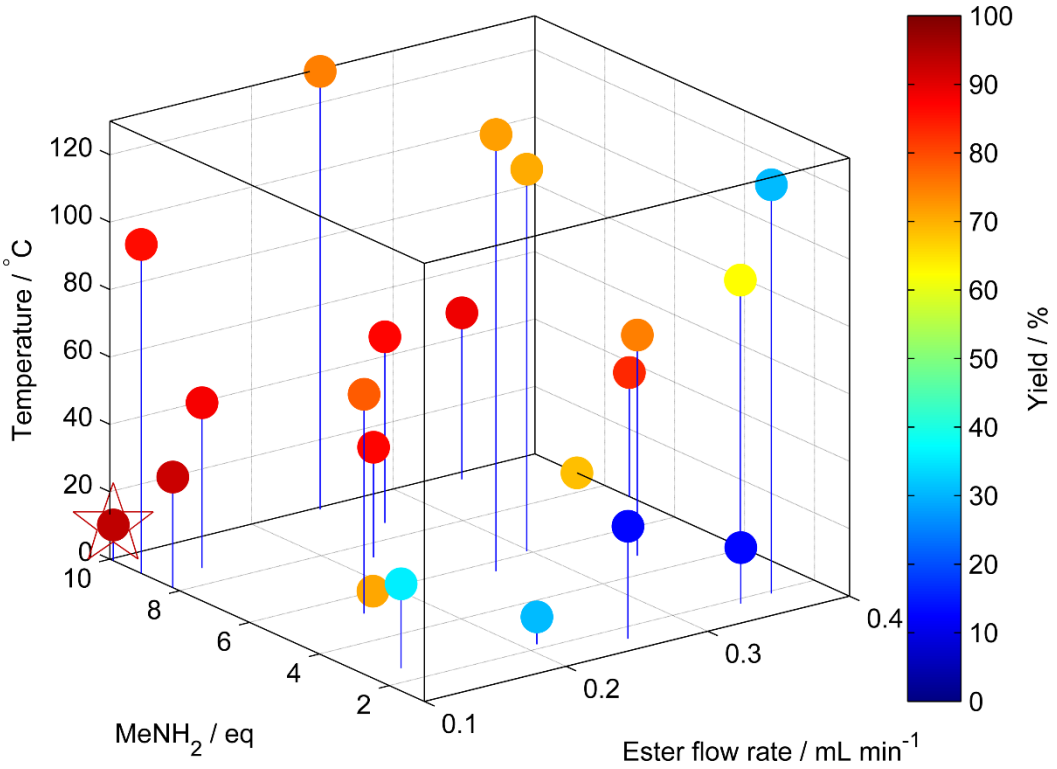

Figure 5.8 Optimisation plot for the SNOBFIT self-optimisation of amide **5.13**. Optimum point highlighted by the star, ester **5.12** flow rate 0.1 mL min^{-1}, $MeNH_2$ 10 eq, 10.6 °C.

The flow rate of the ester **5.12** is inversely proportional to the residence time, therefore the optimum conditions have the minimum flow rate of **5.12** in order to maximise the residence time. The minimum flow rate of **5.12** was also matched by a maximum 10 equivalents of methylamine. Whilst this number is excessive, the optimum function was only looking at maximising the yield of **13** rather than minimising waste. The optimum temperature was low, possibly to reduce the amount

acid **5.14** produced because the high loadings of methylamine would increase the concentration of water in the reaction and the maximum acid yields were recorded at high temperatures.

5.4.2 Response surface optimisation

A CCF design was used to construct RSM models for compounds **5.12**-**5.14**. A central composite circumscribed design was not possible as it would create scientifically impossible experiments (negative flow rates) and it was thought that an inscribed design would not cover enough experimental space.

The reaction conditions were ranked into blocks of ascending temperature and then randomised within these blocks. Traditionally, statistical experiments require full randomisation to eliminate systematic errors that can create bias in the results.[3] However it has been found that results within the same analytical error were obtained for the same design carried out in both ranked and fully randomised orders. Heating and cooling of the reactor is the biggest contributor to the overall optimisation time, therefore it was decided to proceed with the higher intensification of experiments that could be achieved with ascending orders of temperature. The responses of each model are shown in Figure 5.9.

RSM models were fitted using multiple linear regressions (MLR), and the model coefficients determined by creating saturated models with all square and interaction terms and then manually removing any non-significant coefficients.[218] Non-significant terms were determined as those where the probability that the coefficient contributes zero to the overall model (p-value) was greater than 5%. The response for the acid **5.14** was transformed, because of a non-normal distribution of the data, according to the $L_{max}(\lambda)$ value of the Box-Cox plot. This measures the maximum likelihood of the data supporting a transformation (MLE) vs the type of transformation (λ).[175] The MLE value (0.234) was rounded to the nearest integer to give a value of zero, which suggested a logarithm transformation ($y(\lambda) = \log_{10}(y)$, where y is the original response and $y(\lambda)$ is the transformed response). Box-Cox plots of the ester **5.12** and amide **5.13** models did not recommend transformations (Figure 5.10).

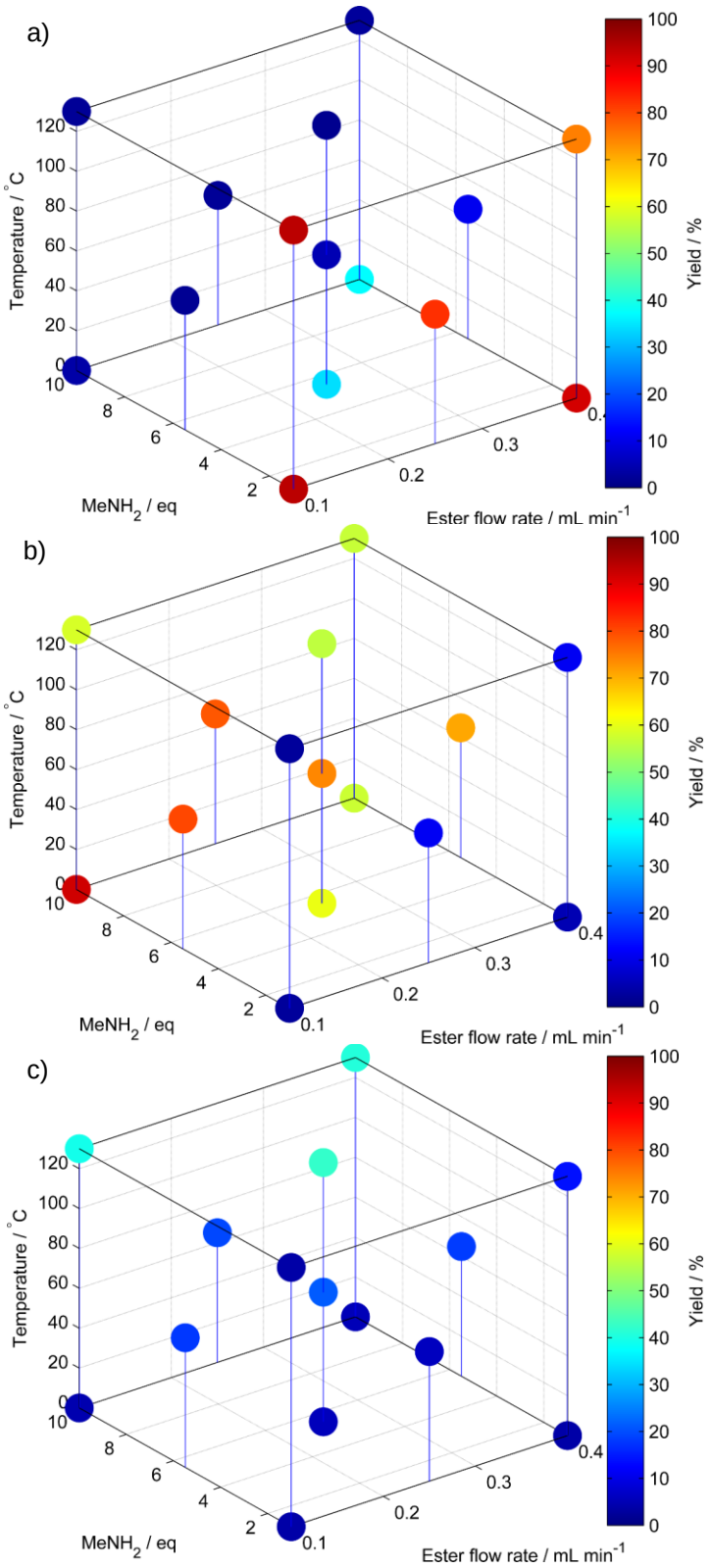

Figure 5.9 Yield of compounds **5.12** (a), **5.13** (b), and **5.14** (c) for each experiment in the CCF design.

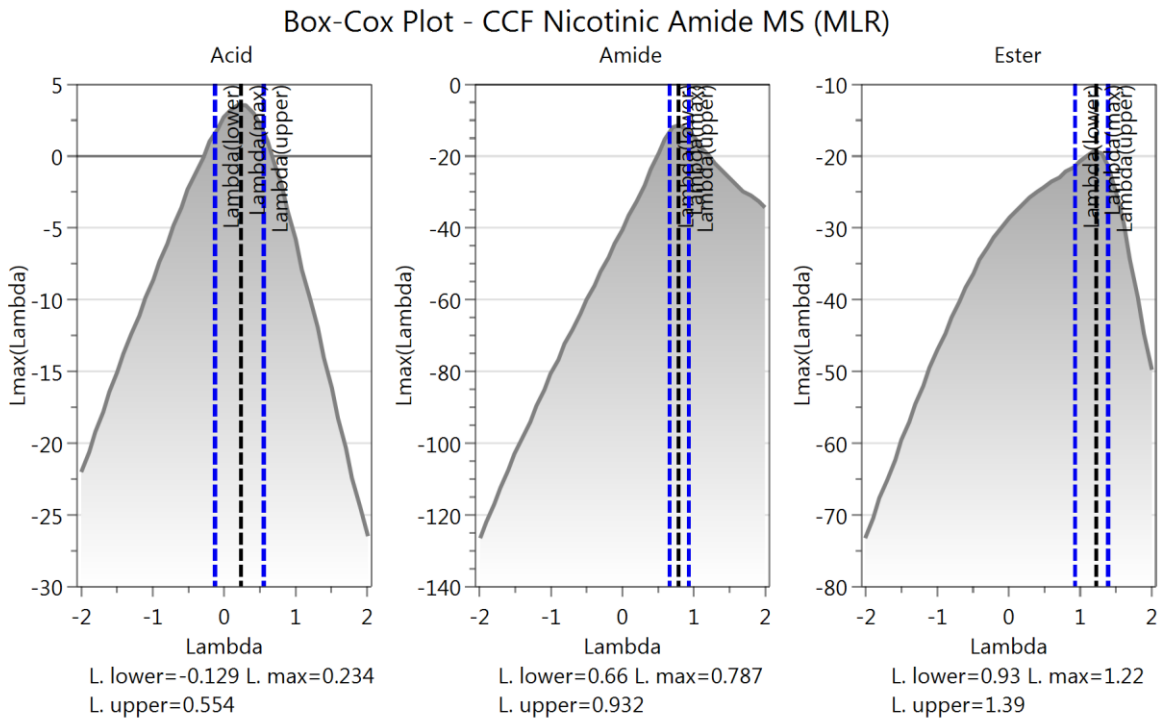

Figure 5.10 Box-Cox plots for the original responses from the CCF design. The $\boldsymbol{L_{max}(\lambda)}$ value (L. max) suggests improved transformations to the original response. The $\boldsymbol{L_{max}(\lambda)}$ value is close to 0 for the acid and therefore suggests a logarithmic transformation. The $\boldsymbol{L_{max}(\lambda)}$ values for the amide and ester are close to 1 and therefore does not recommend a transformation.[175]

After the treatment, all the models had R^2 and Q^2 values of 0.99 and 0.977 for ester **5.12**, 1.00 and 0.98 for amide **5.13** and 0.90 and 0.74 for acid**5.14**, as shown in the summary of fit (Figure 5.11). The fit of models **5.12** and **5.13** are excellent, no doubt attributable to the high reproducibility achievable with automated reactors and precise measurements recorded by the MS through the steady state function. This shows the benefit of such a setup to all synthetic chemistry fields and that the technological barrier to building such equipment is worth the effort.

It is probable that the acid **5.14** model has lower fit values because the spread of data across the experimental space is only between 3 and 40%, whereas the ester **5.12** and amide **5.13** models are between 2 and >90%. In addition the higher acid yields are at the more extreme conditions and a non-uniform spread of data can lead to a poor overall fit. The summary of fit also gives values for the model validity and reproducibility. The model reproducibility is measured by how consistent the responses of the centre-points are in each model, and a very high reproducibility can lead to low

model validity.[8] All three models have excellent reproducibility because the automated equipment allows for very high consistency. As a consequence the value for model validity suffers.

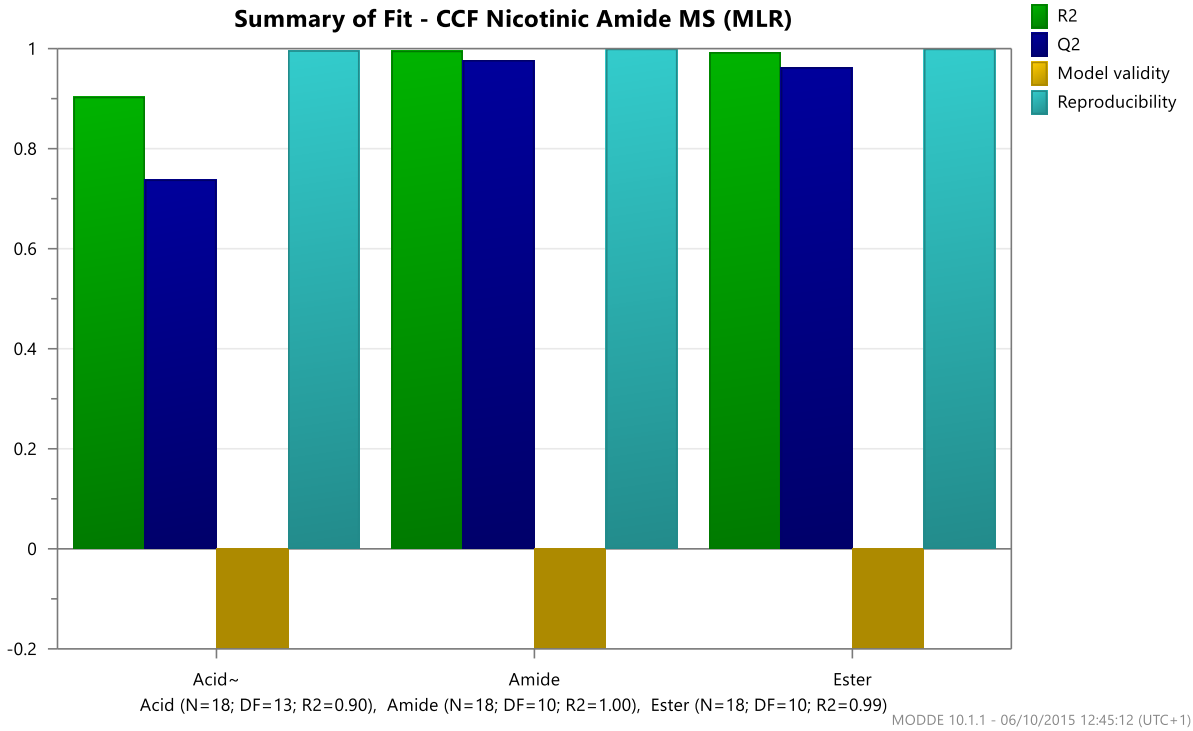

Figure 5.11 Summary of model fit for the acid 5.**14**, amide 5.**13** and ester 5.**12**.

The choice of CCF model allowed for prediction of optimum yield conditions by maximising the response of amide **5.13** and minimising the responses of ester **5.12** and acid **5.14**. The optimum conditions calculated were 0.1 mL min^{-1} ester **5.12**, 9.7 eq $MeNH_2$ and 7 °C, which are consistent with the SNOBFIT optimisation conditions of 0.1 mL min^{-1} ester **5.12**, 10 eq $MeNH_2$ and 10.6 °C. However the ability to plan experiments before carrying them out resulted in an overall run time of 5.5 hours compared to the 12 hours for SNOBFIT.

5.5 Conclusions

Online MS has been explored for monitoring and quantifying the response of an amide bond forming reaction in flow. A calibration model was generated by minimising the regression error between HPLC and MS analysis of identical sample matrices. This calibration model was then used to calculate the yield of desired amide in optimisations using the minimising SNOBFIT algorithm

[8] DoE model terms are explained in more detail in Chapter 4

and CCF response surface model. The optimum conditions generated by both techniques were highly consistent, showing the high reproducibility and low error associated with online MS.

The online analysis for self-optimisation requires fast, quantitative and sensitive data acquisition, which is simple to set up, carry out and analyse. IR has had a lot of success in the online monitoring of flow reactions, exemplified by the commercialisation of the Mettler Toledo ReactIR and FlowIR and its fast data acquisition.[219] However IR data analysis can be increasingly difficult as the structure of the desired compounds becomes more complex or multiple impurities or intermediates are generated. HPLC can discretely separate crude mixtures and quantify individual components but typically requires a chromophore for UV detection and the total acquisition time is often greater than 5 min rather than <1 min achievable with spectroscopic methods.

It is possible that MS can fill the void generated between these two forms of analysis because of its inherent separation of compounds based on their molecular weight, fast data acquisition and simple data analysis. However calibration of online MS can be difficult due to suppression of signal caused by the sample matrix. Whilst quantification techniques have been reported prior to this work,[190, 191] the calibration has been carried out after the experimental work was completed. In the work carried out in this chapter, the calibration model was created first, allowing for rapid automated feedback controlled optimisations using fast and efficient MS analysis.

For MS to be used routinely for reaction monitoring then the method of calibration needs to be simplified. All existing methods, including this work, have been calibrated for all components of the reaction by either comparing the response under the same reactions conditions of different analytical methods, or by preparing calibration solutions of mixtures of numerous components. These approaches assume that only the compounds screened during the calibration will be present in the sample matrix and therefore no further impurities or by-products are formed. These assumptions are valid for simple reactions involving monofunctional compounds, however this is not true of most synthetic transformations. Synthetic routes to pharmaceutical compounds involve the stepwise increase in complexity of a molecule, therefore increasing the numbers of undesired impurity routes. The ability to detect an impurity using the mass or isotope pattern is an advantage of analysing by MS, however quantification is not possible if it has not been included during

calibrations. It may also interfere with the response of compounds that are included, reducing the calibration accuracy.

A possible way around this is to include an internal standard (IS), which the responses of all known and unconfirmed compounds can be normalised to. This would allow quantified analysis of reactions without having to carry out full calibration beforehand. The difficulty with this approach is confirming that the IS response remains a constant ratio to its concentration in the sample and a change in measured product composition is reflected by the reaction conditions and not due to differing suppression effects between compounds relative to the IS in the matrix.

Nevertheless, MS analysis is a very strong asset to online reaction monitoring due to its high sensitivity, inherent separation of compounds and fast data acquisition. Obtaining quantitative signal response is not without its challenges, however as more calibration techniques are developed its use for reaction monitoring will surely increase. This chapter exemplifies how a benchtop MS can be easily integrated into a flow reactor setup and can replace HPLC for fast on-demand data analysis and reaction optimisation.

6. Reducing Material Consumption in Automated Flow Optimisations

6.1 Introduction

Preparative chemical research requires countless hours of manual, unskilled tasks. Reactions are carried out *via* the transfer of chemicals from containers into reaction vessels, which are exposed to various physical conditions, samples are acquired for analysis and then the desired component(s) are extracted through a variety of techniques such as liquid-liquid separation, induced precipitation, trituration, filtration, solvent evaporation, purification, distillation and crystallisation. Multiple reactions are required for methodology, in order to find combinations of reagents, solvents, catalysts etc., which can then undergo extended scopes to show how the reaction changes with different substrate functionalities. Reaction understanding requires multiple screens of different concentrations and temperatures to determine the kinetic parameters of the associated chemical transformation, and the optimisation of continuous variables to find and verify optimum conditions again requires considerable experimentation.

The ability to use the data acquired from analysis to understand the key components of chemical transformations and then decide which follow up experiments are needed is the main focus of chemical research. However a large proportion of a researcher's time is spent carrying out unskilled, labour intensive tasks that could be replaced by automated technology.[53] Sometimes only the data from a reaction is required and the final mixture is simply disposed of, at high cost.[22] Therefore chemical research generates a lot of waste: not only material but the time of a highly trained and educated workforce.

It should be expected that chemical reaction development and the associated technologies are increasingly employing automation and becoming data rich environments. Automated reaction platforms are now routinely used for discovering new chemical transformations,[220-223] synthesising known compounds,[96, 224-226] high throughput screening[227-229] and optimising novel or existing synthetic pathways.[14, 15, 20, 172, 215]

Online analysis and automation are widely applied to microfluidic flow reactors because the integration of this technology is simple.[9, 10, 53, 54, 159, 185] The nature of continuous plug flow means

that at steady state, the chemical composition changes with the distance of the reactor but for any fixed point the composition is constant. Therefore, if analysis is carried out at a fixed point at the end of the reactor, the whole contents of that reactor are pumped to waste before the composition under new reaction conditions reaches the analysis point. It can take anywhere between 1.5 to 3 reactor volumes to reach steady state under these new conditions.[230]

A way to circumvent these problems is to use segmented flow, where a small amount of reaction mixture is carried through the reactor using either a miscible or non-miscible fluid. Below is an abridged list of different gas and liquid flow regimes that result in controlled separation between the two fluid compositions, described in terms of dispersed and continuous phases (Table 6.1 and Figure 6.1).

Table 6.1 Description of microfluidic multiphase flows

Description	Dispersed phase	Continuous phase
Pulsed flow	Liquid	Miscible liquid
Segmented/Slug flow	Liquid	Non-miscible fluid or PFC
Compartmentalised flow	Liquid	PFC followed by non-miscible fluid
Double emulsion	PFC within organic liquid	Aqueous

fluid – gas or liquid, PFC – perfluorinated compound

Interesting phenomena can occur using the different flow regimes. In segmented flow, the individual segments can act as individual reactors allowing increased mixing through physical collisions caused by surface tension between the segments.[231] In double emulsion flow, the bead of PFC within a segment also increases the physical mixing.[232] In continuous flow, reactions can suffer from dispersion, where the increase in friction of the walls of the reactor causes the flow profile shape to become parabolic, resulting in non-constant flow velocities across the cross sectional area of the reactor and uncertainty in the residence time. The surface tension between plugs in segmented flow is generally greater than the frictional forces and therefore dispersion is minimised.[231, 233]

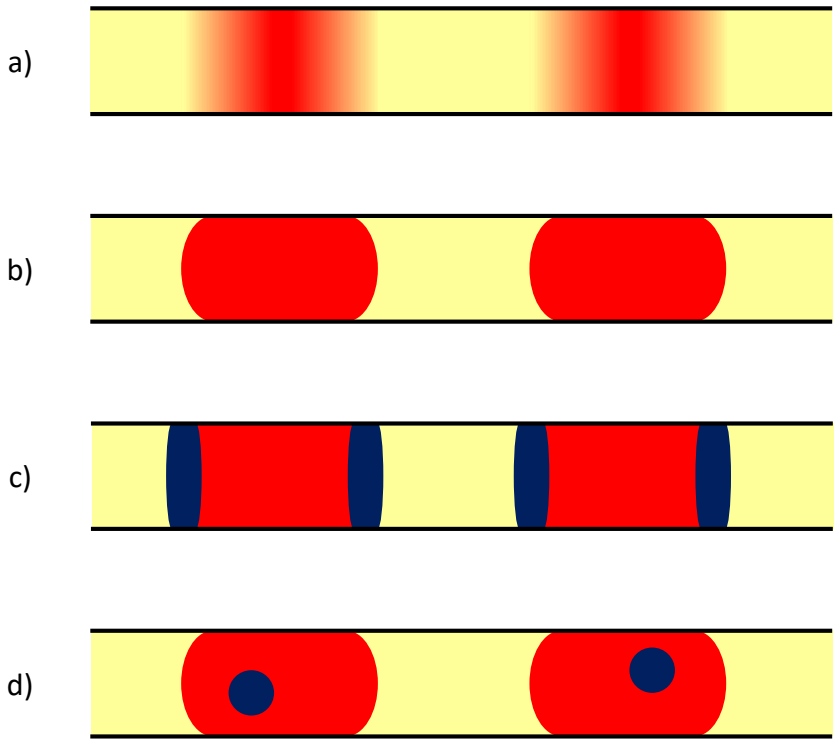

Figure 6.1 Schematic of different flow regimes where the dispersed phase is red, continuous phase is yellow and PFC is blue: a) pulsed flow, b) segmented flow, c) compartmentalised flow, d) double emulsion flow.

The only existing examples using segmented flows in the feedback controlled optimisation of automated flow reactors has been reported by Reizman *et al*. who used slug flow for the selective alkylation of diamines[20] and Suzuki-Miyaura cross couplings.[21, 185] The authors used a series of fractional factorial (FED) experiments to screen discrete variables then used feedback controlled response surface methodology (RSM) to optimise continuous variables for a target function. FEDs were used in order to test if there was disproportionate response across experimental space with the different discrete parameters. An automated liquid handler prepared the reagent solutions which were introduced to the reactor as 14 µL slugs using a sample injection loop and carried using N_2 gas. The amine and base solutions were introduced to the slug through tee-pieces and the reaction quenched the same way using acetic acid. After quenching, the reaction was diluted before analysis using at-line HPLC-MS.

In the first example (Scheme 6.1), DMSO provided the best yield of the desired mono adduct **6.3** out of all the solvents screened: DMF, pyridine, DCE, THF, DMC, MeCN, ^{i}PrOH, DME and toluene. The feedback RSM then optimised the reaction to generate **6.3** in a 62% yield.

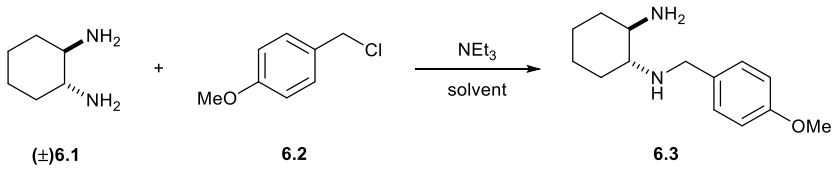

Scheme 6.1 Asymmetric alkylation of trans-1,2-diaminocyclohexane **(±)6.1** with 4-methoxybenzyl chloride **6.2** to form the desired mono adduct **6.3**.

In the second example (Scheme 6.2), pre-catalysts were prepared using a variety of phosphine ligands (Figure 6.2) and used to screen and subsequently optimise the synthesis of four different compounds **6.8**-**6.11** for turnover number (TON) of the catalyst (mol of substrates converted to product per mol of catalyst). The optimum TONs ranged from 17 (35% yield) for **6.9** to 89 (90% yield) for **6.11**.

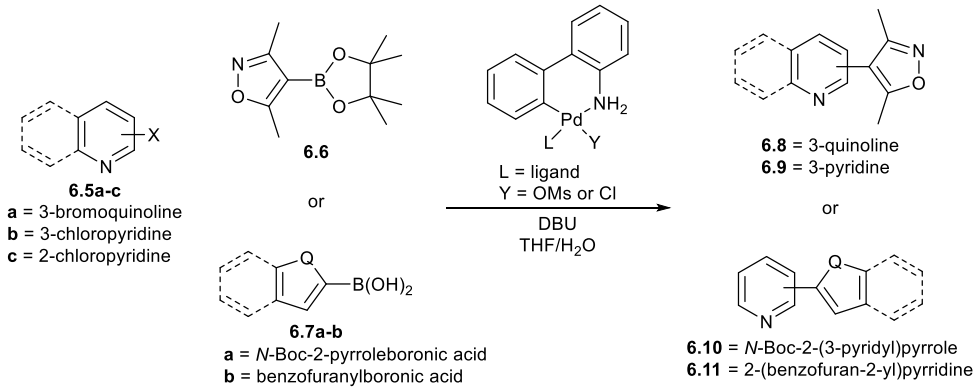

Scheme 6.2 Suzuki-Miyaura cross-coupling between heteroaryl **6.5** and boronic ester **6.6** or boronic acid **6.7**.

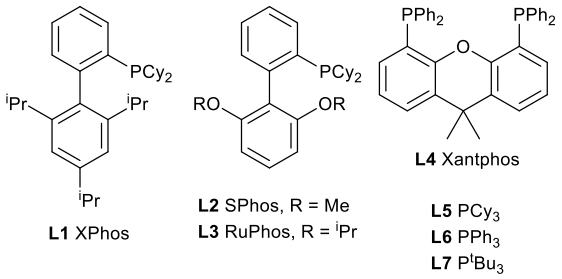

Figure 6.2 Ligands screened in the Suzuki-Miyaura cross-coupling optimisation (Scheme 6.2)

Effective optimisation of discrete and continuous variables in both examples was achieved using this method, which greatly benefitted from the segmented flows approach. The reactor volume was 240 µL, which would have required at least 360 µL of material pumped to reach steady state. However each reaction was contained within a 14 µL segment requiring only 4% of

the material when operating under continuous flow. These calculations assume a steady state of 1.5 reactor volumes.

The main disadvantage with the approach is that the reactor set-up suffered from over complexity. Photosensors were fitted either side of the tee-pieces and sample loops to control the addition of amine and quench solution as well as at-line HPLC-MS sampling. The rig also contained 7 individual sample injection loops that all needed individual programming as well as 4 syringe pumps, vacuum pump, mass flow controller, reactor, HPLC-MS and custom designed automated liquid handler. The use of a liquid handler also meant that any discrete reagents had to be liquid or in solution, thus meaning that solvents and reagents must be prepared in all combinations of reagent/solvent solutions if they are to be screened simultaneously. A common problem for discrete variable screening in automated flow reactors.

This chapter will explore the use of pulsed flows in self-optimising reactors to reduce the amount of material required to complete an optimisation *vs.* continuous flow. It was decided to use pulsed flows as they can be introduced into the existing reactor set-up with minimal disruption and is therefore less technologically complex than the segmented flow setup used by Reizman *et al*.[20, 21, 185] The main disadvantage with pulsed flows is that the reactor can suffer from dispersion, however these effects can be minimised or completely removed if the residence time distribution is characterised before optimisations commence.

Pulsed flow is routinely used in chemical development by industry and academia alike to reduce the amount of material consumed in reactions. The Uniqsis FlowSyn[234] and Vaportec R-Series[235] are fitted with 6 port sample injection loops of various sizes, which can be loaded with reagent and/or substrate and the machines can switch between pumping continuously from a stock solution and carrying the injection loop pulse with solvent. Selected examples include, but are not necessarily limited to, organic functional group transformations[123, 236, 237] using gaseous[238-241] and organometallic reagents;[242-244] multistep synthesis;[238, 239, 245, 246] packed bed reactors[238, 247-249] and photochemistry.[250, 251]

6.2 Calculating Dispersion and Residence Time Distribution

Continuous flow is often described as plug flow, which is an engineering model term to describe an ideal continuous reactor where no fluid mixes back against the flow direction. A plug flow reactor (PFR) can be thought as of as cross-sectional discs of infinitely small thickness that are all stacked together and move in unison in the direction of flow. In reality, a continuous reactor contains non-uniform flow patterns caused by differences in frictional forces across the tubing or oscillations from mechanical motion of the pumps (Figure 6.3). These non-uniform regimes result in uncertainty in the residence time, which can be characterised by residence time distribution.[213]

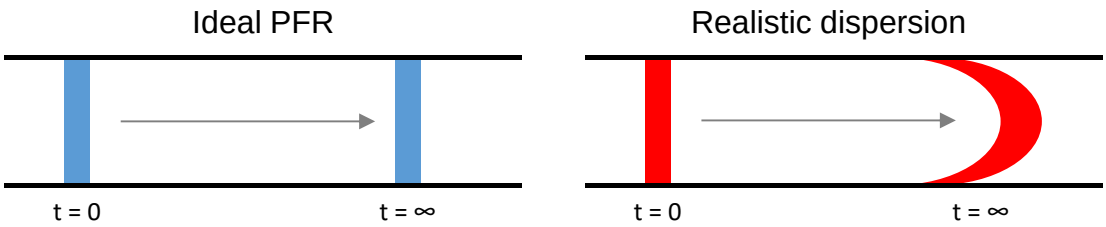

Figure 6.3 Comparison between the flow patterns of an ideal PFR (left) and realistic reactor suffering from dispersion (right).

Residence time distribution (RTD) calculations were carried out using a 3 mL PTFE tubular reactor with internal dimensions (ID) 1/32” (0.79 mm) and external dimensions 1/16” (1.59 mm) and length 6.25 m. A pulse of a biphenyl solution was pumped through the reactor by alternating between two pumps, one containing the solution and one with just solvent and dispersion was measured at 1 and 3 min residence times. For residence times of 1 min, the solvent pump was set to 3 mL min^{-1} for 1 min, then stopped and the biphenyl pump was set to 3 mL min^{-1} for 1 min. This was repeated for a total duration of 50 min. During this time, the sample loop was set to acquire a HPLC sample at a frequency of 125 s. This resulted in 25 chromatograms displaying the composition of biphenyl at 5 s intervals along the 1 min repeated pulse.[60] For residence times of 3 min, the solvent pulse was set to 1 mL min^{-1} for 3 min, then the biphenyl pump set to 1 mL min^{-1} for 3 min. This was repeated for a duration of 216 min with HPLC sampling frequency of 370 s. This resulted in 36 points displaying the composition of biphenyl at 10 s intervals across the 3 min repeated pulse (Figure 6.4).

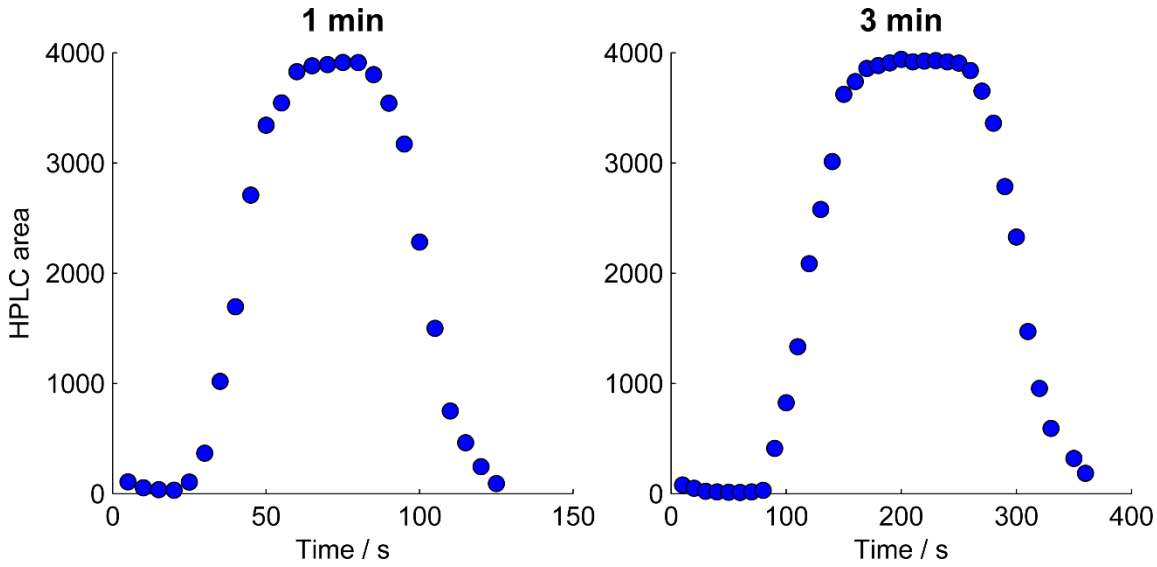

Figure 6.4 Plots of HPLC area of biphenyl vs time for the dispersion experiments. Residence times of 1 min (left) and 3 min (right).

The dispersion is determined by calculating the parameter D, which is the longitudinal dispersion coefficient and characterises the amount of back mixing in continuous flow. This can be converted to the dimensionless term $\frac{D}{uL}$, where u is the flow velocity and L is the length of tubing. For $\frac{D}{uL}$ values of 0, there is perfect plug flow but as $\frac{D}{uL}$ approaches infinity there is large dispersion and mixed flows. Typically any value of $\frac{D}{uL} < 0.01$ can be fitted to the dispersion model for a PFR.

The experiments as described in the previous chapters generated a tracer pulse of HPLC area *vs.* time of pulse (Figure 6.4). This response of the pulse is normalised to create a C curve

$$C = \frac{C_i(t)}{C_{max}} \tag{6.1}$$

where C is the normalised HPLC response, $C_i(t)$ is the HPLC area at time t and C_{max} is the maximum HPLC area across the time span. The time was normalised so that C_{max} occurs at $\theta = 1$

$$\theta = \frac{t}{\bar{t}} \tag{6.2}$$

Next, an E curve was calculated, which fits the data to a Gaussian trend depending on the value of $\frac{D}{uL}$. For small deviations from plug flow ($\frac{D}{uL} < 0.01$), the tracer shape is symmetrical and the E curve calculated by

$$E_\theta = \frac{1}{\sqrt{4\pi\left(\frac{D}{uL}\right)}} exp\left(-\frac{(1-\theta)^2}{4\left(\frac{D}{uL}\right)}\right) \tag{6.3}$$

The E curve was normalised in order to calculate the error (SS_E) between the C and E curves

$$SS_E = \sum \left(C_i(\theta) - E_\theta(\theta)\right)^2 \tag{6.4}$$

The shape of the two tracer pulses are not true Gaussian but have a plateau of C_{max} values, that distort the shape of a fit across all the data points. To rectify this, fitting was carried out on only the right hand side of the tracers because the trailing of a peak is a better indication of dispersion, especially for non-symmetrical curves.[213]

The last point of the plateau was denoted as C_{max} ($\theta = 1$) and the E curve was fitted to the C curve by minimising the error SS_E using generalised reduced gradient non-linear algorithm as part of the Microsoft Excel solver function.

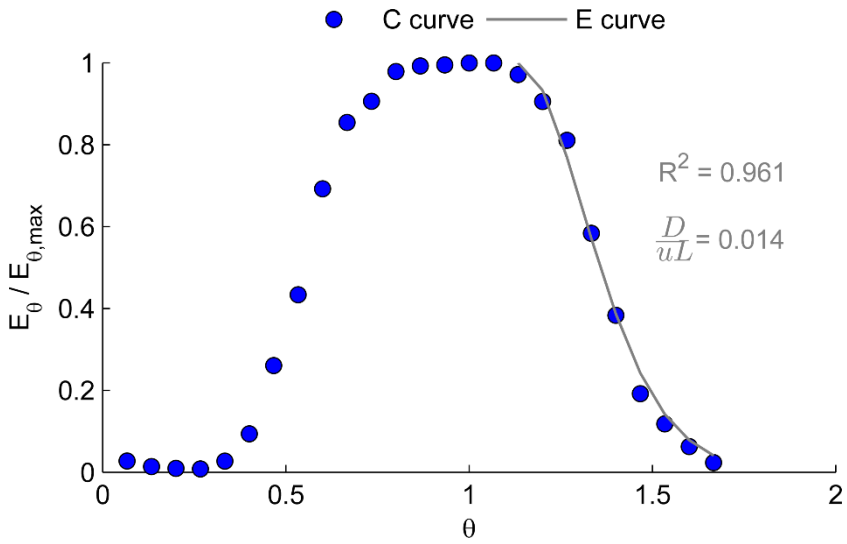

Figure 6.5 ***E*** curve fit layered over ***C*** curve for 1 min residence time distribution experiment

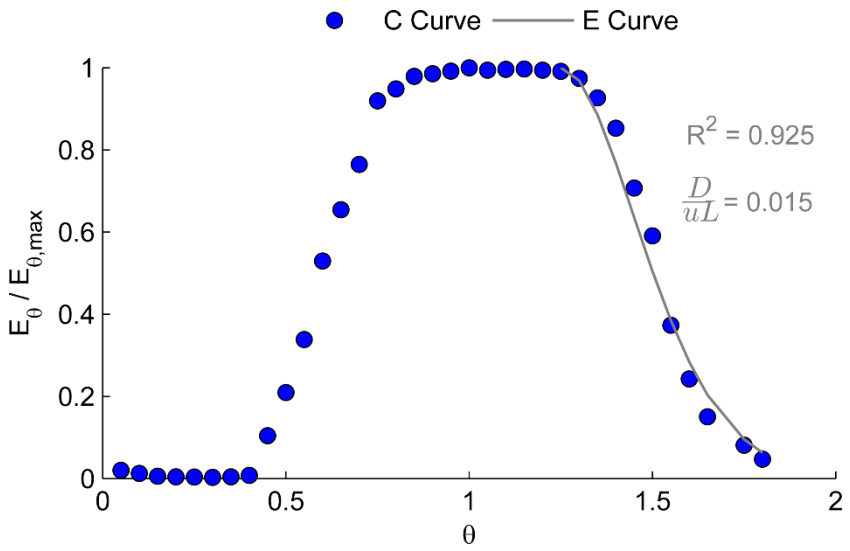

Figure 6.6 ***E*** curve fit layered over ***C*** curve for 3 min residence time distribution experiment

The E curve fits are shown for RTD 1 min experiments in Figure 6.5 and for 3 min experiments in Figure 6.6. Both of the E curve fits show a value for $\frac{D}{uL}$ that is greater than 0.01, indicating that there were deviations from plug flow in the tubular reactor constructed. If this is the case then the E curve is calculated using a different equation from that shown in (6.3)

$$E_\theta = \frac{1}{\sqrt{4\pi\left(\frac{D}{uL}\right)}} exp\left(-\frac{(1-\theta)^2}{4\theta\left(\frac{D}{uL}\right)}\right) \tag{6.5}$$

However when this expression was used there was minimal change to the overall E curve fit and value for $\frac{D}{uL}$.Therefore it was assumed that there was minimal variation from plug flow and therefore minimal dispersion in the reactor.

6.3 Self-Optimisation Using Pulsed Flows

To test the material savings achievable with pulsed flows, a nucleophilic aromatic substitution (S_NAr, Scheme 6.3) was optimised using at-line HPLC and pattern search algorithm.[147] 2,4-difluoronitrobenzene **12** can undergo rapid substitution with morpholine to form the desired regioisomer *ortho* **13** and undesired *para* **14**. Base was required to quench the hydrofluoric acid generated *in situ*, so triethylamine was added to ensure that all of the morpholine was used as a reagent and not a base.[252] Both isomers **13** and **14** can undergo double addition to form the di-substituted **15**, however previous research within the group has shown that the *para* **14** undergoes this transformation faster than **13**.[60]

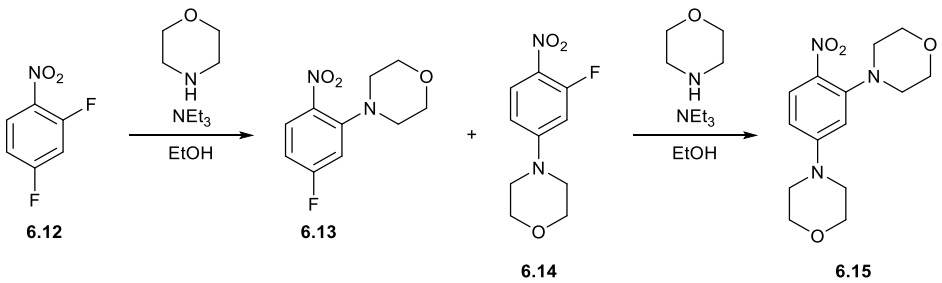

Scheme 6.3 S_NAr reaction between difluoronitrobenzene **6.12** and morpholine to form the desired *ortho* **6.13** and undesired *para* **6.14**, which can both undergo double substitution to form di-substituted **6.15**.

Three pumps were used with reservoirs of nitrobenzene **6.12** (2.03 mol L^{-1}) and biphenyl internal standard (0.10 mol L^{-1}) in EtOH, morpholine in triethylamine (4.17 mol L^{-1}, 1.1 mol eq NEt_3) and neat EtOH. The same 3 mL PTFE tubular reactor was fitted, as was used during the dispersion experiments, as well as a 100 psi BPR (Figure 6.7). The EtOH pump was used to modify the concentration of nitrobenzene species (**6.12-6.15**) during reactions and as the carrier solvent during solvent pulses.

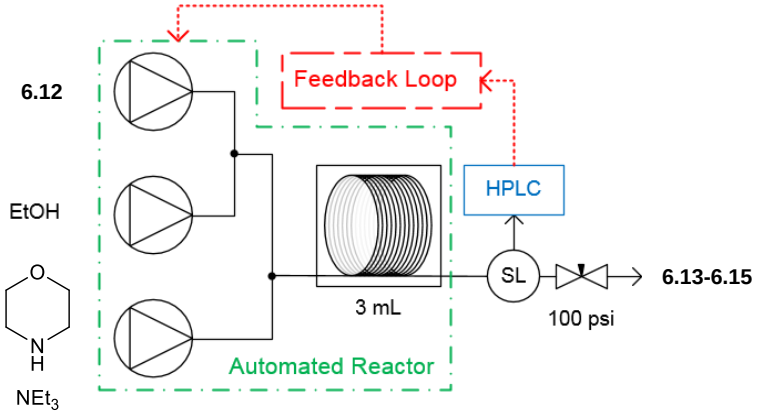

Figure 6.7 Reactor schematic for the S_NAr self-optimisation. SL = Sample loop

6.3.1 Pulse Volume

Firstly it was important to determine the size of reactor volume (RV) pulse that would be used during optimisations. It was hypothesised that 0.5 volumes would be sufficient but this needed to be tested. Several reactions under the same conditions were carried out but differing sizes of reaction pulses were pumped, with ethanol as the miscible solvent carrier.

The flow rates and duration of reaction and solvent pulses were calculated according to the centre of the reaction pulse being at the end of the reactor when a HPLC sample was taken. This

would ensure the centre of the reactor pulse would be at the sample loop when a sample was taken. 4 experiments were carried out for each volume and the analytical response averaged after removal of anomalous results.

To make it easier to calculate the duration of reaction and solvent carrier pulses, the pulses were separated into reaction pulse R and solvent pulses A and B (Figure 6.8). A is the first solvent pulse, which is followed by reaction pulse R then solvent pulse B. The flow rate of all pulses remain constant and the duration of each pulse is calculated

$$R = RV_{pulse} t_{Res} \tag{6.6}$$

$$B = t_{Res} - \frac{R}{2} \tag{6.7}$$

$$A = t_{end} - (R + B) \geq 0 \tag{6.8}$$

where RV_{pulse} is the size of reactor volume pulse, t_{Res} is the residence time and t_{end} is the time for the analysis acquisition to be ready, typically the sample frequency time.

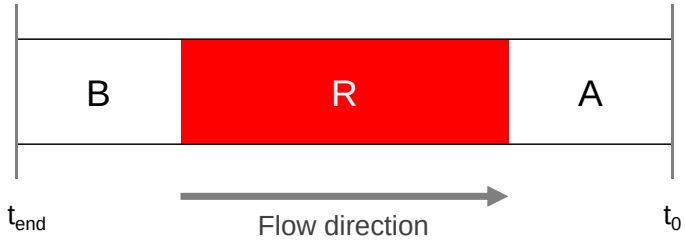

Figure 6.8 Notation of the solvent pulses A and B and reaction pulse R

The change in percentage composition of compounds **6.12-6.15** shows that unreliable responses are recorded at volumes less than 0.5 (Figure 6.9). This means that for pulses of less than 0.5 RV, dispersion was an overriding factor and prevented the expected reaction kinetics. The margin for error for each RV of 0.5 and lower was calculated from the values recorded at RVs 1-2. Firstly the mean response of RVs 1-2 was calculated, then the residual error for the other RVs. For example, the residual error for *ortho* **6.13** at 0.5 reactor volumes

$$SS_{E,(\mathbf{6.13},0.5)} = \sum \left(Y_{i,(\mathbf{6.13},0.5)} - \bar{Y}_{\mathbf{6.13},0.5}\right)^2 = 5.58$$

where Y_i is the yield for experiment i. Next the standard deviation of the residual error for the 3 experiments was calculated

$$\sigma_{(\mathbf{6.13},0.5)} = \sqrt{\frac{5.58}{3}} = 1.36$$

For a confidence interval of 95%, the Z table value for 0.475 (0.95/2) is 1.96 which means the margin for error was

$$error = Z_{1-\frac{\alpha}{2}}\left(\frac{\sigma}{\sqrt{n}}\right) = 1.95 \times \left(\frac{1.36}{\sqrt{3}}\right) = 1.54 \tag{6.9}$$

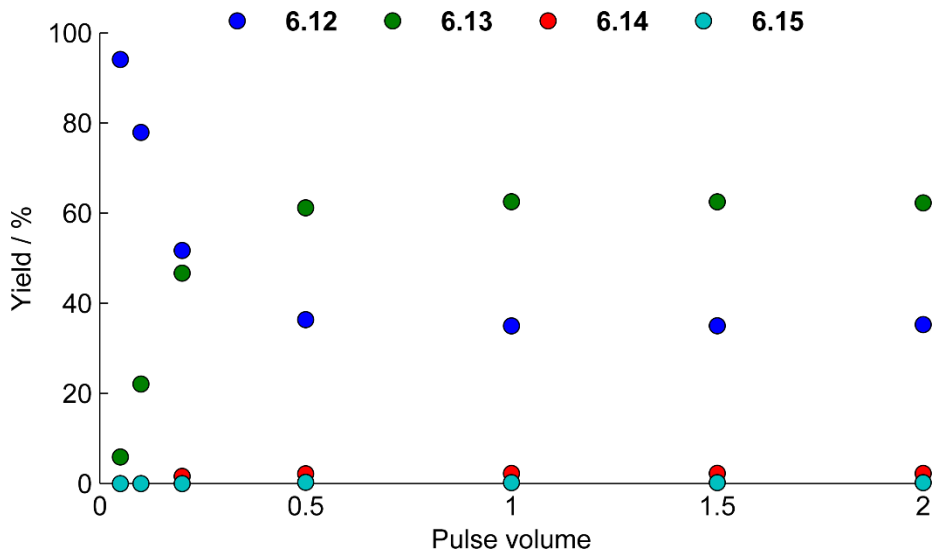

Figure 6.9 Summary of HPLC areas for compounds **6.12-6.15** for changing reactor pulse volumes.

A summary of the yields of all the experiments, along with margins for error, is shown in Table 6.2. The reactions performed in a RV pulse of 0.5 showed a margin for error of $<$ 1.6 %, however part of this error must have been from irreproducibility from equipment as well as analytical error. It could be assumed that these factors were solely responsible for the margins for error for RVs 1-2. If this was the case then the error associated with dispersion can be calculated by subtracting the average margin for error for RV 1-2 from the overall margin for error for 0.5 RV, giving a value of $\sim$ 1%. This low margin for error showed that 0.5 RVs was a suitable pulse volume for optimisations.

Table 6.2 HPLC % area of compounds **6.12**-**6.15** for different rector volume pulses

Reactor volumes	Nitrobenzene **6.12**	*Ortho* **6.13**	*Para* **6.14**	Di **6.15**
2	34.9 (± 0.790)	62.6 (± 0.765)	2.26 (± 0.021)	0.21 (± 0.006)
1.5	35.0 (± 0.440)	62.5 (± 0.422)	2.26 (± 0.013)	0.21 (± 0.007)
1	34.9 (± 0.538)	62.5 (± 0.524)	2.25 (± 0.011)	0.21 (± 0.005)
0.5	**36.37 (± 1.59)**	**61.2 (± 1.54)**	**2.17 (± 0.104)**	**0.27 (± 0.089)**
0.2	51.72 (± 19.0)	46.6 (± 18.0)	1.59 (± 0.760)	0.00 (± 0.241)
0.1	77.92 (± 48.6)	22.0 (± 45.8)	0.00 (± 2.555)	0.00 (± 0.241)
0.05	94.10 (± 66.9)	5.9 (± 64.1)	0.00 (± 2.555)	0.00 (± 0.241)

Margins for error are calculated assuming a 95% confidence interval

6.3.2 Pulsed Flows Optimisation Program

A new optimisation program was written in order to include the changes that would be required for the pulsed flows. A flow chart summarising the key decisions made in the program is displayed in Figure 6.10. In summary, the program is identical to the original when creating the new conditions from the algorithm. Next the program enters the steady state timer, where it calculates the flow rate of the solvent pump and durations of the pulses A, B and R. During the optimisations t_{end} was calculated as the time from which the HPLC would be ready to sample (sum of the time of the previous sample and the method length). This time was calculated before the reactor reached the desired temperature and as a result the pulse A could start after t_{end} resulting in a negative flow rate. For these reasons the minimum value of A was set to zero (6.8).

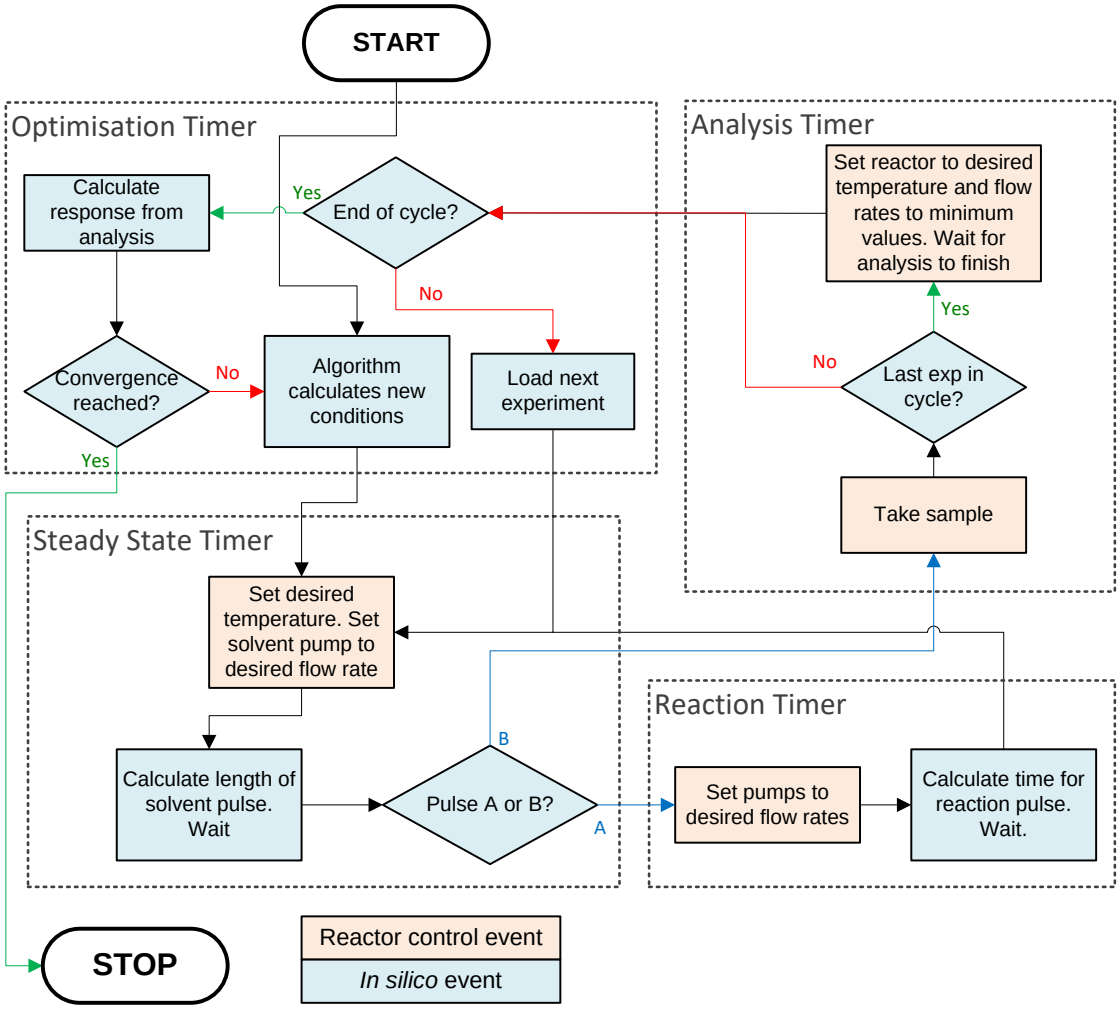

Figure 6.10 Flow chart summary of the optimisation program, which includes the pulsed flows

6.3.3 Space Time Yield Self-Optimisation

The S_NAr reaction (Scheme 6.3) was optimised for the space time yield (STY) of ortho **6.13** using the pattern search algorithm. STY is a measure of reactor productivity and calculates the mass of product per unit time and volume

$$STY = \frac{C_{\mathbf{6.12}} Y_{i(\mathbf{6.13})} MW_{\mathbf{6.13}}}{t_{Res,i}} \tag{6.10}$$

where $C_{\mathbf{12}}$ is the initial concentration of nitrobenzene **6.12** in the reactor, $MW_{\mathbf{6.13}}$ is the molecular weight of *ortho* **6.13** and $t_{Res,i}$ is the residence time of experiment i.

Table 6.3 – Optimisation limits for the STY optimisation of ortho 6.13

Limit	Residence time / min	Morpholine / mol eq	Concentration / mol L^{-1}	Temperature / °C
Lower	1	1.0	0.200	60
Upper	3	2.0	0.500	120

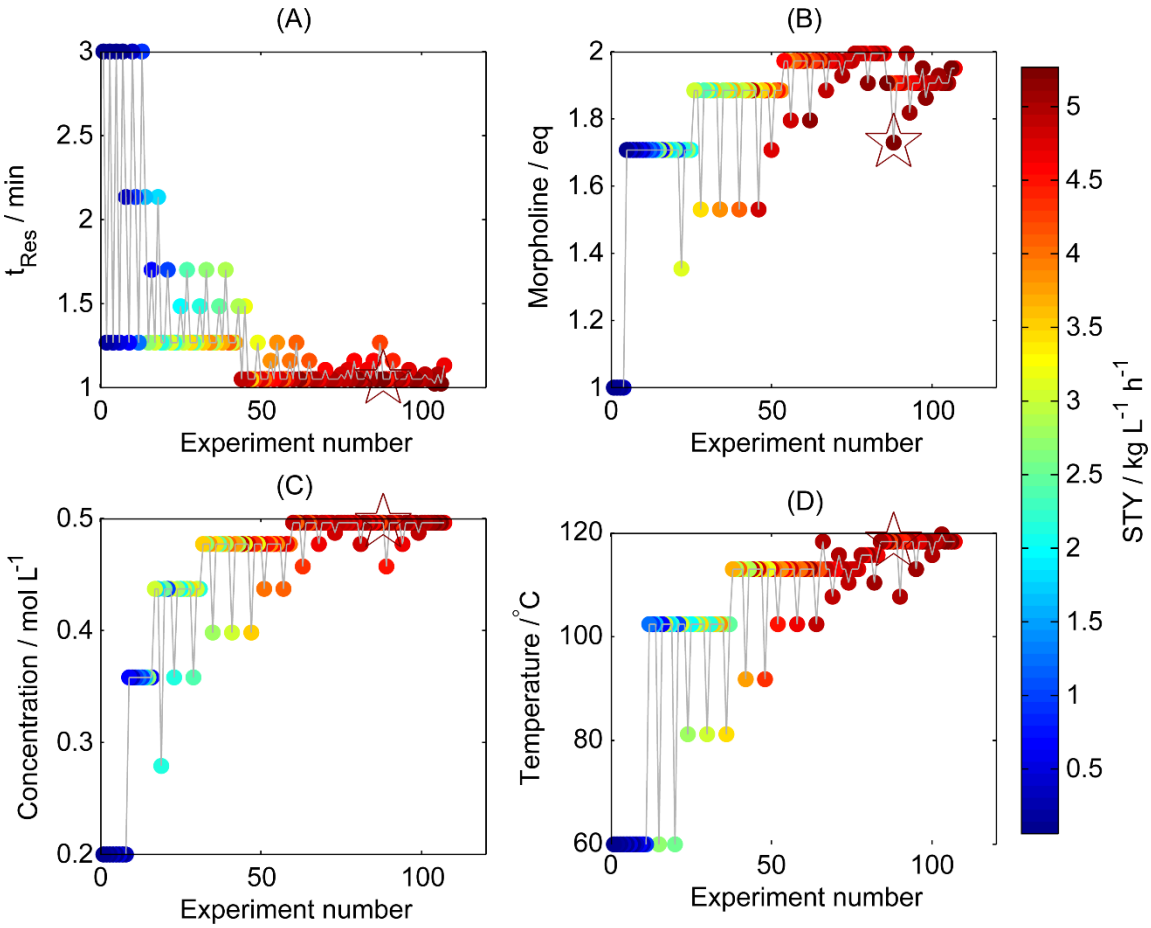

Figure 6.11 Summary of optimisation results. Each plot shows how an individual variables changes as the algorithm reaches the optimum. A – residence time, B – morpholine eq, C – concentration of **6.12**, D – temperature. The colour of the point represents the target metric (STY).

The reaction was optimised according to the limits in Table 6.3. The optimum conditions generated ortho **6.13** in an 82% yield with a STY of 5.27 kg L^{-1} h^{-1}; a summary of results is shown in Figure 6.11. The optimum conditions were 1.05 min, 1.7 eq of morpholine, 0.50 mol L^{-1} and 118.3 °C, which were at (or close to) the maximum limits for morpholine eq, concentration and temperature but minimum residence time. This was in order to maximise the yield of ortho **6.13** whilst reducing the overall residence time to maximise the amount of material pumped per unit time.

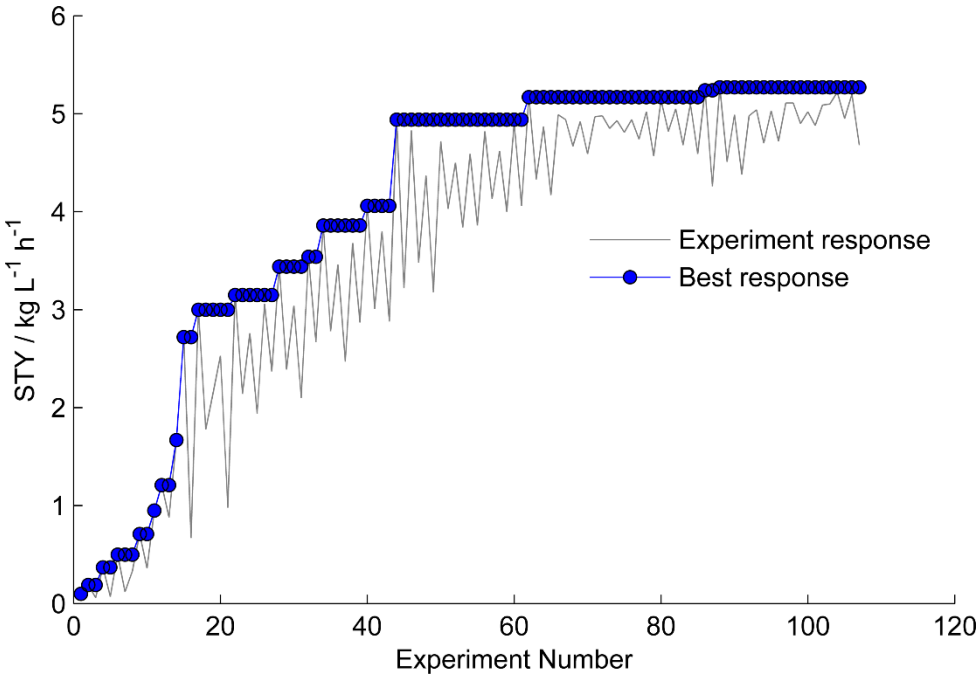

Figure 6.12 Plot displaying the improved optimum with increasing experiment number

Figure 6.12 shows how the optimum improved as the optimisation progressed. The algorithm did not have a built in stopping criterion and was stopped manually after 107 experiments.

6.3.4 Material and Cost Savings

The main objective of the pulsed flows approach was to save material during each experiment. Material savings were calculated based on three separate forms of operation: pulsed flow; step-flow, where the flow rate of all pumps was reduced whilst the reactor was reaching temperature; and full continuous flow operation.

Further analysis of the reactor data showed that reactor pulses varied from 0.54 to 0.72 RV rather than the desired 0.50 RV. This is likely caused by the resolution of the program timers. Instead of calculating the time that the timer should run for then stopping, the timer would repeat its line of code at a fixed period then stop once it had carried out enough repetitions. This was to ensure that the program was constantly checking that all reactor components were at their desired values, ensuring that there were no sudden temperature spikes or pumps that had stopped because of a blockage. The period of each timer ranged from 15 to 20 s. It was important not to reduce this time period because the timer could try to restart whilst already running and cause the program to crash. In experiments with a residence time of 1 min, the time to pump the reaction pulse could

change by as much as a third. It is likely that this caused the deviation in reactor volume. For reactions that require a longer residence time, the error in timer period would be less significant.

In previous step-flow optimisations, where steady state has been calculated, the program has waited for 1.5 RV. Because of the discrepancy with the pulse volume, the potential steady state reactor volumes for each experiment were calculated by adding 1 RV to the pulse volume. Therefore the step flow steady state volumes ranged from 1.54 to 1.72. For continuous flow operation, it was assumed that the pumps were continually pumping at the flow rates calculated by the algorithm during changes in reactor temperature, waiting for steady state and analysis and would only change when new conditions were calculated.

Table 6.4 Comparison of material used during different optimisation approaches

	Nitrobenzene **6.12**		Morpholine	
	Total / g	Per experiment / mg	Total / g	Per experiment / mg
Pulsed Flow	14.5	135	14.7	137
Step Flow	37.1	347	37.7	352
Continuous Flow	74.7	698	75.6	707

The amount of material required for the different flow modes is shown in Table 6.4. The pulsed flows optimisation used a total of 14.5 g of nitrobenzene **6.12** and 14.7 g of morpholine, averaging 135 mg and 137 mg per experiment, respectively. This resulted in savings of 61% and 81% compared to the step flow and continuous flow modes, respectively.

6.4 Optimising For Multiple Targets

STY is a useful metric to improve the productivity of a process but in this case has produced conditions that have not reached full conversion of nitrobenzene **6.12** and is therefore wasting material. According to the kinetic model of this reaction, a slight increase in the residence time is likely to result in a higher conversion and yield without overreacting to form di **6.15**.[60] However this would lower the reactor productivity. A more advantageous approach would be to optimise the reaction for more than one target function. Process mass intensity (PMI) measures the amount of waste in a synthetic step per mass unit of product

$$PMI = \frac{mass_{reactants}}{mass_{product}} \tag{6.11}$$

and the American Chemistry Society Green Chemistry Institute Roundtable also selects it as the best metric for sustainable manufacture.[182] Therefore it was decided to optimise the reaction for both STY and PMI in order to maximise productivity and minimise waste.

6.4.1 Bayesian Approach to Multi-Objective Optimisations

In order to optimise for more than one target, it is possible to create a single function that incorporates multiple targets,[27] however a better strategy is to use a multi-objective optimising algorithm. In multi-objective optimisation, the main objectives are to form a Pareto front, a number of points that form a compromise between the different target functions; and to make this Pareto front as diverse as possible across experimental space.[253]

The algorithm used was the Thompson sampling-evolutionary global optimisation algorithms (TS-EMO), developed at the University of Cambridge.[254, 255] The algorithm uses Thompson sampling and Bayesian analysis to generate and validate surrogate models that satisfy the optimising function, in this case the S_NAr reaction (Scheme 6.3). This algorithm is a second generation version of the multi-objective active learner (MOAL) algorithm,[171] previously used for the multi-target optimisation of an emulsion polymerisation.[26]

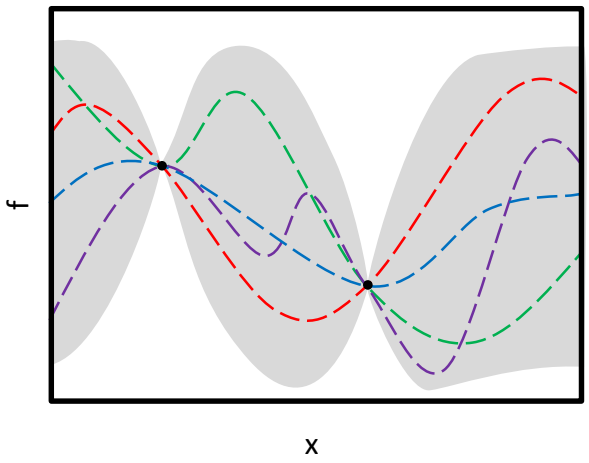

Figure 6.13 Bayesian analysis of surrogate models for a single factor variable, x, with response, f. The black dots signify existing experiments and responses, the coloured dashed lines signify surrogate models that fit the current experiments. The grey shading shows the uncertainty of the response of the unexplored experimental space. Note that the uncertainty is zero for the two experimental data points.

The algorithm starts by generating an initial number of experiments using a latin hypercube generator.[256] From this data, a number of surrogate models are created using Gaussian processes and the algorithm continually minimises the responses by using Thompson sampling, which is a

method of choosing the best potential surrogate model based on the expected maximum improvement over the existing responses.[257] Thompson sampling is a form of Bayesian analysis, which choses new conditions based on the known response of existing experiments (Figure 6.13).

6.4.2 Multi-Objective Self-Optimisation

The S_NAr reaction was optimised using the TS-EMO algorithm according to the limits displayed in Table 6.5. The limits were adjusted from the first optimisation based on the optimum STY and to better test the new algorithm. The residence time limits were reduced and morpholine limits increased with the aim to generate a large Pareto front of short residence times and high equivalents, leading to high STY; and longer residence times and low equivalents, leading to low PMI. The temperature was raised to increase yield in compensation for the shorter residence times.

Table 6.5 Optimisation limits for the multi-objective optimisation of *ortho* **13**

Limit	Residence time / min	Morpholine / mol eq	Concentration / mol L^{-1}	Temperature / °C
Lower	0.5	1.0	0.100	60
Upper	2	5.0	0.500	140

The results of the optimisation are shown in Figure 6.14. It was necessary to transform the responses of both PMI and STY using natural logarithms so that the algorithm would be able to fit better models. The STY response was then converted to negative because the algorithm would minimise any response and STY needed to be maximised.

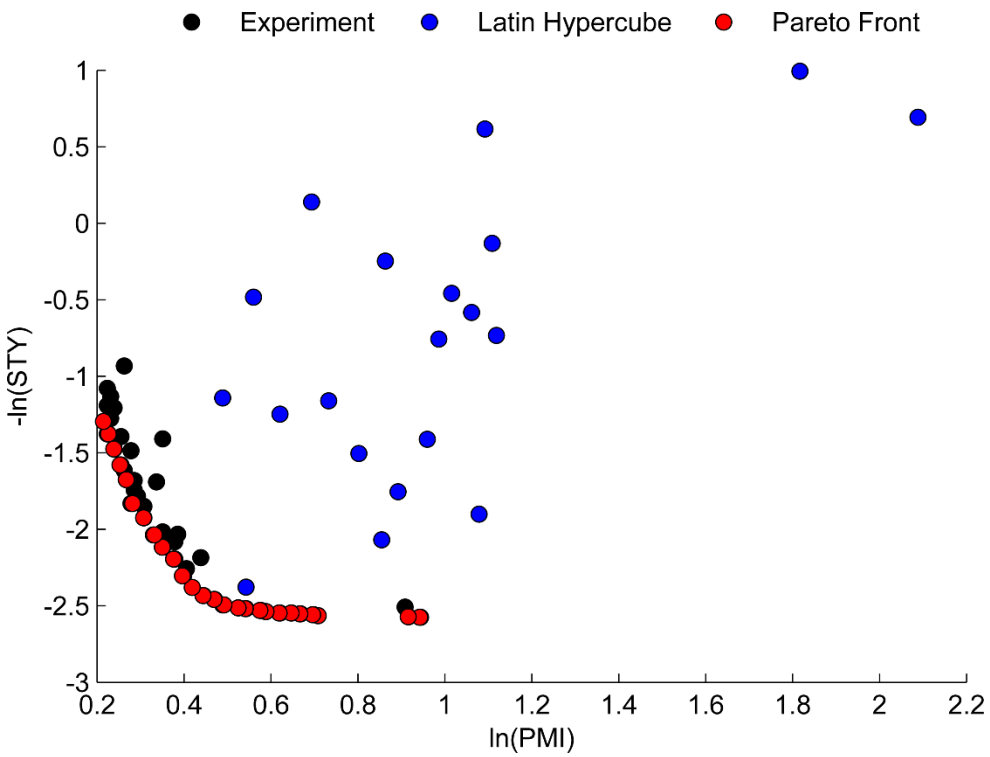

Figure 6.14 Results of the TS-EMO multi-objective optimisation. The x and y axes show the natural logarithm of PMI and the negative natural logarithm of STY, respectively. The blue data points show the initial latin hypercube data; black points show the experiments generated by the surrogate models of the algorithm; and red points show the experiments that converged to a pareto front.

The initial latin hypercube generated 20 experiments with a general trend of low PMI but also low STY. The TS-EMO algorithm then generated a further 48 experiments, creating a dense Pareto front of 26 points. The conditions of the Pareto front are shown in Table 6.6 and all have consistently high temperature (140 ºC) and concentration (0.500 mol L^{-1}). This can be explained by the very fast first step to form the desired ortho/para mono-substituted product, which donates more electron density to the aromatic ring thus making the compound less likely to undergo the second substitution to form the di. Therefore reactions could be carried out at the maximum temperature and morpholine eq without risk of overreaction to the di because of the short residence times.

The compromise in the optimum conditions occurred between the residence time and morpholine eq. Conditions with a short residence time and high eq resulted in a maximum STY and high PMI (Table 6.6, entry 1, 0.50 min, 4.70 eq, 0.500 mol L^{-1}, 140 ºC, STY = 218.62 kg L^{-1} h^{-1}, PMI = 2.57). Conversely, a long residence time and low morpholine eq resulted in a low STY and minimum PMI (Table 6.6, entry 26, 1.62 min, 1.00 eq, 0.500 mol L^{-1}, 140 ºC, STY = 60.76 kg L^{-1} h^{-1}, PMI = 1.24).

Table 6.6 Reaction conditions of Pareto points

Exp no	t_{Res} / min	Morph eq	Conc / mol L^{-1}	Temp / ^{o}C	STY / kg L^{-1} h^{-1}	PMI
1	0.50	4.70	0.500	140.0	13.12	2.565
2	0.50	4.51	0.500	140.0	13.08	2.498
3	0.50	3.28	0.500	140.0	12.99	2.031
4	0.50	3.19	0.500	140.0	12.91	2.005
5	0.50	3.01	0.500	140.0	12.83	1.947
6	0.50	2.89	0.500	140.0	12.76	1.908
7	0.50	2.76	0.500	140.0	12.76	1.856
8	0.50	2.58	0.500	140.0	12.65	1.801
9	0.50	2.49	0.500	139.6	12.55	1.776
10	0.50	2.29	0.500	137.8	12.40	1.717
11	0.50	2.20	0.500	139.4	12.34	1.689
12	0.50	2.00	0.500	140.0	12.10	1.635
13	0.50	1.78	0.500	140.0	11.68	1.598
14	0.50	1.60	0.500	140.0	11.39	1.558
15	0.50	1.34	0.500	140.0	10.80	1.520
16	0.53	1.23	0.500	140.0	10.01	1.486
17	0.60	1.19	0.500	140.0	8.97	1.456
18	0.70	1.37	0.500	140.0	8.30	1.419
19	0.77	1.33	0.500	140.0	7.66	1.393
20	0.81	1.07	0.500	140.0	6.85	1.359
21	0.93	1.13	0.500	140.0	6.24	1.325
22	1.05	1.00	0.500	140.0	5.34	1.306
23	1.18	1.00	0.500	140.0	4.85	1.287
24	1.32	1.00	0.500	140.0	4.37	1.269
25	1.52	1.09	0.500	140.0	3.96	1.253
26	1.62	1.00	0.500	140.0	3.65	1.239

tRes – residence time, Morph – morpholine, Conc – concentration, Temp - temperature, STY – space time yield, PMI – process mass intensity.

An advantage with using a dual-objective algorithm was that it provides a clear compromise between the two targets and allows the user to pick an optimum point based on the response of additional metrics such as cost, yield or selectivity (Figure 6.15). However the main advantage with using this algorithm is the amount of information the user obtains from the data compared to the number of experiments. The algorithm required a total of 68 experiments, which is within the same magnitude as has previously been carried out in other chapters for single objective optimisations.

Not only has the algorithm optimised for two targets but, in generating a Pareto front, has shown much more clearly how the conditions reach a compromise between different targets.

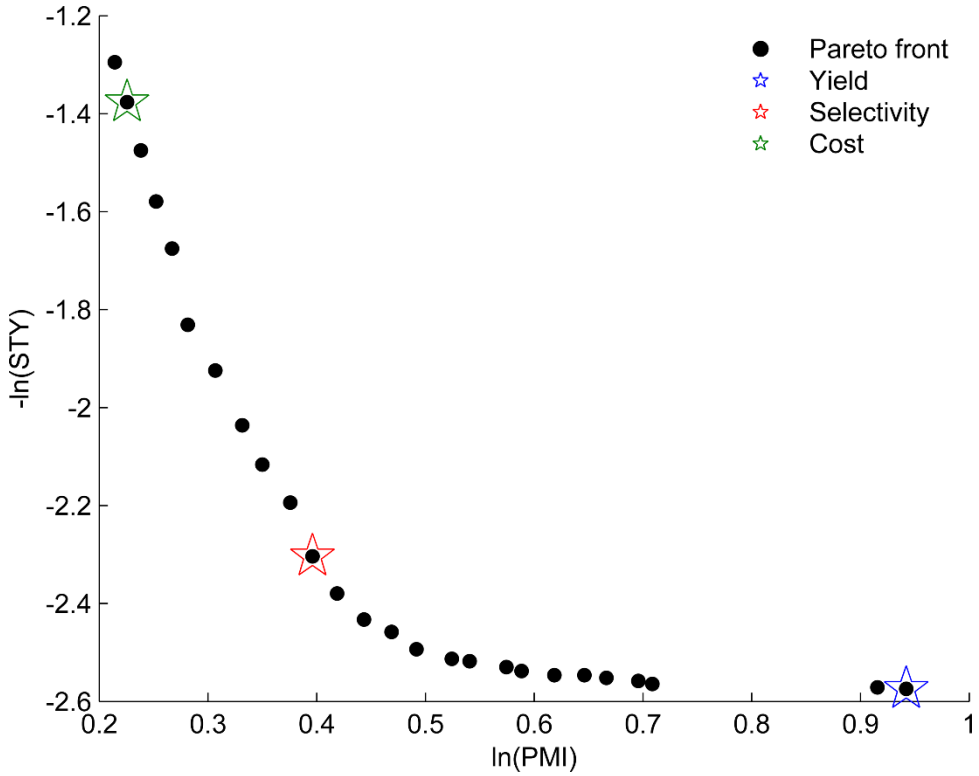

Figure 6.15 Pareto front with optima for other targets highlighted. Blue - % yield (96.6%), red - % selectivity of para (96.7%), green – cost of raw materials £ kg^{-1} (£ 145.85 kg^{-1}).

6.5 Conclusions

The desire to reduce the amount of material consumption in chemical development can clearly be explained by economic and environmental factors. Through automation of chemical reactors, numerous experiments can be carried out that screen multiple physical conditions and choices of substrates, reagents, solvents etc. therefore reducing the number of man-hours designated to performing tedious unskilled tasks. The successful automation of chemical discovery, [220-223] synthesis, [96, 224-226] screening[227-229] and optimisation[14, 15, 20, 172, 215] has not only resulted in more efficient practical work but has also contributed to improving the quality of the desired output, be it physical product or numerical data.

However there is still more that can be done. The self-optimisation of continuous flow reactors can generate a large amount of waste for numerous reasons. Firstly due to the nature of flow chemistry. Although there has been great success with the miniaturisation of flow reactors,[35, 45, 129, 258, 259] any flow reactor will typically use more material than a batch counterpart. The liquid

metering pumps need to be primed, which results in pumping material to waste (except some syringe pumps). When the experimental work is finished, any unused chemicals are disposed of either to prevent contamination or because they are mixed in a solution. In batch, the desired quantity of chemicals is transferred into the reactor with minimal excess waste. Secondly, for most applications only the data is required and the product stream is directly disposed of.[22] Thirdly, more than one reactor volume needs to be pumped before steady state is reached, resulting in material wasted. Finally, a poor choice of algorithm is used, which either stops at a local optimum or does not provide enough information about the reaction system, requiring additional experimentation to take place.

The first problem can be addressed by sensible planning and careful use of equipment to ensure that material is not unnecessarily wasted. The second is a general issue with experimenting for reaction development and optimisation because it is often not practical to keep the reaction contents. However, the best attempts can be made to reduce the amount of material that is used for each reaction, which addresses the third problem. The work in this chapter follows that of Reizman *et al*. to use compartmentalised flow that contains a reaction pulse smaller than the reactor volume. By using gas/liquid segmented flow, Reizman was able to introduce reactor pulses that would not suffer from dispersion and reduced the material required by 96%.[9] However, the reactor setup used was complex and would potentially be intimidating to the novice user. The approach used in this chapter characterised the reactor RTD and showed that the error associated with dispersion from liquid/liquid pulsed flow was minimal and could provide material savings of 67%.[9] Whilst the pulsed flows delivered less saving than the segmented flows, the approach in this chapter could be introduced into an existing automated continuous reactor, whereas a completely new reactor needed to be designed for Reizman's approach.

The next challenge is to further reduce the amount of material used in the pulsed flows. This can be achieved by either reducing the reactor or the pulse volume. Reducing the pulse size would result in too much dispersion to deliver accurate results, and it is highly likely that reducing the volume would lead to a loss of plug flow behaviour due to lower flow velocities to achieve the

[9] Material savings are calculated based on 1.5 reactor volumes to reach steady state under continuous flow vs the volume of the pulse in the compartmentalised flow.

same residence time. However, it would be possible to use tubing with a narrower internal diameter in the reactor, which would provide the opportunity to use smaller pulse volumes and possibly even a smaller reactor size, depending on the RTD results of the new tubing.

The final problem with self-optimisation is a poor choice of algorithm, which does not provide enough information about the system. The simplex algorithm,[137] and its modifications,[138, 139, 149] is an effective algorithm for quickly finding the closest optimum from a starting point, however it can sometimes stop at a local, rather than a global, optimum. The use of global searching algorithms (e.g. SNOBFIT and genetic algorithm) can circumvent this problem by scanning all the experimental space, but can only optimise for one target at a time. The work in this chapter has shown how using a multi-objective algorithm can find a distribution of points that find a compromise between two different targets. With this set of points, optimum points for other targets can be found and optimum conditions for separate three target optimisations were found. Plus, the algorithm required a similar number of experiments (68) to single target global searching algorithms.

In summary, two separate strategies were implemented to reduce material usage in self-optimisation. First, pulsed flows were introduced, which resulted in a material saving of 81% *vs* continuous flow operation. Secondly, a multi-objective algorithm was used, which was able to find a set of compromising optimum conditions between STY and PMI and could be used to further create three-target optimum conditions. This was achieved using a similar number of experiments to single target optimisations and creates a theoretical three-fold material saving.

7. Conclusions

The recurring theme of this thesis has been a reflective look at existing technologies associated with automated optimisation of flow reactors and how to improve them. In the first chapter, a list of disadvantages with existing self-optimisation technologies was identified that needed to be addressed before its widespread use in pharmaceutical process development. These were:

- Applicability to complex pharmaceutical reaction steps
- Integration with existing statistical design techniques
- Combining self-optimisation with different types of online analytical equipment
- Evaluating the correct target function and/or best algorithm
- Minimising the amount of waste material

This thesis has contributed to addressing all of these points in various different formats. In Chapter 3, the final bond-forming step in the synthesis of the API osimertinib (AZD9291) was self-optimised in continuous flow. Osimertinib is an irreversible EGFR tyrosine kinase inhibitor for T790M mutations in non-small cell lung cancer, developed by AstraZeneca (AZ).[160, 161, 168] Phase I clinical trials with osimertinib began in March 2015 and FDA approval was granted 2.5 years later in November 2015.[260] In collaboration with AZ, self-optimisation studies started in early 2014 and it was hypothesised that the rapid technique could help AZ process development scientists, who were working on a much shorter timescale than for most pharmaceutical approval timescales.

Initial optimisations were carried out on a model compound, which highlighted that the potential bottlenecks would be with generating flow conditions that could be pumped continuously without clogging. Once these conditions were discovered reaction screening was rapid and facile and two separate optimisations were carried out in order to maximise the yield of the desired model acrylamide **7** and a potential impurity. The coverage of experimental results across the process design space enabled by the SNOBFIT algorithm provided potential impurity routes, which could be verified using offline LC-MS.

The initial experiments showed that the AZD9291 aniline had much lower reactivity than the model aniline and thus required much more forcing conditions. The AZD9291 optimisations also had a much more complex experimental space and as such had a smaller region of optimum values. This could be caused by more favourable impurity pathways caused by the more forcing conditions

but there was not the same success in mapping these impurity pathways than there was with the model compound.

The biggest positive from the study was that self-optimisation could be used to optimise a pharmaceutical reaction step without consuming large amounts of starting material. The disadvantages was that the lack of restraint applied to the algorithm generated results with very high reagent stoichiometry and the results only focused on the reaction step and not any downstream processes. The first point could be addressed by improved algorithms or target functions, which unfortunately wasn't possible within the scope of this study. The second point obviously requires integration of downstream processing equipment before online analysis. With techniques where an empirical model is obtained, it is possible to see the compromise between reagent stoichiometry, cost and yield.

Chapter 4 addressed this point by using existing DoE fitting techniques and applying them to data obtained from a self-optimisation. It was necessary to change the boundary limits, and with it the experimental design space, in order to obtain models with a good fit and predictability. Once an empirical model was obtained, it was possible to find optimum conditions for different metrics as well as optima that compromised between these different target functions.

A new form of analysis for automated flow reactor optimisation was introduced in Chapter 5 – mass spectrometry (MS). The advantage with MS is that it has a very short acquisition time, will inherently separate compounds based on their molecular weight and can provide quantitative analysis. The disadvantage is that the MS signal can be difficult to calibrate because of a lack of linear response across the whole experimental area. In the chapter, the MS was calibrated to HPLC then used to optimise an amide bond formation using SNOBFIT algorithm and DoE.

However, it has yet to be shown that MS can be used for quantitative analysis of pharmaceutically relevant reactions. All existing calibration techniques have calibrated all known compounds in the reactions including by-products and impurities. In pharmaceutical process development, it is not always possible to identify and isolate all impurities and therefore this technique cannot be used. A more advantageous technique could be to calibrate the desired compound relative to an internal standard, which is commonplace in chromatography and spectroscopy. However the signal of both the analyte and internal standard need to be linear across

the experimental space because an increase in calculated yield could be a result of internal standard suppression rather than actual reaction yield. Another technique could be to simply maximise the raw mass count of the product peak then quantify the optimum response by offline analysis of optimum conditions. However, this does not account for suppression of signal and would only provide information about the optimum and not any other experiments. In conclusion, MS is a very powerful technique but more work is required in its calibration.

The final chapter addressed the need to reduce the amount of material wasted in automated optimisations. This was done in two parts: first, use of sub reactor volume pulses that are suspended between carried solvent; second, use of an algorithm that can optimise for more than one target function at a time. Initial reaction screening showed that 0.5 reactor pulse volume would provide the same results as waiting for 2 reactor volumes for steady state with minimal dispersion. A nucleophilic aromatic substitution was successfully optimised using this pulse volume. Next, a new evolutionary algorithm was used, which could generate a list of optimum values that compromised between maximum productivity and minimum waste.

It has already been proved that it is possible to reduce the pulse size volume by using gas as the carrier fluid in a dispersion-free system.[20, 21, 185] However this reactor setup was incredibly complicated. In order to improve the liquid/liquid pulsed flow carrier system then the reactor volume can be decreased by using narrower tubing. Unfortunately this was out of the scope of this project but plans are already in place to continue the work in this direction.

7.1 Future Work

In the examples in this thesis, there was not strict control over the quenching of reactions and it was assumed that the small injection volume into the HPLC mobile phase would result in a low enough concentration to effectively stop the reaction before components were separated on the column. However the work-up and isolation of a product is incredibly important and can be an area where impurities are created, increased or purged. The ease at which multiple sets of reactors and downstream equipment can be combined in continuous reactors means that it should be easy to include work-up procedures as variables in an optimisation. For example, the flow rate of a quench pump can change the molar equivalents of quenching reagent and physical mixing of that quench,

which in turn can change the impurity profile of the product. In other processes it could be possible that a reaction is carried out in batch then purified using continuous distillation or purification and there doesn't yet exist any automated optimisation of these processes. In summary, it would be highly advantageous to the pharmaceutical industry to see more example of self-optimised unit operations and not just reactions.

Solubility is a problem that haunts many flow chemists and the requirement for homogeneity can drive researchers away from particular reactions or substrates.[95] There have been reactors designed to incorporate solid formation and can result in niche reaction conditions, not achievable in batch.[261] However for these reactors to be adopted in self-optimisation, there needs to be techniques to sample reaction slurries for online analysis.

Another area of improvement is in the area of discrete variable optimisation. Continuous variables (e.g. concentration, time, temperature) are easy to optimise for by changing pump flow rates and reactor temperature. However it is difficult to screen which is the best catalyst, solvent, base or a combination of all using optimising algorithms because they need to correlate to a number. In work by Reizman and Jensen, multiple FEDs were carried out with each different discrete variable then steepest descent algorithm optimised the continuous variables.[20, 21, 185] However there was little intelligent initial screening of the discrete variables and it relied heavily on high throughput screening, where multiple reactions of different discrete variables are carried out then the results compared.[227, 262]

Principal component analysis (PCA) is a technique that separates the properties of multiple discrete variables into two or three principal components.[263] Murray *et al*. used PCA to transform two Pd sources, nine phosphine ligands, four bases and nine solvents into a three dimensional experimental space.[264] With a 3-dimensional space, a series of DoE designs were used to hone in and then find the best combination of catalyst, base and solvent for a Buchwald-Hartwig sulfamidation, reducing the number of experiments from a possible 51 million to only 78. It is surely sensible to use an optimising algorithm to concurrently search the discrete variables and optimise the continuous variables with a tandem PCA-algorithm technique.

The difficulty in screening multiple discrete variables is the reactor setup. If the reactor setup in this thesis was adopted, where each continuous variable is controlled by a piece of equipment,

then each solvent and reagent would need its own pump or a series of switching valves connected to a single pump, assuming everything is liquid. For solid reagents, all combinations of reagent in solvent would need to be prepared, requiring a very large number of pumps. E.g. four solid reagents in four different solvents would require 16 separate pumps. Assuming that there is the physical laboratory space to connect all this equipment, the costs associated would be very high, probably too high for an academic environment.

Therefore the sensible approach would include robotics, with solid and liquid metering systems to prepare pump solutions of various compositions in order to test in the reactor. The disadvantage with this approach is the technological expertise required to operate robotics. The majority of researchers in self-optimisation are chemists/chemical engineers that have learnt to code laboratory equipment as part of their project requirements. Introducing robotics opens up a whole new field of electronic engineering which can be daunting to an adept coder, let alone a novice.

This also fuels the final requirement – a commercially available self-optimisation platform. I.e. a software/hardware package that can be bought and used to integrate all sorts of pumps, reactors and analysis with intelligent program control and minimising algorithms. It has been mentioned a few times in this chapter how equipment is more readily integrated if it is commercially available and does not need specialist individual manufacture. This alone would contribute to the widespread use of automated flow reactors but would be very difficult to implement. There are several different companies that make analytical equipment, and they all use different software programs. This would require collaboration between companies in order to make it easy to integrate all their software together. Protection of intellectual property is paramount to a company's success and integration of multiple forms of technology into one platform is not just a problem for chemical consumers.

7.2 Summary and Outlook

In summary, self-optimisation is a rapid form of finding optimum conditions and recent advances are making it a much more attractive form of technology for the pharmaceutical industry to adopt. The work in this thesis has looked at widespread approaches to improve self-

optimisations by applying it to the synthesis of APIs, combining existing DoE techniques with newer self-optimisation algorithms, introducing new forms of online analysis, reducing the amount of material by carrying out reactions with pulsed flows and using more intelligent algorithms.

However, like all forms of science, there is always scope for improvement. Self-optimising reactors will naturally advance with the progress of flow reactor technologies, but the reactor is just one part of the setup. Analytical methods that can provide quantitative data faster with higher resolution is necessary for self-optimisation advancement but the greatest progress can be made with the feedback loop. More rapid screening of discrete and continuous variables with intelligent algorithms enables faster process development and increases the likelihood of self-optimisation being adopted in the fine chemical industries

8. Experimental

This chapter summarises the practical experimental information, procedures and raw data. Detailed descriptions about the automated flow reactor and general self-optimisation procedures can be found in Chapter 2. Any description of equipment in this chapter applies to offline analytical techniques.

8.1 Analytical Equipment

NMR analysis was carried out using a Bruker Advance 500 MHz or Bruker DPX 300MHz fourier transform machine. Chemical shifts are quoted as parts per million (ppm) with reference to an internal solvent peak of $SiMe_4$. Peaks are quoted as s (singlet), br s (broad singlet), d (doublet), t (triplet), or multiplet (m). LC-MS analysis was collected using an Agilent 1290 UHPLC with Bruker HCT-Ultra detector. Accurate mass MS was carried out using a Bruker MaXis Impact. IR was collected using a Bruker Alpha FT-IR.

8.2 Chapter 3 Procedures

8.2.1 Chemicals

All chemicals were commercially available and used without further purification, unless otherwise stated: 2,4-dimethoxyaniline (Maybridge, 97%), triethylamine (Acros 99%), 3-chloropropionyl chloride (Acros 98%), hydrochloric acid (Fisher, 37%) biphenyl (Aldrich, 99.5% GC), acetonitrile (VWR, 99.9%). Anhydrous acetonitrile was obtained from departmental solvent purification system with a water content of 2.6 ppm. AZD9291 aniline was supplied by AstraZeneca.

8.2.2 Synthesis of *N*-(2,4-dimethoxyphenyl)prop-2-enamide standard, 3.13

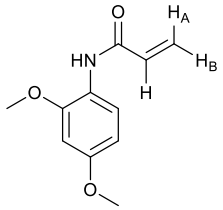

2,4-Dimethoxy aniline (498 mg, 3.25 mmol) and triethylamine (1.15 mL, 8.26 mmol) were dissolved in acetonitrile. The black slurry was cooled to 0 °C (aq ice bath) and 3-chloropronionyl chloride (0.47 mL, 4.92 mmol) was added drop-wise with rigorous stirring. The reaction was stirred at 0 °C for 3 h and then quenched with HCl (2 M, 10 mL). Acetonitrile was removed under vacuum and the resultant residue was washed with dichloromethane (3 x 10 mL) The organic fractions were combined and washed with HCl (2 M, 3 x 10 mL) and then dried (Na_2SO_4) and concentrated under vacuum to leave the crude product as a black flaky solid. Crystalizing from EtOAc–hexane gave the acrylamide **3.13** (512 mg, 2.47 mmol 76%) as dark brown plates, mp 119-121 °C; δ_H (500 MHz, $CDCl_3$, $SiMe_4$) 8.36 (1H, d, *J* 9.0, aryl 6-H), 7.68 (1H, br s, N-H), 6.48-6.50 (2H, m, aryl 3-H and 5-H), 6.40 (1H, dd, *J* 17.0 and 1.0, vinyl 3-H_A), 6.27 (1H, dd, *J* 16.5 and 10.0, vinyl 2-H) 5.72 (1H, dd, *J* 10.0 and 1.0, vinyl 3-H_B), 3.87 (3H, s, methoxy 2-CH_3), 3.80 (3H, s, methoxy 4-CH_3); δ_C (125 MHz, $CDCl_3$, $SiMe_4$) 163.0 (aryl 4-C), 156.5 (CO), 149.2 (aryl 2-C), 133.0 (vinyl 2-C), 131.6 (vinyl 3-C), 121.2 (aryl 1-C), 120.8 (aryl 6-C), 103.8 (aryl 5-C), 98.6 (aryl 3-C) 55.7 (methoxy 2-C), 55.5 (methoxy 4-C); ν_{max}/cm^{-1} (solid); 1453, 1467, 1506, 1536, 1612, 1652, 2942, 2973, 3010, 3233; *m/z* (ESI+) found $[M+H]^+$ 208.0968, $C_{11}H_{14}NO_3$ requires $[M+H]^+$ 208.0968.

8.2.3 Temperature Profile

Pump A reservoir solution: 2,4-dimethoxy aniline (7.70 g, 50.3 mmol) and biphenyl (135 mg, 0.88 mmol) were dissolved in a acetonitrile (156 mL) and water (44 mL) under stirring at ambient temperature. Excess solid was filtered by gravity (0.252 mol L^{-1} aniline, 4.39 mmol L^{-1} IS). Pump B: neat triethylamine (100 mL, 717 mmol, 7.17 mol L^{-1}). Pump C: an oven dried quick fit flask was flushed with nitrogen. 3-chloropropionyl chloride (20 mL, 210 mmol) and anhydrous acetonitrile (75 mL) were added to the flask under nitrogen flow and stirring at ambient temperature (2.2 mol L^{-1}).

The pump flow rates were: A = 0.425 mL min^{-1}, B = 0.078 mL min^{-1}, C = 0.090 mL min^{-1}. A BPR with a fixed pressure of 75 PSI (5 bar) was used and the reactor coil had a volume of 3 mL. A HPLC sample (See section 8.2.5 for method) was taken, 2 reactor volumes after the reactor had

reached the set conditions, at temperatures of 22, 26, 30, 40, 50, 60, 70, 80, 90, 100, 110, 120, 130, 140 and 150 ºC.

8.2.4 Preparation of Pump Reservoir Solutions for Self-Optimisations

Pumps A and B: The desired reagents were dissolved in MeCN and H_2O (7:2, v:v, MeCN:H_2O) under stirring at ambient conditions. 2,4-Dimethoxyaniline solution was filtered before use. Pump C: 3-chloropropionyl chloride was added to a dry quick-fit conical flask, fitted with a septum and purged with nitrogen. Anhydrous acetonitrile was added under stirring and nitrogen flow. The solutions were prepared according to the concentrations in Table 8.1

Table 8.1 Concentrations for Chapter 3 stock solutions

	Pump A		Pump B		Pump C	
	Reagent	Concentration / mol L^{-1}	Reagent	Concentration / mol L^{-1}	Reagent	Concentration / mol L^{-1}
Model	Aniline Biphenyl	0.241 0.0156	NEt_3	3.73	3-chloropropionyl chloride	1.00
AZD9291	Aniline Biphenyl	0.241 0.0156	NEt_3	3.73	3-chloropropionyl chloride	0.500

8.2.5 Model Acrylamide Optimisation

At-line HPLC analysis was carried out using an Agilent 1100 HPLC. Method: Sigma Ascentis Express C18 (50 x 6.6 mm, 2.7 μm) column; A 0.1 % (v:v) aqueous TFA, B 0.1 % (v:v) TFA in MeCN; 5% to 95% B over 8.5 min, to 5% B after 9.5 min, post time 30 s; 1.2 mL min^{-1} , 254 nm, 20 °C.

Table 8.2 Optimisation limits for the model compound optimisation

Limits	Pump A flow / mL min^{-1}	NEt_3 mol eq	Acid chloride mol eq	Temperature / °C
Lower	0.100	4.5	0.9	0
Upper	0.400	20	2.1	130

Table 8.3 List of conditions and yield of acrylamide for the model compound optimisation. Optimum conditions highlighted in bold.

Entry	A / mL min^{-1}	C / eq	B / eq	Temperature / °C	A_x/A_{IS}	Yield %
1	0.495	1.0	7.1	0.1	1.86	26.2

Entry	A / mL min^{-1}	C / eq	B / eq	Temperature / °C	A_x/A_{IS}	Yield %
2	0.369	1.8	15.5	63.4	2.34	35.2
3	0.333	1.9	8.0	96.7	2.43	38.8
4	0.214	1.3	5.3	130.0	2.63	41.9
5	0.480	1.9	13.2	16.0	2.34	35.7
6	0.120	1.2	11.3	31.8	3.26	65.1
7	0.340	1.2	11.3	80.9	2.65	45.3
8	0.360	0.9	6.7	113.4	2.67	47.7
9	0.180	1.5	7.8	47.7	2.94	49.6
10	0.490	1.2	7.3	71.6	2.08	30.0
11	0.490	1.6	12.6	105.4	2.53	39.9
12	0.470	1.1	9.8	121.6	2.90	56.0
13	0.500	0.9	8.6	13.1	1.94	30.4
14	0.100	1.2	4.8	54.2	2.82	46.3
15	0.220	1.7	9.2	64.2	2.93	49.2
16	0.500	1.5	14.8	130.0	3.22	68.7
17	0.100	1.5	15.2	23.4	3.58	77.3
18	0.100	1.5	14.8	80.9	3.53	85.1
19	0.200	1.7	13.9	80.9	3.48	67.9
20	0.360	1.8	17.7	130.0	3.46	77.7
21	0.340	1.5	14.8	130.0	3.55	80.2
22	0.100	2.0	14.6	0.0	3.71	77.0
23	0.100	1.9	18.5	7.5	3.69	79.1
24	0.320	1.2	6.6	76.6	2.20	31.4
25	0.100	2.0	18.0	84.4	3.61	71.3
26	0.100	1.7	13.8	0.0	3.73	75.6
27	0.100	1.9	15.3	76.3	3.79	77.5
28	0.100	2.1	15.5	79.9	3.74	75.4
29	0.150	1.2	9.8	105.5	3.44	64.8
30	0.220	1.2	11.9	130.0	3.77	91.1
31	0.200	1.0	8.7	15.9	3.00	51.5
32	0.100	2.1	19.5	74.8	3.53	81.1
33	0.100	1.4	9.9	82.7	3.56	69.1
34	0.100	1.8	12.9	89.2	3.64	71.7
35	**0.100**	**1.7**	**16.3**	**117.8**	**3.82**	**91.9**

Table 8.4 Composition of impurities from the list of experiments in Table 8.3.

Entry	Conditions				Yield %			
	A / mL min^{-1}	C / eq	B / eq	Temperature / °C	Aniline	Chloroamide	Enolate	Dimer
1	0.495	1.0	7.1	0.1	0.0	68.4	4.4	0.5
2	0.369	1.8	15.5	63.4	0.0	58.2	5.5	0.4
3	0.333	1.9	8.0	96.7	0.3	54	5.7	0.4
4	0.214	1.3	5.3	130.0	0.0	51	6.3	0.6
5	0.480	1.9	13.2	16.0	0.0	57.6	5.5	0.6
6	0.120	1.2	11.3	31.8	0.5	21.1	12.6	0.8
7	0.340	1.2	11.3	80.9	0.3	47.6	6.1	0.5
8	0.360	0.9	6.7	113.4	0.5	47.1	3.8	0.6
9	0.180	1.5	7.8	47.7	0.0	39.3	9.3	0.6
10	0.490	1.2	7.3	71.6	0.0	63.7	5	0.3
11	0.490	1.6	12.6	105.4	0.0	54.4	4.7	0.4
12	0.470	1.1	9.8	121.6	0.7	40.4	1.6	0.5
13	0.500	0.9	8.6	13.1	0.5	63	5.3	0.4
14	0.100	1.2	4.8	54.2	0.0	42.7	9.6	0.5
15	0.220	1.7	9.2	64.2	0.0	40.8	8.7	0.5
16	0.500	1.5	14.8	130.0	0.4	28.2	1.4	0.7
17	0.100	1.5	15.2	23.4	0.5	6.4	15	0.9
18	0.100	1.5	14.8	80.9	0.5	3.5	9.9	0.9
19	0.200	1.7	13.9	80.9	0.0	21.4	10	0.7
20	0.360	1.8	17.7	130.0	0.3	19.1	1.5	0.8
21	0.340	1.5	14.8	130.0	0.5	17.1	0.9	0.8
22	0.100	2.0	14.6	0.0	0.0	7.8	13.9	0.6
23	0.100	1.9	18.5	7.5	0.0	5.7	14.4	0.8
24	0.320	1.2	6.6	76.6	0.0	62	5.5	0.3
25	0.100	2.0	18.0	84.4	0.0	15.8	12.2	0.7
26	0.100	1.7	13.8	0.0	0.0	8.6	14.6	0.9
27	0.100	1.9	15.3	76.3	0.0	7.1	14.1	0.8
28	0.100	2.1	15.5	79.9	0.0	10.2	13.1	0.8
29	0.150	1.2	9.8	105.5	0.0	23.5	10.3	0.7
30	0.220	1.2	11.9	130.0	1.0	5.4	0.8	1
31	0.200	1.0	8.7	15.9	0.0	36.9	9.9	0.6
32	0.100	2.1	19.5	74.8	0.0	4.9	12.6	0.8

Entry	Conditions				Yield %			
	A / mL min^{-1}	C / eq	B / eq	Temperature / °C	Aniline	Chloroamide	Enolate	Dimer
33	0.100	1.4	9.9	82.7	0.0	16.7	13	0.7
34	0.100	1.8	12.9	89.2	0.0	13.9	13.2	0.7
35	0.100	1.7	16.3	117.8	0.0	2.7	3.9	0.9

8.2.6 Model Enolate Optimisation

At-line HPLC analysis was carried out according to the equipment and methods described for the model acrylamide optimisation (8.2.5)

Table 8.5 List of conditions and yield of enolate for the model enolate optimisation. Experiments from the previous acrylamide optimisation are highlighted with grey fill. Optimum conditions highlighted in bold.

Entry	A / mL min^{-1}	C / eq	B / eq	Temperature / °C	A_x/A_{IS}	Yield %
1	0.495	1.0	7.1	0.1	0.31	4.4
2	0.214	1.3	5.3	130.0	0.4	6.2
3	0.369	1.8	15.5	63.4	0.37	5.5
4	0.333	1.9	8.0	96.7	0.36	5.7
5	0.480	1.9	13.2	16.0	0.36	5.4
6	0.120	1.2	11.3	31.8	0.63	12.5
7	0.340	1.2	11.3	80.9	0.36	6
8	0.360	0.9	6.7	113.4	0.21	3.7
9	0.180	1.5	7.8	47.7	0.55	9.3
10	0.490	1.2	7.3	71.6	0.35	5
11	0.490	1.6	12.6	105.4	0.3	4.7
12	0.470	1.1	9.8	121.6	0.09	1.6
13	0.500	0.9	8.6	13.1	0.34	5.3
14	0.100	1.2	4.8	54.2	0.58	9.5
15	0.220	1.7	9.2	64.2	0.52	8.6
16	0.500	1.5	14.8	130.0	0.07	1.4
17	**0.100**	**1.5**	**15.2**	**23.4**	**0.69**	**14.7**
18	0.100	1.5	14.8	80.9	0.41	9.7
19	0.200	1.7	13.9	80.9	0.52	9.8
20	0.360	1.8	17.7	130.0	0.06	1.4
21	0.340	1.5	14.8	130.0	0.04	0.9
22	0.100	2.0	14.6	0.0	0.67	13.7
23	0.100	1.9	18.5	7.5	0.67	14.1
24	0.320	1.2	6.6	76.6	0.38	5.4

Entry	A / mL min^{-1}	C / eq	B / eq	Temperature / °C	A_x/A_{IS}	Yield %
25	0.100	2.0	18.0	84.4	0.62	11.9
26	0.100	1.7	13.8	0.0	0.72	14.4
27	0.100	1.9	15.3	76.3	0.69	13.7
28	0.100	2.1	15.5	79.9	0.65	12.8
29	0.150	1.2	9.8	105.5	0.54	10.1
30	0.220	1.2	11.9	130.0	0.03	0.7
31	0.200	1.0	8.7	15.9	0.58	9.9
32	0.100	2.1	19.5	74.8	0.55	12.2
33	0.100	1.4	9.9	82.7	0.67	12.8
34	0.100	1.8	12.9	89.2	0.67	12.9
35	0.100	1.7	16.3	117.8	0.16	3.8
36	0.100	1.3	12.4	0.0	0.26	8.1
37	0.260	1.5	11.1	23.8	0.5	7.7
38	0.100	1.7	12.8	38.4	0.73	14.1
39	0.100	1.5	10.5	74.7	0.73	14.1
40	0.100	0.9	8.6	93.3	0.12	3.4
41	0.100	1.5	8.6	2.5	0.62	11.4
42	0.100	1.3	9.6	5.1	0.56	10.2
43	0.160	1.9	8.9	32.1	0.57	10.7
44	0.100	1.9	10.4	66.7	0.68	13.5
45	0.370	1.4	6.6	38.3	0.37	5.3
46	0.100	2.0	18.9	44.3	0.64	12.3
47	0.100	1.7	11.7	66.7	0.68	13.7
48	0.100	2.1	11.9	85.9	0.65	13
49	0.100	2.1	18.2	11.8	0.67	13.6
50	0.100	1.5	8.7	37.3	0.72	14.1
51	0.380	1.7	9.2	48.3	0.29	4.3
52	0.100	1.3	8.3	71.5	0	0
53	0.100	1.6	6.3	82.7	0.49	8.1
54	0.310	1.2	8.9	31.8	0.53	8.9
55	0.490	1.3	5.2	68.5	0.33	4.6
56	0.300	1.7	9.5	74.5	0.44	7.2
57	0.500	1.6	8.1	75.2	0.38	5.5
58	0.100	1.8	11.2	76.5	0.68	12.7
59	0.220	1.7	9.6	16.1	0.48	7.8
60	0.270	2.1	12.9	67.7	0.39	6.4
61	0.500	1.3	5.6	69.5	0.3	4.2

8.2.7 Impurity Identification with Offline LC-MS

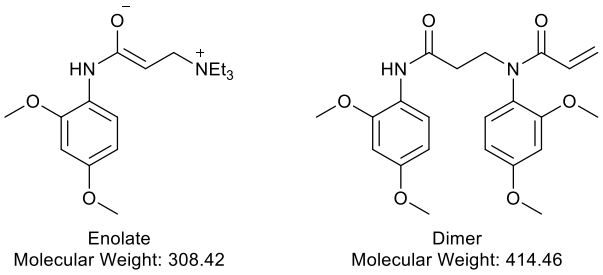

Figure 8.1 Structures and molecular weights of enolate (left) and dimer (right) impurities

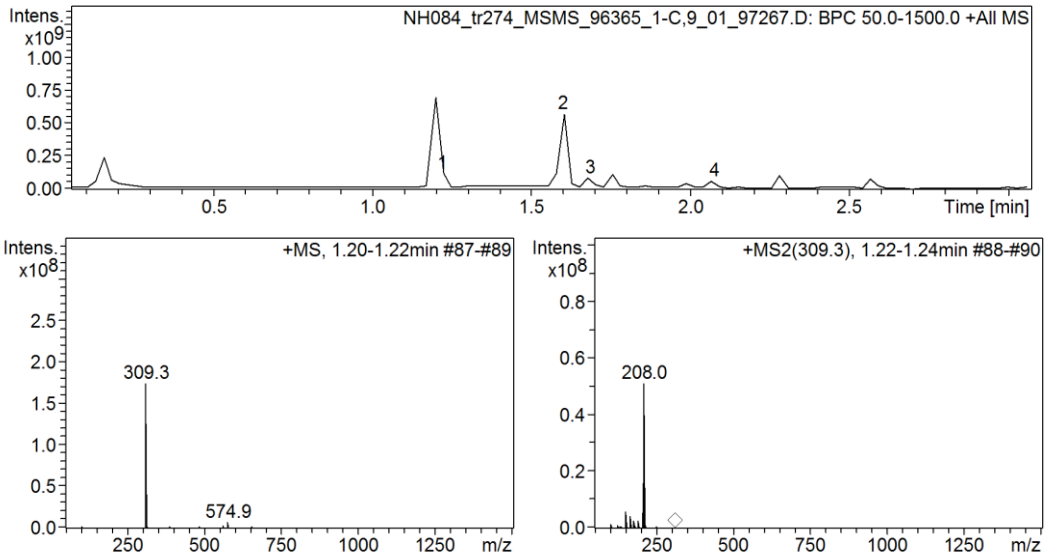

Figure 8.2 LC-MS chromatogram (above) and MS-MS spectra of compound t_R 1.22 min (below), identified as model enolate.

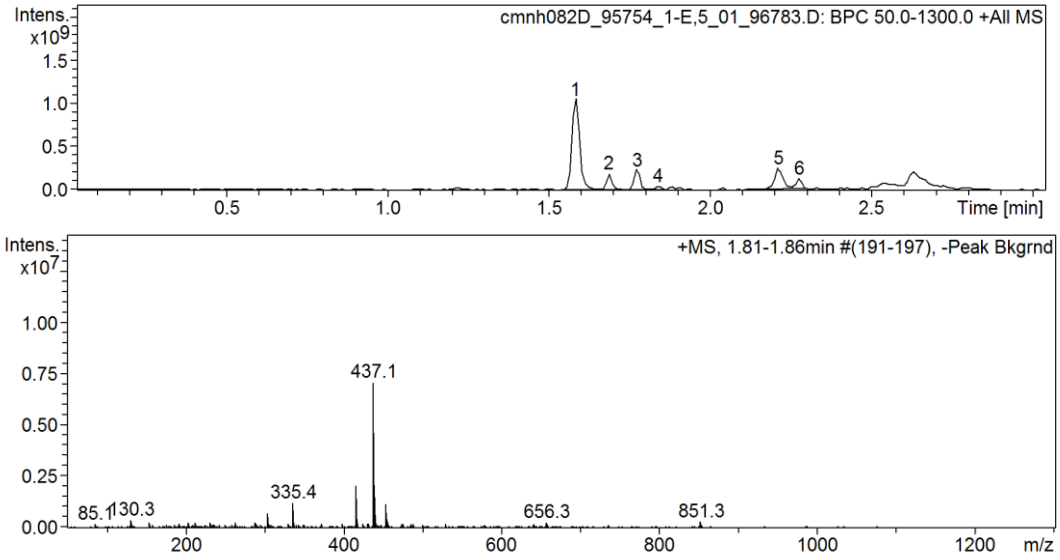

Figure 8.3 LC-MS chromatogram (above) and MS spectrum (below) of compound t_R 1.80 min, identified as model dimer.

8.2.8 AZD9291 Acrylamide Optimisation

At-line HPLC was carried out using an Agilent 1100 HPLC. Method: Waters X-Bridge C18 (150 x 30 mm, 3.5 µm) column; A H_2O, B MeCN, C 10% (v:v) aqueous TFA; 5% to 38% B over 10 min, to 95% B after 15 min to 5% B after 15.1 min, 3% C hold over 15.1 min, post time 3 min (5% B, 3% C); 1.0 mL min^{-1}, 210 nm, 40 °C.

Table 8.6 Optimisation limits for the AZD9291 compound optimisation

Limits	Pump A flow / mL min^{-1}	NEt_3 mol eq	Acid chloride mol eq	Temperature / °C
Lower	0.080	2.2	0.75	80
Upper	0.150	15	3.0	150

Table 8.7 List of conditions and acrylamide yield for the AZD9291 optimisation. Optimum conditions are highlighted in bold.

Entry	A / mL min^{-1}	C / eq	B / eq	Temperature / °C	A_x/A_{IS}	Yield %
1	0.100	1.3	5.0	80.1	1.80	37.1
2	0.118	2.4	9.4	149.8	2.87	68.0
3	0.130	0.9	3.7	141.1	2.97	53.7
4	0.100	1.9	5.0	105.4	3.52	72.3
5	0.120	1.0	3.3	106.3	2.37	47.3
6	0.080	0.8	2.2	150.0	1.99	55.8
7	0.150	1.9	8.6	150.0	2.93	67.8
8	0.080	0.8	2.6	93.6	1.80	41.1
9	0.080	2.8	7.6	99.6	3.82	79.4
10	0.080	2.4	6.3	107.1	2.69	57.1
11	0.100	1.4	5.4	119.4	1.98	51.1
12	0.150	0.8	2.6	147.6	2.21	51.3
13	0.090	3.0	9.5	88.2	2.70	71.2
14	0.120	2.4	6.5	104.4	3.23	77.1
15	0.110	3.0	8.0	106.1	3.59	82.3
16	**0.110**	**2.7**	**10.5**	**123.9**	**4.49**	**88.9**
17	0.120	1.0	3.3	86.6	2.15	48.8
18	0.100	0.9	2.5	106.3	2.41	56.7
19	0.110	1.8	4.8	124.0	3.18	83.2
20	0.090	3.0	9.9	124.2	3.86	85.6
21	0.080	1.8	4.7	103.0	3.34	75.1
22	0.100	1.4	6.7	110.9	2.81	69.3
23	0.130	3.0	13.8	123.3	4.29	83.2

Entry	A / mL min^{-1}	C / eq	B / eq	Temperature / °C	A_x/A_{IS}	Yield %
24	0.090	2.4	6.4	123.3	3.47	81.6
25	0.120	3.0	14.9	141.1	3.77	75.7
26	0.100	3.0	10.6	111.0	3.14	74.0
27	0.090	3.0	13.6	124.1	3.35	74.7
28	0.140	3.0	11.4	138.3	3.77	81.0
29	0.110	1.3	4.3	145.6	3.36	72.0
30	0.120	1.1	5.3	121.7	2.49	61.6
31	0.150	3.0	10.9	123.4	3.69	80.7
32	0.130	3.0	11.1	124.1	3.84	86.5
33	0.130	3.0	14.9	132.6	3.39	86.1
34	0.080	3.0	9.5	103.0	3.93	80.1
35	0.150	3.0	13.1	122.5	3.34	68.5
36	0.090	1.0	2.6	124.9	2.82	62.8
37	0.090	2.4	6.4	125.2	3.37	79.9
38	0.110	2.1	6.7	141.2	3.25	81.3
39	0.130	1.4	5.4	119.4	2.58	65.7
40	0.110	3.0	12.4	122.4	3.56	71.5
41	0.150	2.2	11.0	123.3	2.83	67.3
42	0.150	2.7	13.4	123.8	2.47	68.0

Table 8.8 Composition of impurities from the list of experiments in Table 8.7.

Entry	Conditions				Yield / %					
	A / mL min^{-1}	C / eq	B / eq	Temp / °C	Imp 1	Aniline	Dimer	Chloro-amide	Imp 2	Imp 3
1	0.100	1.3	5.0	80.1	0.3	57.3	1.6	1.2	0.0	0.4
2	0.118	2.4	9.4	149.8	0.3	21.4	4.7	3.1	0.0	0.4
3	0.130	0.9	3.7	141.1	1.9	39.9	0.3	0.0	0.0	0.6
4	0.100	1.9	5.0	105.4	0.3	14.1	4.2	1.8	0.0	0.8
5	0.120	1.0	3.3	106.3	0.6	44.6	2.1	0.6	0.3	0.6
6	0.080	0.8	2.2	150.0	3.0	34.3	0.9	0.0	0.0	0.8
7	0.150	1.9	8.6	150.0	0.7	25.9	0.4	0.0	0.3	0.6
8	0.080	0.8	2.6	93.6	0.7	48.5	2.3	0.6	0.3	0.8
9	0.080	2.8	7.6	99.6	0.0	5.1	6.7	4.0	0.6	0.7
10	0.080	2.4	6.3	107.1	0.4	29.8	2.1	2.1	1.3	0.6
11	0.100	1.4	5.4	119.4	0.8	41.4	0.7	0.4	0.6	1.3
12	0.150	0.8	2.6	147.6	1.4	40.8	0.4	0.4	0.2	0.8
13	0.090	3.0	9.5	88.2	0.3	12.3	4.2	4.5	0.7	0.7
14	0.120	2.4	6.5	104.4	0.4	5.7	4.4	3.6	0.6	0.6

Entry	Conditions				Yield / %					
	A / mL min^{-1}	C / eq	B / eq	Temp / °C	Imp 1	Aniline	Dimer	Chloro-amide	Imp 2	Imp 3
15	0.110	3.0	8.0	106.1	0.3	1.3	4.6	4.6	0.5	0.7
16	0.110	2.7	10.5	123.9	0.0	2.6	1.8	1.1	1.2	0.8
17	0.120	1.0	3.3	86.6	0.2	39.2	2.4	1.4	0.6	0.8
18	0.100	0.9	2.5	106.3	0.8	33.3	2.5	0.7	0.3	1.0
19	0.110	1.8	4.8	124.0	0.4	7.8	1.1	0.7	0.4	0.7
20	0.090	3.0	9.9	124.2	0.5	4.6	0.9	1.3	0.7	0.8
21	0.080	1.8	4.7	103.0	0.3	9.3	4.7	2.0	0.8	0.8
22	0.100	1.4	6.7	110.9	0.4	18.3	2.7	1.4	0.7	0.9
23	0.130	3.0	13.8	123.3	0.0	6.9	2.2	1.7	1.1	0.9
24	0.090	2.4	6.4	123.3	0.4	8.9	0.9	0.8	0.6	0.8
25	0.120	3.0	14.9	141.1	0.0	15.4	1.0	0.8	0.8	0.8
26	0.100	3.0	10.6	111.0	0.0	11.2	3.0	3.1	1.0	0.7
27	0.090	3.0	13.6	124.1	0.0	14.9	0.7	2.1	1.1	0.8
28	0.140	3.0	11.4	138.3	0.0	10.4	0.5	1.0	0.8	1.2
29	0.110	1.3	4.3	145.6	1.2	19.3	0.4	0.3	0.0	1.0
30	0.120	1.1	5.3	121.7	0.7	29.5	0.7	0.5	0.6	1.0
31	0.150	3.0	10.9	123.4	0.0	7.2	1.7	2.3	1.3	0.8
32	0.130	3.0	11.1	124.1	0.0	3.5	1.5	1.8	1.0	0.9
33	0.130	3.0	14.9	132.6	0.0	4.1	0.7	1.4	1.2	0.7
34	0.080	3.0	9.5	103.0	0.0	3.9	4.8	3.3	0.8	1.1
35	0.150	3.0	13.1	122.5	0.0	18.6	1.5	2.1	1.0	0.9
36	0.090	1.0	2.6	124.9	1.4	27.0	0.6	0.2	0.8	1.1
37	0.090	2.4	6.4	125.2	0.5	9.4	0.8	0.8	0.9	0.9
38	0.110	2.1	6.7	141.2	0.5	10.7	0.7	0.0	0.4	1.4
39	0.130	1.4	5.4	119.4	0.4	22.9	1.1	1.0	0.7	0.9
40	0.110	3.0	12.4	122.4	0.0	16.2	1.0	1.5	1.1	1.4
41	0.150	2.2	11.0	123.3	0.0	21.3	1.1	1.6	1.0	1.0
42	0.150	2.7	13.4	123.8	0.0	20.2	1.0	1.2	0.9	1.0

8.3 Chapter 4 Procedures

8.3.1 Chemicals and Procedures

All practical experimental work was carried out by the Bourne group MChem student Mohammed Jeraal. Please see his report for all practical experimental details.[265]

8.3.2 Empirical Model Fitting

All models were fitted using MODDE Pro version 11 (MKS Umetrics) software using multiple linear regressions. Anomalous experiments were measured according to their deleted studentised residuals and removed from models. Model coefficients were removed if their p-value was greater than 0.05. Some model responses were transformed according to their $L_{max}(\lambda)$ values. Please see chapter 4 for detailed explanations of model fitting procedures.

8.3.3 First Model Data

Table 8.9 List of experiments included in the first set of models. Greyed out cells were removed as anomalies.

Entry	P1 / mmol min^{-1}	Acetone eq	NaOH / mmol min^{-1}	Temp / °C	PhCHO / %	BA / %	DBA / %
1	0.736	6.747	0.0421	10.1	95.55	2.69	0
2	1.202	5.579	0.0373	79.9	101.95	2.71	0
3	0.413	4.154	0.0575	55.8	98.04	0	0
4	1.355	4.96	0.0249	33	101.81	2.36	0
5	0.977	1.812	0.0713	21.9	37.43	4.04	0.7
6	1.739	5.435	0.0158	44.5	99.01	0	0
7	0.958	3.205	0.0713	61.9	98.97	0.81	0
8	1.016	2.3	0.099	68	7.97	31.78	4.59
9	1.564	1.533	0.0614	15.9	92.84	1.06	0
10	1.466	2.578	0.0891	38.8	9.89	34.11	8.37
11	0.84	5.923	0.0911	50.3	2.63	52.28	4.72
12	1.349	4.599	0.0218	73.9	4.51	52.01	8.7
13	1.29	6.968	0.099	49.1	3.39	59.67	6.04
14	1.114	2.996	0.0356	50.4	3.38	42.19	10.46
15	1.739	1.812	0.0158	51.8	93.09	0.16	0
16	1.818	3.205	0.0079	72.1	97.83	3.42	0
17	1.603	3.693	0.0079	75.6	94.46	3.41	0
18	0.645	2.578	0.0337	38.7	4.19	36.24	11.11
19	0.45	6.968	0.0158	65.6	4.1	39.58	0.94
20	1.016	4.808	0.0079	66	100.07	2.34	0
21	0.879	5.993	0.0079	66.6	91.89	0	0
22	0.41	6.968	0.0594	33	4.91	61.4	6.19
23	1.329	2.021	0.0218	36	42.18	4.48	0.61
24	1.954	5.087	0.0535	72.2	2.73	49.61	5.3

Entry	P1 / mmol min^{-1}	Acetone eq	NaOH / mmol min^{-1}	Temp / °C	PhCHO / %	BA / %	DBA / %
25	1.818	5.784	0.0614	72.7	2.87	47.19	3.11
26	0.41	4.111	0.0079	73.3	4.62	47.53	9.73
27	1.739	6.968	0.099	33.2	13.06	25.97	1.27
28	0.528	1.812	0.0535	53.3	5.42	29.53	5.88
29	0.391	6.968	0.0574	69.8	5.28	32.11	0.46
30	0.879	5.784	0.0297	72.8	5.38	42.01	1.48
31	1.349	5.435	0.0713	15.8	14.97	5.99	0.29
32	0.391	6.968	0.0812	41.5	4.16	57.97	3.97
33	0.762	4.181	0.0079	46.6	99.29	0	0
34	1.231	3.833	0.099	46.8	4.51	49.11	8.28
35	1.407	6.968	0.0772	50.1	5.02	59.25	6.07
36	0.391	6.968	0.0851	32.5	7.37	65.57	5.81
37	1.114	5.993	0.0356	41.3	11.13	42.26	3.78
38	0.997	6.968	0.0713	46.6	4.56	59.37	5.58
39	1.72	6.968	0.099	52.5	5.63	59.37	6.12
40	1.896	6.968	0.099	53	5.43	60.82	6.23
41	0.977	2.857	0.0356	12.9	29.34	3.57	0.24
42	0.391	6.968	0.0832	28.3	7.18	58.12	5.03
43	0.391	6.968	0.099	35.8	6.76	66	5.87
44	0.625	6.968	0.099	46.2	4.45	58.35	4.12
45	0.391	6.968	0.099	33.6	6.83	59.1	6.21
46	0.919	6.481	0.095	38.1	8.94	53.98	5.8
47	0.645	6.968	0.099	39.2	6.39	60.45	5.88
48	1.954	6.968	0.099	49.9	9.79	55.62	5.6
49	1.466	2.16	0.0594	51.9	8.7	34.44	12.35
50	0.391	6.968	0.0614	37.5	7.48	59.69	5.34
51	0.391	2.021	0.0851	39.1	5.99	32.12	11.85
52	0.704	2.369	0.0673	49	7.08	33.94	8.23
53	1.72	3.624	0.0733	59.9	5.96	45.18	8.83
54	0.391	4.739	0.0752	37.2	6.48	52.1	6.96
55	1.466	4.39	0.0614	50.9	7.88	48.64	8.32
56	0.704	5.017	0.0079	51.7	101.53	2.99	0
57	0.391	6.968	0.0574	62.1	7.05	35.5	0.45
58	0.391	6.968	0.0851	30.6	8.08	58.7	5.82
59	1.739	3.972	0.0416	38.7	30.57	6.87	0.4
60	1.954	6.968	0.099	51.3	8.73	56.29	6.14
61	1.954	5.296	0.0416	56.2	26.25	30.23	2.25

Entry	P1 / mmol min^{-1}	Acetone eq	NaOH / mmol min^{-1}	Temp / °C	PhCHO / %	BA / %	DBA / %
62	1.681	6.062	0.0634	59	7.27	55.24	6.88
63	1.739	6.968	0.0574	38.7	17.48	20.61	0.96
64	1.544	5.017	0.0079	49.7	98.17	0	0
65	1.349	3.624	0.0733	59.4	6.2	43.65	6.6
66	1.954	6.968	0.0871	62.3	7.19	59.24	5.95
67	0.391	6.968	0.0594	32.9	7.95	57.98	5.95
68	1.309	3.415	0.0891	50.3	6.34	45.2	8.87
69	1.837	4.39	0.0614	50.9	13.92	44.85	6.5
70	1.681	5.296	0.099	56.3	6.21	52.66	6.53

P1 = pump 1 benzaldehyde, PHCHO = benzaldehyde yield, BA = benzylideneacetone yield, DBA = dibenzylideneacetone yield

Table 8.10 Model coefficients and ***p***-values

Coefficeint	PHCHO		BA		DBA	
	Value	p-value	Value	p-value	Value	p-value
Constant	0.98	1.1E-26	37.17	7.3E-28	7.43	5.9E-22
P1	0.30	4.0E-07	-5.62	7.5E-03	-2.07	3.2E-07
Acetone	0.02	6.9E-01	7.16	1.6E-04	-2.38	2.2E-08
NaOH	-0.49	1.3E-11	21.98	1.3E-19	3.63	1.8E-14
Temperature	-0.63	1.1E-10	16.38	2.8E-09	2.13	3.3E-05
P1*P1					-1.78	6.6E-03
Ace*Ace						
NaOH*NaOH	0.54	1.1E-07	-12.73	3.0E-06	-3.04	5.6E-07
Temp*Temp			-33.16	9.1E-12	-6.87	8.3E-12
P1*Ace			-8.91	2.2E-03		
P1*NaOH	-0.19	1.2E-02	9.67	8.4E-04	2.54	8.8E-06
P1*Temp			29.17	7.1E-10	6.39	2.6E-10
Ace*NaOH	-0.23	2.6E-02				
Ace*Temp						
NaOH*Temp					-2.68	5.2E-03

P1 = pump 1 benzaldehyde, Ace = Acetone eq, Temp = Temperature, PHCHO = benzaldehyde yield, BA = benzylideneacetone yield, DBA = dibenzylideneacetone yield.

8.3.4 Second Model Data

Table 8.11 List of experiments included in the second set of models. Greyed out cells were removed as anomalies.

Entry	P1 / mmol min^{-1}	Acetone eq	NaOH / mmol min^{-1}	Temp / °C	PhCHO / %	BA / %	DBA / %	PMI	STY / g L^{-1} h^{-1}	Cost / £ kg^{-1}
1	0.736	6.747	0.042	10.1	95.55	2.69	0	266.24	26.7	524.53
2	0.413	4.154	0.057	55.8	98.04	0	0	34551.6	0.1	71245.6
3	0.977	1.812	0.071	21.9	37.43	4.04	0.7	138.59	53.6	310.04
4	0.84	5.923	0.091	50.3	2.63	52.28	4.72	15.66	596.2	31.3
5	0.645	2.578	0.034	38.7	4.19	36.24	11.11	14.74	317.2	32.54
6	0.41	6.968	0.059	33	4.91	61.4	6.19	15.61	341.9	30.61
7	0.528	1.812	0.053	53.3	5.42	29.53	5.88	21.58	211.4	47.54
8	0.391	6.968	0.081	41.5	4.16	57.97	3.97	19.48	307.5	38.18
9	0.762	4.181	0.008	46.6	99.29	0	0	37111.4	0.1	79194.4
10	0.391	6.968	0.085	32.5	7.37	65.57	5.81	17.64	347.8	34.58
11	0.997	6.968	0.071	46.6	4.56	59.37	5.58	12.8	802.9	25.1
12	0.977	2.857	0.036	12.9	29.34	3.57	0.24	140.84	47.3	310.76
13	0.391	6.968	0.083	28.3	7.18	58.12	5.03	19.66	308.3	38.55
14	0.391	6.968	0.099	35.8	6.76	66	5.87	18.98	350.1	37.21
15	0.625	6.968	0.099	46.2	4.45	58.35	4.12	17.06	495.2	33.44
16	0.391	6.968	0.099	33.6	6.83	59.1	6.21	21.2	313.5	41.55
17	0.919	6.481	0.095	38.1	8.94	53.98	5.8	15.33	672.8	30.32
18	0.645	6.968	0.099	39.2	6.39	60.45	5.88	16.25	529.0	31.86
19	0.391	6.968	0.061	37.5	7.48	59.69	5.34	16.62	316.6	32.58
20	0.391	2.021	0.085	39.1	5.99	32.12	11.85	29.92	170.4	63.27
21	0.704	2.369	0.067	49	7.08	33.94	8.23	18.97	324.0	41.26
22	0.391	4.739	0.075	37.2	6.48	52.1	6.96	19.19	276.3	38.91
23	0.704	5.017	0.008	51.7	101.53	2.99	0	173.79	28.5	360.42
24	0.391	6.968	0.085	30.6	8.08	58.7	5.82	19.7	311.3	38.63
25	0.391	6.968	0.059	32.9	7.95	57.98	5.95	16.87	307.5	33.07
26	0.907	5.943	0.014	47.1	5.77	37.85	4.69	14.96	465.5	30.16
27	0.743	6.829	0.107	27.2	2.38	50.95	1.08	18.67	513.2	36.69
28	0.444	11.647	0.142	59.9	15.26	55.64	5.33	29.05	334.8	54.42
29	0.787	9.889	0.042	34.2	6.06	43.8	2.21	18.88	467.8	35.02
30	0.879	8.223	0.127	40.5	3.66	59.45	6.08	16.94	709.1	32.57
31	0.704	13.24	0.147	50.1	6.98	57.22	1.91	24.1	546.1	43.95
32	0.86	13.867	0.018	56.6	6.37	43.33	6.83	20.66	505.4	35.73
33	0.762	13.519	0.059	30.8	6.59	63.48	4.32	16.33	656.3	28.92
34	0.958	12.404	0.149	38.9	4.66	59.59	3.97	20.17	774.0	36.8
35	0.977	11.08	0.149	40.9	4.17	63.5	4.83	17.97	841.7	33.28
36	0.625	10.871	0.048	51	2.68	53.46	2.17	17.34	453.5	31.8

Entry	P1 / mmol min^{-1}	Acetone eq	NaOH / mmol min^{-1}	Temp / °C	PhCHO / %	BA / %	DBA / %	PMI	STY / g L^{-1} h^{-1}	Cost / £ kg^{-1}
37	0.84	13.937	0.149	56.6	3.54	56.73	1.76	23.29	646.7	41.96
38	0.977	13.937	0.083	60	2.81	53.06	1.35	20.21	703.3	35.69
39	0.586	8.92	0.061	27.1	6.03	45.84	3.42	20.23	364.5	38.39
40	0.547	6.481	0.149	41.4	3.4	55.52	6.47	23.11	412.1	45.56
41	0.84	13.937	0.109	45.2	3.56	65.37	3.73	18.25	745.1	32.59
42	0.977	8.501	0.149	45.6	2.7	58.4	5.36	17.79	774.1	34.1
43	0.645	13.937	0.01	49.9	12.37	30.17	1.03	29.28	263.9	50.49
44	0.645	6.899	0.046	33.6	4.09	49.71	5.52	15.19	434.9	29.83
45	0.977	7.386	0.149	36.6	4.97	53.18	5.66	18.71	704.9	36.45
46	0.821	11.219	0.107	45.3	3.51	62.01	4.13	17.54	690.4	32.33
47	0.977	13.937	0.149	45.6	4.11	66.05	4.02	18.99	875.4	34.05
48	0.743	9.268	0.113	42	3.59	58.75	5.14	18.2	591.8	34.51
49	0.704	13.937	0.149	42.8	1.68	66.08	3.97	21.4	630.6	38.79
50	0.762	13.937	0.149	43	1.78	66.61	3.97	20.57	688.7	37.18
51	0.547	13.937	0.109	45.5	3.97	62.89	2.83	21.97	466.8	39.74
52	0.801	8.432	0.099	53.8	2.59	50.87	2.41	18.86	552.9	36.11
53	0.977	13.867	0.095	41.6	2.13	63.61	4.13	17.34	843.2	30.73
54	0.977	5.923	0.139	42.9	2.94	54.01	6.82	16.84	715.9	33.6
55	0.977	10.522	0.149	43.1	3.42	62.34	5.03	17.95	826.3	33.48
56	0.821	13.937	0.149	45.3	4.52	65.82	3.71	20.24	732.8	36.51
57	0.919	10.871	0.048	51	3.38	59.42	4.08	14.49	740.4	26.44
58	0.84	13.937	0.149	44	1.72	65.4	3.93	20.2	745.5	36.4
59	0.684	13.937	0.149	45.4	3.73	64.72	3.4	22.11	600.5	40.1
60	0.977	13.937	0.113	47.5	1.75	63.91	3.67	18.07	847.1	32.16
61	0.84	9.407	0.028	55.5	3.03	57.37	4.13	13.11	653.9	24.44

P1 = pump 1 benzaldehyde, PHCHO = benzaldehyde yield, BA = benzylideneacetone yield, DBA = dibenzylideneacetone yield, PMI = process mass intensity, STY = space time yield.

Table 8.12 Model coefficients and ***p***-values

Coefficeint	PHCHO		BA		DBA		PMI		STY		Cost	
	Value	*p*-value	Value	*p*-value	Value	*p*-value	Value	*p*-value	Value	*p*-value	Value	*p*-value
Constant	5.49	2.5E-15	57.86	0.0E+00	5.56	7.2E-30	16.27	3.5E-35	470.17	0	31.62	3.3E-35
P1	0.41	5.4E-01	-7.56	1.8E-06	0.00	9.9E-01	-2.31	2.6E-05	251.49	3.8E-27	-4.53	2.2E-05
Acetone	-1.69	2.9E-02	17.19	4.6E-16	-4.33	3.6E-20	1.71	1.7E-02	113.59	5.3E-13	-0.53	7.0E-01
NaOH	0.49	4.9E-01	6.61	9.0E-06	0.58	7.8E-03	2.72	1.5E-05	86.78	2.2E-06	5.42	1.0E-05
Temperature	-6.06	1.8E-05	13.26	2.1E-07	-1.35	1.1E-03	-4.69	1.2E-05	90.48	2.8E-05	-8.93	1.7E-05
P1*P1	2.70	2.8E-02			-1.05	3.0E-02	2.59	8.5E-03			5.00	8.8E-03
Ace*Ace			-11.54	3.3E-08	2.99	3.2E-11	3.34	2.1E-05	-115.30	2.4E-08	7.47	2.0E-06
NaOH*NaOH			-5.68	5.3E-03			2.73	3.5E-06	-74.08	1.1E-05	5.07	7.0E-06
Temp*Temp	7.64	6.4E-05	-26.98	2.5E-14	-6.06	2.0E-17	12.95	1.1E-09	-240.85	2.1E-13	25.40	8.2E-10
P1*Ace												
P1*NaOH	-1.99	6.4E-02					-3.05	3.1E-04			-5.76	4.2E-04
P1*Temp	-6.94	6.1E-05	12.30	1.1E-03	5.64	1.9E-11	-6.53	8.2E-04	187.70	8.7E-08	-12.73	7.7E-04
Ace*NaOH							-2.53	1.6E-03	120.16	7.2E-08	-4.31	4.9E-03
Ace*Temp	2.61	9.7E-02					-3.80	6.8E-03			-8.53	2.0E-03
NaOH*Temp							3.46	8.6E-03	-139.29	6.0E-05	6.34	1.3E-02

P1 = pump 1 benzaldehyde, Ace = Acetone eq, Temp = Temperature, PHCHO = benzaldehyde yield, BA = benzylideneacetone yield, DBA = dibenzylideneacetone yield, PMI = process mass intensity, STY = space time yield.

8.4 Chapter 5 Procedures

8.4.1 Chemicals

Methyl nicotinate (99%, Alfa Aesar), methylamine (40% wt in water, Merck; 2 M in methanol, Alfa Aesar), methanol (HPLC grade, Sigma-Aldrich), niacin (99.5%, Acros) were used as starting materials and/or analytical standards. *N*'-methyl nicotinamide standard was synthesized and was determined as >99% by ^{1}H NMR. All commercial chemicals were used without further purification.

8.4.2 Online Analysis Methods

An Advion Expression CMS operating in positive APCI mode was used for collecting online and offline MS spectra. A mobile phase of 1:1 (v:v) H_2O:MeCN was used with 0.1% (v:v) formic acid buffer and flow rate 0.3 mL min^{-1}. An Agilent G1311A quaternary pump was used to pump the mobile phase with separate feeds of H_2O, MeCN and formic acid (10%, v:v). Agilent capillary tubing (0.17 mm ID) delivered mobile phase from the pump to the sample loop, peek tubing (red, 1/16" OD, 0.005" ID) from the sample loop to the MS.

A 5:2 flow splitter was created by attaching 6.5 cm and 16.5 cm peek tubing (red) to a microvolume tee-piece, where the input was mobile phase from the sample loop. The shorter tubing was a waste outlet, and the longer tube was the MS input. The change in back pressure between the different tube lengths was used to control the flow splitter. The mobile phase flow rate into the MS was calculated to be 0.12 mL min^{-1} (calculated based on the approximate pressure drop across the 2 tee-piece outlets).

At-line HPLC analysis was carried out using an Agilent 1100 HPLC. Method: Sigma Ascentis Express C18 (50 x 6.6 mm, 2.7 μm) column; A H_2O, B MeCN, C 10% aqueous formic acid (v:v); 5% to 50% B over 5 min, to 5% B after 5.5 min, 3% hold C over 5.5 min, flow rate 1.2 mL min^{-1}, 254 nm, 20 °C.

8.4.3 Synthesis of *N*'-methyl nicotinamide

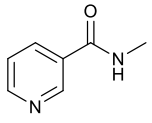

Methyl nicotinate (10.03 g, 73.2 mmol) was added in portions to a cooled solution (0 °C, ice bath) of methylamine in methanol (145 mL, 2 M, 292 mmol). The reaction was allowed to warm to room temperature and stirred for 24 h. The solvent was removed under vacuum to leave the amide as a white solid (9.23 g, 67.8 mmol, 99%) which was used without any further purification, mp 102-104 °C; δ_H: (300 MHz, $CDCl_3$, TMS) 8.96 (1H, dd, *J* 2.4 and 0.9, Ar 2-H), 8.71 (1H, dd, *J* 4.8 and 1.5, Ar 6-H), 8.12 (1H, dt, *J* 2.0 and 7.8, Ar 5-H), 7.38 (1H, ddd, *J* 7.8, 4.8 and 0.9, Ar 4-H), 6.36 (1H, br s, N-H), 3.04 (3H, d, *J* 4.8, NCH_3); MS (APCI+) 137 $[M+H]^+$, 178 $[M+MeCN+H]^+$. Analysis matches existing literature[266]

8.4.4 Pump Reservoir Solutions

Solution reservoirs for the pumps were prepared by dissolving methyl nicotinate (50 g, 36.5 mmol) in methanol (200 mL); and methylamine solution (40% wt aq, 200 mL, 5.15 mol) in distilled water (200 mL). Ester solution concentration = 1.46 mol L^{-1}, methylamine solution = 5.77 mol L^{-1}.

8.4.5 Steady State Determination

Online MS was tested for its ability to be used as real-time analysis to check for steady state in the reactor. The reagent pumps were primed, and then **1** was pumped at 0.2 mL min^{-1} and $MeNH_2$ was pumped at 0.023 mL min^{-1} (2 mol eq) for a period of 30 min, during which a MS sample was taken at 60 s intervals. After the 30 min reagent pulse, methanol was pumped at 1 mL min^{-1} for 10 min. This was to clean the reactor and prevent accumulation in the MS. The process was repeated using 3 and 4 mol eq of $MeNH_2$ carrying out the three flow experiments sequentially. The results were analyzed by internal normalization and linearity was observed when the standard deviation of the previous three points was less than or equal to 1.5%.

8.4.6 Isotope Calculations

There is an overlap in the peaks between **1** and **2** due to the $[M+H]^+$ adduct of **1** masking the $[M+H+1]^+$ isotope adduct of **2**. To correct this, the isotope abundance for each compound was predicted using ChemDraw (ver 13.0.0.3015) and verified experimentally.

The following calculations were used when calculating the MS response:

$$Ester = (P_{137} - (P_{138} \times 0.077)) \times 1.077$$

$$Amide = P_{138} \times 1.077$$

$$Acid = P_{124} \times 1.066$$

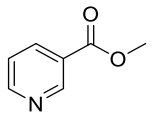

5.12

m/z: 137.05 (100.0%), 138.05 (7.7%)

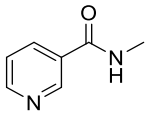

5.13

m/z: 136.06 (100.0%), 137.07 (7.7%)

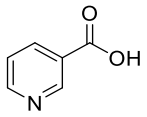

5.14

m/z: 123.03 (100.0%), 124.04 (6.6%)

Figure 8.4 Isotope adundances for compounds **5.12** to **5.14**

8.4.7 MS Calibration

8.4.7.1 HPLC

The HPLC response was calibrated by preparing a single solution containing compounds **5.12**-**5.14** at 0.35 mol L^{-1} in DMSO. HPLC samples were taken at dilution factors of 1, 2, 4 and 8 (corresponding to concentrations of 0.35, 0.175, 0.0875, 0.0438 M) and the relative response factors were calculated by internal normalization. Existing calibration curves showed a linear response up to 1.4 M for **5.12** and **5.13** and 0.5 mol L^{-1} for **5.14**, which is in the same concentration range in which optimizations were carried out.

8.4.7.2 MS

A central composite faced (CCF) Design of Experiment (DoE) was constructed and ran using both HPLC and MS as analysis.

Table 8.13 Summary of experiments in the CCF DoE

Experiment	**5.12** / mL min^{-1}	$MeNH_2$ / mol eq	Temperature / °C
1	0.1	1	0
2	0.1	10	0
3	0.25	5.5	0
4	0.4	1	0
5	0.4	10	0
6	0.1	5.5	65
7	0.25	1	65
8	0.25	5.5	65
9	0.25	5.5	65
10	0.25	5.5	65

11	0.25	5.5	65
12	0.25	10	65
13	0.4	5.5	65
14	0.1	10	130
15	0.25	5.5	130
16	0.4	1	130
17	0.4	10	130
18	0.1	1	130

Table 8.14 Results from HPLC CCF, showing absolute peak area and calibrated internally normalised percentage yield

Experiment	HPLC Area			Percentage Yield / %		
	5.14	**5.13**	**5.12**	**5.14**	**5.13**	**5.12**
1	9.5	126.9	1480.8	0.5	5.7	93.8
2	18.8	548.4	0.0	4.0	96.0	0.0
3	24.5	525.1	247.3	3.3	58.1	38.6
4	5.5	67.9	1469.0	0.3	3.2	96.5
5	15.7	364.8	160.3	3.1	59.8	37.1
6	161.4	761.6	0.0	20.5	79.5	0.0
7	71.6	255.9	1220.4	4.2	12.4	83.4
8	148.2	694.5	12.7	20.2	77.8	2.0
9	151.3	701.4	13.2	20.4	77.5	2.1
10	136.8	659.2	5.1	20.0	79.1	0.9
11	157.5	722.8	28.0	20.1	75.7	4.1
12	94.5	459.1	0.0	20.1	79.9	0.0
13	136.7	652.7	54.1	18.6	72.9	8.5
14	199.6	346.7	0.0	41.3	58.7	0.0
15	361.6	524.2	0.0	45.7	54.3	0.0
16	235.2	245.7	1118.2	13.6	11.6	74.8
17	195.2	313.5	0.0	43.2	56.8	0.0
18	499.4	448.8	782.5	28.2	20.7	51.1

Table 8.15 Results from the MS CCF showing uncalibrated internally normalised percentage yield with isotope correction calculations.

Experiment	**5.14** / %	**5.13** / %	**5.12** / %
1	1.2	3.7	95.5
2	1.1	95.9	2.8
3	1.5	70.6	27.8
4	1.2	6.8	92.5
5	1.5	67.7	30.8
6	4.8	93.4	1.5
7	2.0	16.1	82.3

8	5.3	90.2	4.3
9	5.6	90.2	4.0
10	5.6	90.2	4.0
11	6.0	89.6	4.1
12	5.3	92.7	1.8
13	5.1	85.6	9.1
14	13.2	84.2	2.4
15	14.6	83.7	1.3
16	4.8	17.0	78.5
17	13.9	83.4	2.5
18	1.2	2.0	97.3

The error in the measurement was calculated by using sum of squares, where R_i is the response of compound **i**:

$$Error = \sum_{i=1}^{3} \left(R_{i,HPLC} - R_{i,MS}\right)^2$$

A 'new' yield was calculated by multiplying the existing response by a response factor (initially set to 1). The error in the measurement between the 'new' MS yield and existing HPLC yield was minimized by changing the values of the 3 response factors. Optimum minimized values were calculated using the MS Excel solver add-in (GRG Non-Linear algorithm). A comparison between the calibrated LC and MS responses are shown in Table S4 and

Table 8.16 Comparison between calibrated MS and LC responces

Experiment	Percentage Yield (HPLC)/ %			Calibrated MS response / %		
	5.14	**5.13**	**5.12**	**5.14**	**5.13**	**5.12**
1	0.5	5.7	93.8	3.7	2.5	93.8
2	4.0	96.0	0.0	4.5	91.8	3.8
3	3.3	58.1	38.6	5.6	60.4	34.0
4	0.3	3.2	96.5	3.7	4.7	91.7
5	3.1	59.8	37.1	5.3	57.4	37.3
6	20.5	79.5	0.0	17.8	80.4	1.9
7	4.2	12.4	83.4	6.1	11.3	82.6
8	20.2	77.8	2.0	19.2	75.7	5.1
9	20.4	77.5	2.1	20.1	75.2	4.7
10	20.0	79.1	0.9	20.1	75.2	4.7

11	20.1	75.7	4.1	21.3	73.9	4.8
12	20.1	79.9	0.0	19.3	78.6	2.1
13	18.6	72.9	8.5	18.3	71.0	10.8
14	41.3	58.7	0.0	39.4	58.3	2.3
15	45.7	54.3	0.0	42.5	56.2	1.3
16	13.6	11.6	74.8	13.9	11.3	74.8
17	43.2	56.8	0.0	40.8	56.8	2.4
18	28.2	20.7	51.1	3.7	2.5	93.8

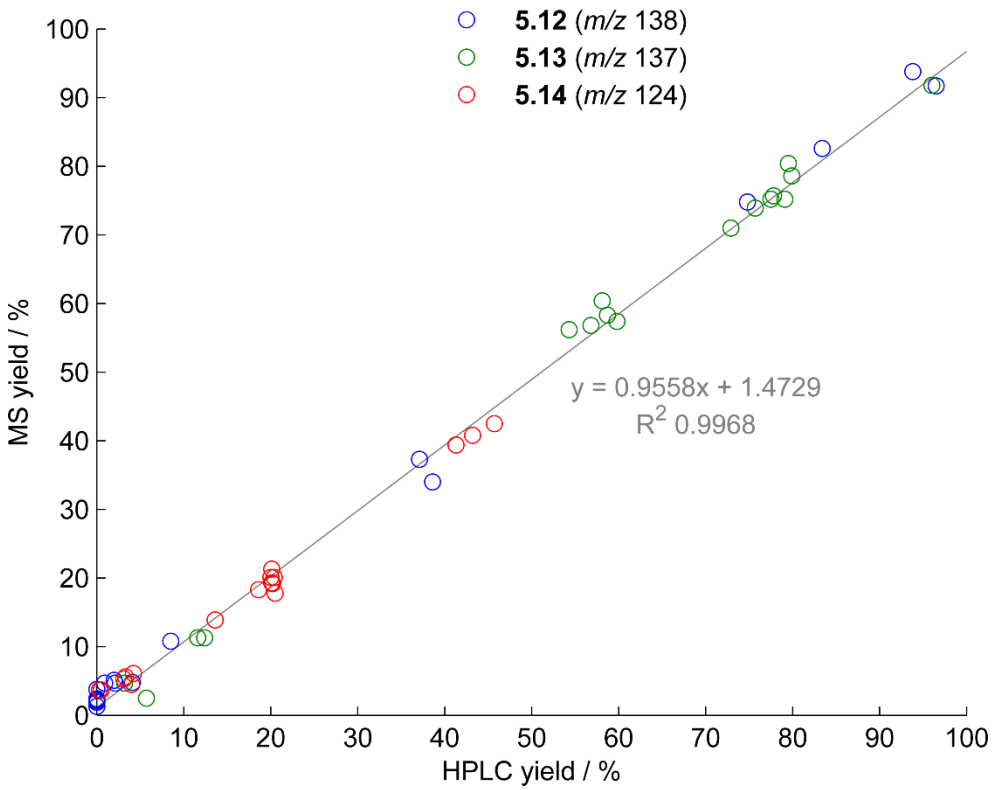

Figure 8.5 Comparison between the calibrated responses by MS and HPLC for each individual compound.

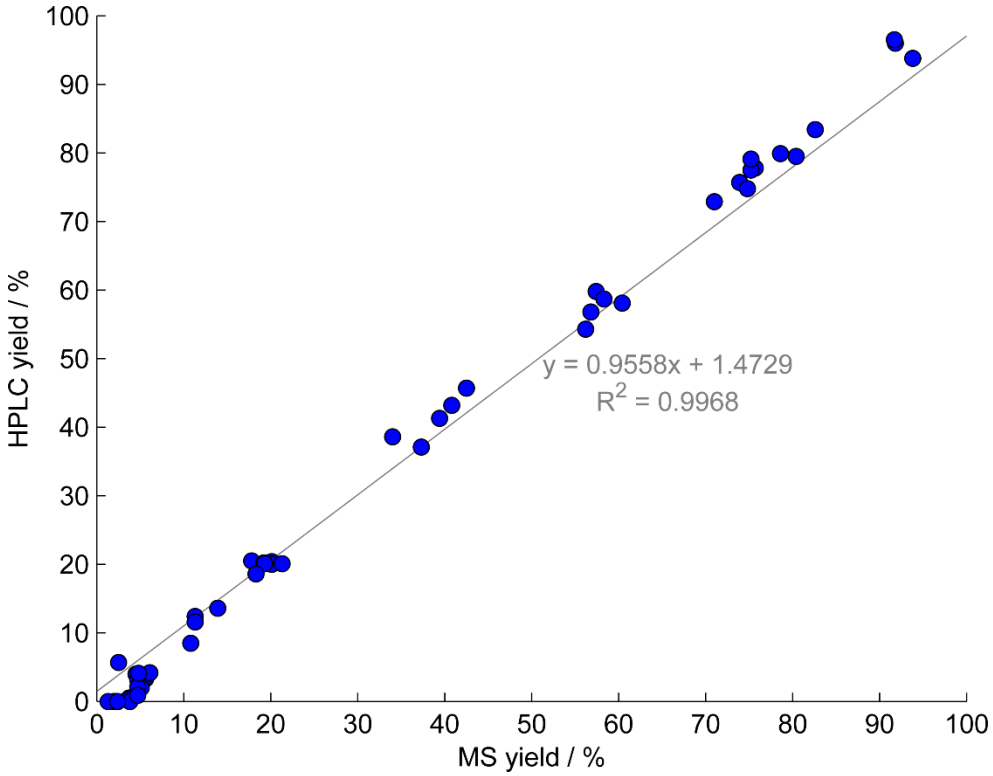

Figure 8.6 Comparison between the calibrated responses by MS and HPLC for all combined compounds.

8.4.8 *N*'-Methyl Nicotinamide Optimisation

Table 8.17 Optimisation limits used in the self-optimisation and design of experiment

Limits	Ester flow / mL min^{-1}	$MeNH_2$ eq	Temperature / °C
Upper	0.100	1	0
Lower	0.400	10	130

Table 8.18 Conditions and responses from the self-optimisation, Optimum conditions are highlighted in bold.

Entry	Ester flow / mL min^{-1}	$MeNH_2$ mol eq	Temperature / °C	Yield %
1	0.187	6.0	0.2	70.8
2	0.264	5.6	129.6	71.8
3	0.256	1.5	33.4	12.8
4	0.344	4.8	65.5	74.7
5	0.343	1.8	16.6	12.6
6	0.341	9.7	49.4	88.9
7	0.392	3.8	81.5	62.2
8	0.100	9.1	97.6	86.3
9	0.209	2.2	8.1	30.7
10	0.123	2.6	25.0	35.9

11	0.298	6.1	113.4	70.7
12	0.367	1.9	121.3	30.6
13	0.400	8.8	0.0	68.4
14	0.222	7.4	32.7	87.0
15	0.400	7.3	36.8	83.5
16	0.246	9.9	130.0	74.9
17	**0.100**	**9.9**	**10.6**	**93.4**
18	0.100	8.2	32.8	92.3
19	0.133	8.7	49.1	88.0
20	0.262	8.7	55.2	87.1
21	0.161	5.2	65.1	78.4

Table 8.19 List of experiments and responses for all compounds in the CCF DoE

Experiment	Ester flow / mL min^{-1}	$MeNH_2$ mol eq	Temperature / °C	Acid / %	Amide / %	Ester / %
1	0.1	1	0	3.7	2.5	93.8
2	0.1	10	0	4.5	91.8	3.8
3	0.25	5.5	0	5.6	60.4	34.0
4	0.4	1	0	3.7	4.7	91.7
5	0.4	10	0	5.3	57.4	37.3
6	0.1	5.5	65	17.8	80.4	1.9
7	0.25	1	65	6.1	11.3	82.6
8	0.25	5.5	65	19.2	75.7	5.1
9	0.25	5.5	65	20.1	75.2	4.7
10	0.25	5.5	65	20.1	75.2	4.7
11	0.25	5.5	65	21.3	73.9	4.8
12	0.25	10	65	19.3	78.6	2.1
13	0.4	5.5	65	18.3	71.0	10.8
14	0.1	10	130	39.4	58.3	2.3
15	0.25	5.5	130	42.5	56.2	1.3
16	0.4	1	130	13.9	11.3	74.8
17	0.4	10	130	40.8	56.8	2.4
18	0.1	1	130	3.7	2.5	93.8

8.4.9 DoE Model Analysis

The CCF design was analyzed and response surface models were fitted using Umetrics Modde (ver 10.1) by including all square and interactions then removing terms with a p-value less than 0.05. The model for **3** (acid) was transformed logarithmically ($y = \log x$) to improve the normality of its distribution. The following figures show a summary of the model displaying Figure

8.7 a) replicates plot, b) summary of fit, c) coefficients and d) residual normality plot for the model of amide **5.13**; Figure 8.8, summary of the fit; Figure 8.9, model coefficients; Figure 8.10, observed *vs* predicted plots for each compound model; and Figure 8.11, contour plot, using the predictor function of the model for amide **5.13**.

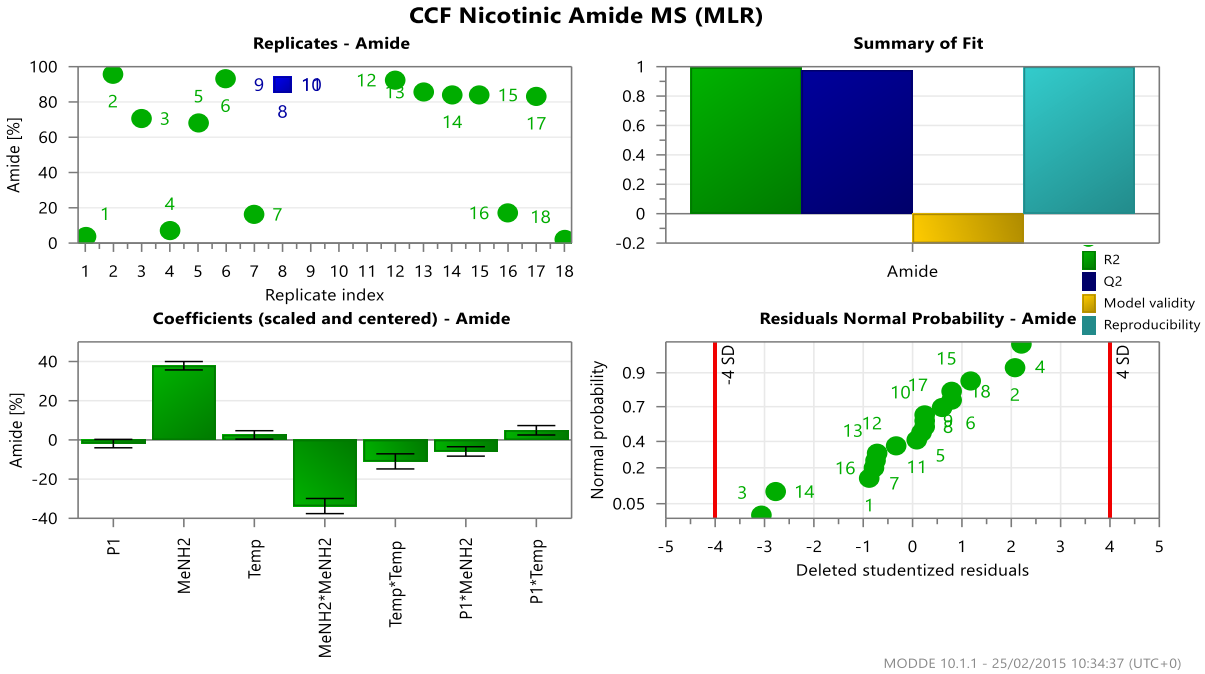

Figure 8.7 Model summary for the model of 2: a) Replicates, shown in blue, highlight the reproducibility of the model; b) summary of fit, displaying $\boldsymbol{R^2}$, which shows the accuracy of the fit, $\boldsymbol{Q^2}$, which shows how accurately the model can predict, vailidity, which is low due to the high reproducibility (i.e. the model does not believe it is valid due to such high reproducibility); c) model coefficients and their weighting; d) normal probability plot, which a good model will fit a straight line with all points within the 4 SD (4 standard deviations) markers.

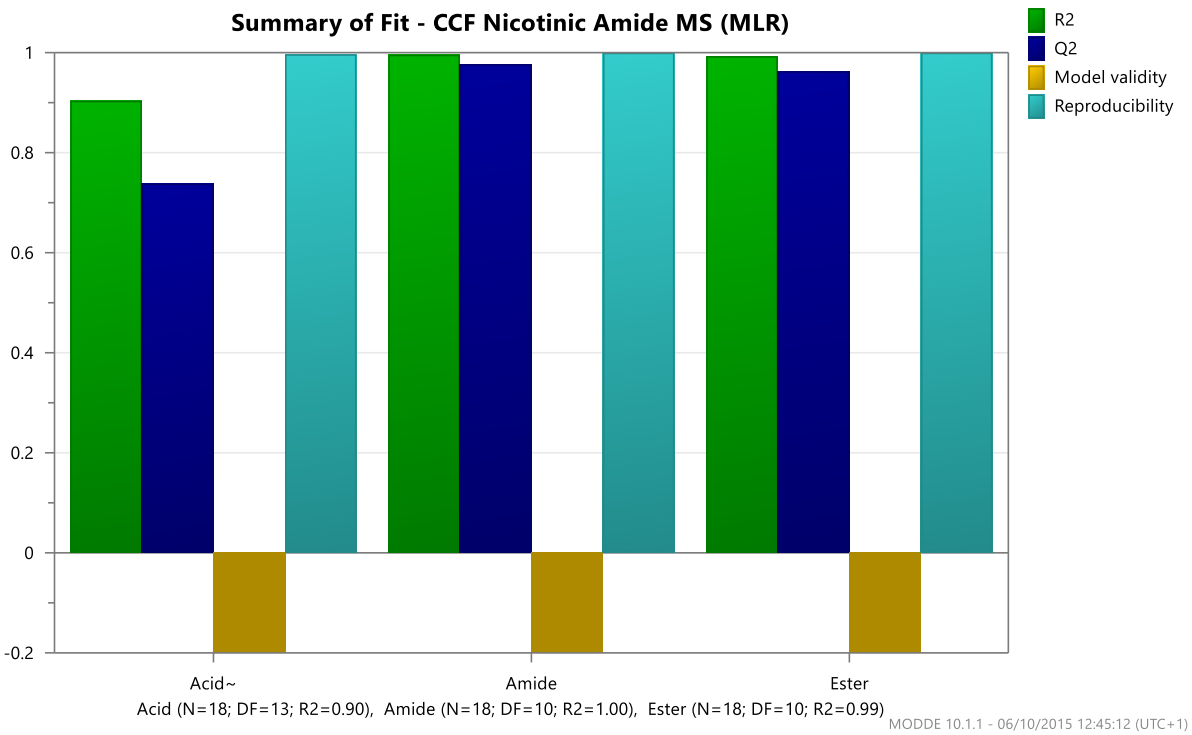

Figure 8.8 Summary of fit for the models of **5.12** (ester), **5.13** (amide) and **5.14** (acid).

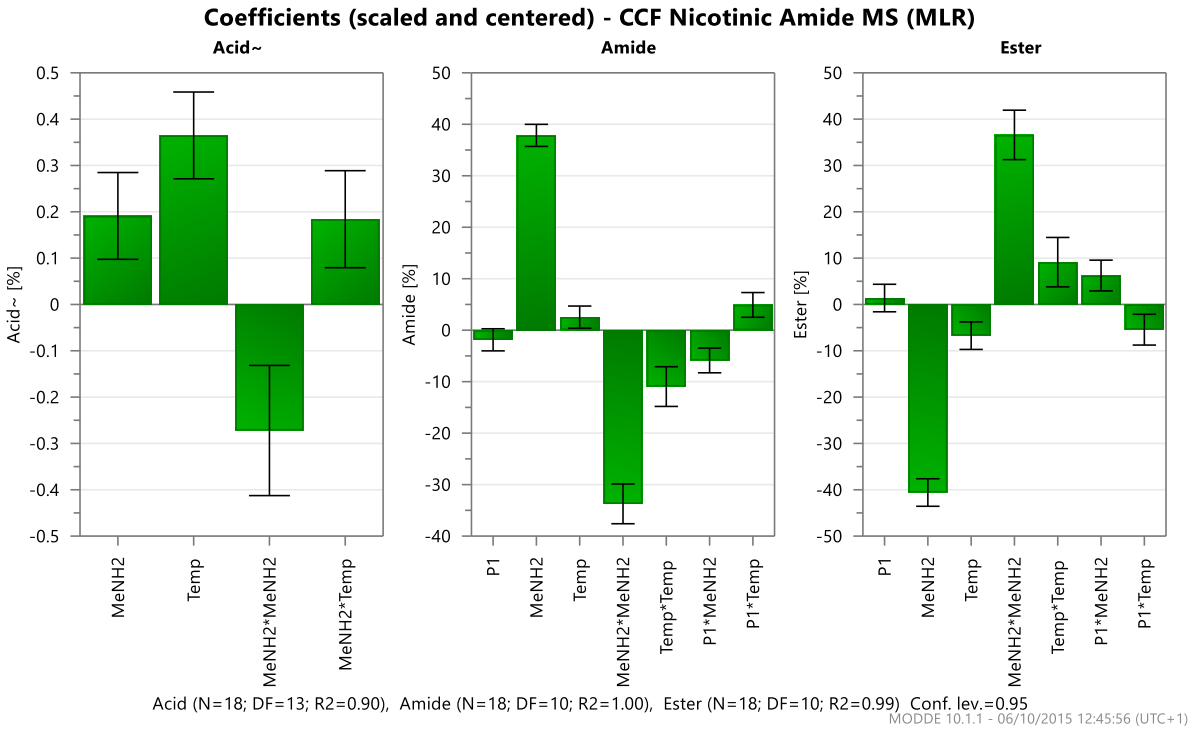

Figure 8.9 Coefficients of each model for compounds **5.12** (ester), **5.13** (amide) and **5.14** (acid).

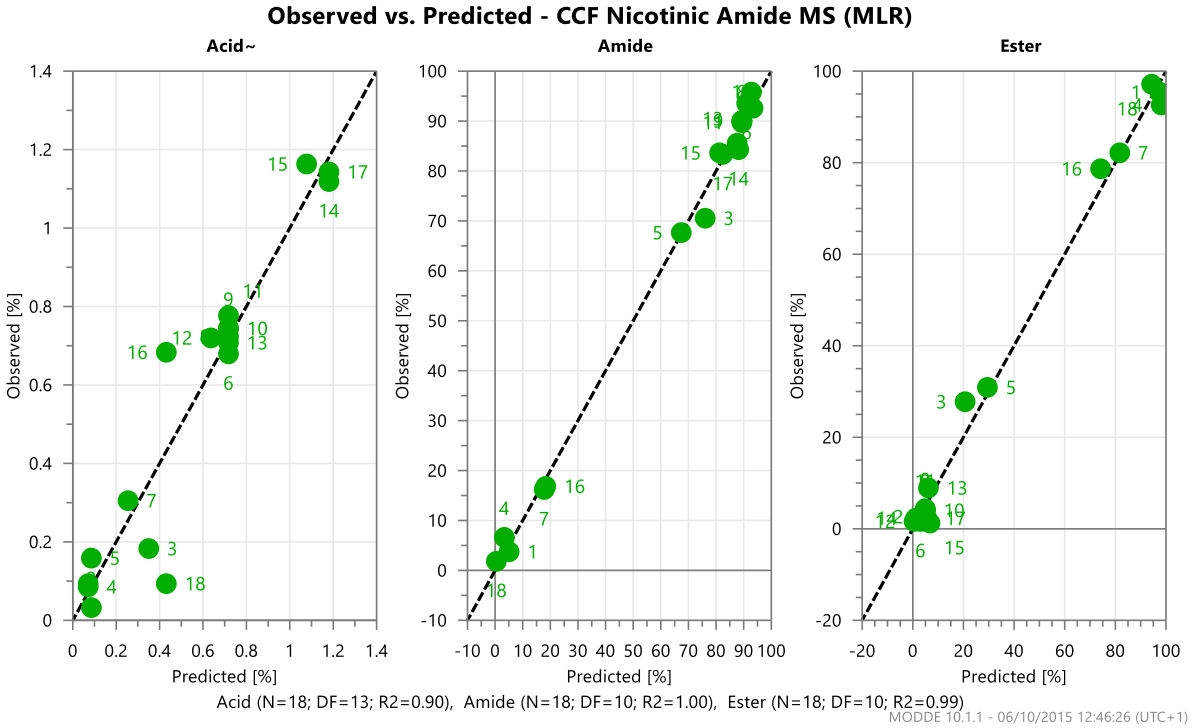

Figure 8.10 Plot of observed *vs* predicted of each model from the compounds

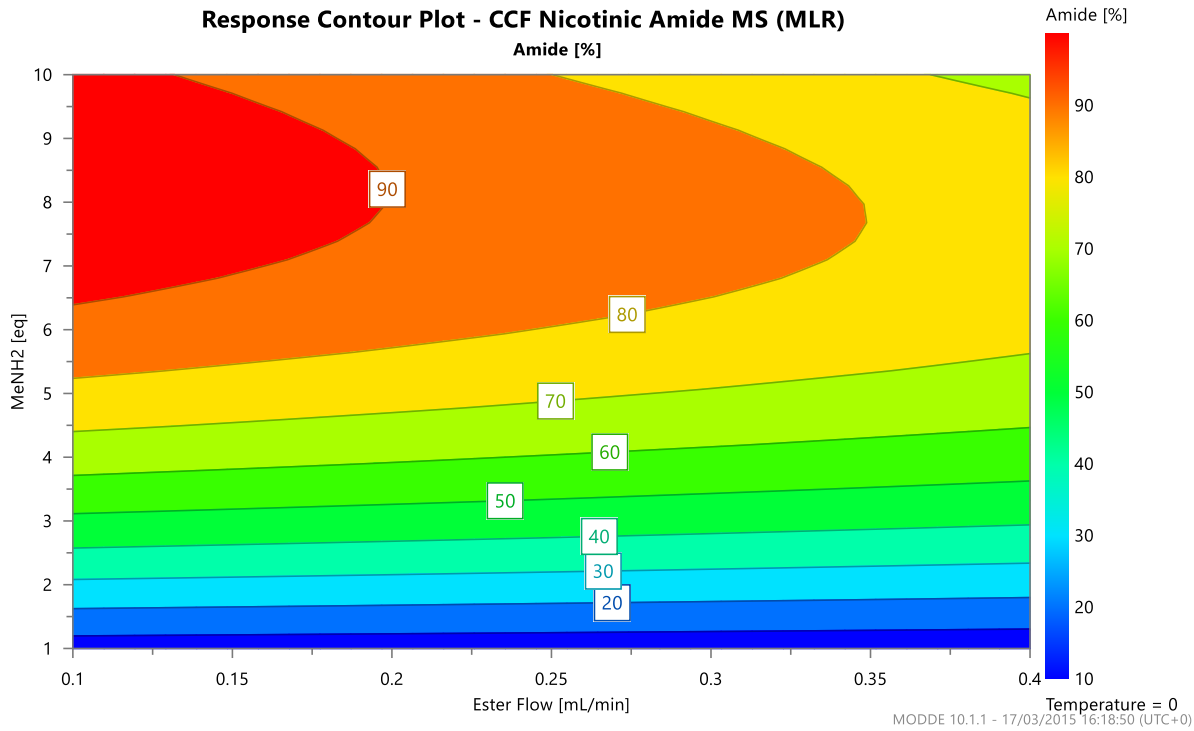

Figure 8.11 Contour plot at showing the effect of ester flow rate (mL/min) and $MeNH_2$ eq on the yield of amide at fixed temperature (0 °C).

8.5 Chapter 6 Procedures

8.5.1 Chemicals

2,4-Difluoronitrobenzene (99%, Aldrich), morpholine (≥99.0%, Merck), triethylamine (99%, Acros), ethanol (99.8%, VWR) and biphenyl (99.5% GC, Aldrich) were all used without further purification. Standards of 4-(5-fluoro-2-nitrophenyl)morpholine, *N*-(3-fluoro-4-nitrophenyl) morpholine and 4,4'-(4-nitro-1,3-phenylene)dimorpholine were synthesised by C. A. Hone.[267]

8.5.2 Measuring Dispersion

Dispersion was measured at residence times (t_{Res}) of 1 and 3 min. A 3 mL tubular reactor internal dimension 1/32" (0.79 mm) and external dimensions 1/16" (1.59 mm) and length of 6.25 m was fitted to 2 separate pumps. The pumps contained reservoir solutions of A: biphenyl in ethanol (0.050 mol L^{-1}) and B: neat ethanol. For 1 min t_{Res}, the solvent (ethanol) pump was set to 3 mL min^{-1} for 1 min then stopped and the biphenyl pump was set to 3 mL min^{-1} for 1 min and this sequence was repeated for 50 min. During this time, the sample loop was set to acquire a HPLC sample at a 125 s intervals. This resulted in 25 chromatograms displaying the composition of biphenyl at 5 s intervals across the 1 min repeated pulse.[60] For 3 min t_{res}, the solvent pulse was set to 1 mL min^{-1} for 3 min, then the biphenyl pump set to 1 mL min^{-1} for 3 min. This was repeated for a duration of 216 min with HPLC sampling frequency of 370 s. The data for these two sets of dispersion experiments are shown in Table 8.20 and Table 8.21.

Table 8.20 List of experiments for the dispersion experiments with 1 min t_{Res}

Entry	Time point / s	HPLC area
1	5	107.64
2	10	55.12
3	15	37.69
4	20	32.66
5	25	106.37
6	30	367.94
7	35	1019.68
8	40	1696.92
9	45	2708.71
10	50	3342.98
11	55	3545.33

12	60	3829.05
13	65	3882.24
14	70	3892.96
15	75	3911.81
16	80	3910.99
17	85	3801.22
18	90	3543.15
19	95	3172.44
20	100	2283.46
21	105	1500.20
22	110	750.75
23	115	462.75
24	120	245.54
25	125	92.61

Table 8.21 List of experiments for the dispersion experiments with 3 min t_{Res}

Entry	Time point / s	HPLC area
1	10	79.74
2	20	49.90
3	30	22.60
4	40	16.53
5	50	14.37
6	60	12.12
7	70	16.82
8	80	31.49
9	90	411.93
10	100	825.72
11	110	1334.26
12	120	2087.43
13	130	2578.46
14	140	3013.16
15	150	3622.97
16	160	3738.19
17	170	3858.24
18	180	3883.66
19	190	3908.44
20	200	3940.44
21	210	3917.88
22	220	3925.23
23	230	3928.72

Entry	Time point / s	HPLC area
24	240	3917.58
25	250	3906.46
26	260	3838.19
27	270	3652.44
28	280	3361.13
29	290	2786.56
30	300	2328.88
31	310	1471.10
32	320	955.52
33	330	592.77
34	350	320.39
35	360	185.50

8.5.3 Preparation of Pump Reservoir Solutions

Reservoir solutions were prepared by dissolving the desired reagents in solvent under stirring at ambient conditions. Pump A: 2,4-difluoronitrobenzene (50 mL, 0.46 mol, 2.03 mol L^{-1}) and biphenyl (3.51 g, 22.7 mmol, 0.101 mol L^{-1}) in ethanol (175 mL); Pump B: morpholine (70 mL, 0.81 mol, 4.17 mol L^{-1}) in triethylamine (124 mL, 0.89 mol, 4.59 mol L^{-1}); Pump C: ethanol.

8.5.4 Determining Pulse Volume

The pump reservoirs were prepared according to the instructions above. The following list of experiments were carried out in sequence and repeated 4 times with HPLC samples acquired at 6 min intervals. The reactor was 1 mL and maintained at constant a temperature of 90 °C. The reaction conditions are 2.75 min residence time (165 s), 1.5 eq of morpholine and a nitrobenzene concentration of 0.30 mol L^{-1}, corresponding to the centre-point of the optimisation limits.

Table 8.22 List of experiments used to determined the minimum possible reactor pulse size

Steady State Volume	Pulse type	Duration / s	Pump A / mL min^{-1}	Pump B / mL min^{-1}	Pump C / mL min^{-1}
2	A	30	0	0	0.364
	R	330	0.054	0.039	0.271
	B	0	N/A	N/A	N/A
1.5	A	71	0	0	0.364

	R	247	0.054	0.039	0.271
	B	41	0	0	0.364
1.0	A	113	0	0	0.364
	R	165	0.054	0.039	0.271
	B	82	0	0	0.364
0.5	A	154	0	0	0.364
	R	82	0.054	0.039	0.271
	B	124	0	0	0.364
0.2	A	179	0	0	0.364
	R	33	0.054	0.039	0.271
	B	148	0	0	0.364
0.1	A	187	0	0	0.364
	R	16	0.054	0.039	0.271
	B	157	0	0	0.364
0.05	A	191	0	0	0.364
	R	8	0.054	0.039	0.271
	B	161	0	0	0.364

Next the accuracy of each experiment was measured using a confidence interval of 95% after removal of anomalous results. Table 8.23 shows the % yield of *ortho* product for each experiment.

Table 8.23 List of % yield of desired *ortho* product after removal of anomalous experiments

Steady State Volume	ortho %
2	61.69
2	63.05
2	62.07
1.5	63.14
1.5	61.93
1.5	62.46
1.5	62.52
1	63.14
1	61.98
1	63.01
1	62.04
0.5	61.12
0.5	61.22
0.5	61.25

0.2	45.95
0.2	48.73
0.2	45.39
0.1	22.95
0.1	23.03
0.1	20.26
0.05	5.37
0.05	5.97
0.05	7.14
0.05	5.11

The mean of each steady state pulse volume was calculated by simply dividing the sum of yields by the population number (n). Next the "real" mean was calculated by calculating the mean from the volumes 1-2 as it was determined these values were at true steady state and did not suffer from dispersion. The residual error (SS_E) was calculated by squaring the difference between each yield value and the "real" mean value

$$SS_E = \sum (Y_i - \bar{Y})^2$$

where Y_i is the yield of a particular experiment and $\bar{Y}$ is the "real" mean value. The standard deviation (σ) for each steady state volume was calculated

$$\sigma = \sqrt{\frac{SS_E}{n}}$$

Next, the Z-value for a confidence interval of 95% was calculated, where $\alpha = 0.05$. This is carried out by finding the value for 0.475 ($(1-\alpha)/2$) in cumulative distribution table of a standard normal distribution (Z-table). For 0.475 the Z-value is 1.96. Therefore the error can be calculated

$$error = Z_{\frac{1-\alpha}{2}}\left(\frac{\sigma}{\sqrt{n}}\right)$$

Table 8.24 shows a summary of calculations for *ortho* product.

Table 8.24 Statistical analysis of the results from Table 8.23**.**

Steady State volume	Mean	SS_E	Std	Conf	Error
2	62.27	1.074659	0.518329	0.95	0.508
1.5	62.51	0.753329	0.433973	0.95	0.425

1	62.54	1.185654	0.544439	0.95	0.534
0.5	61.20	4.673808	1.248173	0.95	1.412
0.2	46.69	750.7423	15.81921	0.95	17.901
0.1	22.08	4892.09	40.38189	0.95	45.696
0.05	5.90	12792.22	65.29986	0.95	63.994

8.5.5 Pattern Search STY Optimisation

The optimisation target function was space time yield (STY, units: kg L^{-1} h^{-1})

$$STY = \frac{C_{(SM)} Y_{i(ortho)} MW_{(ortho)}}{t_{Res,i}}$$

where $C_{(SM)}$ is the concentration of 2,4-dilfuoronitrobenzene, $Y_{i,(ortho)}$ is the yield of *ortho* for experiment i, $MW_{(ortho)}$ is the molecular weight of *ortho* and $t_{Res,i}$ is the residence time.

Table 8.25 Limits for the STY optimisation using pattern search algorithm

Limit	t_{Res} / min	Morpholine / mol eq	Concentration / mol L^{-1}	Temperature / °C
Lower	1	1.0	0.200	60
Upper	3	2.0	0.500	120

Table 8.26 List of results from the STY pattern search optimisation. Optimum conditions highlighted in bold

Entry	t_{Res} / min	Morpholine eq	Concentration / mol L^{-1}	Temperature / °C	STY / kg L^{-1} h^{-1}
1	3.000	1.000	0.200	60.0	0.10
2	1.268	1.000	0.200	60.0	0.19
3	3.000	1.000	0.200	60.0	0.06
4	1.268	1.000	0.200	60.0	0.37
5	3.000	1.707	0.200	60.0	0.07
6	1.268	1.707	0.200	60.0	0.50
7	3.000	1.707	0.200	60.0	0.12
8	2.134	1.707	0.200	60.0	0.33
9	1.268	1.707	0.358	60.0	0.71
10	3.000	1.707	0.358	60.0	0.36
11	2.134	1.707	0.358	60.0	0.95
12	1.268	1.707	0.358	102.4	1.21
13	3.000	1.707	0.358	102.4	0.88
14	2.134	1.707	0.358	102.4	1.67

Entry	t_{Res} / min	Morpholine eq	Concentration / mol L^{-1}	Temperature / °C	STY / kg L^{-1} h^{-1}
15	1.268	1.707	0.358	60.0	2.72
16	1.701	1.707	0.358	102.4	0.67
17	1.268	1.707	0.437	102.4	3.00
18	2.134	1.707	0.437	102.4	1.78
19	1.268	1.707	0.279	102.4	2.15
20	1.268	1.707	0.437	60.0	2.53
21	1.701	1.707	0.437	102.4	0.98
22	1.268	1.354	0.437	102.4	3.15
23	1.268	1.707	0.358	102.4	2.14
24	1.268	1.707	0.437	81.2	2.76
25	1.484	1.707	0.437	102.4	1.94
26	1.268	1.884	0.437	102.4	3.06
27	1.701	1.884	0.437	102.4	2.37
28	1.268	1.530	0.437	102.4	3.44
29	1.268	1.884	0.358	102.4	2.39
30	1.268	1.884	0.437	81.2	3.04
31	1.484	1.884	0.437	102.4	2.10
32	1.268	1.884	0.477	102.4	3.54
33	1.701	1.884	0.477	102.4	2.67
34	1.268	1.530	0.477	102.4	3.86
35	1.268	1.884	0.398	102.4	2.78
36	1.268	1.884	0.477	81.2	3.46
37	1.484	1.884	0.477	102.4	2.47
38	1.268	1.884	0.477	113.0	3.68
39	1.701	1.884	0.477	113.0	2.87
40	1.268	1.530	0.477	113.0	4.06
41	1.268	1.884	0.398	113.0	3.01
42	1.268	1.884	0.477	91.8	3.80
43	1.484	1.884	0.477	113.0	2.88
44	1.051	1.884	0.477	113.0	4.94
45	1.484	1.884	0.477	113.0	3.22
46	1.051	1.530	0.477	113.0	4.83
47	1.051	1.884	0.398	113.0	3.48
48	1.051	1.884	0.477	91.8	4.37
49	1.268	1.884	0.477	113.0	3.18
50	1.051	1.707	0.477	113.0	4.72
51	1.051	1.884	0.437	113.0	4.03
52	1.051	1.884	0.477	102.4	4.50
53	1.160	1.884	0.477	113.0	3.84

Entry	t_{Res} / min	Morpholine eq	Concentration / mol L^{-1}	Temperature / °C	STY / kg L^{-1} h^{-1}
54	1.051	1.972	0.477	113.0	4.59
55	1.268	1.972	0.477	113.0	3.86
56	1.051	1.795	0.477	113.0	4.82
57	1.051	1.972	0.437	113.0	4.13
58	1.051	1.972	0.477	102.4	4.62
59	1.160	1.972	0.477	113.0	4.00
60	1.051	1.972	0.496	113.0	4.90
61	1.268	1.972	0.496	113.0	4.06
62	1.051	1.795	0.496	113.0	5.17
63	1.051	1.972	0.457	113.0	4.33
64	1.051	1.972	0.496	102.4	4.87
65	1.160	1.972	0.496	113.0	4.17
66	1.051	1.972	0.496	118.3	4.99
67	1.051	1.884	0.496	113.0	4.94
68	1.051	1.972	0.477	113.0	4.67
69	1.051	1.972	0.496	107.7	4.92
70	1.106	1.972	0.496	113.0	4.59
71	1.051	1.972	0.496	115.7	4.97
72	1.051	1.928	0.496	113.0	4.98
73	1.051	1.972	0.487	113.0	4.85
74	1.051	1.972	0.496	110.4	4.93
75	1.079	1.972	0.496	113.0	4.81
76	1.051	1.994	0.496	113.0	4.94
77	1.106	1.994	0.496	113.0	4.74
78	1.051	1.994	0.496	115.7	5.02
79	1.160	1.994	0.496	115.7	4.57
80	1.051	1.906	0.496	115.7	5.14
81	1.051	1.994	0.477	115.7	4.82
82	1.051	1.994	0.496	110.4	5.05
83	1.106	1.994	0.496	115.7	4.68
84	1.051	1.994	0.496	118.3	5.10
85	1.160	1.994	0.496	118.3	4.59
86	1.051	1.906	0.496	118.3	5.24
87	1.268	1.906	0.496	118.3	4.26
88	**1.051**	**1.729**	**0.496**	**118.3**	**5.27**
89	1.051	1.906	0.457	118.3	4.51
90	1.051	1.906	0.496	107.7	4.99
91	1.160	1.906	0.496	118.3	4.38
92	1.051	1.994	0.496	118.3	4.98

Entry	t_{Res} / min	Morpholine eq	Concentration / mol L^{-1}	Temperature / °C	STY / kg L^{-1} h^{-1}
93	1.051	1.818	0.496	118.3	5.04
94	1.051	1.906	0.477	118.3	4.70
95	1.051	1.906	0.496	113.0	5.03
96	1.106	1.906	0.496	118.3	4.72
97	1.051	1.950	0.496	118.3	5.11
98	1.051	1.862	0.496	118.3	5.11
99	1.051	1.906	0.487	118.3	4.90
100	1.051	1.906	0.496	115.7	5.02
101	1.079	1.906	0.496	118.3	4.88
102	1.051	1.928	0.496	118.3	5.09
103	1.051	1.906	0.496	119.7	5.10
104	1.024	1.906	0.496	118.3	5.22
105	1.079	1.906	0.496	118.3	4.95
106	1.024	1.950	0.496	118.3	5.20
107	1.133	1.950	0.496	118.3	4.68

8.5.6 Multi-Objective Optimisation

The target functions were STY and process mass intensity (PMI)

$$PMI = \frac{mass_{reactants}}{mass_{products}}$$

Table 8.27 Limits for the multi-objective optimisation using TS-EMO algorithm.

Limit	t_{Res} / min	Morpholine / mol eq	Concentration / mol L^{-1}	Temperature / °C
Lower	0.5	1.0	0.100	60
Upper	2	5.0	0.500	140

Table 8.28 List of experiments from the multi-objective TS-EMO optimisation. Optimum conditions highlighted in bold.

Entry	t_{Res} / min	Morpholine eq	Concentration / mol L^{-1}	Temperature / °C	PMI	STY / kg L^{-1} h^{-1}
1	1.45	2.04	0.165	60.5	6.15	0.37
2	1.24	2.43	0.361	64.8	3.06	2.08
3	0.81	4.59	0.484	71.6	2.94	6.69
4	0.69	1.97	0.141	74.7	8.07	0.50
5	1.49	3.31	0.194	79.4	3.03	1.14
6	1.04	1.27	0.334	80.7	2.89	1.79
7	1.96	3.19	0.229	84.2	2.37	1.28

Entry	t_{Res} / min	Morpholine eq	Concentration / mol L^{-1}	Temperature / °C	PMI	STY / kg L^{-1} h^{-1}
8	0.98	4.05	0.456	88.8	2.44	5.78
9	1.66	4.75	0.214	92.2	2.76	1.58
10	1.74	3.43	0.425	97.1	2.08	3.19
11	1.27	1.73	0.111	103.9	2.98	0.54
12	1.58	1.44	0.264	105.1	1.75	1.62
13	0.59	3.70	0.388	111.6	2.35	7.91
14	1.17	3.84	0.400	115.2	2.23	4.50
15	0.74	4.37	0.248	116.3	2.61	4.10
16	1.82	2.73	0.134	122.6	2.00	0.87
17	1.92	4.96	0.313	124.8	2.68	2.13
18	0.88	1.12	0.295	132.0	1.63	3.13
19	1.35	2.91	0.357	134.5	1.86	3.48
20	0.53	2.28	0.465	139.4	1.72	10.78
21	0.50	4.09	0.500	111.0	2.48	12.28
22	0.97	1.00	0.500	140.0	1.33	5.71
23	0.50	1.34	0.500	140.0	1.52	10.80
24	0.64	1.00	0.500	140.0	1.44	8.01
25	2.00	1.00	0.500	129.1	1.25	2.94
26	0.50	2.29	0.500	137.8	1.72	12.40
27	0.81	1.07	0.500	140.0	1.36	6.85
28	1.18	1.00	0.500	140.0	1.29	4.85
29	0.50	2.89	0.500	140.0	1.91	12.76
30	0.50	1.78	0.500	140.0	1.60	11.68
31	0.60	1.19	0.500	140.0	1.46	8.97
32	0.69	1.00	0.500	140.0	1.42	7.51
33	1.27	1.00	0.500	121.5	1.42	4.09
34	1.02	1.19	0.499	126.7	1.40	5.42
35	0.75	1.43	0.500	129.7	1.47	7.63
36	0.61	1.43	0.500	130.6	1.55	8.89
37	1.80	1.10	0.500	140.0	1.27	3.34
38	0.77	1.33	0.500	140.0	1.39	7.66
39	1.52	1.09	0.500	140.0	1.25	3.96
40	0.50	2.00	0.500	140.0	1.63	12.10
41	0.92	1.22	0.500	139.9	1.36	6.36
42	**0.50**	**4.51**	**0.500**	**140.0**	**2.50**	**13.08**
43	0.61	1.56	0.500	140.0	1.50	9.55
44	1.08	1.14	0.500	140.0	1.33	5.37
45	0.50	3.19	0.500	140.0	2.01	12.91
46	0.50	2.58	0.500	140.0	1.80	12.65

Entry	t_{Res} / min	Morpholine eq	Concentration / mol L^{-1}	Temperature / °C	PMI	STY / kg L^{-1} h^{-1}
47	1.05	1.00	0.500	140.0	1.31	5.34
48	1.32	1.00	0.500	140.0	1.27	4.37
49	1.88	1.00	0.425	134.5	1.30	2.54
50	1.73	1.00	0.460	137.9	1.26	3.10
51	1.60	1.00	0.490	139.8	1.26	3.58
52	0.53	1.23	0.500	140.0	1.49	10.01
53	0.50	4.70	0.500	140.0	2.57	13.12
54	0.50	1.60	0.500	140.0	1.56	11.39
55	0.62	1.00	0.499	140.0	1.46	8.01
56	0.92	1.00	0.500	140.0	1.34	5.95
57	1.79	1.00	0.500	140.0	1.25	3.29
58	0.70	1.37	0.500	140.0	1.42	8.30
59	**1.62**	**1.00**	**0.500**	**140.0**	**1.24**	**3.65**
60	0.93	1.13	0.500	140.0	1.32	6.24
61	1.26	1.00	0.500	134.1	1.32	4.42
62	1.41	1.00	0.500	134.2	1.29	4.03
63	0.50	2.20	0.500	139.4	1.69	12.34
64	0.50	2.49	0.500	139.6	1.78	12.55
65	0.50	3.01	0.500	140.0	1.95	12.83
66	0.50	2.76	0.500	140.0	1.86	12.76
67	0.50	3.28	0.500	140.0	2.03	12.99
68	1.12	1.00	0.500	140.0	1.30	5.03

Table 8.29 List of experiments in Pareto front in order from optimum STY to optimum PMI

Entry[a]	t_{Res} / min	Morpholine eq	Concentration / mol L^{-1}	Temperature / °C	PMI	STY / kg L^{-1} h^{-1}
53	0.50	4.70	0.500	140.0	2.57	13.12
42	0.50	4.51	0.500	140.0	2.50	13.08
67	0.50	3.28	0.500	140.0	2.03	12.99
45	0.50	3.19	0.500	140.0	2.01	12.91
65	0.50	3.01	0.500	140.0	1.95	12.83
29	0.50	2.89	0.500	140.0	1.91	12.76
66	0.50	2.76	0.500	140.0	1.86	12.76
46	0.50	2.58	0.500	140.0	1.80	12.65
64	0.50	2.49	0.500	139.6	1.78	12.55
26	0.50	2.29	0.500	137.8	1.72	12.40
63	0.50	2.20	0.500	139.4	1.69	12.34
40	0.50	2.00	0.500	140.0	1.63	12.10
30	0.50	1.78	0.500	140.0	1.60	11.68

54	0.50	1.60	0.500	140.0	1.56	11.39
23	0.50	1.34	0.500	140.0	1.52	10.80
52	0.53	1.23	0.500	140.0	1.49	10.01
31	0.60	1.19	0.500	140.0	1.46	8.97
58	0.70	1.37	0.500	140.0	1.42	8.30
38	0.77	1.33	0.500	140.0	1.39	7.66
27	0.81	1.07	0.500	140.0	1.36	6.85
60	0.93	1.13	0.500	140.0	1.32	6.24
47	1.05	1.00	0.500	140.0	1.31	5.34
28	1.18	1.00	0.500	140.0	1.29	4.85
48	1.32	1.00	0.500	140.0	1.27	4.37
39	1.52	1.09	0.500	140.0	1.25	3.96
59	1.62	1.00	0.500	140.0	1.24	3.65

a – relates to the entry in Table 8.28

Table 8.30 List of experiments from Paerto front displaying different target functions

Entry	PMI	STY / kg L^{-1} h^{-1}	Ortho %	Selectivity %	Cost / £ kg^{-1}
53	2.565	13.1172	96.6	93.9	155.2238
42	2.498	13.0801	96.4	93.6	154.4462
67	2.031	12.9896	95.7	94.8	148.405
45	2.005	12.9096	95.1	94.9	148.8133
65	1.947	12.8272	94.5	95.1	148.6954
29	1.908	12.7624	94.0	95.1	148.774
66	1.856	12.7559	94.1	95.3	147.8451
46	1.801	12.6535	93.2	95.4	148.1953
64	1.776	12.5549	92.5	95.5	148.7739
26	1.717	12.399	91.4	95.7	149.3435
63	1.689	12.3368	90.9	95.9	149.6126
40	1.635	12.0956	89.1	96.0	151.3827
30	1.598	11.6764	86.0	96.2	155.4122
54	1.558	11.3868	83.9	96.4	158.1052
23	1.520	10.7985	79.6	96.5	164.8236
52	1.486	10.0054	78.5	96.7	166.3514
31	1.456	8.9676	79.2	96.6	164.5994
58	1.419	8.29794	86.0	96.2	152.7523
38	1.393	7.65563	86.7	96.2	151.2616
27	1.359	6.85096	81.3	96.4	159.5242
60	1.325	6.24299	85.2	96.3	152.615
47	1.306	5.34426	82.7	96.5	156.3514
28	1.287	4.84947	84.0	96.3	153.9317

48	1.269	4.37047	85.2	96.3	151.7636
39	1.253	3.96485	89.0	96.0	145.8481
59	1.239	3.64542	87.2	96.2	148.2828

References

1. H.-J. Federsel, *Drug Discov. Today*, 2006, **11**, 966-974.
2. S. A. Weissman and N. G. Anderson, *Org. Process Res. Dev.*, 2015, **19**, 1605-1633.
3. M. R. Owen, C. Luscombe, Lai, S. Godbert, D. L. Crookes and D. Emiabata-Smith, *Org. Process Res. Dev.*, 2001, **5**, 308-323.
4. P. Poechlauer, J. Colberg, E. Fisher, M. Jansen, M. D. Johnson, S. G. Koenig, M. Lawler, T. Laporte, J. Manley, B. Martin and A. O'Kearney-McMullan, *Org. Process Res. Dev.*, 2013, **17**, 1472-1478.
5. P. Poechlauer, J. Manley, R. Broxterman, B. Gregertsen and M. Ridemark, *Org. Process Res. Dev.*, 2012, **16**, 1586-1590.
6. I. R. Baxendale, R. D. Braatz, B. K. Hodnett, K. F. Jensen, M. D. Johnson, P. Sharratt, J.-P. Sherlock and A. J. Florence, *J. Pharmaceut. Sci.*, 2014, **104**, 781-791.
7. M. Baumann and I. R. Baxendale, *Beilstein J. Org. Chem.*, 2015, **11**, 1194-1219.
8. M. Rasheed and T. Wirth, *Angew. Chem., Int. Ed.*, 2011, **50**, 357-358.
9. D. C. Fabry, E. Sugiono and M. Rueping, *React. Chem. Eng.*, 2016, **1**, 126-133.
10. V. Sans and L. Cronin, *Chem. Soc. Rev.*, 2016, **45**, 2032-2043.
11. S. Krishnadasan, R. J. C. Brown, A. J. de Mello and J. C. de Mello, *Lab Chip*, 2007, **7**, 1434-1441.
12. J. P. McMullen and K. F. Jensen, *Org. Process Res. Dev.*, 2010, **14**, 1169-1176.
13. J. P. McMullen and K. F. Jensen, *Org. Process Res. Dev.*, 2011, **15**, 398-407.
14. J. P. McMullen, M. T. Stone, S. L. Buchwald and K. F. Jensen, *Angew. Chem., Int. Ed.*, 2010, **49**, 7076-7080.
15. A. J. Parrott, R. A. Bourne, G. R. Akien, D. J. Irvine and M. Poliakoff, *Angew. Chem., Int. Ed.*, 2011, **50**, 3788-3792.
16. R. A. Bourne, R. A. Skilton, A. J. Parrott, D. J. Irvine and M. Poliakoff, *Org. Process Res. Dev.*, 2011, **15**, 932-938.
17. D. N. Jumbam, R. A. Skilton, A. J. Parrott, R. A. Bourne and M. Poliakoff, *J. Flow Chem.*, 2012, **2**, 24-27.
18. R. A. Skilton, A. J. Parrott, M. W. George, M. Poliakoff and R. A. Bourne, *Appl. Spectrosc.*, 2013, **67**, 1127-1131.
19. B. J. Reizman and K. F. Jensen, *Org. Process Res. Dev.*, 2012, **16**, 1770-1782.
20. B. J. Reizman and K. F. Jensen, *Chem. Commun.*, 2015, **51**, 13290-13293.
21. B. J. Reizman, Y.-M. Wang, S. L. Buchwald and K. F. Jensen, *React. Chem. Eng.*, 2016, **1**, 658-666.
22. R. A. Skilton, R. A. Bourne, Z. Amara, R. Horvath, J. Jin, M. J. Scully, E. Streng, S. L. Y. Tang, P. A. Summers, J. Wang, E. Perez, N. Asfaw, G. L. P. Aydos, J. Dupont, G. Comak, M. W. George and M. Poliakoff, *Nat. Chem.*, 2015, **7**, 1-5.
23. Z. Amara, E. S. Streng, R. A. Skilton, J. Jin, M. W. George and M. Poliakoff, *Eur. J. Org. Chem.*, 2015, **2015**, 6141-6145.
24. V. Sans, S. Glatzel, F. J. Douglas, D. A. Maclaren, A. Lapkin and L. Cronin, *Chem. Sci.*, 2014, **5**, 1153-1157.
25. V. Sans, L. Porwol, V. Dragone and L. Cronin, *Chem. Sci.*, 2015, **6**, 1258-1264.
26. C. Houben, N. Peremezhney, A. Zubov, J. Kosek and A. A. Lapkin, *Org. Process Res. Dev.*, 2015, **19**, 1049-1053.
27. D. E. Fitzpatrick, C. Battilocchio and S. V. Ley, *Org. Process Res. Dev.*, 2015, **20**, 386–394.
28. D. Cortés-Borda, K. V. Kutonova, C. Jamet, M. E. Trusova, F. Zammattio, C. Truchet, M. Rodriguez-Zubiri and F.-X. Felpin, *Org. Process Res. Dev.*, 2016, **20**, 1979-1987.
29. V. Hessel, *Chem. Eng. Technol.*, 2009, **32**, 1655-1681.
30. V. Hessel, B. Cortese and M. H. J. M. de Croon, *Chem. Eng. Sci.*, 2011, **66**, 1426-1448.
31. V. Hessel, D. Kralisch, N. Kockmann, T. Noël and Q. Wang, *ChemSusChem*, 2013, **6**, 746-789.
32. D. L. Browne, M. Baumann, B. H. Harji, I. R. Baxendale and S. V. Ley, *Org. Lett.*, 2011, **13**, 3312-3315.
33. D. L. Browne, B. H. Harji and S. V. Ley, *Chem. Eng. Technol.*, 2013, **36**, 959-967.

34. J. A. Newby, D. W. Blaylock, P. M. Witt, R. M. Turner, P. L. Heider, B. H. Harji, D. L. Browne and S. V. Ley, *Org. Process Res. Dev.*, 2014, **18**, 1221-1228.
35. J.-i. Yoshida, A. Nagaki and T. Yamada, *Chem. - Eur. J.*, 2008, **14**, 7450-7459.
36. J.-i. Yoshida, Y. Takahashi and A. Nagaki, *Chem. Commun.*, 2013, **49**, 9896-9904.
37. Y. Su, N. J. W. Straathof, V. Hessel and T. Noël, *Chem. - Eur. J.*, 2014, **20**, 10562-10589.
38. D. M. Roberge, N. Bieler, M. Mathier, M. Eyholzer, B. Zimmermann, P. Barthe, C. Guermeur, O. Lobet, M. Moreno and P. Woehl, *Chem. Eng. Technol.*, 2008, **31**, 1155-1161.
39. C. B. McPake and G. Sandford, *Org. Process Res. Dev.*, 2012, **16**, 844-851.
40. B. J. Deadman, R. M. O'Mahony, D. Lynch, D. C. Crowley, S. G. Collins and A. R. Maguire, *Org. Biomol. Chem.*, 2016, **14**, 3423-3431.
41. C. J. Mallia and I. R. Baxendale, *Org. Process Res. Dev.*, 2016, **20**, 327-360.
42. B. J. Deadman, S. G. Collins and A. R. Maguire, *Chem. - Eur. J.*, 2015, **21**, 2298-2308.
43. S. G. Newman, L. Gu, C. Lesniak, G. Victor, F. Meschke, L. Abahmane and K. F. Jensen, *Green Chem.*, 2014, **16**, 176-180.
44. B. Gutmann, J.-P. Roduit, D. Roberge and C. O. Kappe, *Angew. Chem. Int. Ed.*, 2010, **49**, 7101-7105.
45. R. L. Hartman, J. P. McMullen and K. F. Jensen, *Angew. Chem., Int. Ed.*, 2011, **50**, 7502-7519.
46. D. M. Roberge, B. Zimmermann, F. Rainone, M. Gottsponer, M. Eyholzer and N. Kockmann, *Org. Process Res. Dev.*, 2008, **12**, 905-910.
47. D. T. McQuade and P. H. Seeberger, *J. Org. Chem.*, 2013, **78**, 6384-6389.
48. P. Watts and S. J. Haswell, *Chem. Soc. Rev.*, 2005, **34**, 235-246.
49. B. Gutmann, D. Cantillo and C. O. Kappe, *Angew. Chem., Int. Ed.*, 2015, **54**, 6688-6728.
50. T. Razzaq and C. O. Kappe, *Chem. - Asian J.*, 2010, **5**, 1274-1289.
51. D. Webb and T. F. Jamison, *Chem. Sci.*, 2010, **1**, 675-680.
52. B. P. Mason, K. E. Price, J. L. Steinbacher, A. R. Bogdan and D. T. McQuade, *Chemical Reviews*, 2007, **107**, 2300-2318.
53. S. V. Ley, D. E. Fitzpatrick, R. J. Ingham and R. M. Myers, *Angew. Chem. Int. Ed.*, 2015, **54**, 3449-3464.
54. S. V. Ley, D. E. Fitzpatrick, R. M. Myers, C. Battilocchio and R. J. Ingham, *Angew. Chem., Int. Ed.*, 2015, **54**, 10122-10136.
55. K. F. Jensen, *AIChE Journal*, 2017, **63**, 858-869.
56. S. Borukhova, T. Noel, B. Metten, E. de Vos and V. Hessel, *Green Chem.*, 2016, **18**, 4947-4953
57. S. Borukhova, T. Noël and V. Hessel, *Org. Process Res. Dev.*, 2016, **20**, 568-573.
58. S. Borukhova, T. Noel, B. Metten, E. de Vos and V. Hessel, *ChemSusChem*, 2013, **6**, 2220-2225.
59. D. R. Snead and T. F. Jamison, *Chem. Sci.*, 2013, **4**, 2822-2827.
60. C. A. Hone, N. Holmes, G. R. Akien, R. A. Bourne and F. L. Muller, *React. Chem. Eng.*, 2017,**2**, 103-108.
61. B. Gutmann, P. Elsner, A. O'Kearney-McMullan, W. Goundry, D. M. Roberge and C. O. Kappe, *Org. Process Res. Dev.*, 2015, **19**, 1062-1067.
62. H. Kim, K.-I. Min, K. Inoue, D. J. Im, D.-P. Kim and J.-i. Yoshida, *Science*, 2016, **352**, 691-694.
63. T. Kawaguchi, H. Miyata, K. Ataka, K. Mae and J.-I. Yoshida, *Angew. Chem., Int. Ed.*, 2005, **44**, 2413-2416.
64. Z. Amara, J. Bellamy, F. B., R. Horvath, S. J. Miller, A. Beeby, A. Burgard, K. Rossen, M. Poliakoff and M. W. George, *Nat. Chem.*, 2015, **7**, 489-495.
65. K. Gilmore, D. Kopetzki, J. W. Lee, Z. Horvath, D. T. McQuade, A. Seidel-Morgenstern and P. H. Seeberger, *Chem. Commun.*, 2014, **50**, 12652-12655.
66. D. Kopetzki, F. Lévesque and P. H. Seeberger, *Chem. - Eur. J.*, 2013, **19**, 5450-5456.
67. F. Lévesque and P. H. Seeberger, *Angew. Chem. Int. Ed.*, 2012, **51**, 1706-1709.
68. K. Watts, A. Baker and T. Wirth, *J. Flow Chem.*, 2014, **4**, 2-11.
69. J.-i. Yoshida, *Chem. Commun.*, 2005, 4509-4516.
70. I. R. Baxendale and M. R. Pitts, *Chim. Oggi Chem. Today*, 2006, **24**, 41.
71. T. N. Glasnov and C. O. Kappe, *Macromol. Rapid Commun.*, 2007, **28**, 395-410.

72. S. Ceylan, C. Friese, C. Lammel, K. Mazac and A. Kirschning, *Angew. Chem. Int. Ed.*, 2008, **47**, 8950-8953.
73. A. Kirschning, L. Kupracz and J. Hartwig, *Chem. Lett.*, 2012, **41**, 562-570.
74. R. L. Hartman, J. R. Naber, N. Zaborenko, S. L. Buchwald and K. F. Jensen, *Org. Process Res. Dev.*, 2010, **14**, 1347-1357.
75. S. Kuhn, T. Noel, L. Gu, P. L. Heider and K. F. Jensen, *Lab Chip*, 2011, **11**, 2488-2492.
76. N. P. Tu, J. E. Hochlowski and S. W. Djuric, *Molec. Divers.*, 2012, **16**, 53-58.
77. R. D. Chambers, D. Holling, R. C. H. Spink and G. Sandford, *Lab Chip*, 2001, **1**, 132-137.
78. R. D. Chambers, M. A. Fox, D. Holling, T. Nakano, T. Okazoe and G. Sandford, *Lab Chip*, 2005, **5**, 191-198.
79. J. R. Breen, G. Sandford, D. S. Yufit, J. A. K. Howard, J. Fray and B. Patel, *Beilstein Journal of Organic Chemistry*, 2011, **7**, 1048-1054.
80. P. Poechlauer, S. Braune, B. Dielemans, B. Kaptein, R. Obermueller and M. Thathagar, *Chim. Oggi Chem. Today*, 2012, **30**, 4.
81. M. O'Brien, P. Koos, D. L. Browne and S. V. Ley, *Org. Biomol. Chem.*, 2012, **10**, 7031-7036.
82. A. Adamo, P. L. Heider, N. Weeranoppanant and K. F. Jensen, *Ind. Eng. Chem. Res.*, 2013, **52**, 10802-10808.
83. J. J. John, S. Kuhn, L. Braeken and T. Van Gerven, *Chem. Eng. Process.*, 2017, **113**, 35-41.
84. B. J. Deadman, C. Battilocchio, E. Sliwinski and S. V. Ley, *Green Chem.*, 2013, **15**, 2050-2055.
85. R. L. Hartman, J. R. Naber, S. L. Buchwald and K. F. Jensen, *Angew. Chem. Int. Ed.*, 2010, **49**, 899-903.
86. B. Z. Cvetkovic, O. Lade, L. Marra, V. Arima, R. Rinaldi and P. S. Dittrich, *RSC Adv.*, 2012, **2**, 11117-11122.
87. S. V. Ley, I. R. Baxendale, R. N. Bream, P. S. Jackson, A. G. Leach, D. A. Longbottom, M. Nesi, J. S. Scott, R. I. Storer and S. J. Taylor, *J. Chem. Soc., Perkin Trans. 1*, 2000, **0**, 3815-4195.
88. B. J. Deadman, D. L. Browne, I. R. Baxendale and S. V. Ley, *Chem. Eng. Technol.*, 2015, **38**, 259-264.
89. D. Rossi, R. Jamshidi, N. Saffari, S. Kuhn, A. Gavriilidis and L. Mazzei, *Cryst. Growth Des.*, 2015, **15**, 5519-5529.
90. H. Zhang, R. Lakerveld, P. L. Heider, M. Tao, M. Su, C. J. Testa, A. N. D'Antonio, P. I. Barton, R. D. Braatz, B. L. Trout, A. S. Myerson, K. F. Jensen and J. M. B. Evans, *Cryst. Growth Des.*, 2014, **14**, 2148-2157.
91. S. Mascia, P. L. Heider, H. Zhang, R. Lakerveld, B. Benyahia, P. I. Barton, R. D. Braatz, C. L. Cooney, J. M. B. Evans, T. F. Jamison, K. F. Jensen, A. S. Myerson and B. L. Trout, *Angew. Chem. Int. Ed.*, 2013, **52**, 12359-12363.
92. I. R. Baxendale, C. M. Griffiths-Jones, S. V. Ley and G. K. Tranmer, *Synlett*, 2006, **2006**, 0427-0430.
93. A. R. Bogdan, S. L. Poe, D. C. Kubis, S. J. Broadwater and D. T. McQuade, *Angew. Chem. Int. Ed.*, 2009, **48**, 8547-8550.
94. D. R. Snead and T. F. Jamison, *Angew. Chem., Int. Ed.*, 2015, **54**, 983-987.
95. R. L. Hartman, *Org. Process Res. Dev.*, 2012, **16**, 870-887.
96. A. Adamo, R. L. Beingessner, M. Behnam, J. Chen, T. F. Jamison, K. F. Jensen, J.-C. M. Monbaliu, A. S. Myerson, E. M. Revalor, D. R. Snead, T. Stelzer, N. Weeranoppanant, S. Y. Wong and P. Zhang, *Science*, 2016, **352**, 61-67.
97. J. S. Moore and K. F. Jensen, *Org. Process Res. Dev.*, 2012, **16**, 1409-1415.
98. W. Ferstl, S. Loebbecke, J. Antes, H. Krause, M. Haeberl, D. Schmalz, H. Muntermann, M. Grund, A. Steckenborn, A. Lohf, J. Hassel, T. Bayer, M. Kinzl and I. Leipprand, *Chem. Eng. J. (Amsterdam, Neth.)*, 2004, **101**, 431-438.
99. W. Ferstl, T. Klahn, W. Schweikert, G. Billeb, M. Schwarzer and S. Loebbecke, *Chem. Eng. Technol.*, 2007, **30**, 370-378.
100. R. Herzig-Marx, K. T. Queeney, R. J. Jackman, M. A. Schmidt and K. F. Jensen, *Anal. Chem.*, 2004, **76**, 6476-6483.

101. S. Hübner, U. Bentrup, U. Budde, K. Lovis, T. Dietrich, A. Freitag, L. Küpper and K. Jähnisch, *Org. Process Res. Dev.*, 2009, **13**, 952-960.
102. M. Rueping, T. Bootwicha and E. Sugiono, *Beilstein J. Org. Chem.*, 2012, **8**, 300-307.
103. C. F. Carter, H. Lange, S. V. Ley, I. R. Baxendale, B. Wittkamp, J. G. Goode and N. L. Gaunt, *Org. Process Res. Dev.*, 2010, **14**, 393-404.
104. Z. Qian, I. R. Baxendale and S. V. Ley, *Chem. - Eur. J.*, 2010, **16**, 12342-12348.
105. S. Mozharov, A. Nordon, D. Littlejohn, C. Wiles, P. Watts, P. Dallin and J. M. Girkin, *J. Am. Chem. Soc.*, 2011, **133**, 3601-3608.
106. A. Caceres, M. Jaimes, G. Chavez, B. Bravo, F. Ysambertt and N. Marquez, *Talanta*, 2005, **68**, 359-364.
107. D. L. Olson, T. L. Peck, A. G. Webb, R. L. Magin and J. V. Sweedler, *Science*, 1995, **270**, 1967-1970.
108. H. Wensink, F. Benito-Lopez, D. C. Hermes, W. Verboom, H. J. G. E. Gardeniers, D. N. Reinhoudt and d. B. A. van, *Lab Chip*, 2005, **5**, 280-284.
109. M. V. Gomez, H. H. J. Verputten, A. Diaz-Ortiz, A. Moreno, l. H. A. de and A. H. Velders, *Chem. Commun.*, 2010, **46**, 4514-4516.
110. L. Ciobanu, D. A. Jayawickrama, X. Zhang, A. G. Webb and J. V. Sweedler, *Angew. Chem., Int. Ed.*, 2003, **42**, 4669-4672.
111. A. Rehorek and A. Plum, *Anal. Bioanal. Chem.*, 2006, **384**, 1123-1128.
112. L. Zhu, R. G. Brereton, D. R. Thompson, P. L. Hopkins and R. E. A. Escott, *Analytica. Chimica. Acta.*, 2007, **584**, 370-378.
113. J. Antes, D. Boskovic, H. Krause, S. Loebbecke, N. Lutz, T. Tuercke and W. Schweikert, *Chem. Eng. Res. Des.*, 2003, **81**, 760-765.
114. B. Walsh, J. R. Hyde, P. Licence and M. Poliakoff, *Green Chem.*, 2005, **7**, 456-463.
115. J. G. Stevens, R. A. Bourne and M. Poliakoff, *Green Chem.*, 2009, **11**, 409-416.
116. J. G. Stevens, R. A. Bourne, M. V. Twigg and M. Poliakoff, *Angew. Chem., Int. Ed.*, 2010, **49**, 8856-8859.
117. D. Fabris, *Mass Spectrom. Rev.*, 2005, **24**, 30-54.
118. D. L. Browne, S. Wright, B. J. Deadman, S. Dunnage, I. R. Baxendale, R. M. Turner and S. V. Ley, *Rapid Commun. Mass Spectrom.*, 2012, **26**, 1999-2010.
119. S. E. Hamilton, F. Mattrey, X. Bu, D. Murray, B. McCullough and C. J. Welch, *Org. Process Res. Dev.*, 2014, **18**, 103.
120. F. Dalitz, M. Cudaj, M. Maiwald and G. Guthausen, *Prog. Nucl. Magn. Reson. Spectrosc.*, 2012, **60**, 52-70.
121. Spinsolve 60 NMR spectrometer: http://www.magritek.com/products/spinsolve60/, Last Accessed 17th April 2017.
122. Picospin 80 NMR spectrometer: https://www.thermofisher.com/order/catalog/product/912A0832, Last Accessed 17th April 2017.
123. B. Ahmed-Omer, E. Sliwinski, J. P. Cerroti and S. V. Ley, *Org. Process Res. Dev.*, 2016, **20**, 1603-1614.
124. C. J. Smith, N. Nikbin, S. V. Ley, H. Lange and I. R. Baxendale, *Org. Biomol. Chem.*, 2011, **9**, 1938-1947.
125. G. Chaplain, S. J. Haswell, P. D. I. Fletcher, S. M. Kelly and A. Mansfield, *Australian Journal of Chemistry*, 2013, **66**, 208-212.
126. Y. Roggo, P. Chalus, L. Maurer, C. Lema-Martinez, A. Edmond and N. Jent, *J. Pharm. Biomed. Anal.*, 2007, **44**, 683-700.
127. A. E. Cervera-Padrell, J. P. Nielsen, M. Jønch Pedersen, K. Müller Christensen, A. R. Mortensen, T. Skovby, K. Dam-Johansen, S. Kiil and K. V. Gernaey, *Org. Process Res. Dev.*, 2012, **16**, 901-914.
128. J. Wiss, M. Länzlinger and M. Wermuth, *Org. Process Res. Dev.*, 2005, **9**, 365-371.
129. D. M. Roberge, L. Ducry, N. Bieler, P. Cretton and B. Zimmermann, *Chem. Eng. Technol.*, 2005, **28**, 318-323.
130. H. Meyer, O. Biermann, R. Faller, D. Reith and F. Muller-Plathe, *J. Chem. Phys.*, 2000, **113**, 6264-6275.
131. M. E. Swartz, *J. Liq. Chromatogr. Relat. Technol.*, 2005, **28**, 1253-1263.
132. J. J. van Deemter, F. J. Zuiderweg and A. Klinkenberg, *Chem. Eng. Sci.*, 1956, **5**, 271-289.
133. S. Fekete, K. Ganzler and J. Fekete, *J. Pharm. Biomed. Anal.*, 2011, **54**, 482-490.

134. F. Gritti, I. Leonardis, J. Abia and G. Guiochon, *J. Chromatogr.*, 2010, **1217**, 3819-3843.
135. A. B. Kanu, P. Dwivedi, M. Tam, L. Matz and H. H. Hill, *J. Mass. Spectrom.*, 2008, **43**, 1-22.
136. W. Huyer and A. Neumaier, *ACM Trans. Math. Softw.*, 2008, **35**, 1-25.
137. W. Spendley, G. R. Hext and F. R. Himsworth, *Technometrics*, 1962, **4**, 441-461.
138. J. A. Nelder and R. Mead, *Comput. J.*, 1965, **7**, 308-313.
139. M. W. Routh, P. A. Swartz and M. B. Denton, *Anal. Chem.*, 1977, **49**, 1422-1428.
140. R. S. Oakes, A. A. Clifford and C. M. Rayner, *J. Chem. Soc., Perkin Trans. 1*, 2001, doi: 10.1039/B101219N, 917-941.
141. T. Stelzer, S. Y. Wong, J. Chen and A. S. Myerson, *Org. Process Res. Dev.*, 2016, **20**, 1431-1438.
142. D. Whitley, *Stat Comput*, 1994, **4**, 65-85.
143. S. Forrest, *Science*, 1993, **261**, 872-878.
144. Mathworks, *How the Genetic Algorithm Works*, https://uk.mathworks.com/help/gads/how-the-genetic-algorithm-works.html, Last Accessed 17th April 2017.
145. R. Hooke and T. A. Jeeves, *J. ACM*, 1961, **8**, 212-229.
146. W. C. Davidon, *SIAM J. Optimiz.*, 1991, **1**, 1-17.
147. Mathworks, *How Pattern Search Polling Works*, http://uk.mathworks.com/help/gads/how-pattern-search-polling-works.html, Last Accessed 17th April 2017.
148. P. W. Araujo and R. G. Brereton, *TrAC, Trends Anal. Chem.*, 1996, **15**, 63-70.
149. E. Morgan, K. W. Burton and G. Nickless, *Chemometr. Intell. Lab.*, 1990, **8**, 97-107.
150. P. F. A. van der Wiel, R. Maassen and G. Kateman, *Anal. Chim. Acta*, 1983, **153**, 83-92.
151. J. H. Mathews, in *Numerical Methods Using MATLAB*, ed. K. D. Fink, Pearson Prentice Hall, Upper Saddle River, NJ, 4th edn., 2004, ch. 8, pp. 430-435.
152. G. E. P. Box, W. G. Hunter and J. S. Hunter, in *Statistics for Experimenters*, Wiley, New York, 1978, ch. 10, pp. 306-351.
153. T. Lundstedt, E. Seifert, L. Abramo, B. Thelin, Å. Nyström, J. Pettersen and R. Bergman, *Chemometr. Intell. Lab.*, 1998, **42**, 3-40.
154. G. E. P. Box, W. G. Hunter and J. S. Hunter, in *Statistics for Experimenters*, Wiley, New York, 1978, ch. 12, pp. 374-418.
155. D. C. Montgomery, in *Design and Analysis of Experiments*, Wiley, Singapore, 8th edn., 2013, ch. 8, pp. 320-393.
156. S. A. Raw, B. A. Taylor and S. Tomasi, *Org. Process Res. Dev.*, 2011, **15**, 688-692.
157. G. E. P. Box, W. G. Hunter and J. S. Hunter, in *Statistics for Experimenters*, Wiley, New York, 1978, ch. 15, pp. 510-539.
158. D. C. Montgomery, in *Design and Analysis of Experiments*, Wiley, Singapore, 8th edn., 2013, ch. 8, pp. 320-393.
159. N. Holmes and R. A. Bourne, in *Chemical Process Technology for a Sustainable Future*, eds. T. M. Letcher, J. L. Scott and D. A. Paterson, RSC Publishing, 1st edn., 2014, ch. 3, pp. 28-45.
160. M. R. V. Finlay, M. Anderton, S. Ashton, P. Ballard, P. A. Bethel, M. R. Box, R. H. Bradbury, S. J. Brown, S. Butterworth, A. Campbell, C. Chorley, N. Colclough, D. A. E. Cross, G. S. Currie, M. Grist, L. Hassall, G. B. Hill, D. James, M. James, P. Kemmitt, T. Klinowska, G. Lamont, S. G. Lamont, N. Martin, H. L. McFarland, M. J. Mellor, J. P. Orme, D. Perkins, P. Perkins, G. Richmond, P. Smith, R. A. Ward, M. J. Waring, D. Whittaker, S. Wells and G. L. Wrigley, *J. Med. Chem.*, 2014, **57**, 8249-8267.
161. D. Cross, S. Ashton, C. Nebhan, C. Eberlein, M. R. V. Finlay, G. Hughes, V. Jacobs, M. Mellor, M. Red Brewer, C. Meador, J. Orme, P. Spitzler, S. Powell, A. Rahi, P. Taylor, R. A. Ward, P. Daunt, A. Galer, T. Klinowska, G. Richmond and W. Pao, *Mol. Cancer Ther.*, 2013, **12**, A109.
162. D. Wilson, C. Finnie and S. A. Raw, WO2015101791A1, 2015.
163. *Guidance for Industry Q3B(R2) Impurities in New Drug Products*, Food and Drug Administration, US Department of Health and Human Services, Rockvile, MD, USA, July 2006 (http://www.fda.gov/downloads/Drugs/GuidanceComplianceRegulatoryInformation/Guidances/ucm073389.pdf), Last Accessed 17th April 2017
164. M. M. Rauhut and H. Currier, *US. Pat.*, US3074999, 1963.

165. D. Basavaiah, A. J. Rao and T. Satyanarayana, *Chem. Rev.*, 2003, **103**, 811-892.
166. A. B. Baylis and M. E. D. Hillman, *Ger. Pat.*, DE2155113 (A1), 1972.
167. A. B. Baylis and M. E. D. Hillman, *US. Pat.*, US3743669 (A), 1973.
168. S. Galbraith, *Chin. Clin. Oncol.*, 2014, **3**.
169. Solvent model was generated using the DynoChem utility: "Early phase solvent selection: solubility prediction" available from: https://dcresources.scale-up.com, Last Accessed 17th April 2017.
170. D. Prat, J. Hayler and A. Wells, *Green Chem.*, 2014, **16**, 4546-4551.
171. N. Peremezhney, E. Hines, A. Lapkin and C. Connaughton, *Eng. Optim*, 2014, **46**, 1593-1607.
172. N. Holmes, G. R. Akien, A. J. Blacker, R. L. Woodward, R. E. Meadows and R. A. Bourne, *React. Chem. Eng.*, 2016, **1**, 366-371.
173. C. R. Conrad and M. D. Dolliver, *Org. Synth.*, 1932, **12**, 22.
174. J. D. Gibbons and J. W. Pratt, *Am. Stat.*, 1975, **29**, 20-25.
175. G. E. P. Box and D. R. Cox, *J. Roy. Stat. Soc. B Met.*, 1964, **26**, 211-252.
176. G. E. P. Box, W. G. Hunter and J. S. Hunter, in *Statistics for Experimenters*, Wiley, New York, 1978, ch. 7, pp. 208-244.
177. G. E. P. Box and J. S. Hunter, *Ann. Math. Stat.*, 1957, **28**, 195-241.
178. R. H. Myers, D. C. Montgomery and C. M. Anderson-Cook, in *Response Surface Methodology*, Wiley, 2008, ch. 6, pp. 219-280.
179. G. Derringer and R. Suich, *J. Qual. Technol.*, 1980, **12**, 214-219.
180. N. R. Costa, J. Lourenço and Z. L. Pereira, *Chemometr. Intell. Lab.*, 2011, **107**, 234-244.
181. D. Ott, S. Borukhova and V. Hessel, *Green Chem.*, 2016, **18**, 1096-1116.
182. C. Jimenez-Gonzalez, C. S. Ponder, Q. B. Broxterman and J. B. Manley, *Org. Process Res. Dev.*, 2011, **15**, 912-917.
183. R. F. Kazmierczak., *Optimizing Complex Bioeconomic Silulations Using and Efficient Search Heuristic* DAE Research Report No. 704C61, October 1996.
184. F. Mattrey, S. Dolman, J. Nyrop and J. Skrdla, *Am. Pharm. Rev.*, 2012, **15**.
185. B. J. Reizman and K. F. Jensen, *Acc. Chem. Res.*, 2016, doi: 10.1021/acs.accounts.6b00261.
186. T. W. T. Bristow, A. D. Ray, A. O'Kearney-McMullan, L. Lim, B. McCullough and A. Zammataro, *J. Am. Soc. Mass Spectrom.*, 2014, **25**, 1794-1802.
187. K. M. Roscioli, X. Zhang, S. X. Li, G. H. Goetz, G. Cheng, Z. Zhang, W. F. Siems and H. H. Hill Jr, *Int. J. Mass. Spectrom.*, 2013, **336**, 27-36.
188. J. S. Mathieson, M. H. Rosnes, V. Sans, P. J. Kitson and L. Cronin, *Beilstein J. Nanotechnol.*, 2013, **4**, 285-291.
189. W. Zhao, Z. Jusys and R. J. Behm, *Anal. Chem.*, 2010, **82**, 2472-2479.
190. Z. Zhu, J. E. Bartmess, M. E. McNally, R. M. Hoffman, K. D. Cook and L. Song, *Anal. Chem.*, 2012, **84**, 7547-7554.
191. A. W. Owen, E. A. J. McAulay, A. Nordon, D. Littlejohn, T. P. Lynch, J. S. Lancaster and R. G. Wright, *Anal. Chim. Acta*, 2014, **849**, 12-18.
192. Agilent Technologies, Basic of LC/MS Primer, available open acces http://www.agilent.com/cs/library/support/documents/a05296.pdf, Last Accessed 17th April 2017.
193. B. Zhou, J. F. Xiao, L. Tuli and H. W. Ressom, *Mol. BioSyst.*, 2012, **8**, 470-481.
194. D.-X. Li, L. Gan, A. Bronja and O. J. Schmitz, *Anal. Chim. Acta*, 2015, **891**, 43-61.
195. E. M. Thurman, I. Ferrer and D. Barceló, *Anal. Chem.*, 2001, **73**, 5441-5449.
196. P. J. Taylor, *Clin. Biochem.*, 2005, **38**, 328-334.
197. L. Tang and P. Kebarle, *Anal. Chem.*, 1993, **65**, 3654-3668.
198. R. Bonfiglio, R. C. King, T. V. Olah and K. Merkle, *Rapid Comm. in Mass Spec.*, 1999, **13**, 1175-1185.
199. R. King, R. Bonfiglio, C. Fernandez-Metzler, C. Miller-Stein and T. Olah, *J. Am. Soc. Mass Spectrom.*, 2000, **11**, 942-950.
200. M. Adamczyk, J. R. Fishpaugh, J. C. Gebler, P. G. Mattingly and K. Shreder, *Eur. Mass Spectrom.*, 1998, **4**, 121-125.
201. M. C. Mitchell, V. Spikmans, A. Manz and A. J. de Mello, *J. Chem. Soc., Perkin Trans. 1*, 2001, doi: 10.1039/B009037I, 514-518.

202. M. C. Mitchell, V. Spikmans and A. J. d. Mello, *Analyst*, 2001, **126**, 24-27.
203. J. Griep-Raming, S. Meyer, T. Bruhn and J. O. Metzger, *Angew. Chem. Int. Ed.*, 2002, **41**, 2738-2742.
204. S. Meyer, R. Koch and J. O. Metzger, *Angew. Chem. Int. Ed.*, 2003, **42**, 4700-4703.
205. L. S. Santos, L. Knaack and J. O. Metzger, *Int. J. Mass. Spectrom.*, 2005, **246**, 84-104.
206. M. Brivio, A. Liesener, R. E. Oosterbroek, W. Verboom, U. Karst, A. van den Berg and D. N. Reinhoudt, *Anal. Chem.*, 2005, **77**, 6852-6856.
207. Y. Takahashi, R. Sakai, K. Sakamoto, Y. Yoshida, M. Kitaoka and T. Kitamori, *J. Mass Spec. Soc. Jap.*, 2006, **54**, 19-24.
208. S. Fritzsche, S. Ohla, P. Glaser, D. S. Giera, M. Sickert, C. Schneider and D. Belder, *Angew. Chem., Int. Ed.*, 2011, **50**, 9467-9470.
209. P. Dell'Orco, J. Brum, R. Matsuoka, M. Badlani and K. Muske, *Anal. Chem.*, 1999, **71**, 5165-5170.
210. Advion Expression CMS, version of spectrometer used no longer available, please visit http://advion.com/products/expression/ fo rmore information, Last Accessed 17th April 2017.
211. J. Nichols and M. Foster, *US Pat.*, US20010038071, 2001.
212. H. Cai, J. P. Kiplinger, W. K. Goetzinger, R. O. Cole, K. A. Laws, M. Foster and A. Schrock, *Rapid Comm. in Mass Spec.*, 2002, **16**, 544-554.
213. O. Levenspiel, *Chemical Reaction Engineering*, 3rd edn., Wiley, 1999.
214. F. E. Valera, M. Quaranta, A. Moran, J. Blacker, A. Armstrong, J. T. Cabral and D. G. Blackmond, *Angew. Chem. Int. Ed.*, 2010, **49**, 2478-2485.
215. J. S. Moore and K. F. Jensen, *Angew. Chem. Int. Ed.*, 2014, **53**, 470-473.
216. M. C. McMaster, in *GC/MS: A Practical User's Guide*, Wiley, Second edn., 2007, ch. Appendix C, pp. 165-166.
217. J. R. De Laeter, J. K. Boehlke, B. P. De, H. Hidaka, H. S. Peiser, K. J. R. Rosman and P. D. P. Taylor, *Pure Appl. Chem.*, 2003, **75**, 683-800.
218. Response surfaces were generated and analysed using MODDE v11 (Umetrics)
219. For more details on Mettler Toledo online IR analysis visit http://www.mt.com/gb/en/home/products/L1_AutochemProducts/ReactIR.html, Last Accessed 17th April 2017.
220. M. W. Kanan, M. M. Rozenman, K. Sakurai, T. M. Snyder and D. R. Liu, *Nature*, 2004, **431**, 545-549.
221. A. B. Beeler, S. Su, C. A. Singleton and J. A. Porco, *J. Am. Chem. Soc.*, 2007, **129**, 1413-1419.
222. A. McNally, C. K. Prier and D. W. C. MacMillan, *Science*, 2011, **334**, 1114-1117.
223. L. Weber, K. Illgen and M. Almstetter, *Synlett*, 1999, **1999**, 366-374.
224. O. J. Plante, E. R. Palmacci and P. H. Seeberger, *Science*, 2001, **291**, 1523-1527.
225. J. Li, S. G. Ballmer, E. P. Gillis, S. Fujii, M. J. Schmidt, A. M. E. Palazzolo, J. W. Lehmann, G. F. Morehouse and M. D. Burke, *Science*, 2015, **347**, 1221-1226.
226. R. J. Ingham, C. Battilocchio, D. E. Fitzpatrick, E. Sliwinski, J. M. Hawkins and S. V. Ley, *Angew. Chem. Int. Ed.*, 2015, **54**, 144-148.
227. J. P. Stambuli and J. F. Hartwig, *Curr. Opin. Chem. Biol.*, 2003, **7**, 420-426.
228. A. Buitrago Santanilla, E. L. Regalado, T. Pereira, M. Shevlin, K. Bateman, L.-C. Campeau, J. Schneeweis, S. Berritt, Z.-C. Shi, P. Nantermet, Y. Liu, R. Helmy, C. J. Welch, P. Vachal, I. W. Davies, T. Cernak and S. D. Dreher, *Science*, 2015, **347**, 49-53.
229. A. Bellomo, N. Celebi-Olcum, X. Bu, N. Rivera, R. T. Ruck, C. J. Welch, K. N. Houk and S. D. Dreher, *Angew. Chem. Int. Ed.*, 2012, **51**, 6912-6915.
230. N. Hawbaker, E. Wittgrove, B. Christensen, N. Sach and D. G. Blackmond, *Org. Process Res. Dev.*, 2016, **20**, 465-473.
231. H. Song, J. D. Tice and R. F. Ismagilov, *Angew. Chem., Int. Ed.*, 2003, **42**, 768-772.
232. V. Misuk, A. Mai, Y. Zhao, J. Heinrich, D. Rauber, K. Giannopoulos and H. Löwe, *J. Flow Chem.*, 2015, **5**, 101-109.
233. H. Song, D. L. Chen and R. F. Ismagilov, *Angew. Chem. Int. Ed.*, 2006, **45**, 7336-7356.
234. Uniqsis FlowSyn http://www.uniqsis.com/paFlowSystem.aspx, Last Accessed 17th April 2017.

235. Vapourtec R-Series https://www.vapourtec.com/products/r-series-flow-chemistry-system-overview/, Last Accessed 17th April 2017.
236. P. Rullière, P. Cyr and A. B. Charette, *Org. Lett.*, 2016, **18**, 1988-1991.
237. P. G. McCaw, B. J. Deadman, A. R. Maguire and S. G. Collins, *J. Flow Chem.*, 2016, **6**, 226-233.
238. S.-H. Lau, S. L. Bourne, B. Martin, B. Schenkel, G. Penn and S. V. Ley, *Org. Lett.*, 2015, **17**, 5436-5439.
239. V. D. Pinho, B. Gutmann, L. S. M. Miranda, R. O. M. A. de Souza and C. O. Kappe, *J. Org. Chem.*, 2014, **79**, 1555-1562.
240. C. J. Mallia, P. M. Burton, A. M. R. Smith, G. C. Walter and I. R. Baxendale, *Beilstein J. Org. Chem.*, 2016, **12**, 1598-1607.
241. C. J. Mallia, G. C. Walter and I. R. Baxendale, *Beilstein J. Org. Chem.*, 2016, **12**, 1503-1511.
242. M. R. Becker, M. A. Ganiek and P. Knochel, *Chem. Sci.*, 2015, **6**, 6649-6653.
243. M. R. Becker and P. Knochel, *Angew. Chem. Int. Ed.*, 2015, **54**, 12501-12505.
244. J. A. Newby, D. W. Blaylock, P. M. Witt, J. C. Pastre, M. K. Zacharova, S. V. Ley and D. L. Browne, *Org. Process Res. Dev.*, 2014, **18**, 1211-1220.
245. J. Jacq and P. Pasau, *Chem. - Eur. J.*, 2014, **20**, 12223-12233.
246. M. de Léséleuc, É. Godin, S. Parisien-Collette, A. Lévesque and S. K. Collins, *J. Org. Chem.*, 2016, **81**, 6750-6756.
247. S. Doherty, J. G. Knight, M. A. Carroll, A. R. Clemmet, J. R. Ellison, T. Backhouse, N. Holmes, L. A. Thompson and R. A. Bourne, *RSC Adv.*, 2016, **6**, 73118-73131.
248. M. V. Rojo, L. Guetzoyan and I. R. Baxendale, *Org. Biomol. Chem.*, 2015, **13**, 1768-1777.
249. J. Bao and G. K. Tranmer, *Tetrahedron Lett.*, 2016, **57**, 654-657.
250. D. Cantillo, O. de Frutos, J. A. Rincón, C. Mateos and C. O. Kappe, *Org. Lett.*, 2014, **16**, 896-899.
251. J. Guerra, D. Cantillo and C. O. Kappe, *Catal. Sci. Technol.*, 2016, **6**, 4695-4699.
252. A. G. O'Brien, Z. Horváth, F. Lévesque, J. W. Lee, A. Seidel-Morgenstern and P. H. Seeberger, *Angew. Chem., Int. Ed.*, 2012, **51**, 7028-7030.
253. K. Deb, K. Sindhya and J. Hakanen, in *Decision Sciences: Theory and Practice*, eds. R. N. Sengupta, A. Gupta and J. Dutta, CRC Press, 2016, ch. 3, pp. 145-184.
254. E. Bradford, A. Schweidtmann and A. Lapkin, *Unpublished material*.
255. A. Schweidtmann, MSc report, University of Cambridge, 2017.
256. M. D. McKay, R. J. Beckman and W. J. Conover, *Technometrics*, 1979, **21**, 239-245.
257. S. Agrawal and N. Goyal, *Analysis of Thompson Sampling for the Multi-armed Bandit Problem*, JMLR, Workshop and Conference Proceedings vol 23, 2012, pp. 39.31-39.26.
258. D. M. Roberge, M. Gottsponer, M. Eyholzer and N. Kockmann, *Chim. Oggi*, 2009, **27**, 8-11.
259. J. P. McMullen and K. F. Jensen, *Annu. Rev. Anal. Chem.*,, 2010, **3**, 19-42.
260. S. L. Greig, *Drugs*, 2016, **76**, 263-273.
261. P. Filipponi, A. Gioiello and I. R. Baxendale, *Org. Process Res. Dev.*, 2016, **20**, 371-375.
262. S. M. Senkan, *Nature*, 1998, **394**, 350-353.
263. S. Wold, K. Esbensen and P. Geladi, *Chemomtr. Intell. Lab.*, 1987, **2**, 37-52.
264. P. M. Murray, S. N. G. Tyler and J. D. Moseley, *Org. Process Res. Dev.*, 2013, **17**, 40-46.
265. M. I. Jeraal, MChem report, University of Leeds, 2014.
266. C. J. Pouchert and J. Behnke, in *Aldrich Library of 13C and 1H FT NMR Spectra*, 1993, p. 339B.
267. C. A. Hone, Ph.D. Thesis, University of Leeds, 2016.